Directional Growth of Wind Generated Waves

by

Sun Hong Kwon

Dissertation submitted to the Faculty of the
Virginia Polytechnic Institute and State University
in partial fulfillment of the requirements for the degree of
Doctor of Philosophy
in
Aerospace and Ocean Engineering

APPROVED:

Wayne L. Neu, Chairman

Paul Kaplan

Joseph A. Schetz

Karl E. Sundkvist

Adorjan G. Szeless

February, 1986

Blacksburg, Virginia

Directional Growth of Wind Generated Waves

by

Sun Hong Kwon

Wayne L. Neu, Chairman

Aerospace and Ocean Engineering

(ABSTRACT)

The Spectral Ocean Wave Model (SOWM) is a numerical wave prediction model which calculates directional wave spectra from input wind fields. As do the majority of wave models, it uses a point spectral growth mechanism, i.e., it applies the energy balance equation in a directionally integrated form. The directionality of its growth is obtained from an assumed spreading function on the wind direction.

In this study, the energy balance equation is applied in directional form using directional atmospheric energy source functions. The B function of Miles' instability mechanism is derived following the analysis of Phillips and it is tuned to the directionally integrated form used in the SOWM. Two infinite ocean wave models are used to compare the behavior of the point and directional growth mechanisms under various wind conditions. The directional form shows more flexibility in responding to directionallly varying winds while the point spectral form creates excess energy spread widely over direction when operating in the presence of swell.

Acknowledgements

The author sincerely wishes to express his thanks to Dr. Wayne L. Neu for his valuable time and insight provided during the entire course of the study. Without his help, it would have been very difficult to carry out this study.

The author would also like to thank other members of his committee, Dr. Paul Kaplan, Dr. Joseph A. Schetz, Dr. Karl E. Sundkvist, and Dr. Adorjan G. Szeless for their suggestions and for reading through the first draft of this dissertation.

Special thanks are due to Mr. David Whitaker for his assistance during the use of Perkin Elmer computer. The author would like to thank Mr. Uday Shanker for his help associated with computer and script details. The author wishes to express his thanks to Mr. B. Balachandran and other Ocean Engineering graduate students for their friendship and help. The author also thanks all the other graduate students who have been my good friends.

The author would like to thank his parents for their love and support. The author is especially grateful to his wife for her constant encouragement and patience.

Table of Contents

List of Illustrations

NOMENCLATURE

a - wave amplitude

A - linear growth term

BE - exponential growth term

c - wave speed

$\bar{c}$ - average phase speed of wave

c_g - group velocity

$E(f, \theta)$ - directional frequency spectrum

$E(f,)$ - point spectrum

E_∞ - fully developed spectrum

E_d - spectral component after dissipation

E_e - total energy to the wind direction

E_0 - spectral component before dissipation

f - frequency

$F(\theta)$ - spreading function

g - gravitational acceleration

$\vec{k}$ - wave number

p - pressure

R - autocorrelation function

Δt - time step

Δx, Δy - grid spacing

$\vec{u}$ - total velocity

$\vec{U}$ - mean velocity

$\vec{U}_p$ - wave induced velocity perturbation

$\vec{u}'$ - atmospheric turbulent fluctuation

$\vec{u}^*$ - friction velocity

$\vec{u}_{6.1}$ - wind velocity at 6.1 m above sea surface

$\vec{u}_{19.5}$ - wind velocity at 19.5 m above sea surface

$\vec{u}_c$ - convection velocity of the eddies

S - sum of source function

S_{in} - energy input from the air

S_{nl} - nonlinear wave-wave interaction

S_{ds} - energy dissipation

z_0 - roughness length

z_m - matched layer height

α - angle between wind and wave

β - constant (= 0.074)

γ - constant (= 0.0081)

δ - displacement of mean streamline

ε - $c \sin\theta \frac{\Delta t}{\Delta x}$

θ - direction of propagation

κ - ratio of ω and u_c

Λ - turbulent scaling factor

λ - $\sqrt{\sigma^2 + \varepsilon^2}$

ν - kinematic viscosity

Π - pressure spectrum

ρ_a - density of air

ρ_w - density of water

σ - $c \cos \theta \frac{\Delta t}{\Delta y}$

τ_0 - total stress

τ_t - turbulent Reynolds stress

τ_w - wave induced Reynolds stress

τ_v - viscous stress

Ψ - stream function

Ω - vorticity

ω - angular frequency

1. Introduction

Since the early work of Miles (1957, 1959, 1960) and Phillips (1957) great advances have been made in the theory of wind wave generation. A number of operational wave forcasting models exist which perform with varying degrees of accuracy depending largely on the complexity of the situation they are asked to model. Since our understanding of the wave generation process is far from complete, wind wave models must rely heavily on empirical formulas. As long as the conditions a model is asked to simulate correspond with those under which the data for its empirical foundation were obtained, the model performs fairly well. When presented with situations of increased complexity, however, the performance of a model is bound to deteriorate. This was nicely illustrated in the Sea Wave Modeling Project (SWAMP Group, 1985).

In order to improve the performance of a wave model, it seems important to retain in the model as much detail and generality of the physics as possible. A large step in this direction was made by Pierson, et al. (1966) with the development of a model which computed directional wave spectra and allowed for the propagation of wave energy. After undergoing several refinements (Inoue, 1967; Lazanoff and Stevenson, 1975) it has

evolved into the Spectral Ocean Wave Model (SOWM) as described by Pierson (1982). The SOWM is an operational wave model in use by the U.S. Navy Fleet Numerical Oceanography Center.

The SOWM is classified as a first generation decoupled propagation model in that the wave growth is dominated by wind energy input as opposed to nonlinear wave interaction effects and the spectrum is discretized into frequency-direction bands. Each band is allowed to evolve more or less independently and propagate at its own group velocity in its own direction. Other models of this type include those of Barnett (1968), Ewing (1971) and Gelci and Chavy (1978).

Second generation discrete models, referred to as coupled discrete models rely heavily on nonlinear interactions in their growth mechanisms. These include the models of Resio (1981) and Golding (1983). The remaining class of models, the coupled hybrid models, are parametric models. These attempt to compute a set of parameters of a point spectrum, typically the JONSWAP spectrum (Hasselmann, et al., 1973), to represent the windsea part of the spectrum and require assumptions as to how the windsea becomes swell and vice versa. Thus they implicitly employ nonlinear energy transfer as the dominant mechanism controlling the spectral shape. Models of this type include those of Hasselmann, et al. (1976) and Gunther, et al. (1979). Several models other than those referred to above and falling in all three classes are described by the SWAMP Group (1985).

The focus of this dissertation is on the directional properties of the wave generation mechanism. By the design of the parametric models, the windsea part of the spectrum at least, must obtain its directionality from a spreading function centered on the wind direction. Some of these models allow the existence of swell whose direction of propa-

gation is independent of the windsea, however, the directionality of any energy generated by the model must still be that of a spreading function. The discrete models are not inherently so confined. Since they are discretized in direction, they may allow the directionality of the energy growth to be determined by the directionality of the growth mechanism. Further, since the growth rate of the spectrum is strongly dependent on sea state, the directionality (and, in general, magnitude) of the energy growth depends on the directionality of the existing spectrum.

Unfortunately, most discrete models employ a point spectral growth mechanism and spread the energy growth over direction bands with a spreading function. This is done presumably due to the lack of a form of the atmospheric energy input as a function of the angle between the wind and wave. Barnett (1968) proposed a simple form depending only on the cosine of this angle and this is the form which is employed in those few models which include a directional atmospheric input. The coupled discrete models, however, use a spreading function to account for nonlinear wave interaction by redistributing energy based on a parameterization of the point spectrum and/or base their parameterization on spectra of assumed directionalities. Until evaluation of the full Boltzmann integral form of the nonlinear wave interaction source term can be performed in an amount of time small enough to allow its incorporation into a wave model, the inclusion of nonlinear wave interactions will involve some dependence on a spreading function. Some progress has been made in this direction by Hasselmann and Hasselmann (1985).

In this study, we thus focus our attention on the decoupled propagation models in general and the SOWM in particular with the aim of developing and demonstrating a fully directional wave growth mechanism. An analytic, directional atmospheric energy input

function is presented and is tuned to the directionally integrated form used in the SOWM. An infinite ocean wave model is developed based on this function as is a similar model which parallels the operation of the SOWM. These models are used to demonstrate the differences in performance of the point spectral and directional wave generation mechanisms under identical wind inputs. Calculations are made for the cases of a steady wind, a wind oscillating in direction, the relaxation of a fully developed spectrum under a sudden 90° change in wind direction with and without a change in wind speed and the spectral growth in the presence of swell for a steady wind. A propagation scheme is then added to each model to examine the case of a finite region corrupted by swell.

2. Structure of the model

The rate of change of the wave spectrum can be described by the energy balance equation proposed by Hasselmann (1960)

$$\frac{\partial E(f, \theta; \vec{x}, t)}{\partial t} + \vec{C}_g \nabla E(f, \theta; \vec{x}, t) = S(f, \theta; \vec{x}, t) = S_{in} + S_{nl} - S_{ds} \qquad (2.1)$$

where $E(f, \theta; \vec{x}, t)$ is the two-dimensional directional frequency wave spectrum being a function of position $\vec{x}$, time t, wave frequency f, and direction of propagation θ. C_g is the group velocity of the spectral component and S represents the sum of individual source functions. S_{in}, S_{nl}, and S_{ds} represent the wind input, nonlinear wave interaction and dissipation source functions respectively. The nonlinear wave-wave interaction is neglected in this theory as it is in the SOWM. It is generally accepted that the nonlinear interaction is important for wave growth (SWAMP Group, 1985).

The energy input from the wind S_{in} is represented as

$$S_{in} = A(u, f, \alpha) + B(u^*, f, \alpha) E(f, \theta; \vec{x}, t) \qquad (2.2)$$

where u is the wind velecity, u^* is the friction velocity and α is the angle between the wind and wave directions. The A term represents energy transfer from the turbulent pressure fluctuations to the wave field according to the theory of Phillips (1957) and results in a linear growth of the spectrum. The BE term represents the interaction of an already disturbed surface with the wind.

Without the dissipation term, equation (2.1) becomes

$$\frac{\partial E(f, \theta; \vec{x}, t)}{\partial t} + \vec{C}_g \nabla E(f, \theta; \vec{x}, t) = A(u, f, \alpha) + B(u^*, f, \alpha) E(f, \theta; \vec{x}, t) \qquad (2.3)$$

Since equation (2.3) is linear, each spectral component can grow independently. Also, according to equation (2,3) the spectral component can grow to an infinite value with time, but in the real situation, dissipation will limit the growth. Wave breaking is thought to be the main mechanism of dissipation. The dissipation function S_{ds} is applied implicitly for wave energy propagating within $\pm 90°$ of the wind direction in a manner analogous to its implementation in the SOWM. The growth of the spectrum is limited by a fully developed spectrum in a manner which will be discussed latter.

If we consider an infinite ocean with a homogeneous wind field, the wave spectrum is not a function of position. The numerical model for this case requires only one spacial grid point and no propagation scheme. Equation (2.3) then becomes

$$\frac{dE(f, \theta; t)}{dt} = A(u, f, \alpha) + B(u^*, f, \alpha) E(f, \theta; t) \qquad (2.4)$$

The directional treatment of the wave growth mechanism is the focus of this study. Before we refer to our model, it is helpful to examine the relation of the energy balance

used in the SOWM to equation (2.4). A directional frequency spectrum can be obtained by multiplying the frequency spectrum by a spreading function:

$$E(f, \theta) = E(f)F(\theta) \tag{2.5}$$

The spreading function used in the SOWM is that which was derived by the SWOP project (Cote, et al., 1960). It was considered to be a function of wind speed and frequency as well as direction and is given by

$$F(\omega, \alpha, u) = \frac{1}{\pi}[1 + (0.5 + 0.82e^{-\frac{1}{2}(\frac{\omega u}{g})^4}) \cos 2\alpha + 0.32e^{-\frac{1}{2}(\frac{\omega u}{g})^4} \cos 4\alpha]$$

$$\text{for } -\frac{\pi}{2} < \alpha < \frac{\pi}{2} \tag{2.6}$$

where $\omega = 2\pi f$ and $F(\omega,\alpha,u) = 0$, elsewhere.

Using equation (2.5), equation (2.4) can be rewritten as

$$\frac{\partial E(f;t)F(\alpha)}{\partial t} = A(u, f, \alpha) + B(u^*, f, \alpha)E(f;t)F(\alpha) \tag{2.7}$$

Integrate equation (2.7) over the parameter α from $-\pi/2$ to $\pi/2$ and consider that

$$\int_{-\pi/2}^{+\pi/2} F(\theta)d\theta = 1.$$

Then equation (2.7) becomes

$$\int_{-\pi/2}^{+\pi/2} \frac{\partial E(f;t)F(\alpha)}{\partial t} d\alpha = \int_{-\pi/2}^{+\pi/2} A(u, f, \alpha)d\alpha + \int_{-\pi/2}^{+\pi/2} B(u^*, f, \alpha)E(f;t)F(\alpha)d\alpha \tag{2.8}$$

If we let

$$A'(u, f) = \int_{-\pi/2}^{+\pi/2} A(u, f, \alpha) d\alpha \tag{2.9}$$

and

$$B'(u, f) = \int_{-\pi/2}^{\pi/2} B(u^*, f, \alpha) F(\alpha) d\alpha \tag{2.10}$$

then we have

$$\frac{\partial E(f;t)}{\partial t} = A'(u,f) + B'(u^*,f)E(f) \tag{2.11}$$

This directionally integrated energy balance equation, modified to limit spectral values to a fully developed limit, is what is used by the SOWM. Notice that it assumes that the spectrum is always centered on the wind direction, although the SOWM does not constrain it to be. The directional spectrum is obtained by spreading the growth resulting from this directionally integrated equation at each time step about the wind direction and adding it to the pre-existing directional spectrum, thus forcing the new spectral growth to have the angular distribution of the spreading function.

The model presented in this dissertation solves the energy balance equation in the directional form, equation (2.4). It does not require the introduction of the artificial angular spreading function and it retains the directionality of the growth. Note that the spectral growth rate is highly dependent on the spectral value through the BE term. The directionality (and magnitude) of the growth will thus depend on the directional properties of the spectrum. This dependence is destroyed if the growth is obtained from equation (2.11).

The directional properties of the functions $\Lambda(u,f,\alpha)$ and $B(u^*,f,\alpha)$ are vital to the success of this model. The forms of these functions which are used in this study are presented in sections 3 and 4. The details of the growth mechanism implementation are given in section 5.

3. The A term

The $A(u,f,\alpha)$ term is based on the theory of Phillips (1957). Phillips' mechanism represents the generation of waves on an initially calm water surface through the turbulent atmospheric pressure fluctuations. It is too weak to explain the major growth of the wave field but it can explain the growth of waves from initially calm water to a certain level where other mechanisms become dominant. Within Phillips' theory, that the waves develop most rapidly by means of a resonance mechanism which occurs when a component of the surface pressure distribution moves at the same speed as the free surface wave with the same wave number. More will be said about this resonance later.

The form of the A function used here is similar to that used by Barnett (1968) and is simply a nonintegrated form of the function used in the SOWM. A summary of the mathematical background is as follows.

Hasselmann (1960) has shown that the A function can be represented in terms of the three-dimensional spectrum of the random atmospheric pressure fluctuations $\Pi(k,\omega)$. That is

$$A = \frac{4\pi^2 k\omega^3}{\rho_w^2 g^3}\Pi(\vec{k}, \omega) \tag{3.1}$$

where $\omega = 2\pi f$, k is the magnitude of the wave number $\vec{k} = (k_1, k_2)$, and ρ_w is the density of sea water. The spectrum of the random atmospheric pressure fluctuations is the Fourier transform of the autocorrelation function of the pressure fluctuations. If we let $R(\vec{\xi}, \tau)$ be this correlation function, given by

$$R(\vec{\xi}, \tau) = \overline{p(\vec{x}, t)p(\vec{x} + \vec{\xi}, t + \tau)} \tag{3.2}$$

where p is the pressure at the water surface and the overbar denotes the mean value, the pressure spectrum $\Pi(\vec{k}, \omega)$ is

$$\Pi(\vec{k}, \omega) = \mathrm{Re}\{\frac{1}{(2\pi)^3}\int_{-\infty}^{+\infty} R(\vec{\xi}, \tau)e^{-i(\vec{k}\cdot\vec{\xi} - \omega\tau)}d\vec{\xi}\, d\tau\} \tag{3.3}$$

Priestly (1965) attempted to measure the frequency spectrum

$$K(\vec{\xi}, \omega) = \frac{1}{2\pi}\int_{-\infty}^{+\infty} R(\vec{\xi}, \tau)e^{i\omega\tau}d\tau \tag{3.4}$$

His measurements showed that it could be represented as

$$K(\vec{\xi}, \omega) = \varphi(\omega)e^{-\mu_1|\xi_1| - \mu_2|\xi_2| - i\kappa\xi_1} \tag{3.5}$$

where μ_1, μ_2 and $\varphi(\omega)$ are determined from the experiment as

$$\mu_1 = .33\kappa^{1.28}$$

$$\mu_2 = .52\kappa^{0.95} \tag{3.6}$$

where $\kappa = \frac{\omega}{u_c}$, u_c being the convection velocity of the eddies.

With this, equation (3.3) becomes

$$\Pi(\vec{k}, \omega) = \mathrm{Re}\{\frac{1}{(2\pi)^2}\int_{-\infty}^{+\infty}\varphi(\omega)e^{-\mu_1|\xi_1| - \mu_2|\xi_2| - i\kappa\xi_1 - \vec{ik}.\vec{\xi}}d\vec{\xi}\} \tag{3.7}$$

After some manipulation, equation (3.7) can be expressed as

$$\Pi(\vec{k}, \omega) = \frac{4\varphi(\omega)}{(2\pi)^2}\left[\frac{\mu_1}{\mu_1^2 + (k_1 - \kappa)^2}\right]\left[\frac{\mu_2}{\mu_2^2 + k_2^2}\right] \tag{3.8}$$

According to Priestly, φ (ω) was found to be of the form

$$\varphi(\omega) = \Lambda\psi(\omega) \tag{3.9}$$

where Λ is a turbulent scaling factor which varies with wind speed, ψ(ω) is given as $\psi(\omega) \cong \frac{1.23}{\omega^2}$. Snyder and Cox (1966) expected Λ to vary as the fourth power of the wind speed from a fit to Priestly's data. Barnett (1968) argued that Λ proportional to the sixth power of the wind speed gave a better fit to the available data. In this study the fourth power of the wind speed is chosen to agree with the form used in the SOWM. If we let $k_1 = k \cos\alpha$ and $k_2 = k \sin\alpha$, and substitute known values into equation (3.8), we have

$$\Pi(\vec{k}, \omega) = \frac{1.23A^*}{\pi^2\omega^2}u^4\left[\frac{0.33k^{1.28}}{0.1089\kappa^{2.56} + (k\cos\alpha - \kappa)^2}\right]$$

$$\cdot\left[\frac{0.52k^{0.95}}{0.2704\kappa^{1.9} + k^2\sin^2\alpha}\right] \tag{3.10}$$

where A* is a constant to be determined. Using equation (3.1) and (3.8), A can now be written as

$$A(u,f,\alpha) = \frac{0.211A^{*}k\omega u^{4}}{\rho_w^2 g^3}\left[\frac{k^{1.28}}{0.1089\kappa^{2.56} + (k\cos\alpha - \kappa)^2}\right]$$

$$\cdot\left[\frac{k^{0.95}}{0.2704\kappa^{1.9} + k^2\sin^2\alpha}\right] \tag{3.11}$$

According to Priestly's measurements, μ_1 tends to be constant for $\kappa < 0.02$. Thus, two expressions of $A'(u,f)$ in equation (2.9) are used in the SOWM depending on the value of κ. The value of the coefficient A^* is determined from the measurements of Snyder and Cox with additional data supplied by Cardone (1969). Since this data was related to the wind velocity at 6.1 m above the sea surface the convection velocity is taken as $u_{6.1}$. The form of the A function is then

$$A(f, u_{6.1},\alpha) = A_1(f, u_{6.1}, \alpha), \quad \text{if } \frac{\omega}{u_{6.1}} \le 0.02 \tag{3.12}$$

$$A(f, u_{6.1},\alpha) = A_2(f, u_{6.1}, \alpha), \quad \text{if } \frac{\omega}{u_{6.1}} > 0.02$$

where

$$A_1(f, u_{6.1}, \alpha) = \frac{4.793\text{x}10^{-16}\omega^4 u_{6.1}^3}{Q_1(\omega, u_{6.1}, \alpha)R_1(\omega, u_{6.1}, \alpha)} \tag{3.13}$$

$$A_2(f, u_{6.1}, \alpha) = \frac{7.167\text{x}10^{-14}\omega^{5.25} u_{6.1}^{1.75}}{Q_2(\omega, u_{6.1}, \alpha)R_2(\omega, u_{6.1}, \alpha)} \tag{3.14}$$

and

$$Q_1 = 0.2704\left(\frac{\omega}{u_{6.1}}\right)^2 + \left(\frac{\omega^2}{g}\sin\theta\right)^2 \tag{3.15}$$

$$R_1 = 4.87\text{x}10^{-6} + \left(\frac{\omega^2}{g}\cos\theta - \frac{\omega}{u_{6.1}}\right)^2 \tag{3.16}$$

$$Q_2 = Q_1 \tag{3.17}$$

$$R_2 = 0.1089\left(\frac{\omega^2}{g}\right)^{2.5} + \left(\frac{\omega^2}{g}\cos\theta - \frac{\omega}{u_{6.1}}\right)^2 \tag{3.18}$$

A_1 and A_2 are in m ^{2}/rad, $u_{6.1}$ is in m/sec, and g is in m/sec ^{2}.

It should be noted that the numerical constants appearing in equation (3.13) and (3.14) are not those given in Pierson. He gives the form of A used in the computer code where for computational convenience it has been multiplied by the minimum frequency bandwidth (1/180 sec) and the number of seconds in his 3 hour time step. His value for A is also off by a factor of two which was applied separately in the SOWM code.

4. The BE term

The $B(u^*,f,\alpha)E(f,\theta;t)$ term is the result of the interaction of the air flow with the already disturbed water surface. Miles (1957) considered the perturbation of the mean shear flow in the air by the disturbed water surface, but he neglected the effects of atmospheric turbulence. He considered the undisturbed air flow to be quasi-laminar, inviscid and incompressible. Phillips (1966) extended the analysis to consider the interaction of the wave induced air flow perturbations with the free stream turbulence. Phillips' theory is summarized as follows.

We will use a system of Cartesian coodinate (x,y,z) where x is the direction of wave propagation and z is taken vertically upwards as shown in figure 1. Consider the motion in a frame of reference moving with the wave speed c. The total velocity of the air flow over the waves is broken down as

$$\vec{u} = \vec{U}(z) + \vec{U}_p(x,z) + \vec{u}'(x,y,z,t) \qquad (4.1)$$

where $\vec{U}$ is the mean velocity, $\vec{U}_p = (U_p, V_p, W_p)$ is the wave induced velocity perturbation and $\vec{u'}$ is the random atmospheric turbulent fluctuation. Assuming incompressibility, we can define a stream function Ψ as

$$\frac{\partial \Psi}{\partial z} = U \cos\alpha - c + U_p$$

$$\frac{\partial \Psi}{\partial x} = - W_p \tag{4.2}$$

Since U_p and W_p are periodic along x-direction, the streamline of the mean motion is

$$\Psi = \int_{z_m}^{z} \{U(\xi) \cos\alpha - c\} d\xi + \varphi(z) e^{ikx} = \text{const.} \tag{4.3}$$

The matched layer height z_m is the height where the mean wind velocity matches the phase velocity of the wave. Outside of this layer, the mean streamlines simply undulate about their mean levels. Away from the matched layer, the streamlines Ψ = const. undulate about z_l , i.e.

$$\delta = \frac{\tilde{W}_p(z_l) \cos[kx + \varepsilon(z)]}{k[U(z_l) \cos\alpha - c]} \tag{4.4}$$

where c is the wave speed and $\tilde{W}_p(z_l)$ is the amplitude of $W_p(z_l)$.

At matched layer, the streamlines are given as

$$\Psi = \frac{1}{2}(z - z_m)^2 U'(z_m) \cos\alpha - \frac{\tilde{W}_p(z) \cos[kx + \varepsilon(z)]}{k} \tag{4.5}$$

The thickness δ_m of the matched layer is the maximum dispalcement of the mean streamline of the colsed loops. Using equation (4.5) , we can get

$$\delta_m = \{\frac{4\bar{W}_p(z_m)}{kU'(z_m)\cos\alpha}\}^{\frac{1}{2}} \tag{4.6}$$

The momentum equation is averaged over the y-direction to yield

$$U_j\frac{\partial U_{pi}}{\partial x_j} + U_{pj}\frac{\partial U_i}{\partial x_j} + U_{pj}\frac{\partial U_{pi}}{\partial x_j} + \frac{\partial}{\partial x_j}\overline{u'_i u'_j}$$

$$= -\frac{1}{\rho}\frac{\partial \bar{p}}{\partial x_i} + \nu\frac{\partial^2}{\partial x_j^2}(U_i + U_{pi}) \tag{4.7}$$

The mean stress balance can be obtained by taking the average over x of equation (4.7) as

$$\frac{\partial}{\partial x_j}\overline{U_{pi}U_{pj}} + \frac{\partial}{\partial x_j}\overline{u'_i u'_j} = -\frac{1}{\rho}\frac{\partial \bar{p}}{\partial x_i} + \nu\frac{\partial^2 U_i}{\partial x_j^2} \tag{4.8}$$

The component of equation (4.8) in the x-direction is

$$\frac{\partial}{\partial z}\{\overline{U_p W_p} + \overline{u'w'} - \nu\frac{\partial}{\partial z}(U\cos\alpha)\} = 0. \tag{4.9}$$

This means that the total stress can be represented as

$$\tau_0 = \tau_w + \tau_t + \tau_v = \text{const.} \tag{4.10}$$

where τ_w , τ_t , τ_v represent the wave induced Reynolds stress, the turbulent Reynolds stress and the viscous stress respectively.

For an inviscid flow

$$\tau_0 = \tau_w \tag{4.11}$$

According to Phillips (1966), equation (4.11)is a sufficient approximation even when the flow is turbulent since $\tau_w > > \tau_t, \tau_w$.

τ_w has relation with the product of the vorticy Ω and W_p as

$$\Omega W_p = (\frac{\partial U_p}{\partial z} - \frac{\partial W_p}{\partial x})W_p$$

$$= \frac{\partial}{\partial z}U_p W_p + \frac{\partial}{\partial x}(\frac{1}{2}U_p^2 - \frac{1}{2}W_p^2) \tag{4.12}$$

Integrate from z to infinity and take the x average, then

$$\tau_w(z) = -\rho\overline{U_p W_p(z)} = \rho\int_z^\infty \overline{\Omega W_p}dz \tag{4.13}$$

Let z = 0

$$\tau_w(0) = \rho\int_0^\infty \overline{\Omega W_p}dz \tag{4.14}$$

This is related to B by

$$\frac{B}{f} = \frac{2\tau_w(0)}{\rho_w c^2 k^2 a^2} \tag{4.15}$$

where ρ_w is the water density and a is the wave amplitude. The variations in mean vorticity are represented as

$$|\Omega| \propto |\, U''(z)\delta\cos\alpha\,| \tag{4.16}$$

where $U''(z)\cos\alpha$ is the mean vorticity gradient and δ is the displacement of a mean streamline about its average height.

Using equation (4.4), (4.6) and (4.16), we can form expressions for $\overline{\Omega W_p}$. Outside the matched layer, we have

$$\overline{\Omega W_p} = -M\frac{U''(z)\overline{W_p^2(z)}\cos\alpha}{k|U(z)\cos\alpha - c|} \tag{4.17}$$

while in the matched layer,

$$(\overline{\Omega W_p})_m = -M_m U''(z_m)W_p(z_m)\delta_m\cos\alpha \tag{4.18}$$

where M and M_m are correlation coefficients.

In inviscid flow we find $\overline{\Omega W_p} = 0$ outside the matched layer since Ω and Wp are in exact quadrature. In turbulent flow, however, we can expect a non-zero correlation and hence a non-zero M.

Combining equation (4.14) and (4.18), the contribution of the wave-induced Reynolds stress across the matched layer is

$$\tau_w|_m = M_m\rho(\overline{\Omega W_p})_m\delta_m$$

$$= -M_m\rho\, U''(z_m)W_p(z_m)\delta_m^2\cos\alpha$$

$$= M_m\rho\{\frac{-U''\overline{W_p^2}}{kU'}\} \tag{4.19}$$

Equation (4.19) was originally derived by Miles (1957). Thus the total wave induced Reynolds stress at $z = 0$ is given by combining equation (4.14), (4.17) and (4.19)

$$\tau_w(0) = M_m\rho\{\frac{(-U'')\overline{W}_p^2}{kU'}\} + M\rho\int_0^\infty \frac{(-U'')\overline{W}_p^2 \cos\alpha}{k|U\cos\alpha - c|}dz \qquad (4.20)$$

where the matched layer should be excluded from the range of the integral. Expressions for W_p are given by Phillips as follows.

Outside the matched layer

$$W_p = -iNka\{U(z)\cos\alpha - c\}e^{-kz}e^{ikx} \qquad (4.21)$$

Where N is a constant to be determined. Inside the matched layer

$$W_p = \frac{-iNak^3e^{ikx}}{U'(z_m)\cos\alpha}\int_{z_m}^\infty \{U(z)\cos\alpha - c\}^2 e^{-kz}dz \qquad (4.22)$$

From equation (4.15), (4.20), (4.21) and (4.22)

$$\frac{B}{f} = \frac{\rho_a}{\rho_w}\frac{1}{c^2k}\{\frac{M_mN^2k^4}{\cos^2\alpha}(\frac{-U''}{(U')^3})_{z_m}(\int_{z_m}^\infty [U(z)\cos\alpha - c]^2e^{-kz}dz)^2$$

$$+ M\int_0^\infty N^2(-U'')\cos\alpha|U\cos\alpha - c|e^{-2kz}dz\} \qquad (4.23)$$

The mean wind profile can be taken as

$$U(z) = \frac{u^*}{\kappa}\ln(\frac{z}{z_0}) \qquad (4.24)$$

where κ is Von Karman's constant and z_0 is the roughness length. From the definition of matched layer height, we can get an expression for roughness length and matched layer height using the equation (4.24) as

$$z_o = z_m \exp\{\frac{-\kappa c}{u^* \cos\alpha}\} \tag{4.25}$$

It was first suggested by Charnock (1955), based on dimensional grounds, that the expression for z_0 be represented as

$$z_0 \propto \frac{u^{*2}}{g} \tag{4.26}$$

if the flow is aerodynamically rough. Values for the constant of proportionality of 0.078 and 0.035 were used in Inoue's calculation (1967). Wu (1968) suggested a value of 0.0112 as being more appropriate. In this study Wu's expression is adopted and

$$z_0 = 0.0112\frac{u^{*2}}{g} \tag{4.27}$$

is used in evaluating equation (4.23). With this assumption and equation (4.24), equation (4.23) is reduced to a function of u^*/c and α only. We must now determine the remaining constants in this equation. Phillips suggested $M_m = \pi$, $M = 1.6\text{x}10^{-2}$, $N^2 = 1/3$ for $z > z_m$ and $N^2 = 1$ for $z < z_m$. Inoue used these values to evaluate equation (4.23) and found that for low u^*/c his result was several orders of magnitude larger than observational data. His computational result decreases as u^*/c increases while the observational data show the opposite trend until the two come into approximate agreement. For larger u^*/c the two run roughly parallel with the data being somewhat higher. He did not mention why he had such a discrepancy. He abandoned this approach and used a curve fit to the observational data for his B function. Since the data was from

point spectral measurements, his B was necessarily the directionally integrated form as given by equation (2.21). The function he found and that which is used in the SOWM is

$$B(u^*, f) = f\{0.00139e^{-7000[(\frac{u^*}{c})-0.031]^2}$$

$$+ 0.725(\frac{u^*}{c})^2 e^{-0.0004(\frac{c}{u^*})^2}\} \qquad (4.28)$$

To study the behavior of equation (4.23) more closely, we have to look at its second term. The major contribution to this integral for low u* is in the region from the water surface to z_m . It behaves as

$$I = \int_0^{z_m} \frac{1}{z^2} |\ln\frac{z}{z_m}| e^{-2kz} dz \qquad (4.29)$$

Using a series expansion, this can be written as

$$I = \int_0^{z_m} \{\frac{1}{z^2} - \frac{2k}{z} + 2k^2 - \frac{8k^3}{3!}z + ...\} |\ln\frac{z}{z_m}| dz \qquad (4.30)$$

If we carry out the integration for the first three terms, we have

$$I = -\frac{1}{z}(|\ln\frac{z}{z_m}| + 1) - k(\ln\frac{z}{z_m})^2 + 2k^2(z|\ln\frac{z}{z_m}| - z) + ...\Big]_0^{z_m} \qquad (4.31)$$

Thus as z approaches zero equation (4.30) has strong singularities. This is due to the form of the mean velocity profile assumed. Although Inoue retained zero as the lower limit, it is obvious that the integration range should not extend below the roughness height z_0. Even with z_0 as the lower limit, however, the value of I is very large for small u^*/c since in this range z_m is large and $\frac{z_0}{z_m}$ is still very small.

To study this integral in detail the variable of integration is nondimensionalized through the transformation $kz = t$. Equation (4.29) with z_o substituted for the lower limit becomes

$$I = k\int_{kz_o}^{kz_m} \frac{1}{t^2} \left| \ln \frac{t}{kz_m} \right| e^{-2t} dt \tag{4.32}$$

Using equations (4.25) and (4.27), we have

$$kz_m = 0.0112 \frac{u^{*2}}{g} k \exp\left\{\frac{\kappa c}{u^* \cos\alpha}\right\}$$

$$kz_o = 0.0112 \frac{u^{*2}}{g} k \tag{4.33}$$

For deep water

$$\frac{k}{g} = \frac{1}{c^2} \tag{4.34}$$

Thus

$$kz_m = 0.0112 \left(\frac{u^*}{c}\right)^2 \exp\left\{\frac{\kappa c}{u^* \cos\alpha}\right\}$$

$$kz_o = 0.0112 \left(\frac{u^*}{c}\right)^2 \tag{4.35}$$

Equation (4.32) can be represented as

$$I = k\int_{0.0112(u^*/c)^2}^{0.0112(u^*/c)^2 \exp\left\{\frac{\kappa c}{u^* \cos\alpha}\right\}} \frac{1}{t^2} \left| \ln \frac{t}{0.0112\left(\frac{u^*}{c}\right)^2 \exp\left\{\frac{\kappa c}{u^* \cos\alpha}\right\}} \right| e^{-2t} dt \tag{4.36}$$

The integrand is plotted in Figure 1 for several values of u*/c. Notice that this is a semi-log plot. The limits of the integration are shown in Table 1. The upper limit, kz_m , is very large for small u*/c but drops rapidly as u*/c increases. The lower limit, however, remains well within the strong peak of the integrand. Phillips suggested the lower limit h_0 defined as the height where $U = 10\ u^*$. Values of kh_0 are also given in Table 1. This lower limit is still too small, for small u*/c, to yield reasonable values for I. For large u*/c h_0 is greater than z_m and there is no contribution to the second term in equation (4.23) from the region below the matched layer.

The strong singularity of the integrand at the origin is a result of the logarithmic velocity profile assumed for the mean flow. From these calculations, it appears that the mean velocity must have much less curvature near the surface than is given by the logarithmic profile. Takeda (1963) has measured departures from a logarithmic form very close to the water surface and his measurement confirms the inadequacy of the logarithmic profile close to the water surface.

In this study, rather than attempting to derive a more appropriate mean velocity profile, Gauss-Laguerre quadrature is used in an effort to avoid the singularity at the origin. Thus we are integrating a polynomial fit to the integrand which does not follow the strong peak near the origin. In effect, we are assuming the mean velocity profile which would give us the integrand matching this polynomial fit. The result of evaluating equation (4.23) in this manner, using the values of the constants suggested by Phillips, and integrating over direction according to equation (2.10) is shown as the lowest curve in Figure 3. The solid line in this figure is Inoue's curve fit to the observational data, equation (4.28). Now the computational result increases as u*/c increases following the observational data in the low u*/c region but the magnitude is too small. The constants

M and M_m in equation (4.23) were adjusted to give agreement with the data, requiring the values 1.2 and 12, respectively. The result using these constants is the remaining curve in Figure 3. It shows good agreement with Inoue's curve.

Figure 4 shows the directional behavior of B. It is found that as u^* increases, a local maximum forms and moves away from the wind direction. A possible physical explanation for this behavior was suggested by Manton (1972). Although he considered the case of the wind and wave in the same direction, he pointed out that the interaction between the mean flow and the wave induced perturbations would be strongest when the mean strain rate at z_m matches the wave induced motion, i.e. when

$$\left(\frac{dU}{dz}\right)_{z=z_m} = \omega \tag{4.37}$$

Letting $U = U \cos \alpha$ and assuming a logarithmic profile for U, equation (4.37) becomes an equation for the angle at which we expect this local maximum of B. The angles thus predicted and angles found from the B function differ by almost constant values. Much better agreement is obtained if the derivative in equation (4.37) is evaluated at the height where $U = c/2$, i.e. half way between the surface and the matched layer on a mean velocity scale. By adjusting this elevation slightly to the point where $U = c/1.85$, we find that this condition can very accurately predict the location of the local maximum.

5. Application of the fully developed spectrum and details of the model

As does the SWOM, our model prevents the wave spectrum from growing above an assumed fully developed limit by balancing the input from the wind with the dissipation without explicitly modeling the dissipation for waves traveling with the wind. We need to introduce the concept of a fully developed spectrum here. Consider an infinite ocean which is initially calm. A steady wind starts to blow with a constant direction over the sea. After a sufficient length of time, the wave field will reach a steady state where the energy input from the wind balances the energy loss in wave breaking. The wave spectrum at this state is called a fully developed spectrum.

The fully developed spectrum is an idealized concept and its existence is still under question (Komen, Hasselmann and Hasselmann, 1984). Due to the structure of the model, however, a limiting directional wave spectrum must be assumed as a function of wind speed. The form used here (and in the SOWM) is the Pierson-Moskowitz (1964)

spectrum with the directionality of the SWOP spreading function equation (2.6). The fully developed spectrum is thus

$$E_{\infty}(\omega, \alpha, u) = E_{\infty}(\omega, u)F(\omega, \alpha, u)$$

where

$$E_{\infty}(\omega, u) = \gamma g^2 \omega^{-5} e^{-[\beta(\frac{\omega_o}{\omega})^4]} \tag{5.1}$$

and $\omega = 2\pi f$, $\omega_0 = g/u$, u being the mean wind speed measured at 19.5 m above the sea surface, $\gamma = 8.1 \times 10^{-3}$ and $\beta = 0.074$.

According to Inoue (1967), energy dissipation may be assumed to be a function of the ratio of the spectrum to the fully developed spectrum. Then equation (2.2) can be written as

$$\frac{\partial E(f, \theta, t)}{\partial t} = A(u,f, \alpha) + B(u^*, f, \alpha)E(f, \theta; t)$$

$$- [A(u,f, \alpha) + B(u^*,f, \alpha)E(f, \theta;t)][\frac{E(f, \theta;t)}{E_{\infty}(f, \alpha,u)}]^2 \tag{5.2}$$

A closed form solution may be obtained if we multiply A by $[1 - (\frac{E}{E_{\infty}})^2]^{\frac{1}{2}}$. In the initial stage that change does not affect the growth very much due to the small magnitude of $\frac{E}{E_{\infty}}$. In the later stage of the growth BE term is much greater than the A term. Thus the change in the growth is again small. Thus equation (5.2) can be modified as

$$\frac{dE}{dt} = \{A[1 - (\frac{E}{E_{\infty}})^2]^{\frac{1}{2}} + BE\}[1 - (\frac{E}{E_{\infty}})^2] \tag{5.3}$$

The solution of equation (5.3) can then be expressed analytically as

$$E = \frac{A[e^{Bt} - 1]}{B}\{1 + [\frac{A(e^{Bt} - 1)}{BE_\infty}]^2\}^{-\frac{1}{2}} \tag{5.4}$$

or, if we let

$$G(t) = \frac{A[e^{Bt} - 1]}{BE_\infty}$$

then equation (5.4) becomes

$$E = \frac{G(t)}{\sqrt{1 + G^2(t)}}E_\infty \tag{5.5}$$

which clearly shows that E is bounded by E_∞

Equation (5.4) (or (5.5)) is applied in a directional form in a manner analogous to its directionally integrated application in the SOWM. At each time step, each frequency-direction band that lies within $\pm 90°$ to the wind direction is allowed to grow if its initial value is less than $0.95E_\infty(f, \theta)$. If $0.95E_\infty \leq E < E_\infty$, E is set equal to its fully developed value. If the initial value exceeds E_∞, no growth is allowed. Thus under a steady wind, each component will grow until it reaches its fully developed limit. Once all bands have reached saturation, the spectrum reaches a steady state.

If the wind now turns, since the fully developed spectrum is tied to the wind direction, some bands (within $\pm 90°$ to the wind direction) will exceed their fully developed limit while others will not and some may be empty. If these underdeveloped bands are allowed to grow, the total energy present will exceed that in our fully developed sea. This situation also arises in the SOWM but is given special treatment here. We allow normal

growth in those direction bands less than fully developed and attenuate the energy in over developed bands to maintain the same total energy in each frequency band.

Waves traveling at angles greater than $\pm 90°$ to the wind direction are explicitly dissipated in the same manner as is done in the SOWM. The rate of dissipation depends on the total energy traveling within $\pm 90°$ to the wind direction and the relative angle between wind and wave. The expression used in this dissertation is

$$E_d(f, \theta, t) = E_0(f, \theta, t)[e^{-s\Delta t(E_e(t))^{\frac{1}{2}}f^4}]^{r(\theta)} \tag{5.6}$$

where E_d is spectral component after dissipation. E_0 is spectral component before dissipation. E_e is total energy of the wind sea traveling within $\pm 90°$ to the wind direction. And where $r(\theta) = 0$ for $\theta \le 90°, \theta \ge 270°$. $r(\theta) = 3$ for $90° < \theta \le 135°, 225° \le \theta < 270°$. $r(\theta) = 4.5$ for $135° < \theta \le 165°, 195° \le \theta < 225°$. $r(\theta) = 6$ for $165° < \theta < 195°$. $s = 754.6\ (\frac{sec^4}{m})$ and Δt is the time step in hours.

For a finite ocean, second term in the right hand side of equation (2.3) is nonzero and must be modeled by a propagation scheme. A modified Lax-Wendroff scheme due to Gadd (1978, 1980) is used to propagate the wave energy in two dimensions. This scheme was originally applied by Gadd to numerical weather prediction and was first applied to ocean waves by Golding (1983). For one-dimensional propagation at speed c, the finite difference expression is represented as

$$E_{j+1/2}^{n+1/2} = \frac{1}{2}(E_j^n + E_{j+1}^n) - \frac{1}{2}\mu(E_{j+1}^n - E_j^n)$$

$$E_j^{n+1} = E_j^n - \mu\{(1 + q)(E_{j+1}^{n+1/2} - E_{j-1}^{n+1/2}) - \frac{q}{3}(E_{j+3/2}^{n+1/2} - E_{j-3/2}^{n+1/2})\} \tag{5.7}$$

where

$$\sigma = c\frac{\Delta t}{\Delta x}, \quad q = \frac{3}{4}(1 - \sigma^2) \tag{5.8}$$

j signifies spacial position and n the time level. For points one grid length from a boundary, q is set to zero. Along the boundary, upstream differences are used for outflow components while inflow values are specified. For two-dimensional propagation, the scheme takes the form

$$E^{n+/2}_{i+1/2,j+1/2} = \frac{1}{4}(E^n_{i+1,j+1} + E^n_{i+1,j} + E^n_{i,j+1} + E^n_{i,j})$$

$$- \frac{1}{4}\{\sigma[E^n_{i+1,j+1} + E^n_{i+1,j} - E^n_{i,j+1} - E^n_{i,j}]$$

$$+ \varepsilon[E^n_{i+1,j+1} + E^n_{i,j+1} - E^n_{i+1,j} - E^n_{i,j}]\} \tag{5.9}$$

$$E^{n+1}_{i,j} = E^n_{i,j} - \frac{(1+q)}{2}\{\sigma[E^{n+1/2}_{i+1/2,j+1/2} + E^{n+1/2}_{i+1/2,j-1/2} - E^{n+1/2}_{i-1/2,j+1/2} - E^{n+1/2}_{i-1/2,j-1/2}]$$

$$\varepsilon[E^{n+1/2}_{i+1/2,j+1/2} + E^{n+1/2}_{i-1/2,j+1/2} - E^{n+1/2}_{i+1/2,j-1/2} - E^{n+1/2}_{i-1/2,j-1/2}]\}$$

$$+ \frac{q}{9}\{\sigma[E^{n+1/2}_{i+3/2,j+1/2} + E^{n+1/2}_{i+3/2,j-1/2} - E^{n+1/2}_{i-3/2,j+1/2} - E^{n+1/2}_{i-3/2,j-1/2}]$$

$$\varepsilon[E^{n+1/2}_{i+1/2,j+3/2} + E^{n+1/2}_{i-1/2,j+3/2} - E^{n+1/2}_{i+1/2,j-3/2} - E^{n+1/2}_{i-1/2,j-3/2}]\}$$

$$+ \frac{q}{18}\{\sigma[E^{n+1/2}_{i+3/2,j+3/2} + E^{n+1/2}_{i+3/2,j-3/2} - E^{n+1/2}_{i-3/2,j+3/2} - E^{n+1/2}_{i-3/2,j-3/2}] \tag{5.10}$$

$$\varepsilon[E^{n+1/2}_{i+3/2,j+3/2} + E^{n+1/2}_{i-3/2,j+3/2} - E^{n+1/2}_{i+3/2,j-3/2} - E^{n+1/2}_{i-3/2,j-3/2}]\}$$

$$\sigma = c\cos\theta\frac{\Delta t}{\Delta x},\quad \varepsilon = c\sin\theta\frac{\Delta t}{\Delta y},\quad q = \frac{3}{4}(1-\lambda^2)$$

$$\lambda^2 = \sigma^2 + \varepsilon^2 \tag{5.11}$$

where θ is the direction of propagation and $\lambda^2 \leq 1$ is the stability criterion for the two-dimensional scheme.

The input at each time step is the wind speed at 19.5 m above the sea surface in knots, the wind direction in degrees and the time increment in hours. An initial spectrum is specified which may or may not be zero. An important part of the model is the calculation of the friction velocity, u^*, used directly in $B(u^*,f,\alpha)$ and in determining the velocity at 6.1 m for use in $A(u_{6.1},f,\alpha)$. If the sea is initially calm, u^* is calculated for the first time step from the logarithmic mean velocity profile by assuming a roughness height as given by equation (4.16). Once the spectrum has nonzero values, we take

$$u^* = \frac{\kappa(u-\bar{c})}{\ln\left(\frac{z}{0.075H_{\frac{1}{3}}}\right)} \tag{5.12}$$

where $H_{\frac{1}{3}}$ is the significant wave height, and c is the average phase speed defined as

$$\bar{c} = \frac{g}{2\pi}\frac{\sqrt{\overline{\Sigma E(f_i)}}}{\sqrt{\overline{\Sigma f_i^2 E(f_i)}}} \tag{5.13}$$

Equation (5.12) is also used in the SOWM (Inoue).

As mentioned in the introduction, two model codes were written. One using the formulation of the SOWM code and one, the directional formulation described above. In the following, the former is referred to as VSOWM while the latter is called VPINK.

Both models use 53 frequency bands, each of width 0.005 Hz, from 0.04 Hz to 0.3 Hz and 36 directional bands each 10° wide. In a test of CPU time necessary to complete 14 time steps with the infinite ocean models, VPINK required 2.3 times the time needed to run VSOWM. This is for essentially only a growth routine. For a finite ocean with propagation, both models use 27 frequency bands and 18 directional bands to save computational time.

6. Computational results and discussion

All computations, except for one case, were performed for a 40 knot wind speed (at 19.5 m). A three hour time step was used except where noted. The results are presented in both point spectral form and in polar contour plots of the directional spectra. The point spectra usually include a dashed curve. This is the Pierson-Moskowitz spectrum which is our fully developed spectrum. The contour plots include an arrow which indicates the wind direction. Contours are drawn at increments of 10% of the maximum spectral value present in each plot.

The first case presented is that of wave growth on an initially calm sea under the influence of a steady wind. The results from VPINK are given in Figures 5 and 6 while Figures 7 and 8 are from VSOWM. The point spectra, Figures 5 and 7, show similar results except that the VPINK growth appears somewhat retarded relative to the VSOWM growth. The reason for this is suggested by the contour plots and is illustrated in Figures 9 and 10. The VPINK B function gives a larger growth rate at small angles and smaller growth rate at large angles than that given to the SOWM by the SWOP spreading function. Since this is also the directionality chosen for the fully developed

spectrum of VPINK, the spectral components near the wind direction reach saturation while those away from the wind are still growing at a slow rate. Notice that for VSOWM, each direction band must reach saturation at the same time while this is not the case for VPINK. Figure 11 shows that the difference in significant wave height predicted by the models is small.

Early wave growth is considered by again taking a 40 knot wind blowing over an initially calm sea but with a time step of 0.2 hours. Figures 12 and 13 are for VPINK while Figures 14 and 15 are for VSOWM. These figures clearly show a bimodal spectrum due to the A term growth maximum near f = 0.09 Hz (a function of wind speed) and the B term spectral peak which moves toward lower frequencies as the spectrum evolves. Figures 13 also show the A term resonance as predicted by Phillips and mentioned earlier. The resonance mechanism predicts maximum wave growth when

$$u \cos \alpha = c \tag{6.1}$$

or for deep water,

$$f \cos \alpha = \frac{g}{2\pi u} \tag{6.2}$$

since $c = g/2\pi f$. Since the A function is based on $u_{6.1}$, the velocity at 6.1 m must be used here. Equation (6.2) describes a vertical line appearing on a polar plot as in Figures 13. This cannot be produced by the SOWM as is evidenced by Figures 15.

For the next case, the wind direction is allowed to vary by 10° at each time step, sweeping back and forth between +20°. This illustrates two points. First, the growth rates of VPINK (Figures 16 and 17) and VSOWM (Figures 18 and 19) agree much more closely than in the first case. This indicates that the typical fluctuation of wind direction

may have a significant impact on the wave field directionality. The second point is illustrated by the rather large number of contour plots included for this case. Once the wave energy present within 90° to the wind direction at a given frequency reaches its saturation level, the directional relaxation mechanism discussed in section 5 becomes active in VPINK. In the VSOWM, however, the evolution of the spectrum ceases. In Figures 17, we see that the VPINK spectrum continues to follow the wind vector (with some time lag) while the VSOWM spectrum in Figures 19 "freezes" from outside in as each frequency reaches saturation. After the 27 hour time step, only those frequencies below the modal frequency respond to the changing wind direction, quite the opposite of what we would expect to occur naturally.

The fourth comparison is a case where we have an initially fully developed sea as shown in Figure 20. The wind direction is suddenly turned 90° and subsequently held steady. The response of VPINK is shown in Figures 21 and 22 and that of VSOWM is given in Figures 23 and 24. At each time step both models first calculate the growth then dissipate the wave energy traveling against the wind. In the first time step, due to its point spectral growth mechanism, VSOWM calculates a larger amount of growth than does VPINK. Then, since the rate of dissipation depends on the wave energy traveling with the wind, VSOWM dissipates more energy than VPINK. A second point to be made in comparing Figures 22a and 24a is that the initial growth for VSOWM appears in the wind direction while for VPINK, the energy present to the left of the wind direction causes the initial growth rate to be larger in that direction. As time increases, we again find that VSOWM "freezes up" with considerable energy traveling in the original direction while VPINK continues to evolve into a fully developed spectrum in the new direction.

The fifth case involves a change in wind direction as well as wind speed. The initial condition is that of the previous case and is given in Figure 20. At t = 0, the wind turns 90° and drops to 30 knots. VPINK results are given in Figures 25 and 26. VSOWM results are in Figures 27 and 28. This case shows dramatic differences but exposes what may be a problem for VPINK. Since the wind speed drops from 40 knots to 30 knots, the magnitude of the spectral values drop dramatically. The directional relaxation mechanism discussed in section 5 drops the energy $\pm 90°$ to the wind direction to the fully developed value for a 30 knot wind. This then effects the rate of dissipation of the energy traveling against the wind. The VPINK behavior is more realistic than that of VSOWM for this case however. VSOWM "freezes up" after the first time step and only allows the dissipation of the energy traveling against the wind.

The final infinite ocean comparison is for the important case of wave generation in the presence of swell. The initial condition is shown in Figure 29 and was chosen based on the fully developed spectrum for a 40 knot wind. The frequency range of the swell is from 0.04 to 0.06 Hz. The components of the fully developed spectrum in the bands of the wind direction and this frequency range were placed in the 20°-30° direction band. One half of the components in the fully developed spectrum bands on either side of the wind direction band were placed in both the 10°-20° and 30°-40° bands. A steady 40 knot wind at 0° was then turned on. Figures 30 and 31 show the results from VPINK while the VSOWM results are given in Figures 32 and 33. The point spectrum plots also include the initial spectrum as a dashed line. The presence of the swell gives only a small difference in the development of the rest of the spectrum for VPINK, however, it makes a great deal of difference to VSOWM. The growth of the low frequency bands is greatly accelerated with the 0.06 Hz band reaching saturation in the second time step. Further, this growth is spread over $\pm 90°$ to the wind direction, creating new low frequency

components long before they should exist. Thus VSOWM creates excess low frequency energy spread widely over direction due to the presence of a narrow band swell. The effect of this on significant wave height is shown in Figure 34. The maximum difference in significant wave height is greater than 1 m, however, the frequency content of the predicted sea may be more important.

To further investigate the effect of the swell, a finite ocean with propagation is considered. A test case whose geometry is shown in Fig 35 was considered. A 40 knot wind is blowing diagonally (45 °) over an initially calm ocean of dimensions 750 km x 750 km. A grid spacing of $\Delta x = \Delta y = 50$ km and a time step $\Delta t = 0.5$ hours were used. The Courant number, $\frac{c\Delta t}{\Delta x}$ was 0.70 for the lowest frequency (largest c) waves. The wave field is zero on the upwind boundaries except at the incoming swell locations which are shown in figure 35. The swell is coming normal to the boundary. The frequency range is again from 0.040 to 0.06 Hz and the magnitudes were chosen as follows The components of the fully developed spectrum in the bands of the wind direction were placed at location (8,0). One half of the fully developed spectral components in these bands were placed at locations (7,0) and (9,0). Typical points are selected to investigate the spectral behavior. Figures 36 to 41 show the results from VPINK while the VSOWM results are shown in figures 42 to 47. The rapid low frequency growth of VSOWM which was seen above is now allowed to propagate over the full windward 180°. When we consider the location (11,5), this energy spread has major spectral components even though that location is off the original swell direction. This is clearly shown in figures 45(a) and 45(b). Those propagated spectral components due to excess spreading will experience growth which will amplify the artificial low frequency swell. Thus a chain reaction can be set up corrupting a large region with excess low frequency wave energy. Figure 39(b) from VPINK clearly shows the skewed directional spectrum due to the effect of different

fetches for waves traveling to the right or left of the wind. Figure 41(b) from VSOWM does not show that effect to such an extent because VSOWM restricts any new growth to be centered on the wind direction.

7. Conclusions

A directional growth mechanism has been developed and significant differences between its performance and that of a point spectral growth mechanism have been demonstrated. Two areas of concern have been pointed out regarding the performance of the SOWM. Those are the freezing of the windward spectral components when the fully developed limit is exceeded and the creation of excess low frequency energy when growth occurs in the presence of swell. Lazanoff and Stevenson (1975) describe several high energy case studies made for verification of the SOWM. Among the inaccuracies noted were the propagation of wave energy in improper directions and frequency shifts of spectral peaks. The problems discussed above may very well be responsible for these discrepancies. It also seems likely that the twenty year hindcast wave climatology produced with the SOWM (Bales, Cummins and Comstock, 1982) overestimate both the low frequency wave energy present and its directional spread.

The form of the mean wind velocity profile near the surface was found to be of great importance to the B function. Further work is needed to specify its proper form. Other problems which need further attention in VPINK are the immediate reduction of wave

energy when the wind speed drops and the mismatch of the directionality of the growth and the fully developed spectrum. Both of these problems could be addressed within the framework of the present model, however, both are also the result of the substitution of the fully developed spectrum for an explicit dissipation function. A form of this function has been explored in detail by Komen, et al. (1984) and the feasibility of its use in this model should be investigated.

8. References

Bales, S.L., W.E. Cummins and E.N. Comstock (1982): Potential impact of twenty year hindcast wind and wave climatology on ship design. Marine Technology, Vol. 19, No. 2.

Barnett, T.P. (1968): On the generation, dissipation, and prediction of ocean wind waves. J. Geophys. Res. 73, 513-529.

Bryant, P.J. (1966): Ph.D. Dissertation, University of Cambridge.

Cardone, V.J. (1969): Specification of the wind distribution in the marine boundary layer for wave forecasting. New York University, Department of Meteorology and Oceanography, TR 69-1, 11 pp.

Charnock, H. (1955): Wind stress on water surface. Quart. J. Roy. Met. Soc. 81, 639.

Cote, L.J., J.O. Davis, W. Marks, R.J. McGough, E. Mehr, W.J. Pierson, Jr., F.J. Ropek, G. Stephenson, and R.C. Vetter (1960): The directional spectrum of a wind generated sea as determined from data obtained by the Stereo Wave Observation Project. Meteor. Pap. , Vol. 2, No. 6, 88 pp., New York University Press, NY.

Ewing, J.A. (1971): A numerical wave prediction method for the North Atlantic Ocean. Dtsch. Hydrogr. Z. 24, 241-261.

Gadd, A.J. (1978): A numerical advection scheme with small phase errors. Quart. J. R. Met. Soc. , Vol 104, 583-594.

Gadd, A.J. (1978): A split explicit integration scheme for numerical weather prediction, ibid., Vol 104, 569-582.

Gadd, A.J. (1980): Two refinements of the split explicit integration scheme, ibid., Vol 106, 215-220.

Gelci, R. and P. Chavy (1978): Seven years of numerical wave prediction with the DSAS model in the turbulent fluxes through the sea surface. Wave Dynamics and Prediction (A. Favre and K. Hasselmann, eds.) Plenum press,New York, 565-591.

Golding, B. (1983): A wave prediction system for real-time sea state forecasting. Quart. J. R. Met. Soc. ,109, 393-416.

Gunther, H., W. Rosenthal and K. Richter (1979): Application of the parametrical surface wave prediction model to rapidly varying wind fields during JONSWAP 1973. J. Geophys. Res., 84(18), 4855-4864.

Hasselmann, K. (1960): Grundgleichungen der Seegangsveroussage. Schiffstechnik, 7, 191.

Hasselmann, K., T.P. Barnett, E. Bouws, H. Carlson, D.E. Cartwright, K. Enke, J.A. Ewing, H. Grenopp, D.G. Hasselmann, P. Kruesman, A. Meerburg, P. Muller, D.J. Olbers, K. Richter, W.Sell and H. Walden (1973): Measurements of wind wave growth and swell decay during the joint North Sea Wave Project (JONSWAP). Dtsch. Hydrogr. Z., Suppl. A. 8(12).

Hasselmann, K., D.B. Ross, P. Muller and W. Sell (1976): A parametrical wave prediction model. J. Phys. Oceanogr., 6, 200-228.

Hasselmann, K., A. Favre (1978): Turbulent fluxes through the sea surface ,wave dynamics and prediction. Plenum Press, New York.

Hasselmann, S. and K. Hasselmann (1985): Computations and parametrization of the nonlinear energy transfer in a gravity wave spectrum. Part 1: A new method for efficient computations of the exact nonlinear transfer integral. J. Phys. Oceanogr., 15. 1369-1377

Inoue, T. (1967): On the growth of the spectrum of a wind generated sea according to a modified Miles-Phillips mechanism and its application to wave forecasting. TR-67-5,

Geophysical Science Labrotary Report, NY University, School of Engineering and Science.

Komen, G.T., S. Hasselmann and K. Hasselmann (1984): On the existence of a fully developed wind-sea spectrum. J. Phys. Oceanogr., 14, 1271- 1285.

Lazanoff, S.M. and N. M. Stevenson (1975): An evaluation of a hemispheric operational wave spectral model. Tech. Note 75-3, Fleet Numerical Weather Center, Monterey, CA.

Manton, J.W. (1957): On the generation of sea waves by a turbulent wind. Boundary Layer Met., 2, 348-364.

Miles, J.W. (1957): On the generation of surface waves by shear flow, Part 1, J. Fluid Mech., , 185-204; Part 2, J. Fluid Mech., 6, 568-582, (1959); Part 3, J. Fluid Mech., 6, 583-598 (1959); Part 4, J. Fluid Mech., 7, 469-478 (1960).

Phillips, O.M. (1957): On the generation of surface waves by turbulent wind, J. Fluid Mech., 2, 417-445.

Phillips, O.M. (1966): The dynamics of the upper ocean, Cambridge University Press, NY.

Pierson, W.J. and L.I. Moscowitz (1964): A proposed spectral form for fully developed seas based on the similarity theory of S.A. Kitaigorodskii. J. Geophys. Res., 69(24), 5181-5203.

Pierson, W.J., L. Tick and L. Baer (1966): Computer based procedures for preparing global wave forecasts and wind field analyses capable of using wave data obtained by a space craft. Poc. 6th Naval Hydrodynamics Symp., Vol. 2, 1.

Pierson, W.J. (1982): The spectral ocean wave model (SOWM), A northern hemisphere computer model for specifying and forecasting ocean wave spectra. DTNSRDC-82/011.

Resio, D.T. (1981): The estimation of wind-wave generation in a discrete spectral model. J. Geophys. Oceanogr., 11, 510-525.

Synder, O.H. and C.S.Cox (1966): A field study of the wind generation in a discrete spectral model for specifying and forecasting ocean wave. J. Marine Res., 24(2),141-178.

SWAMP group (1985): Ocean wave modeling. Plenum Press, NY and London.

Takeda, A. (1963): Wind profiles over sea waves. J. Ocean. Soc., Japan, 19, 16-22.

Wu, J. (1968): Labaratory studies of wind wave interactions. J. Fluid Mech., 34, Part 1, 91-111.

9. Figures

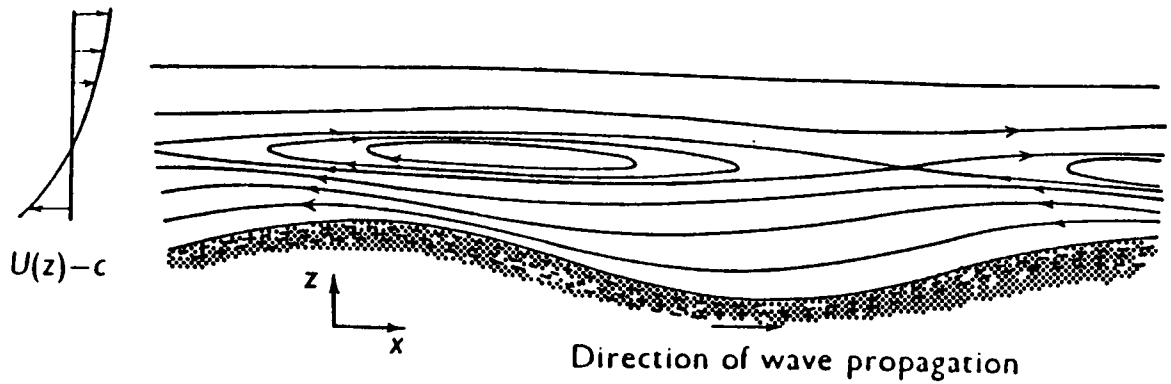

Fig. 1. Mean streamlines and velocity profile in a frame of reference moving with the wave.
from Phillips (1966)

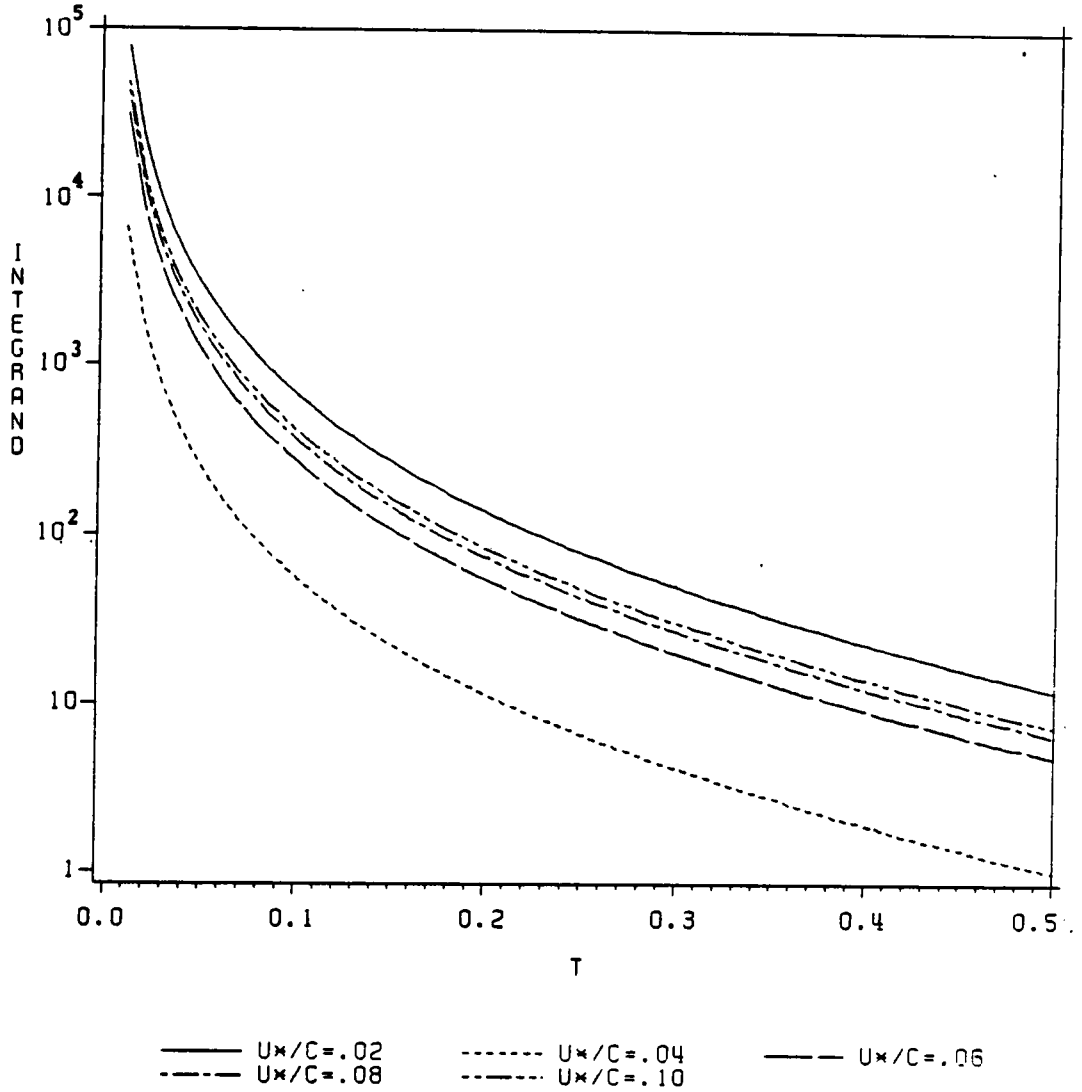

Fig. 2. The integrand of equation 4.36

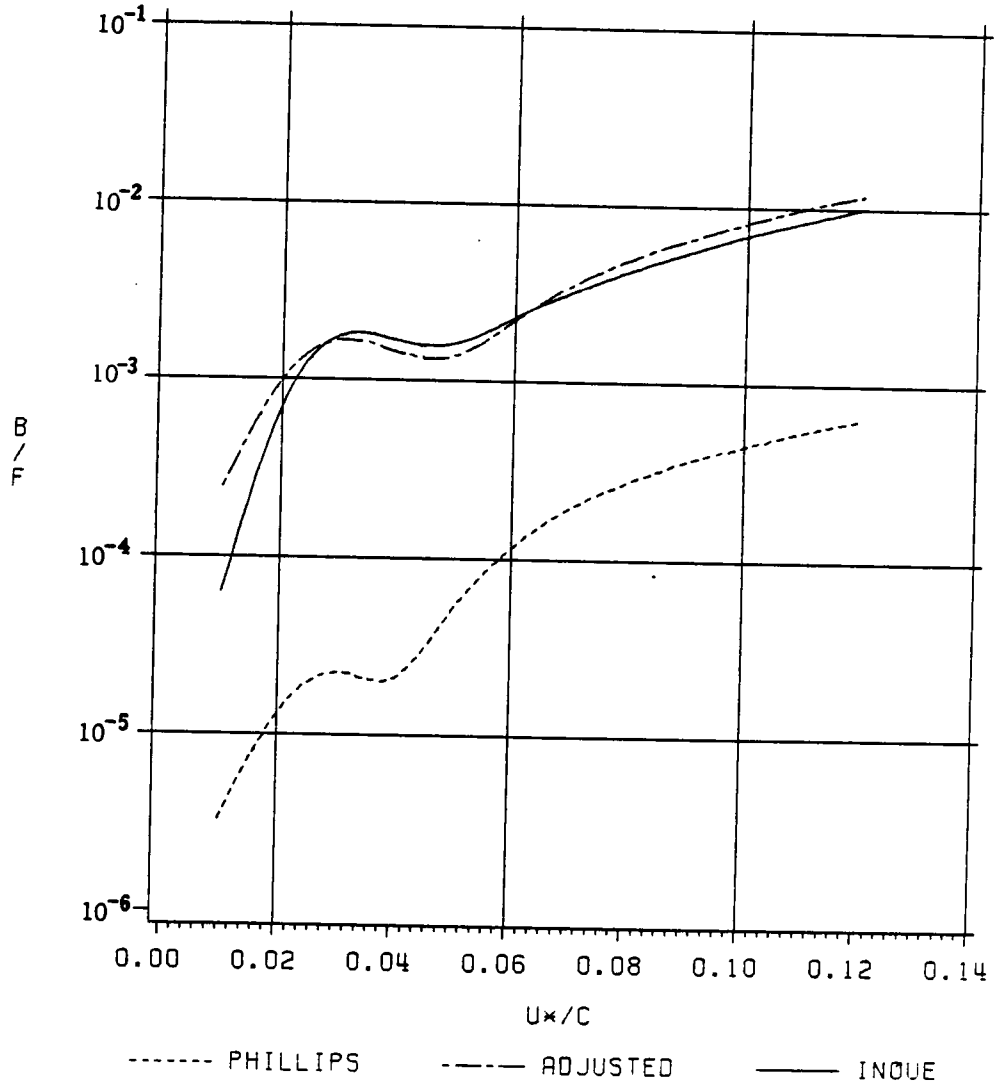

Fig. 3. Evaluation of the B fucntion in directionally integrated form.

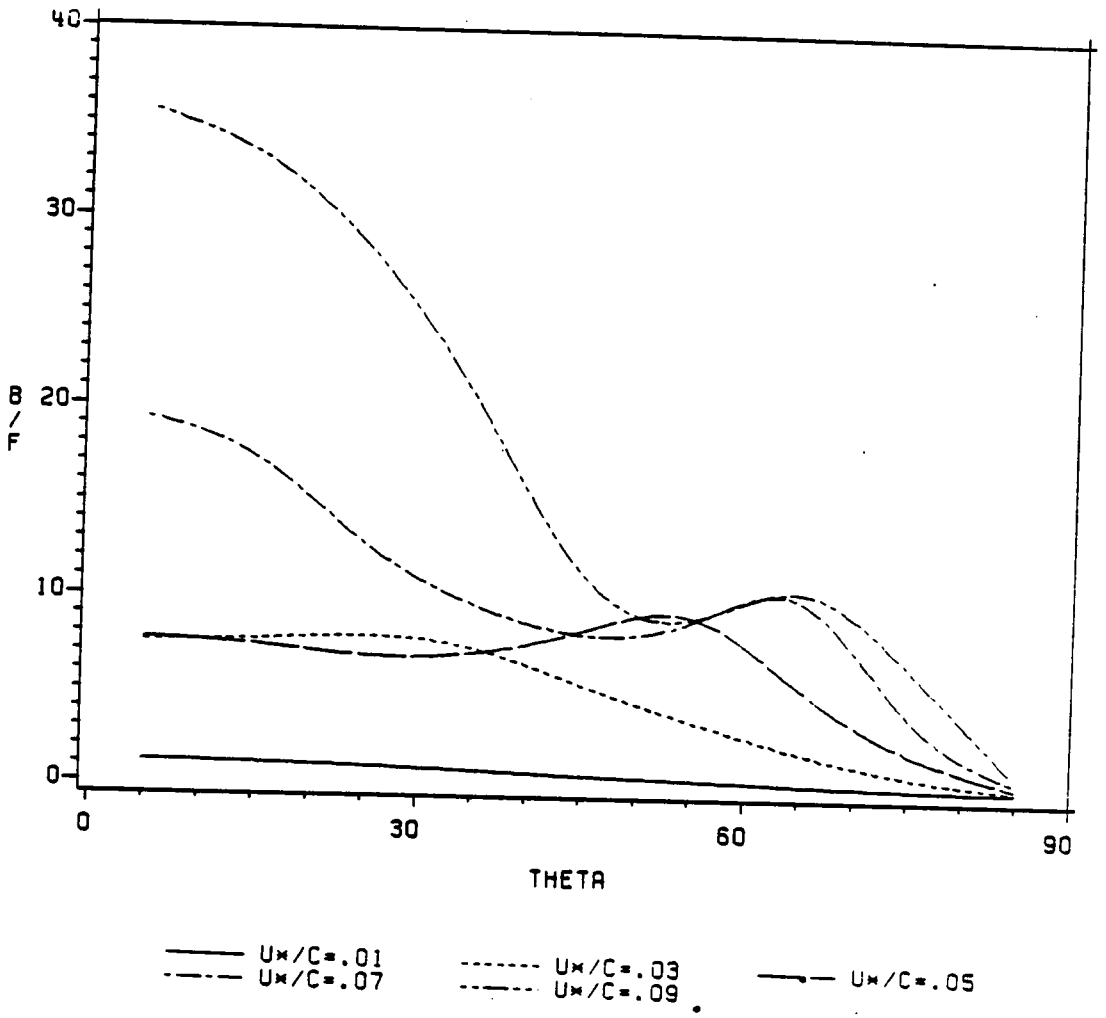

Fig. 4. Directional behavior of the B function

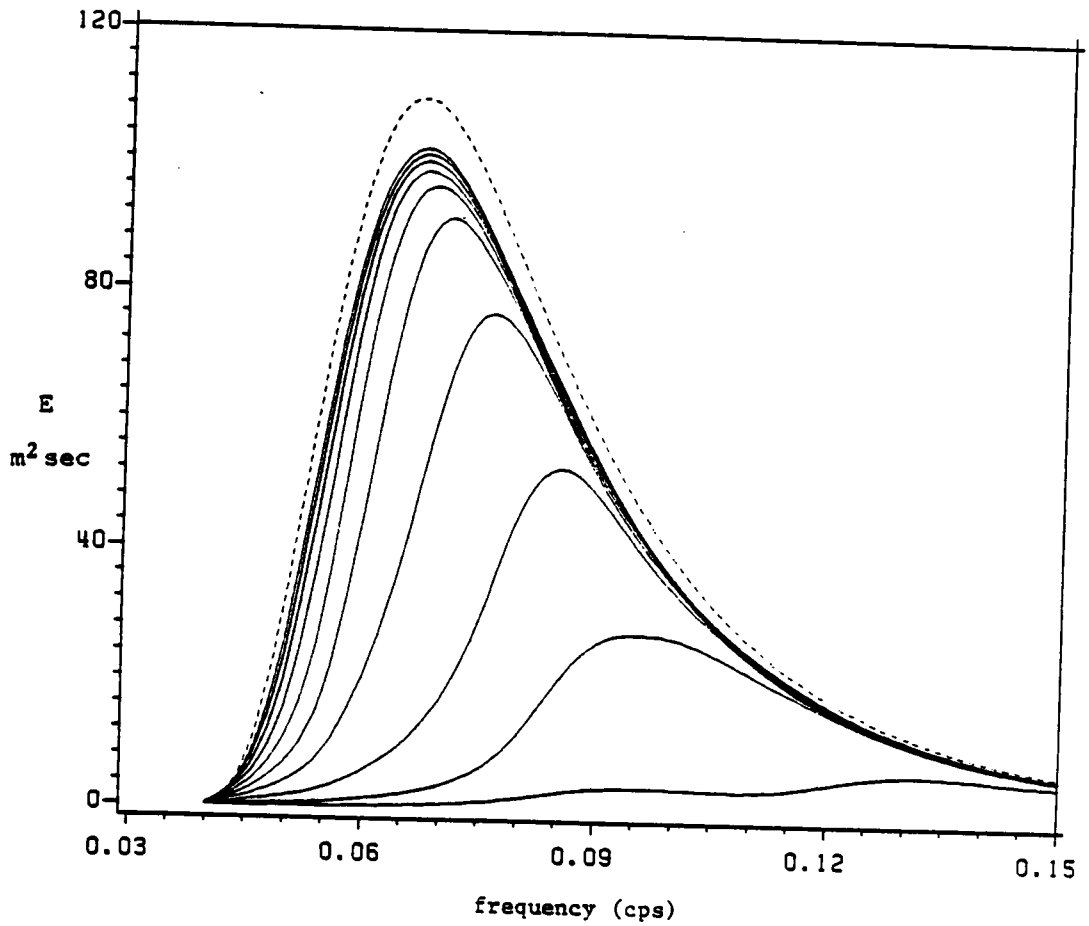

Fig. 5. Point spectrum evolution for a steady 40 knot wind from VPINK in 3 hour time increments

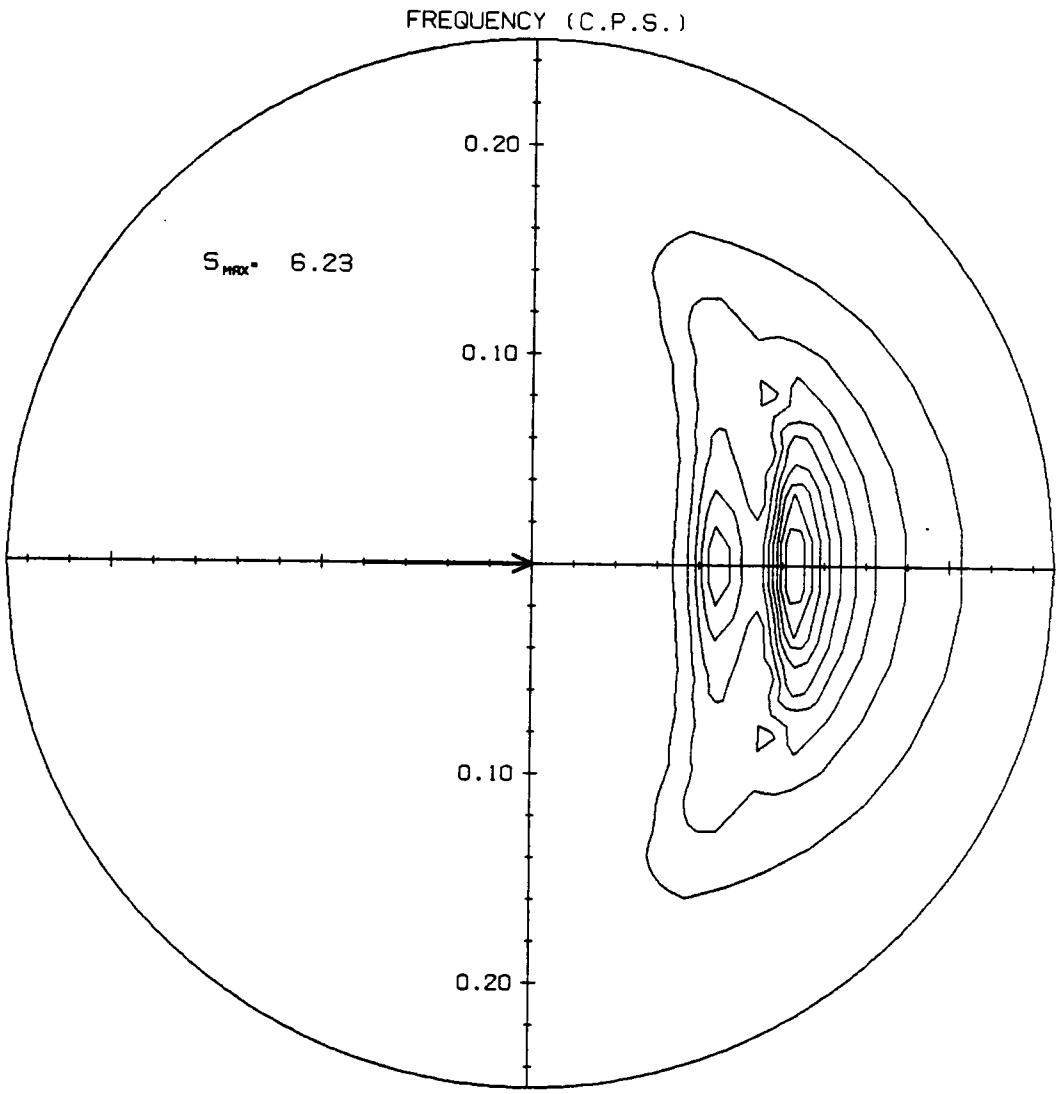

Fig. 6a. Contour plots of 2-D spectrum evolution for a steady 40 knot wind from VPINK. T=3 hours

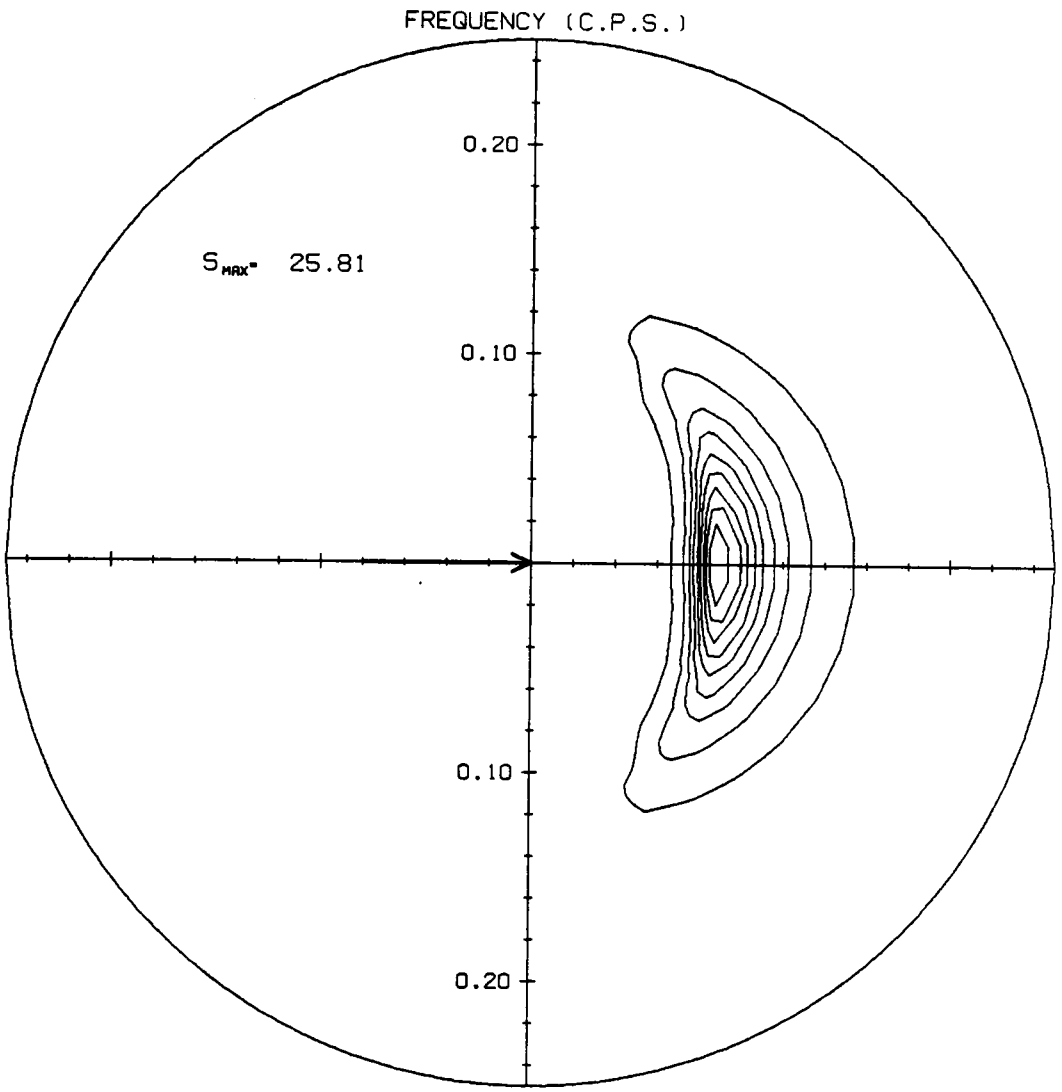

Fig. 6b. T=6 hours

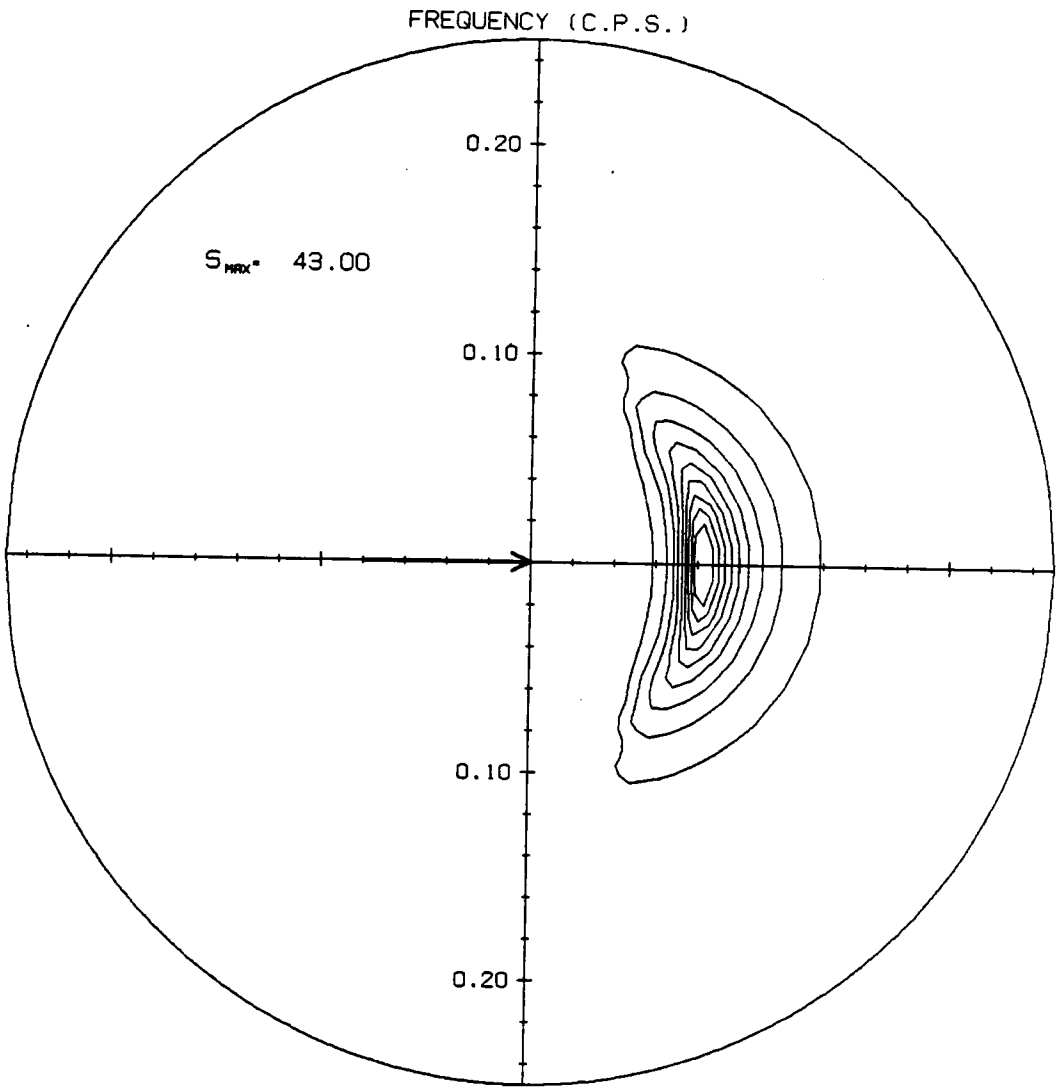

Fig. 6c. T=9 hours

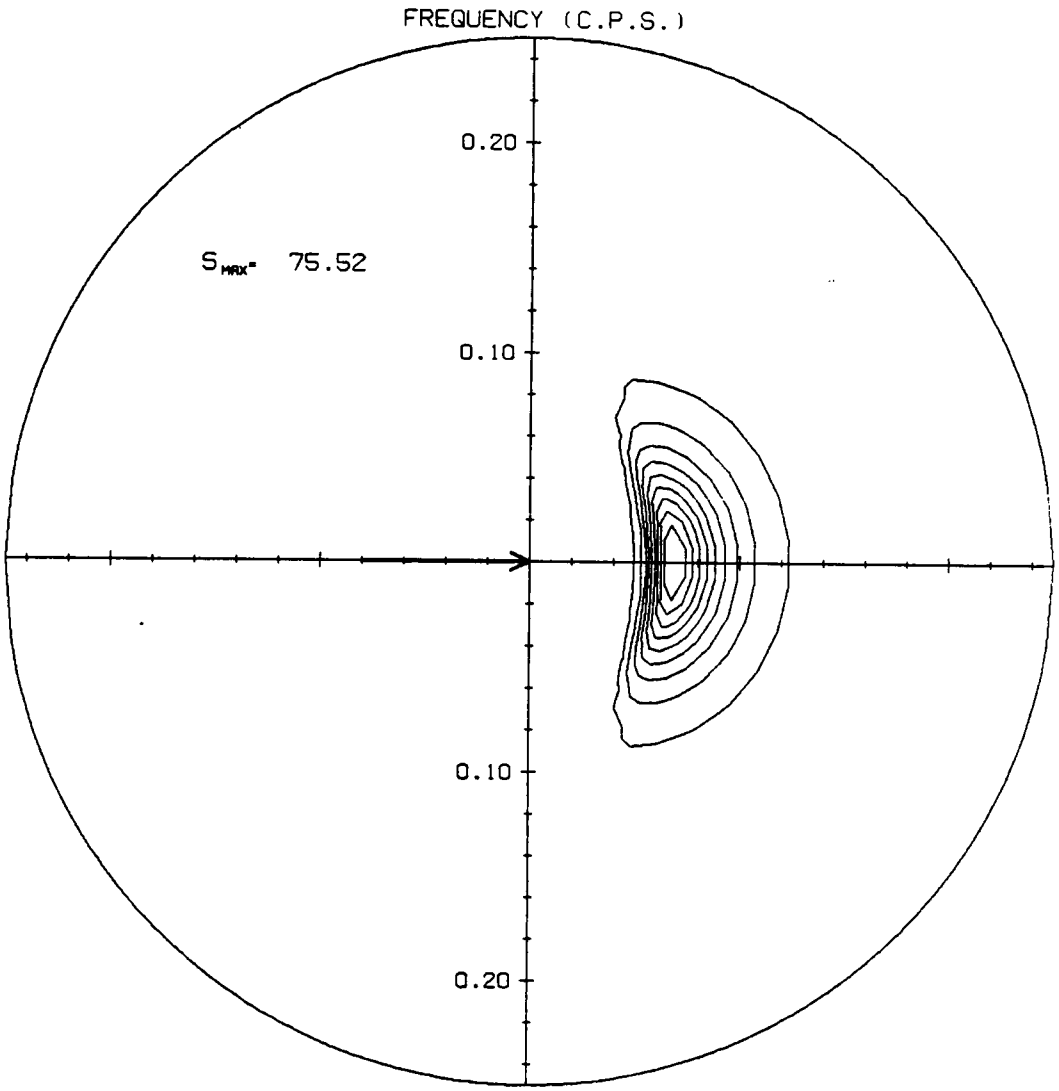

Fig. 6d. T=15 hours

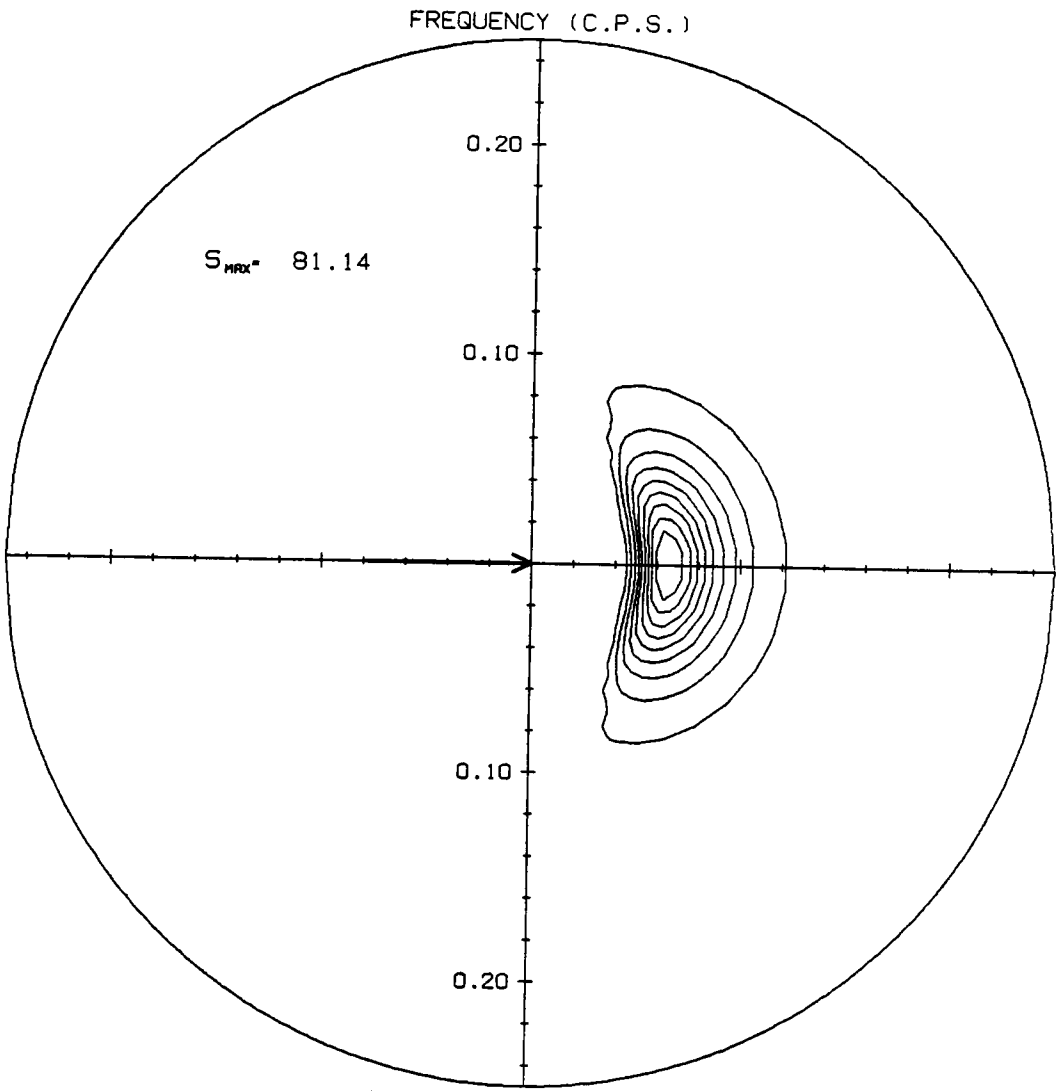

Fig. 6e. T=30 hours

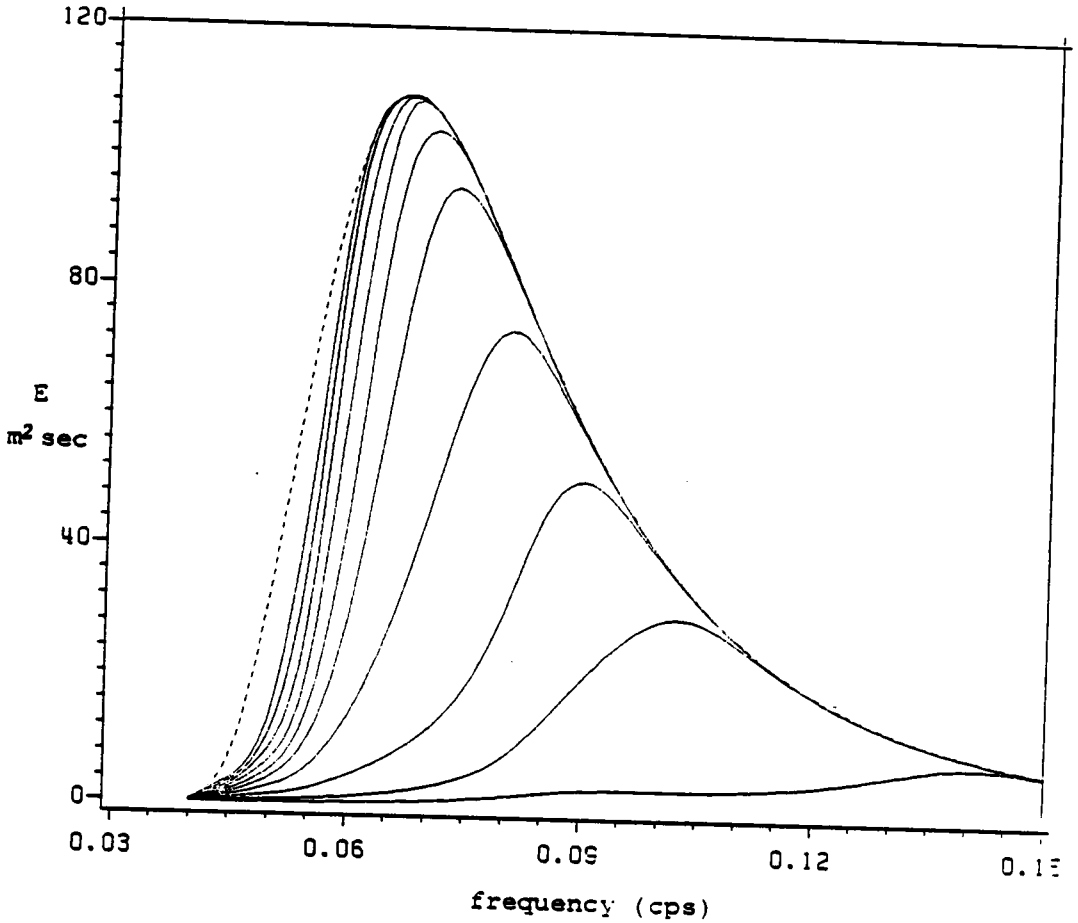

Fig. 7. Point spectrum evolution for a steady 40 knot wind from VSOWM in 3 hour time increments

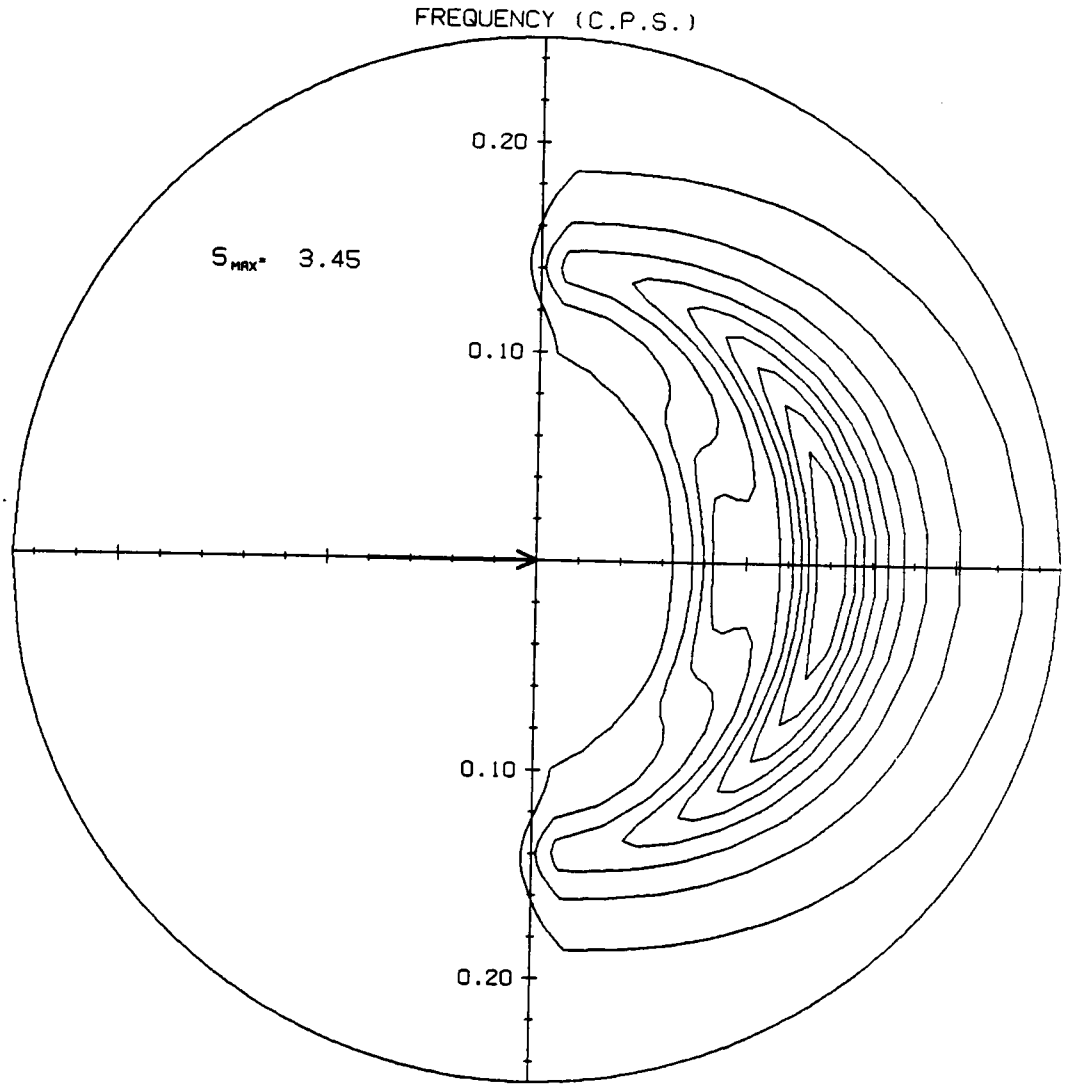

Fig. 8a. Contour plots of 2-D spectrum evolution for a steady 40 knot wind from VSOWM. T=3 hours

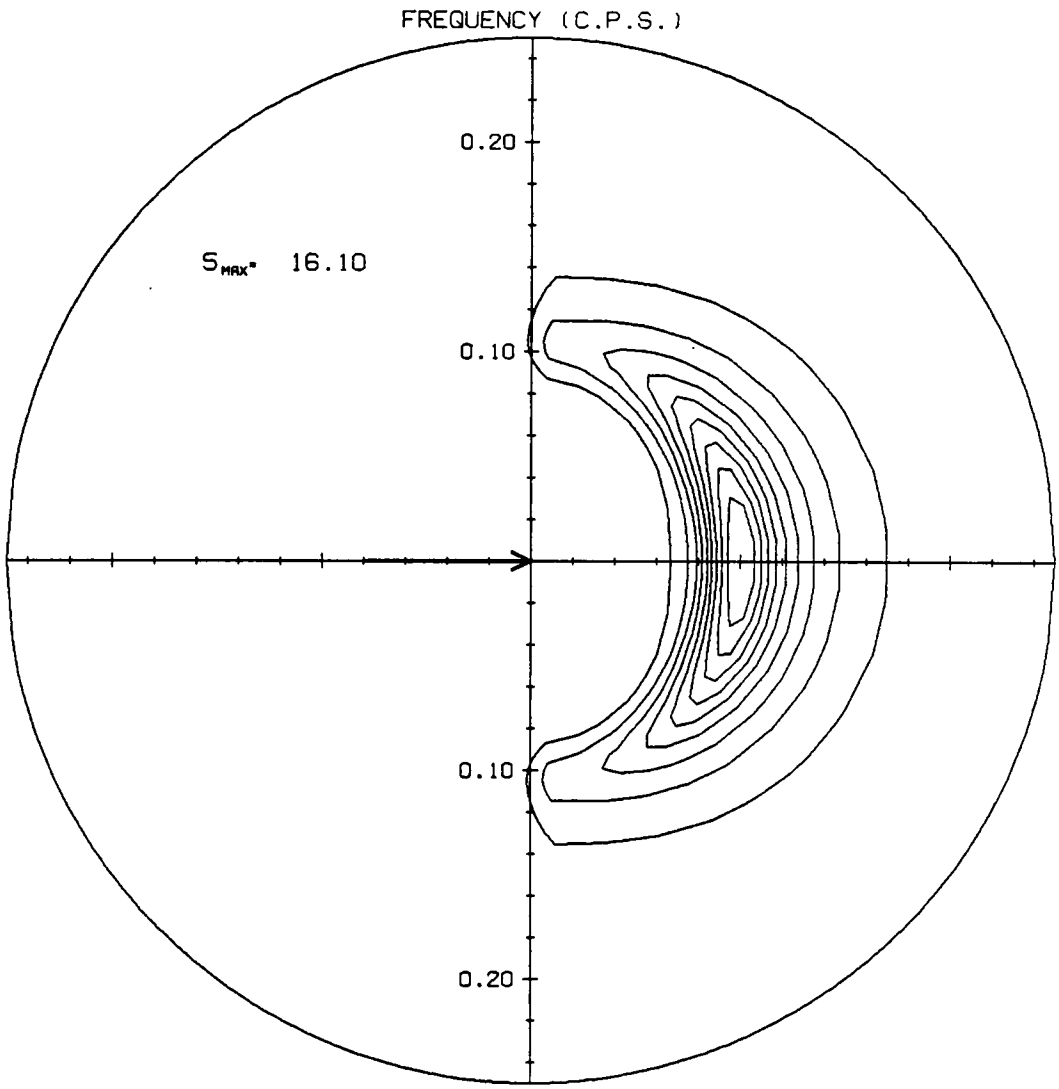

Fig. 8b. T=6 hours

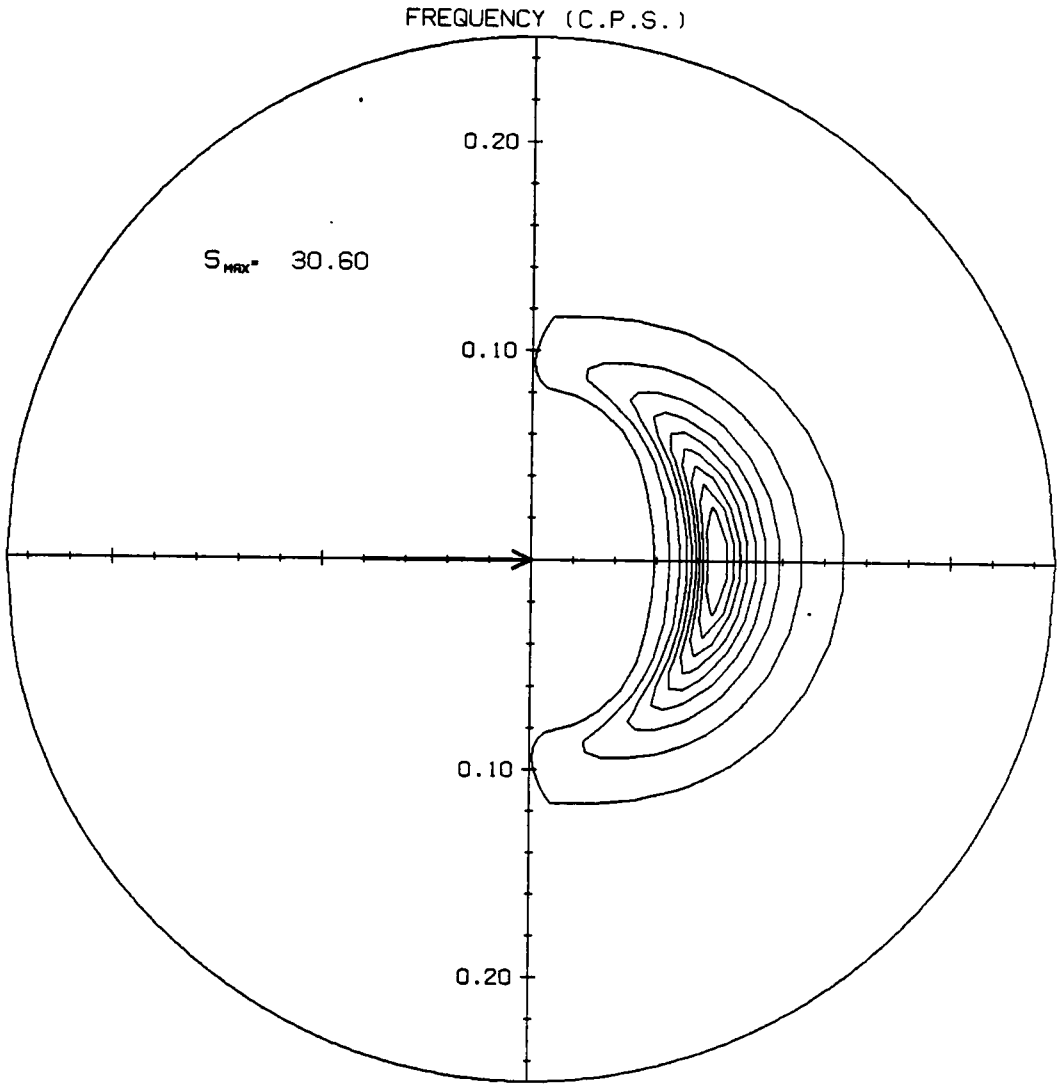

Fig. 8c. T=9 hours

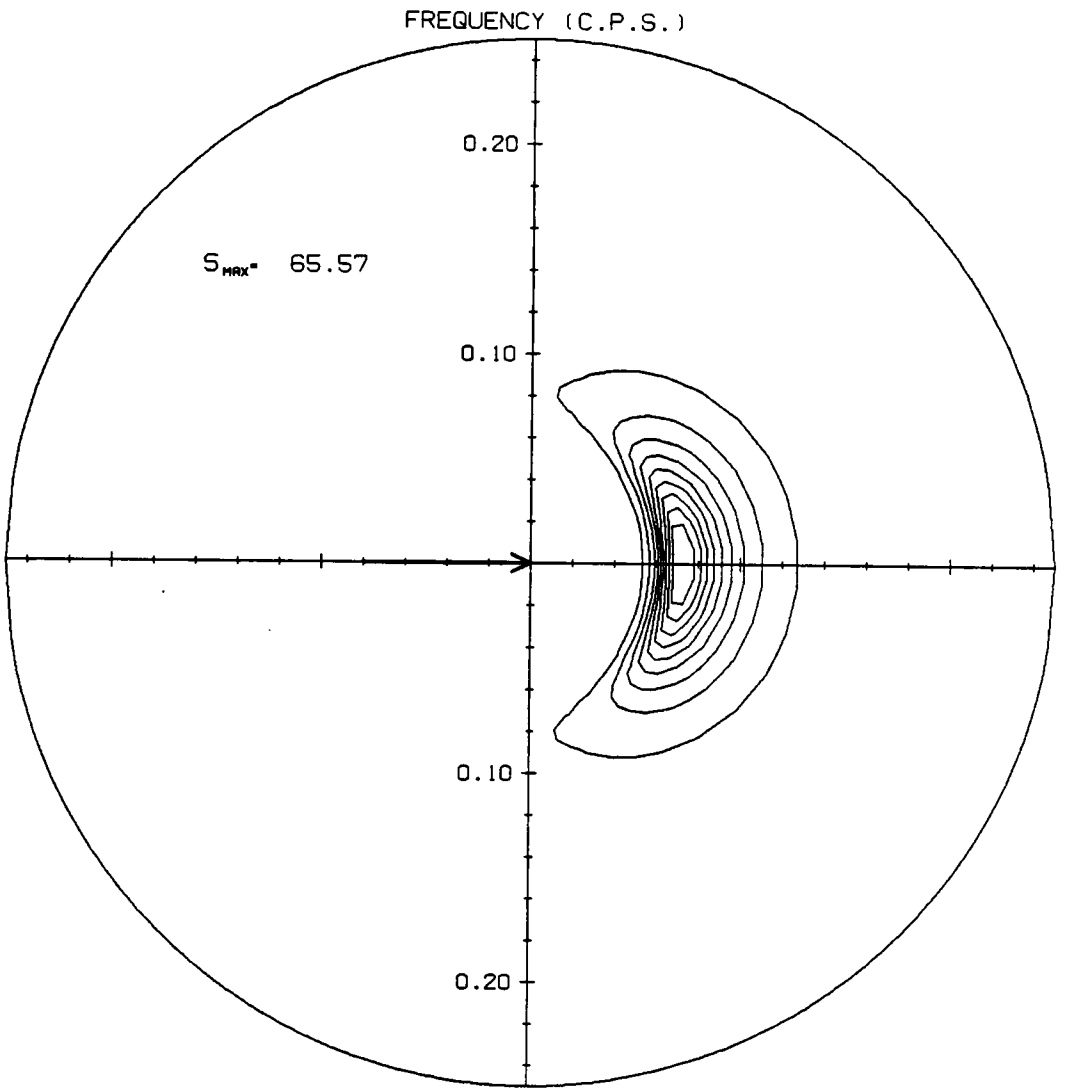

Fig. 8d. T=15 hours

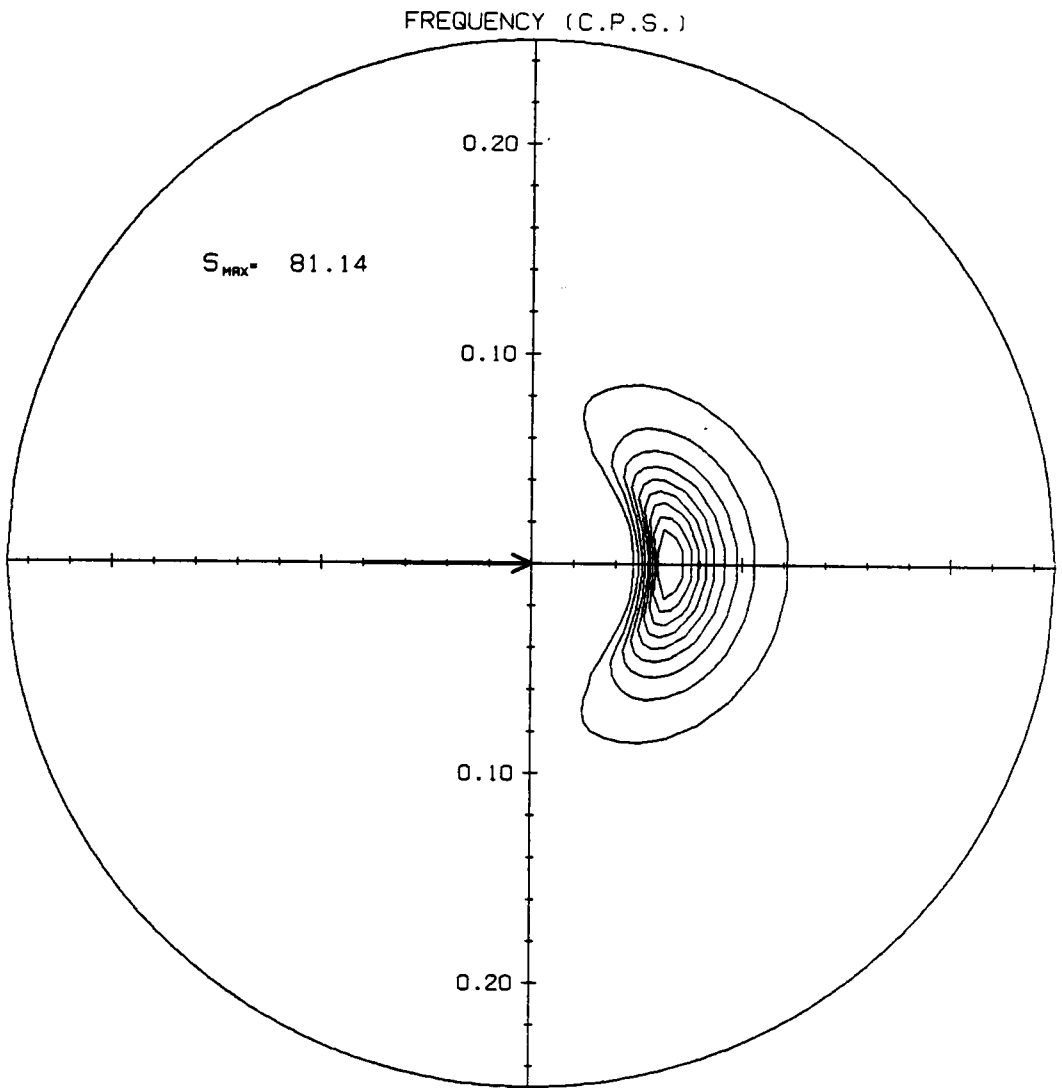

Fig. 8e. T=30 hours

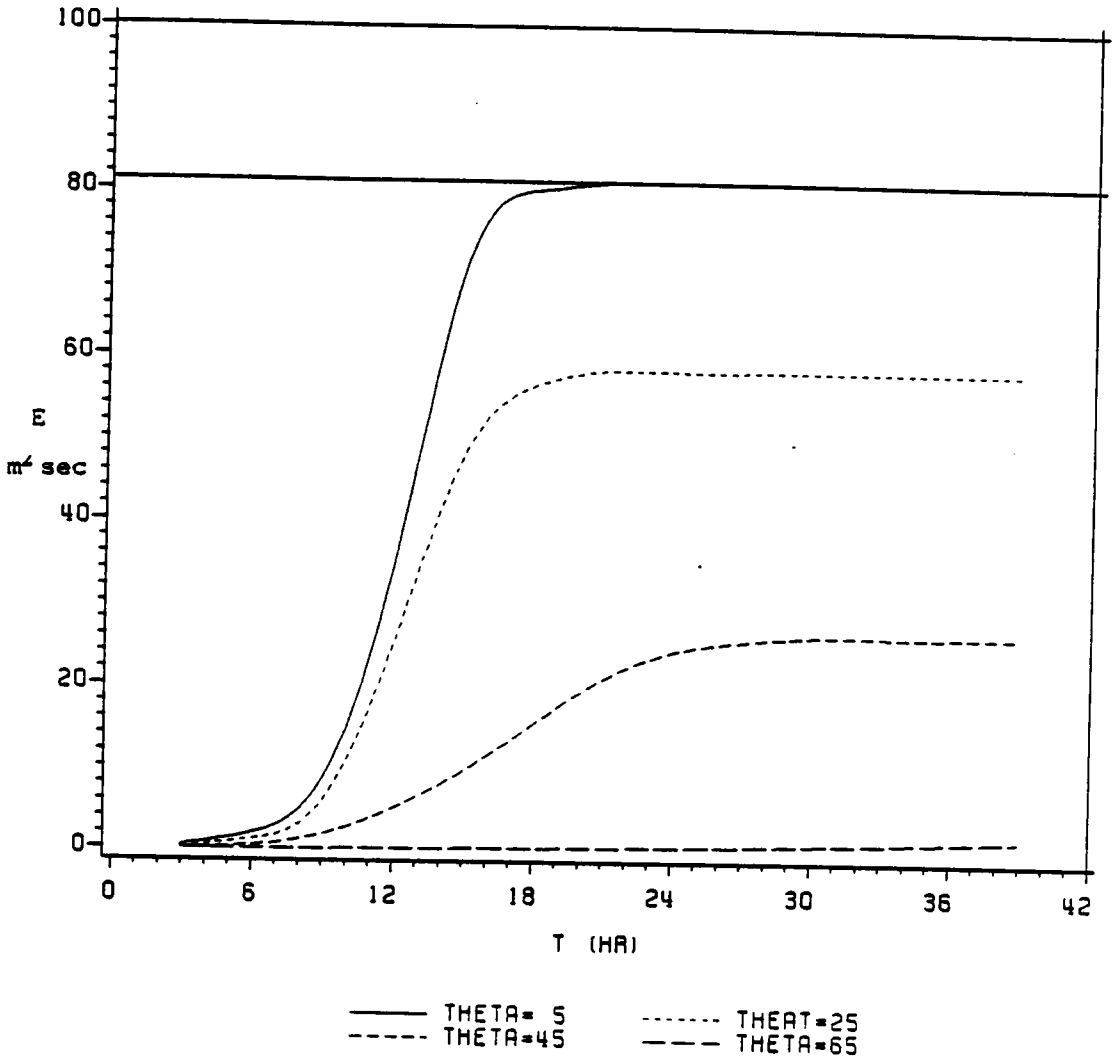

Fig. 9. Growth of the 2-D VPINK spectrum at f=0.065 Hz for a steady 40 knot wind

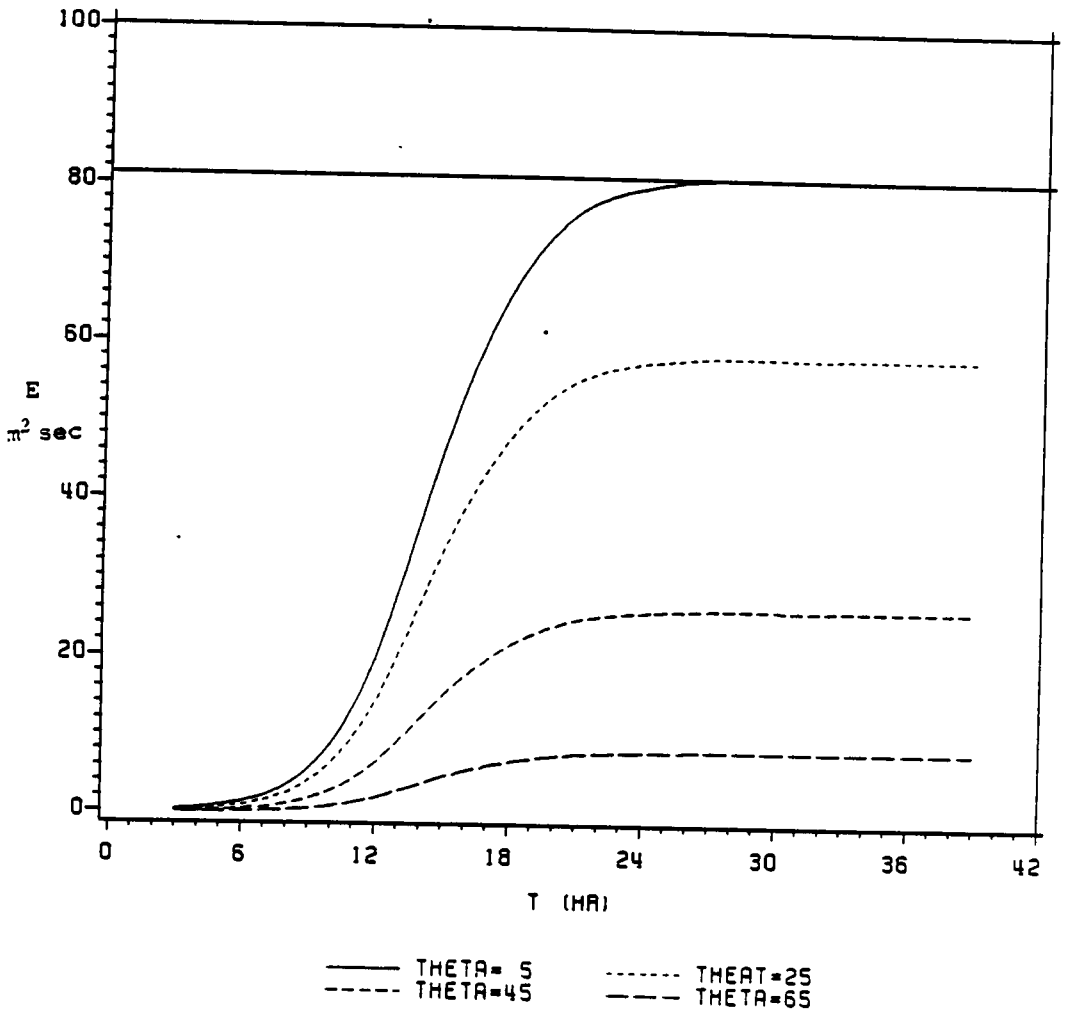

Fig. 10. Growth of the 2-D VSOWM spectrum at f=0.065 Hz for a steady 40 knot wind

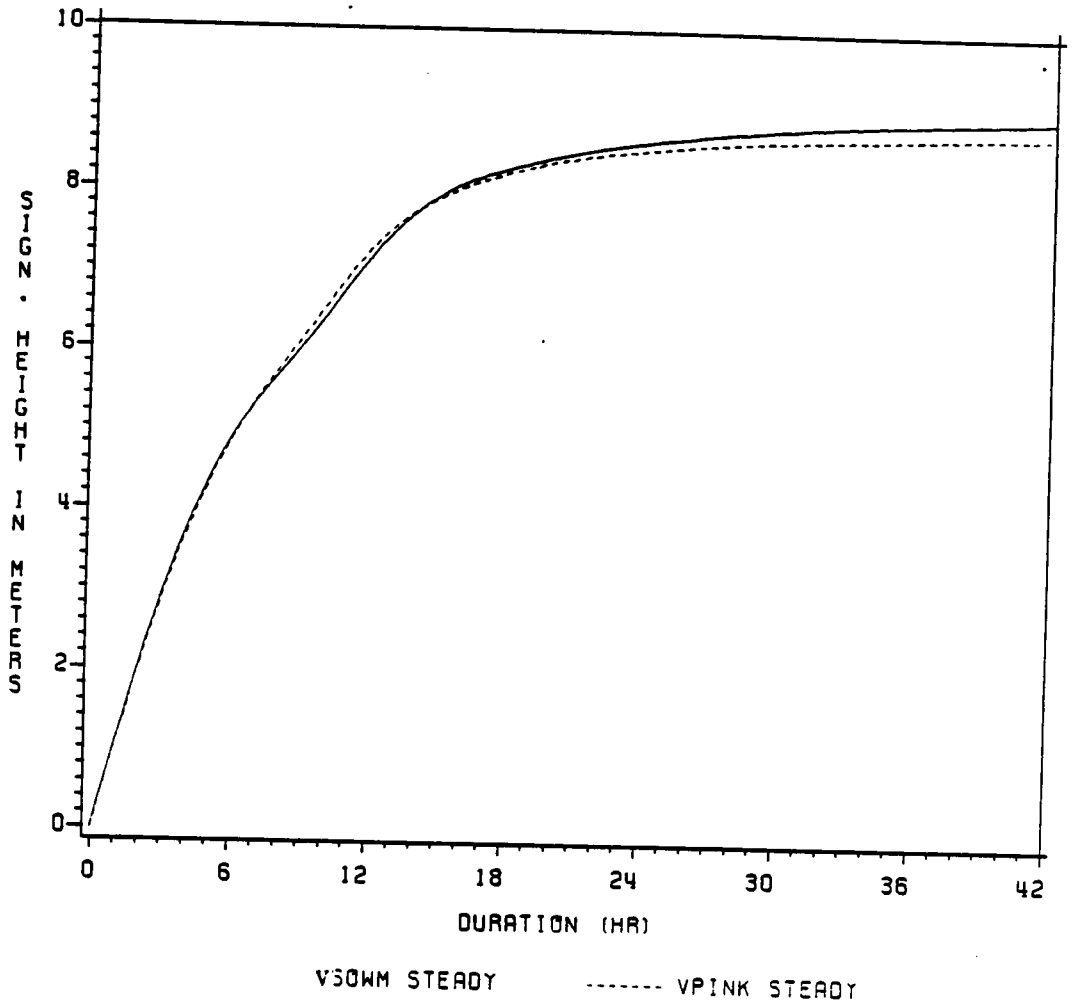

Fig. 11. Significant wave height vs. duration for a steady 40 knot wind

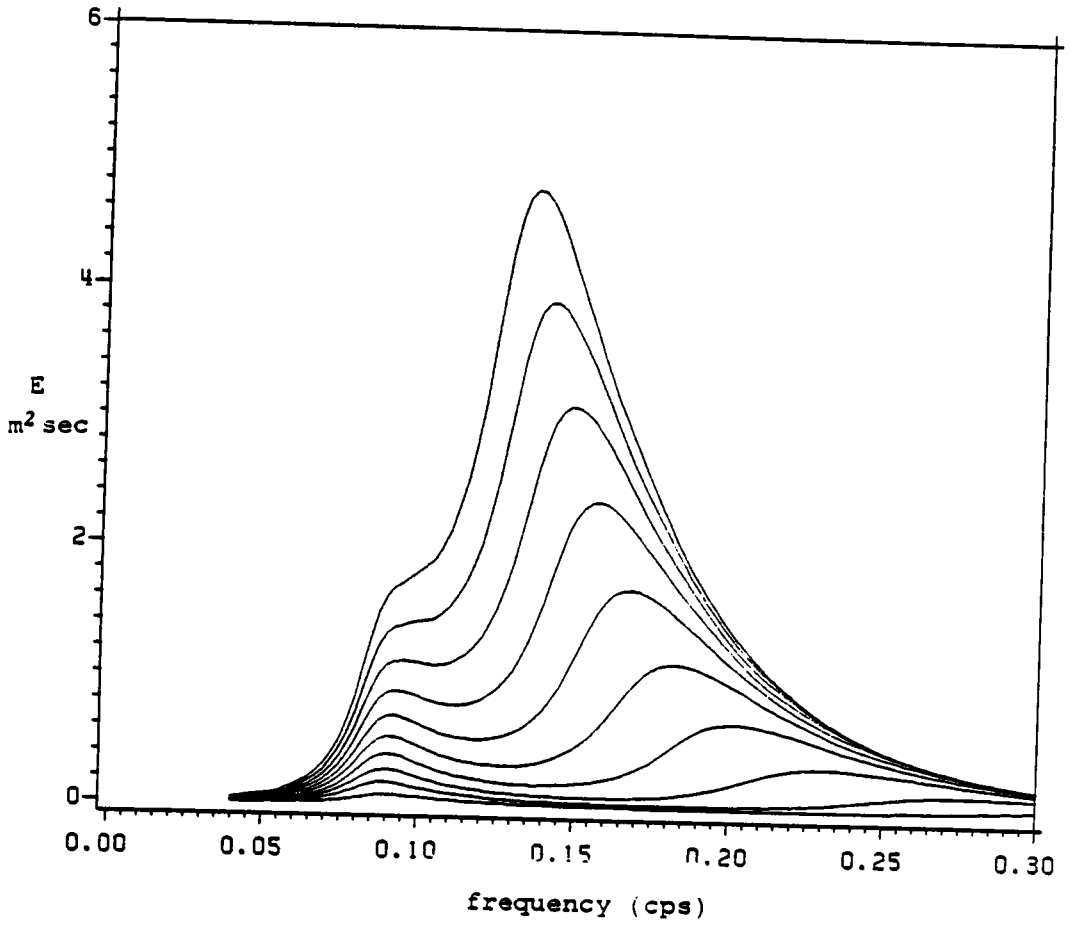

FIG. 12. Point spectrum evolution for a 40 knot wind at early times VPINK. Time increment 0.2 hours

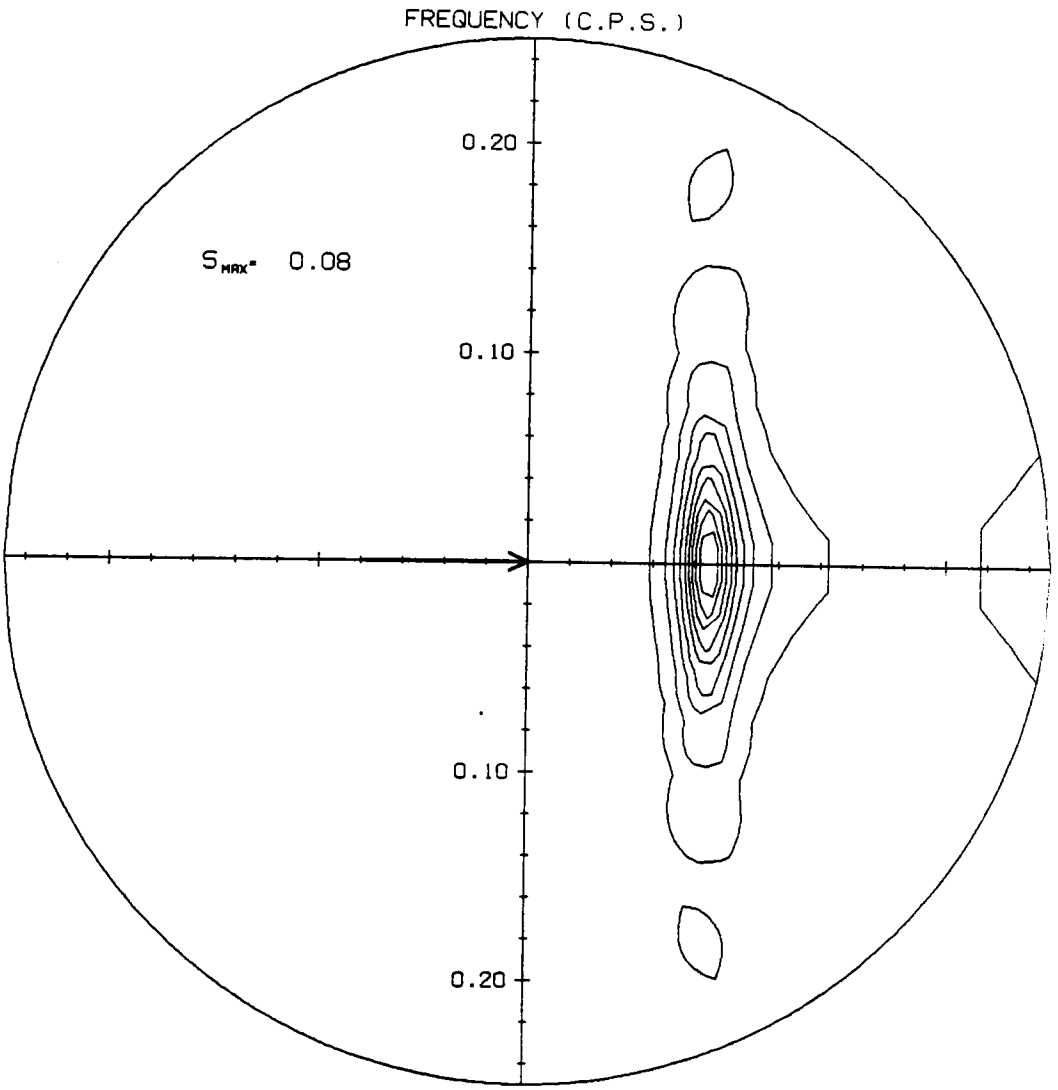

Fig. 13a. Contour plots of 2-D spectrum evolution for a 40 knot wind at early times from VPINK T=0.2 hours

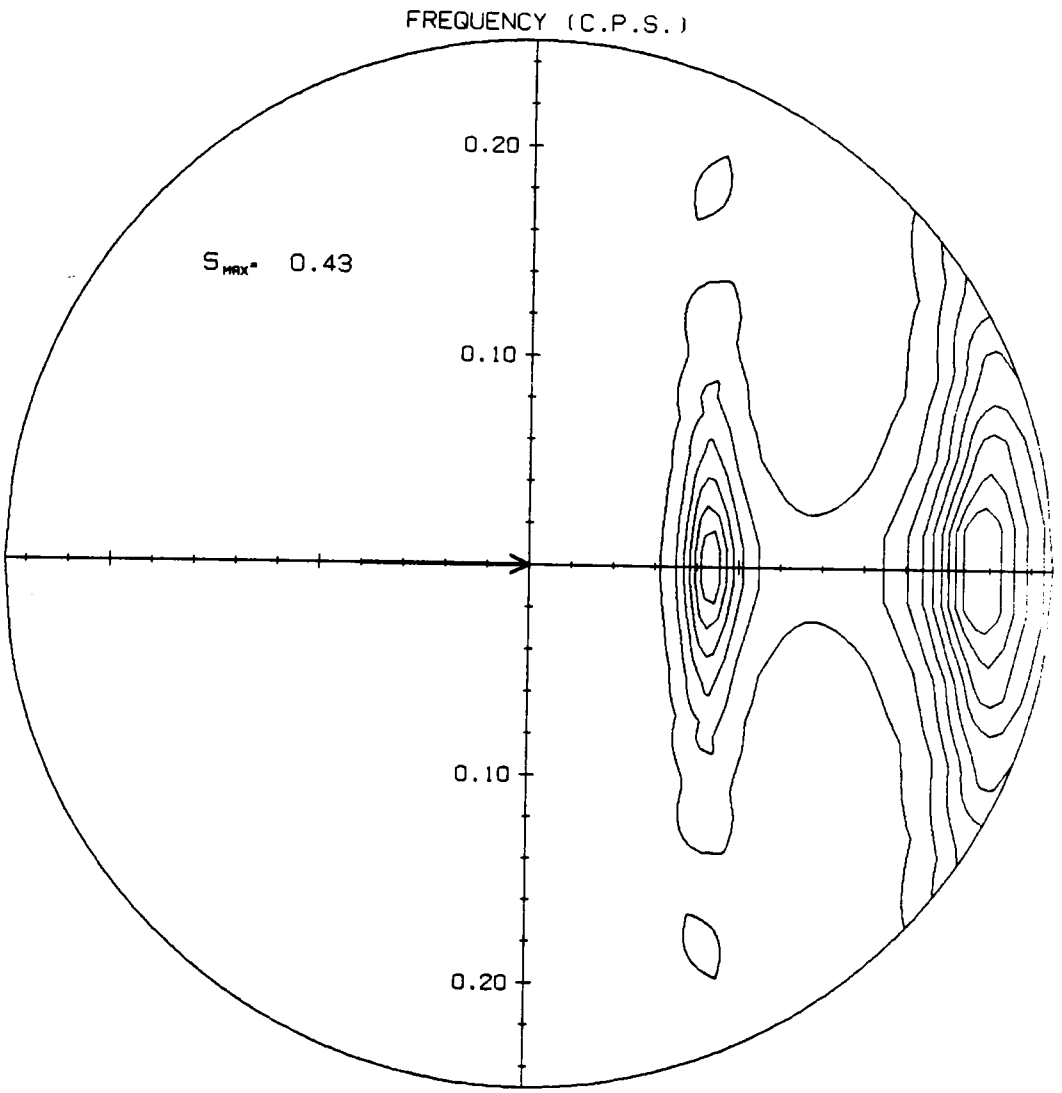

Fig. 13b. T=0.6 hours

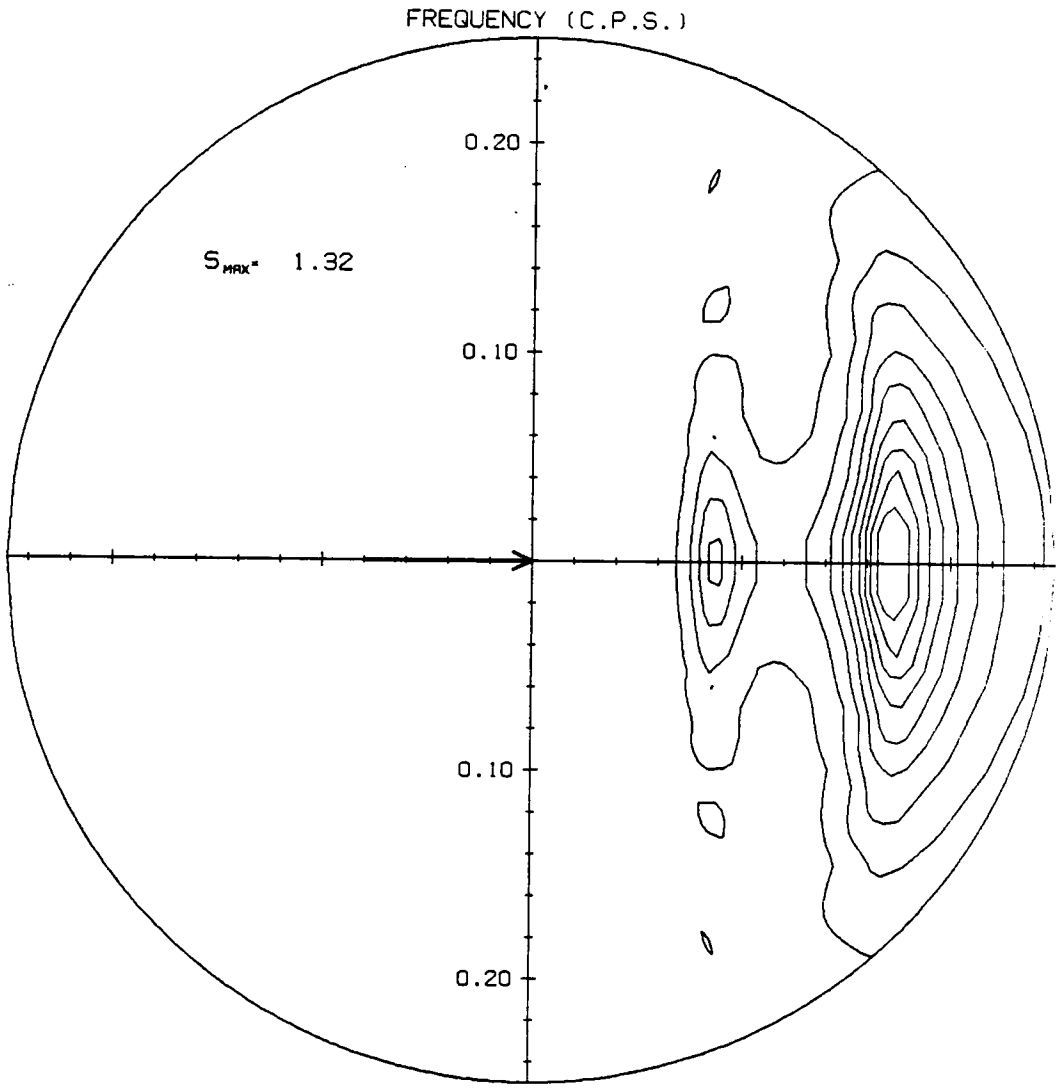

Fig. 13c. T=1.0 hours

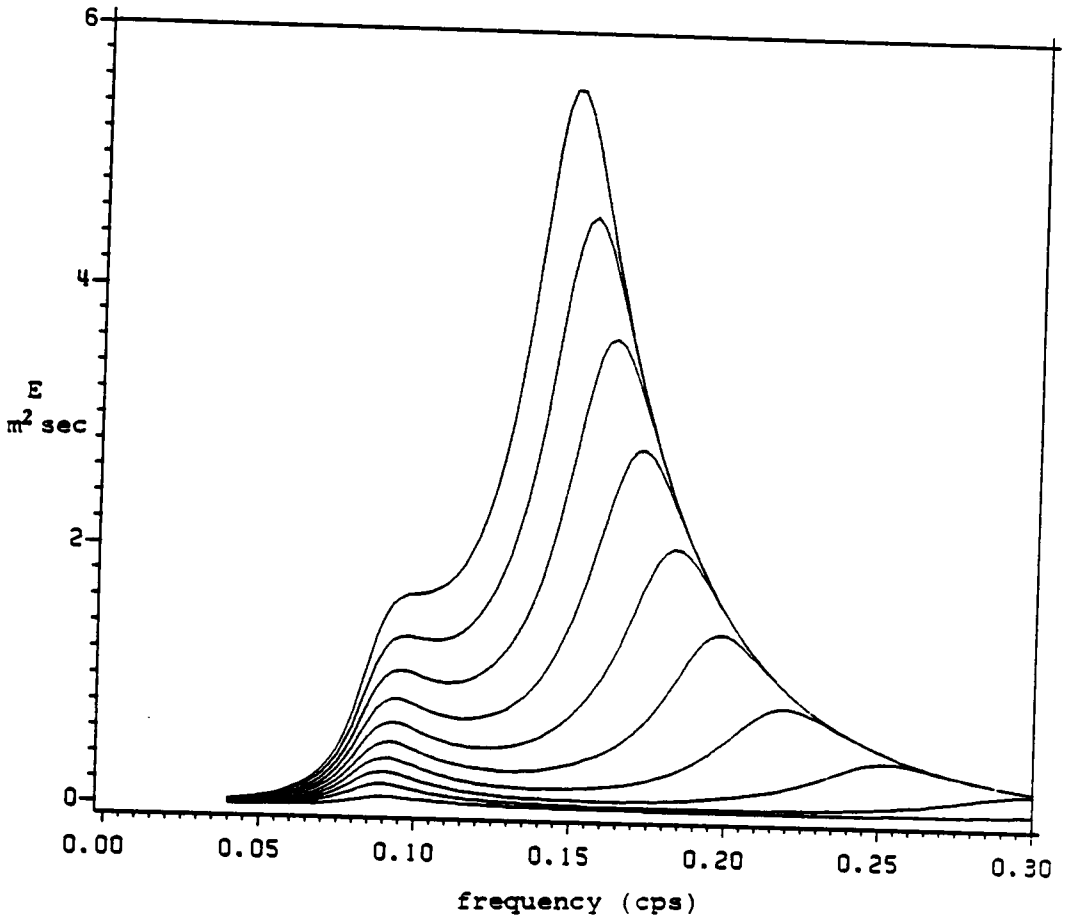

Fig. 14. Point spectrum evolution for a 40 knot wind at early times from VSOWM in 0.2 hour time increments

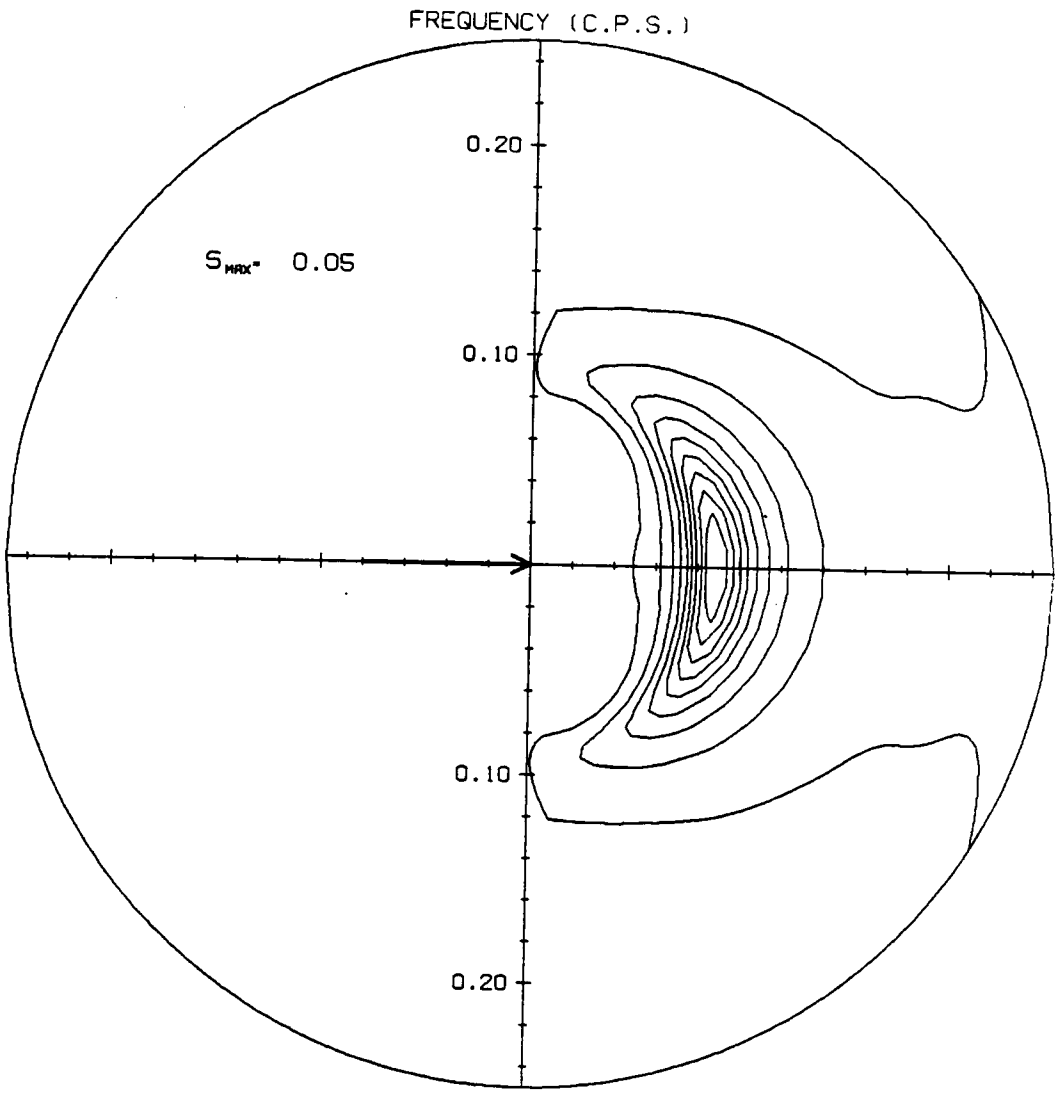

Fig. 15a. Contour plots of 2-D spectrum evolution for a 40 knot wind at early times from VSOWM. T=0.2 hours

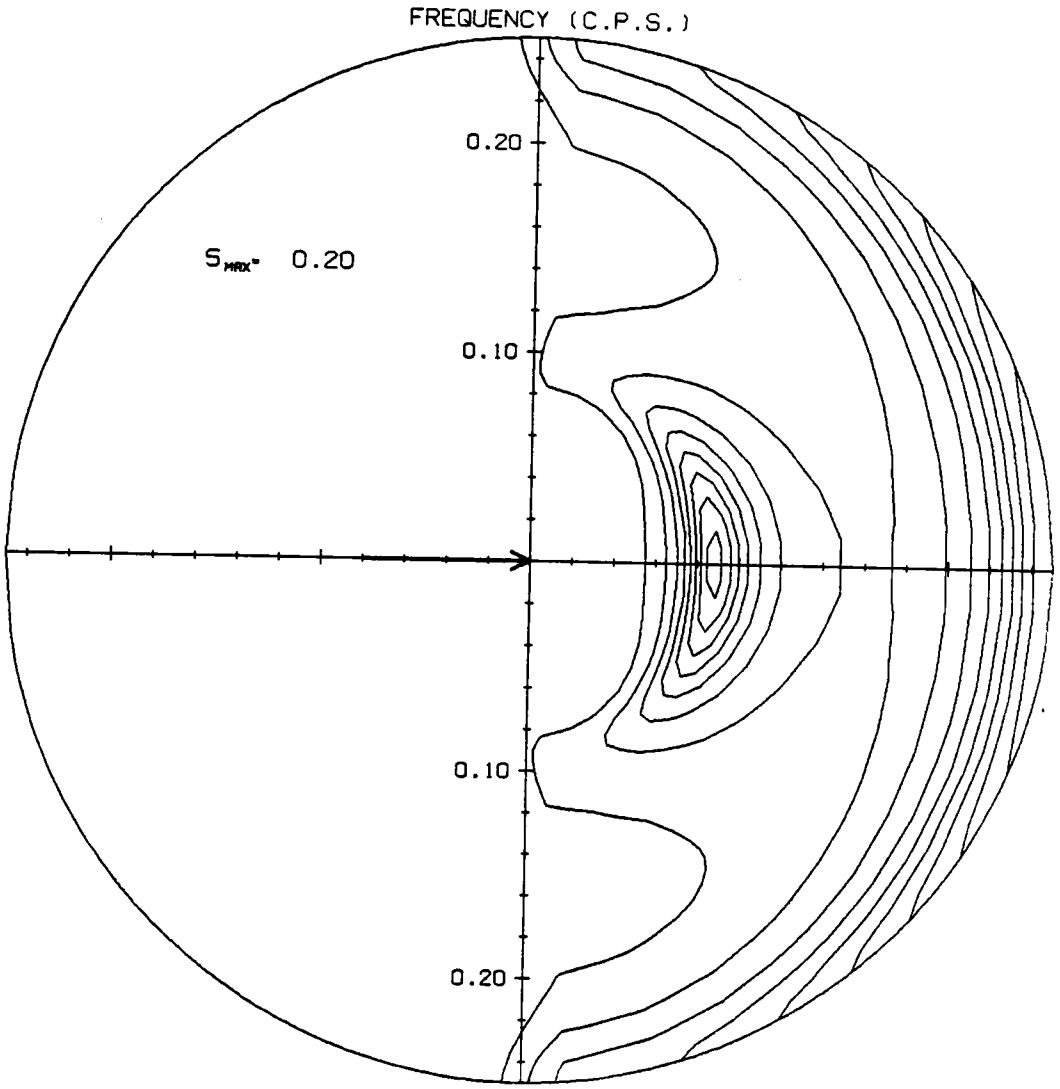

Fig. 15b. T=0.6 hours

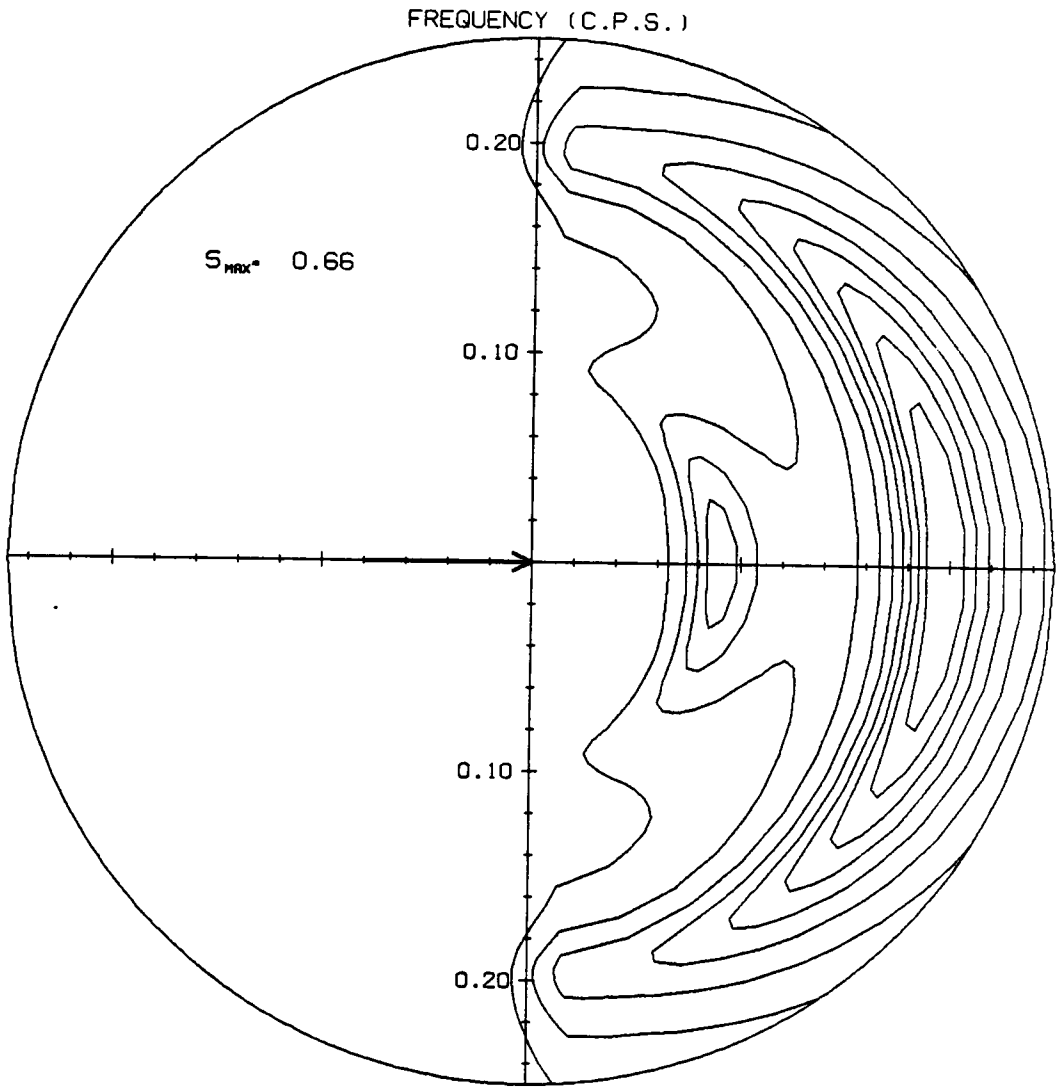

Fig. 15c. T=1.0 hours

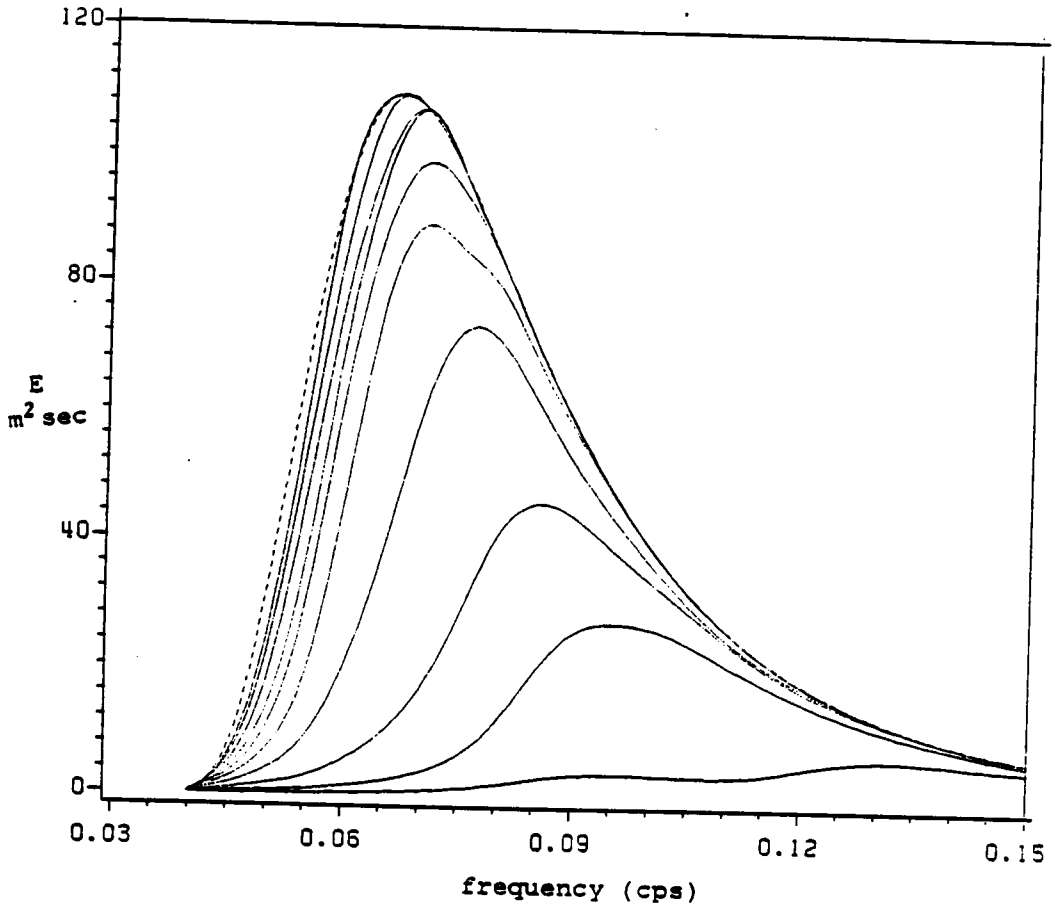

Fig. 16. Point spectrum evolution for a 40 knot wind oscillating in direction from VPINK

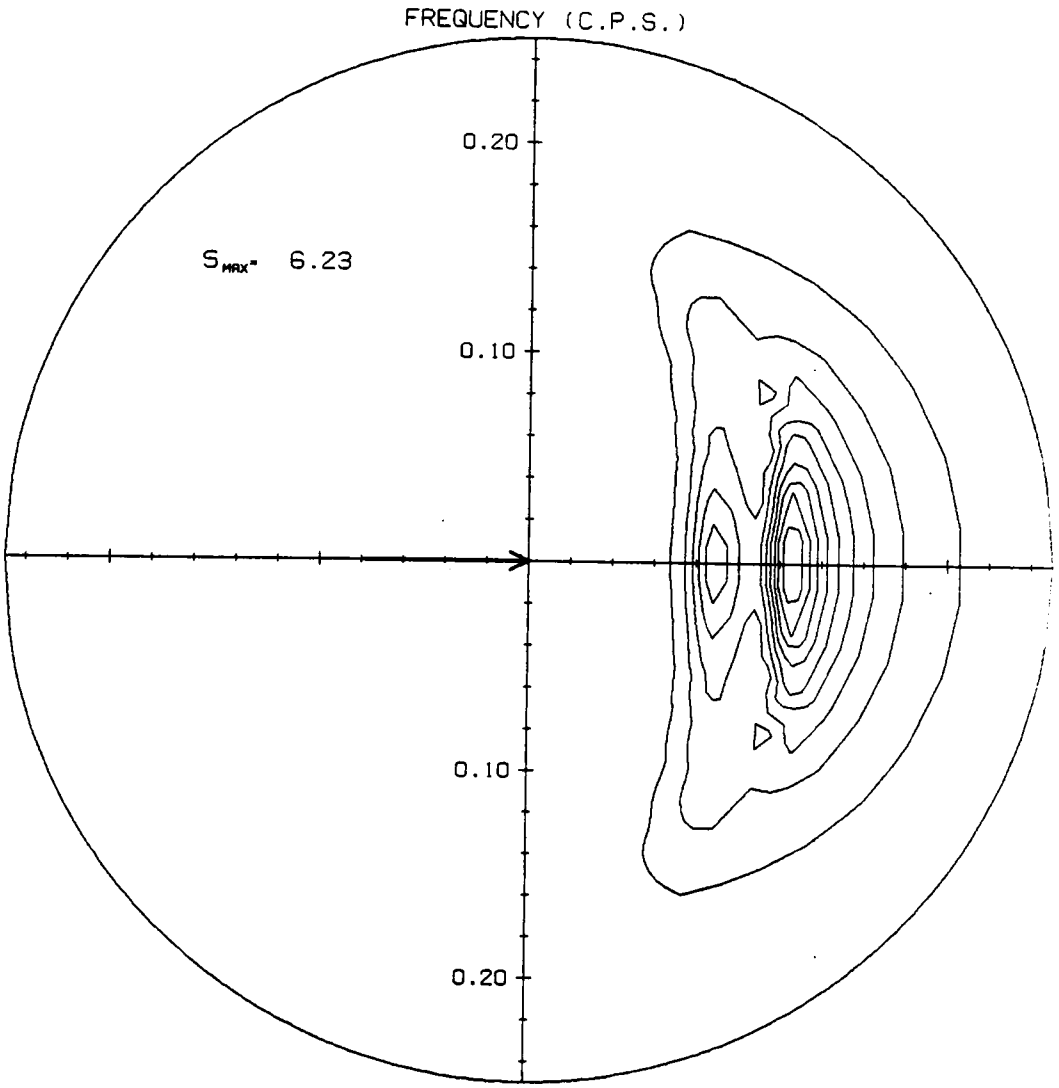

Fig. 17a. Contour plots of 2-D spectrum evolution for an oscillating 40 knot wind from VPINK. T=3 hours

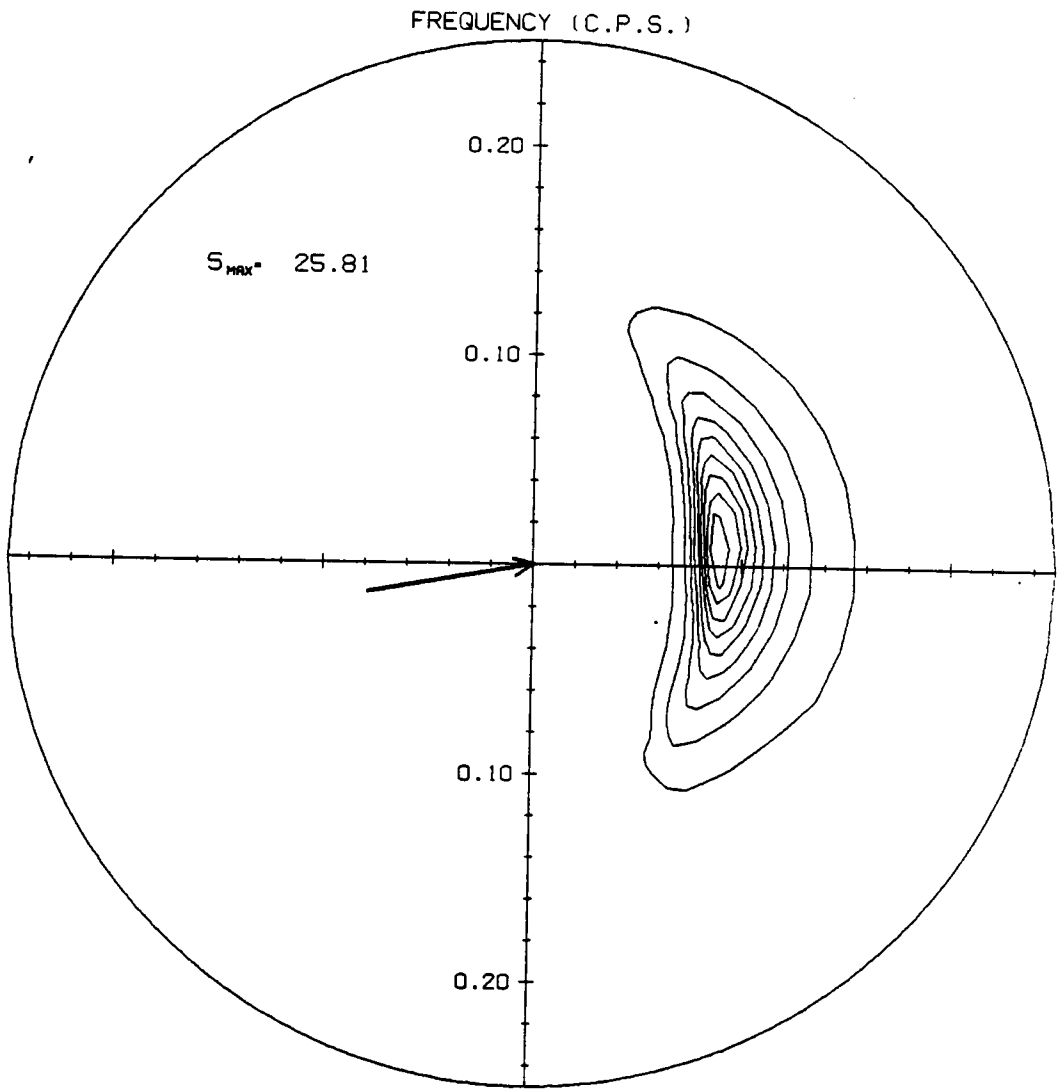

Fig. 17b. T=6 hours

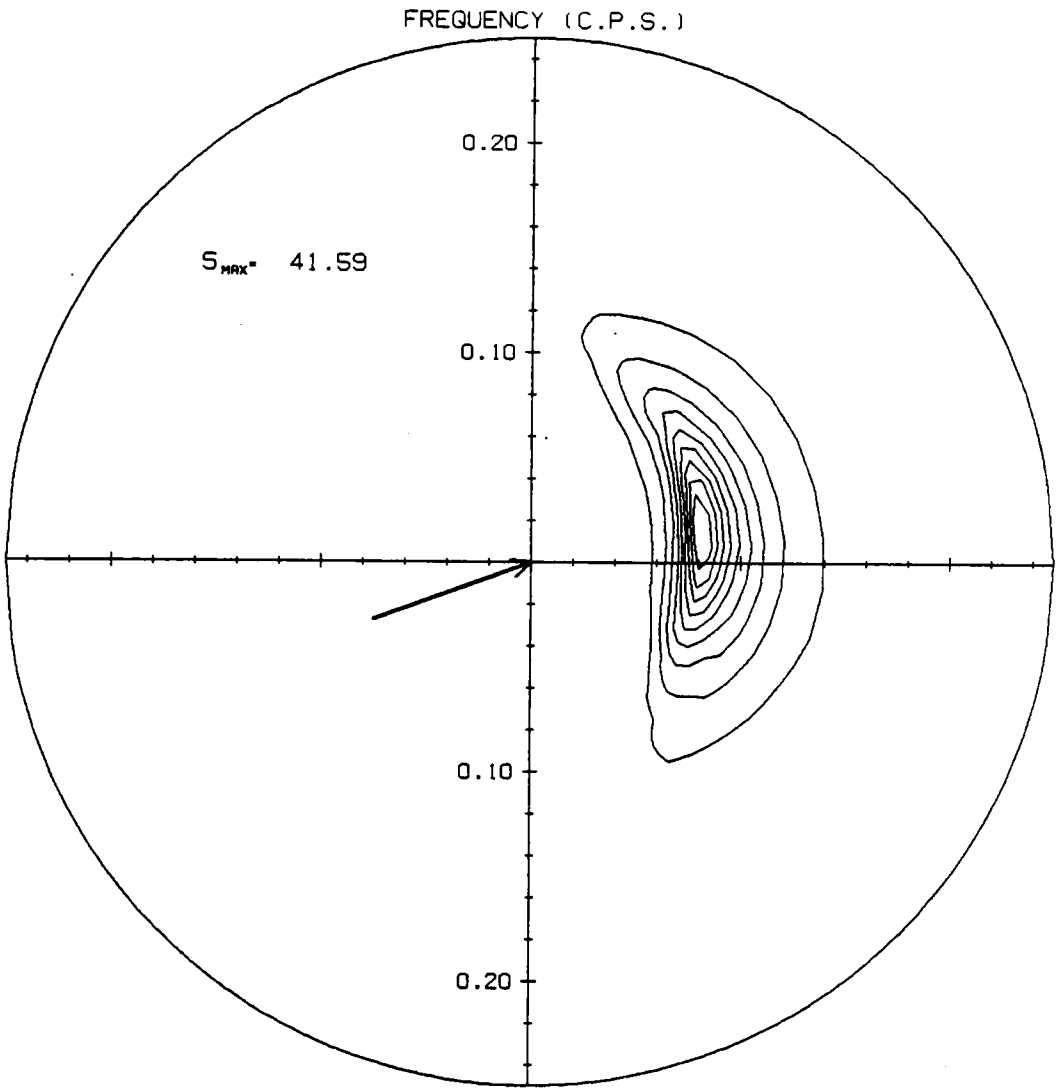

Fig. 17c. T=9 hours

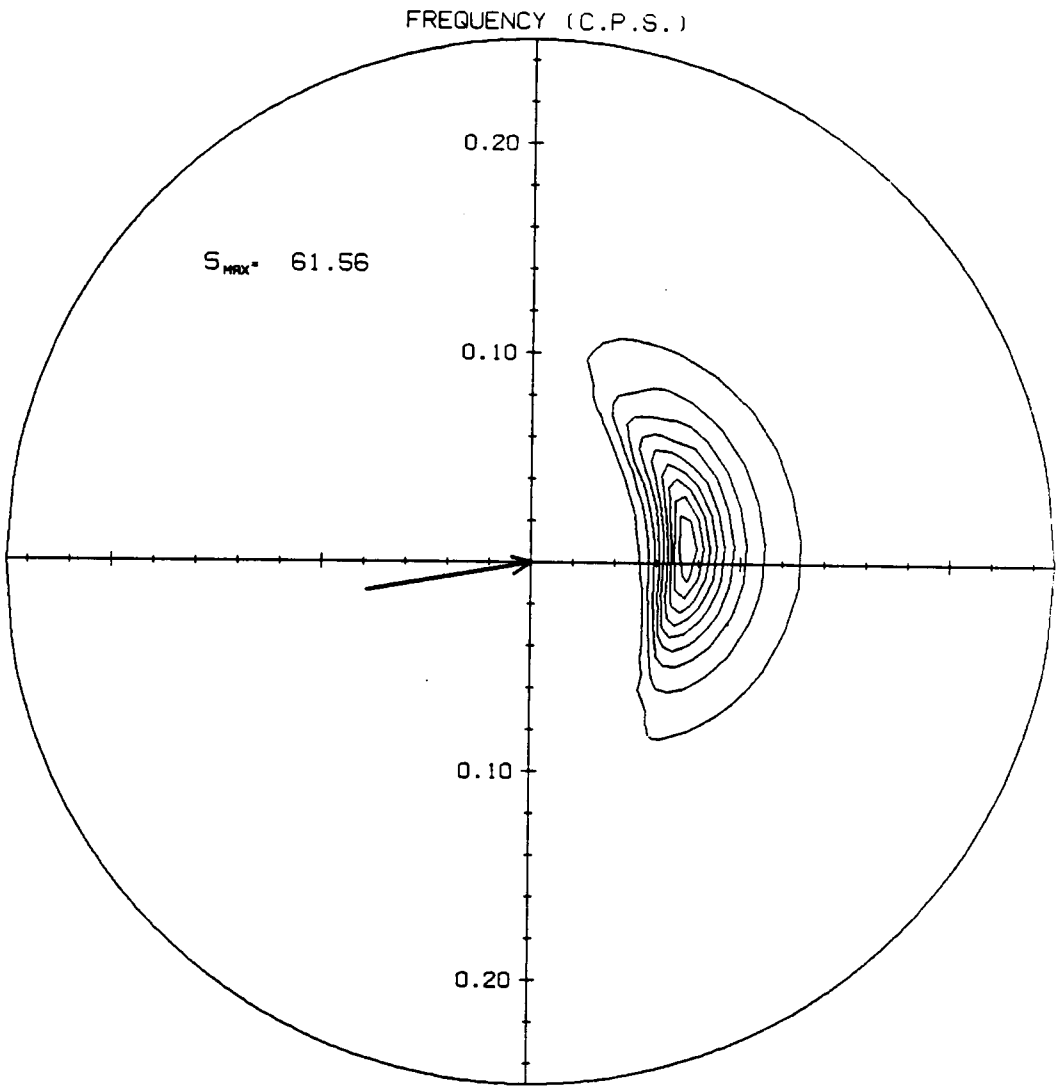

Fig. 17d. T=12 hours

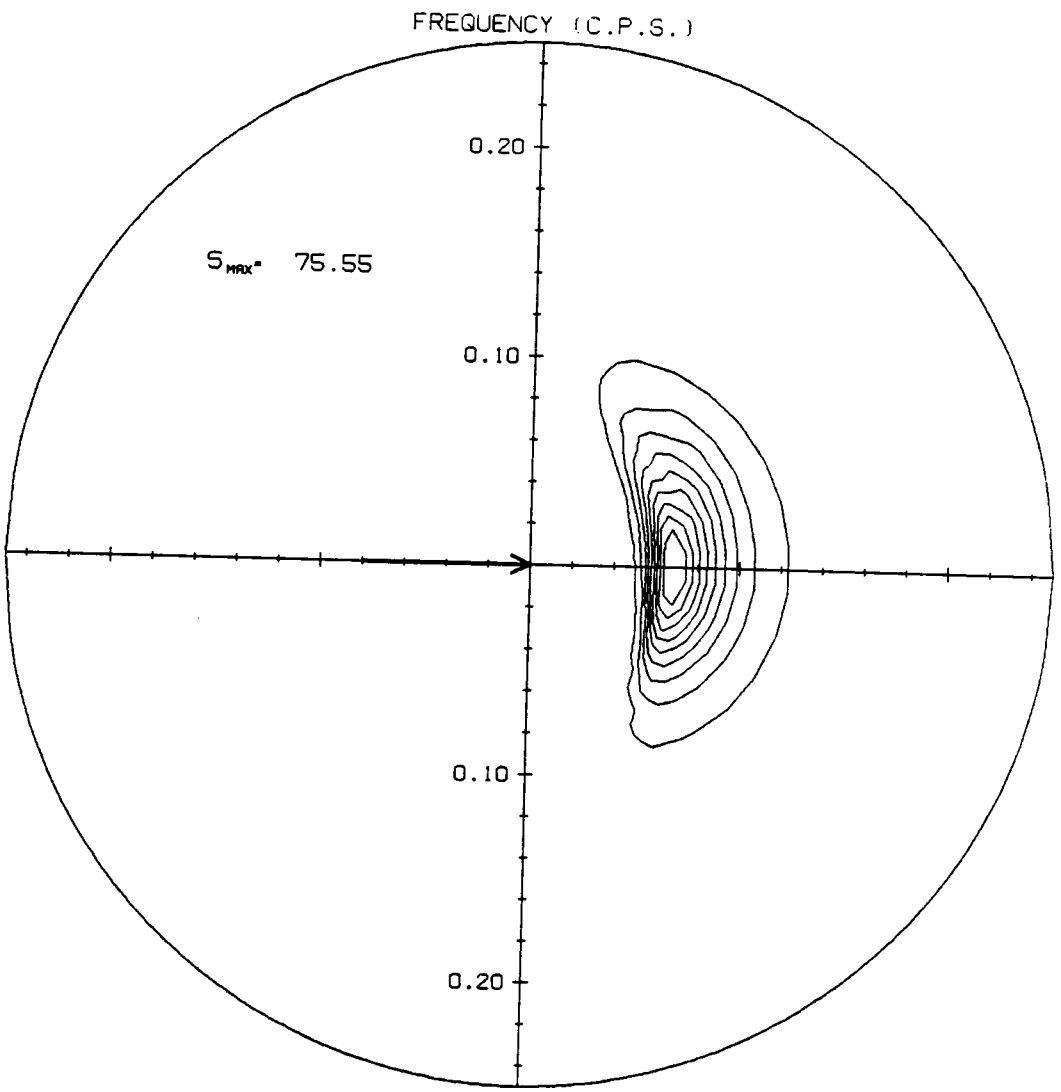

Fig. 17e. T=15 hours

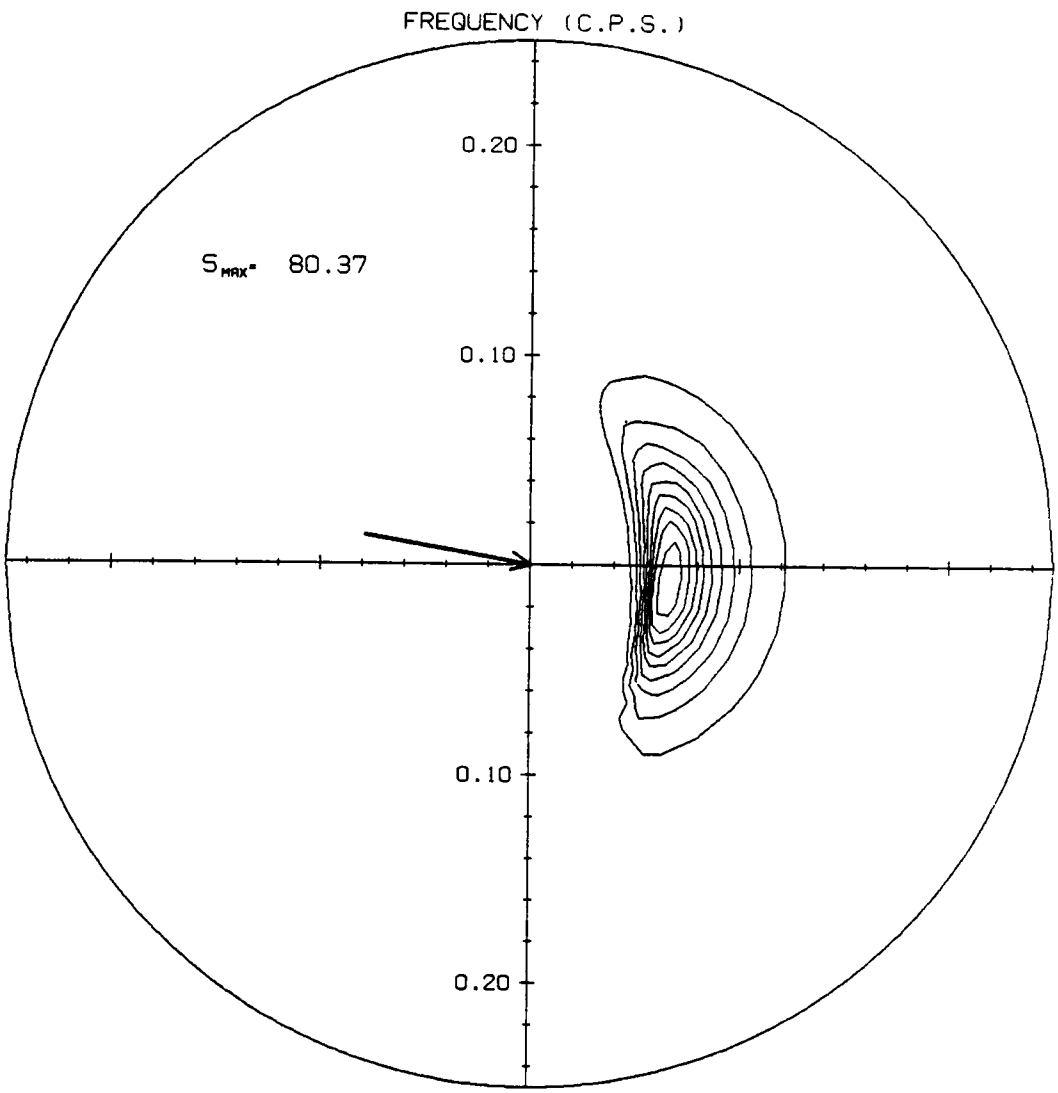

Fig. 17f. T=18 hours

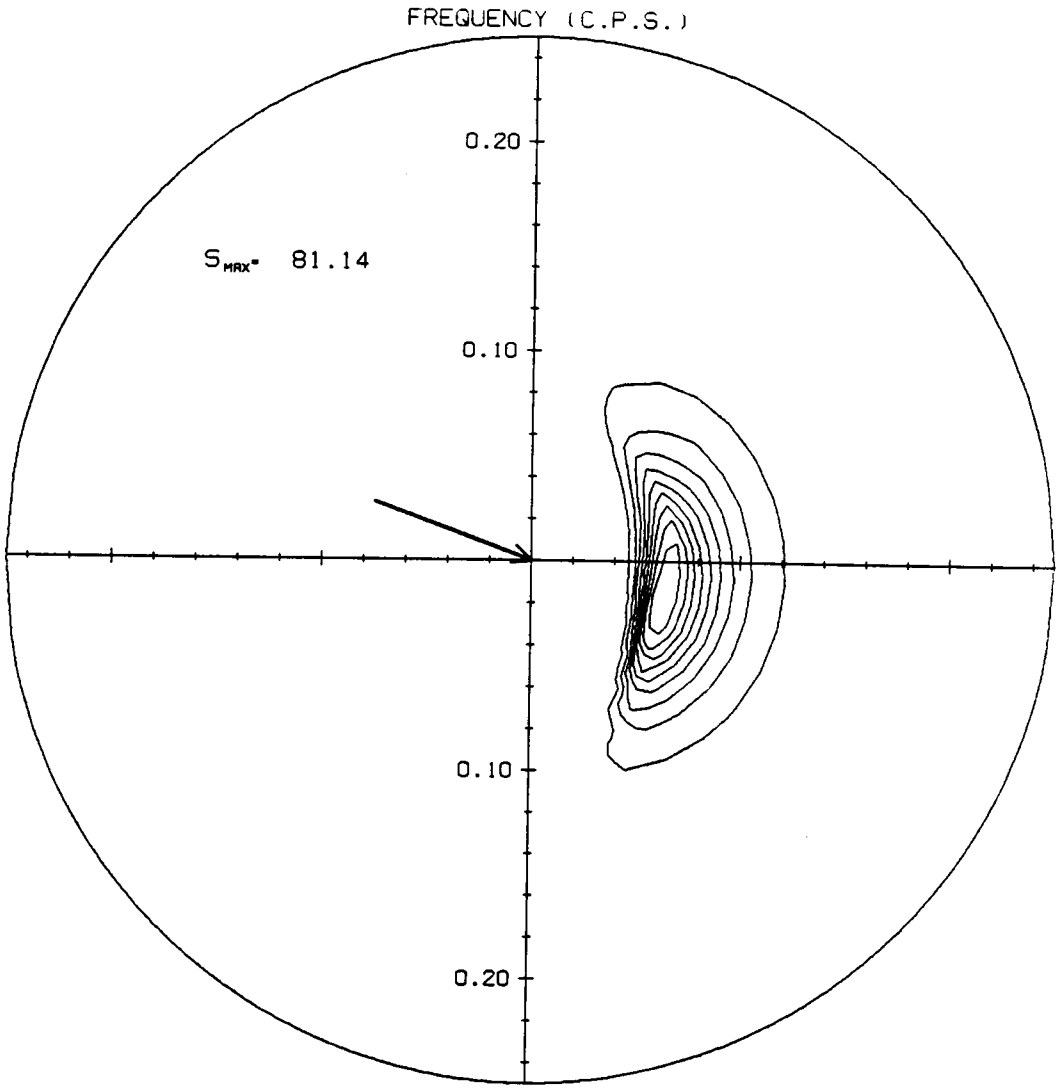

Fig. 17g. T=21 hours

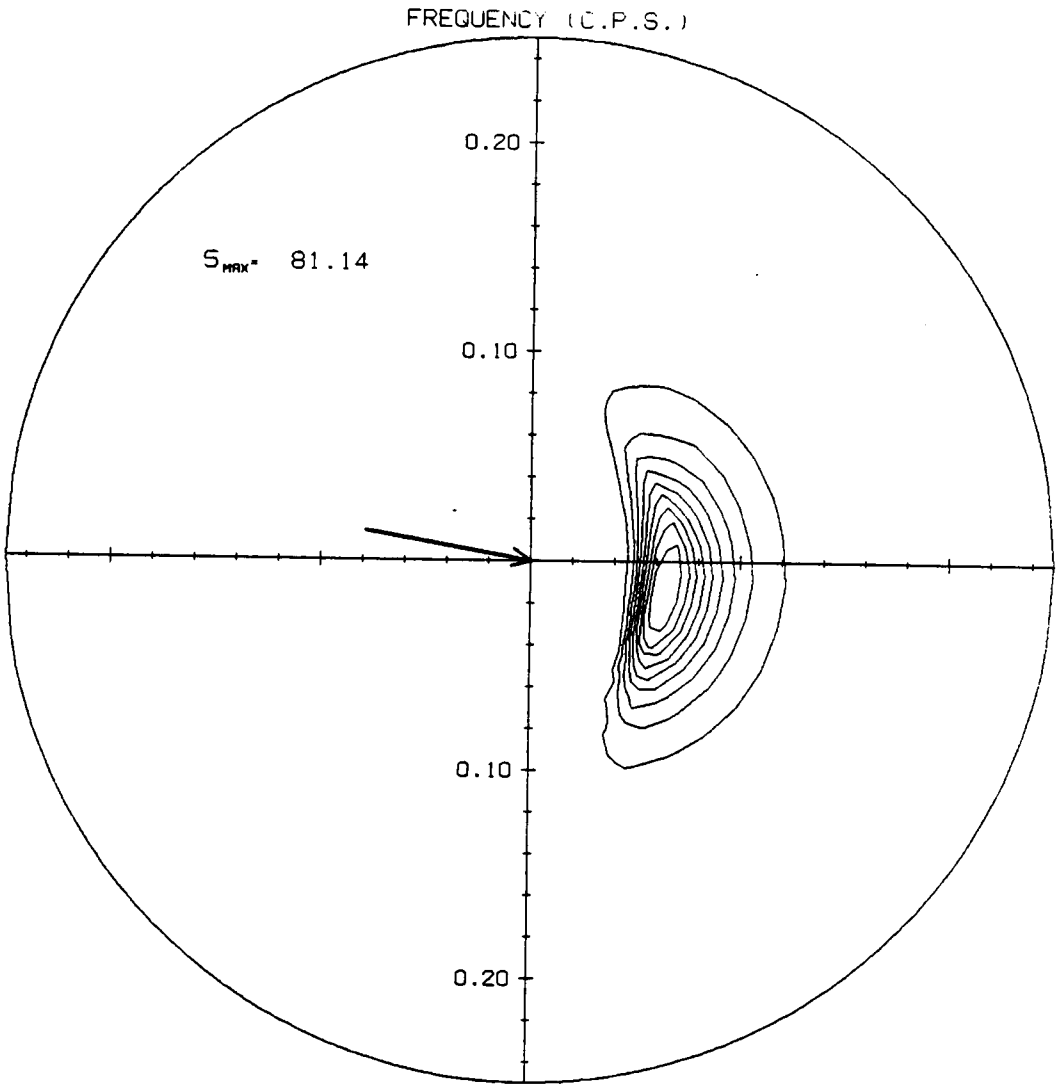

Fig. 17h. T=24 hours

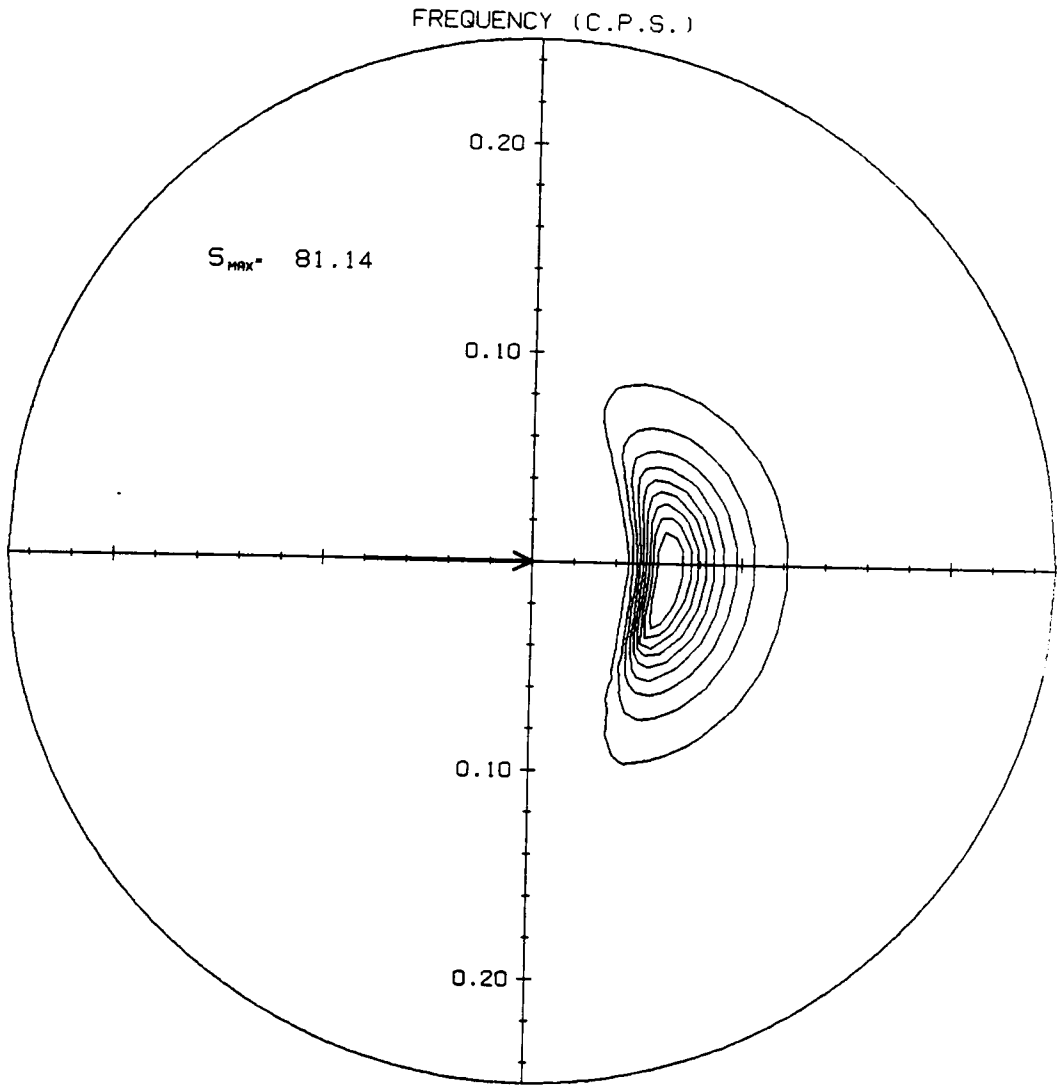

Fig. 17i. T=27 hours

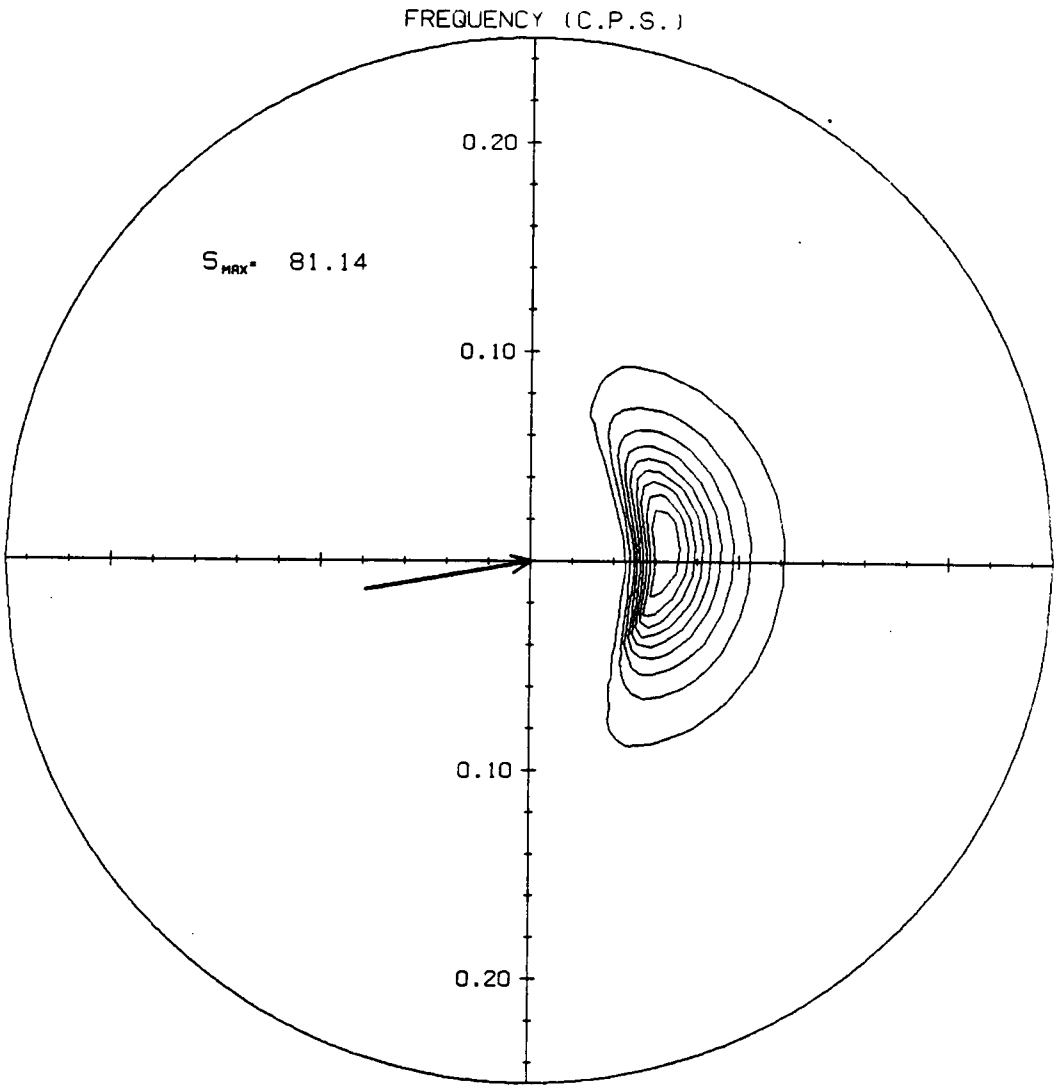

Fig. 17j. T=30 hours

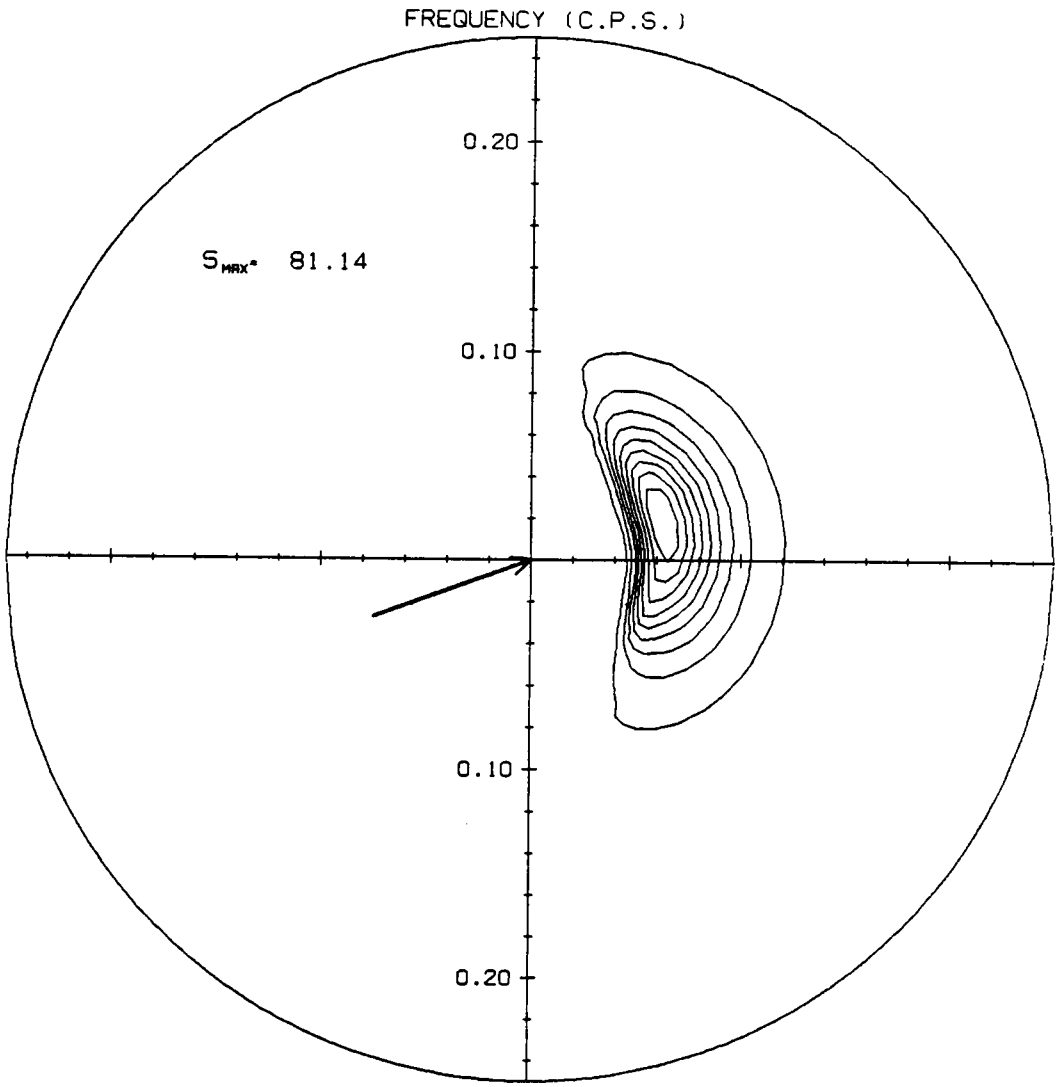

Fig. 17k. T=33 hours

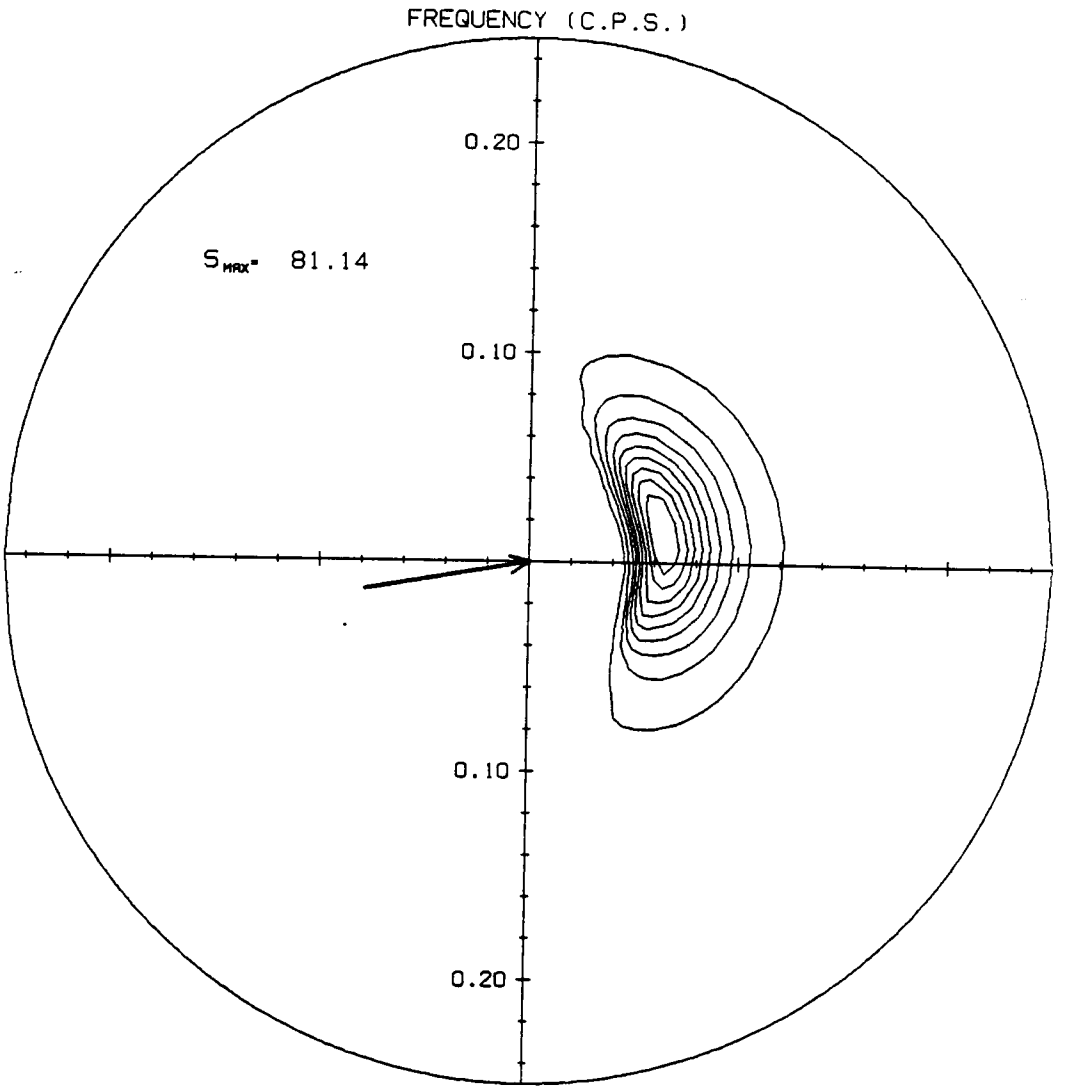

Fig. 171. T=36 hours

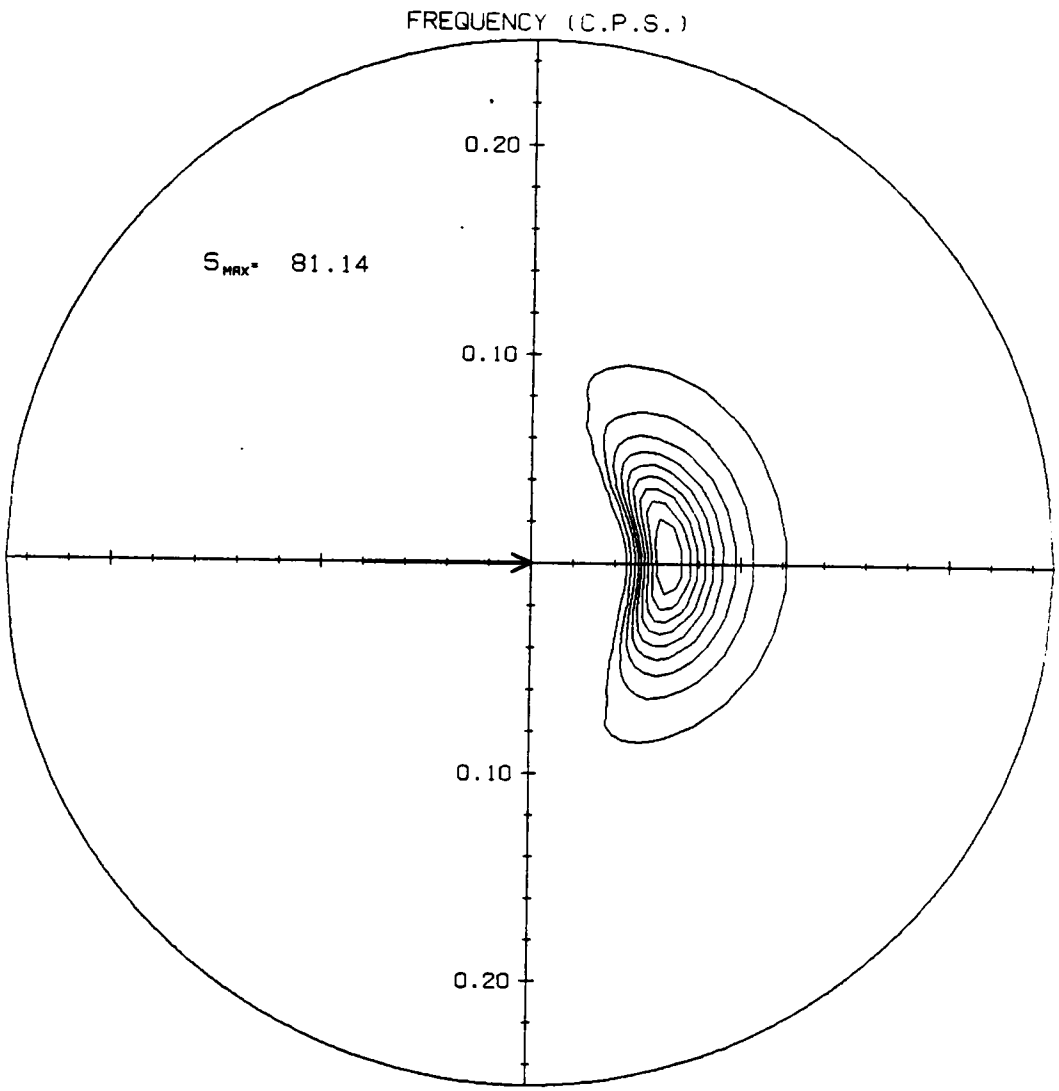

Fig. 17m. T=39 hours

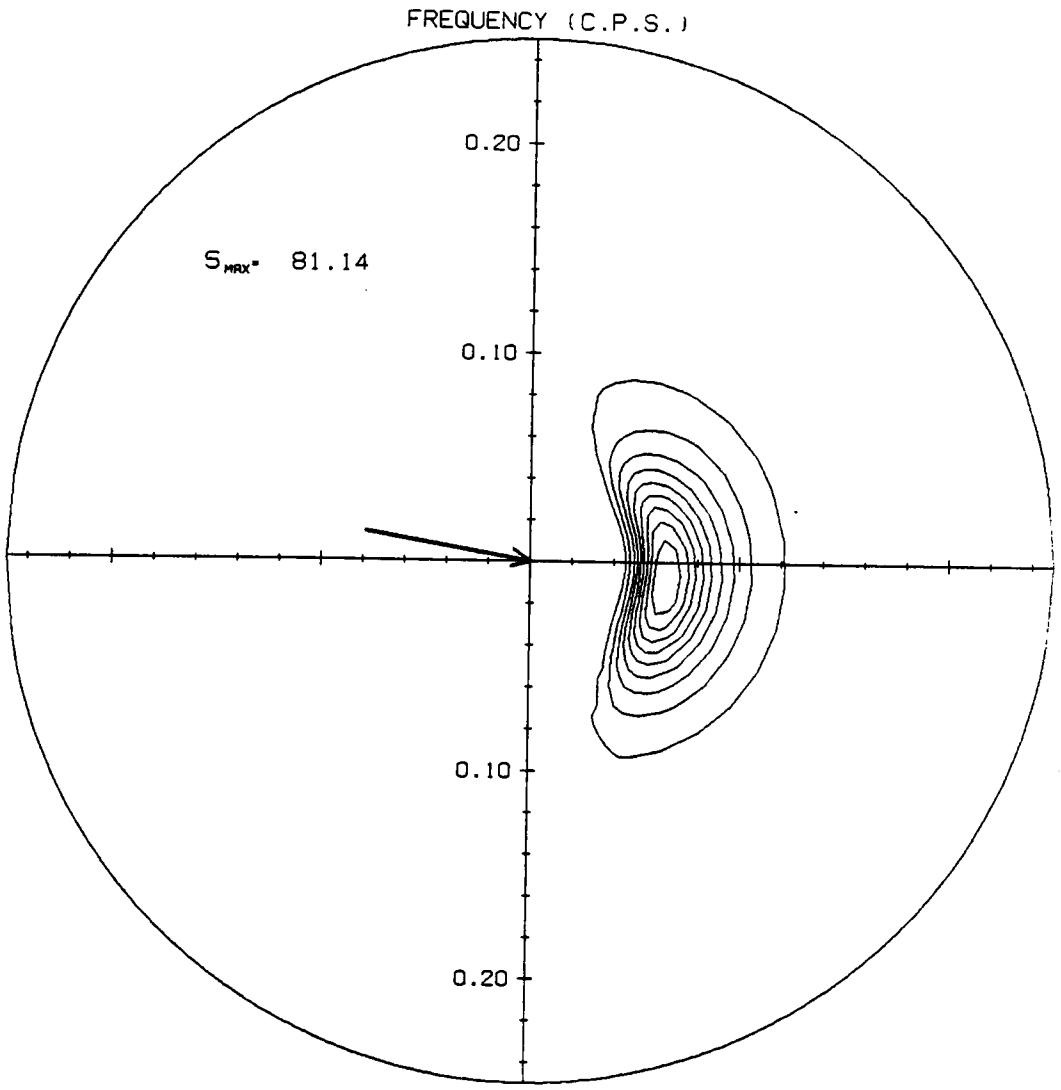

Fig. 17n. T=42 hours

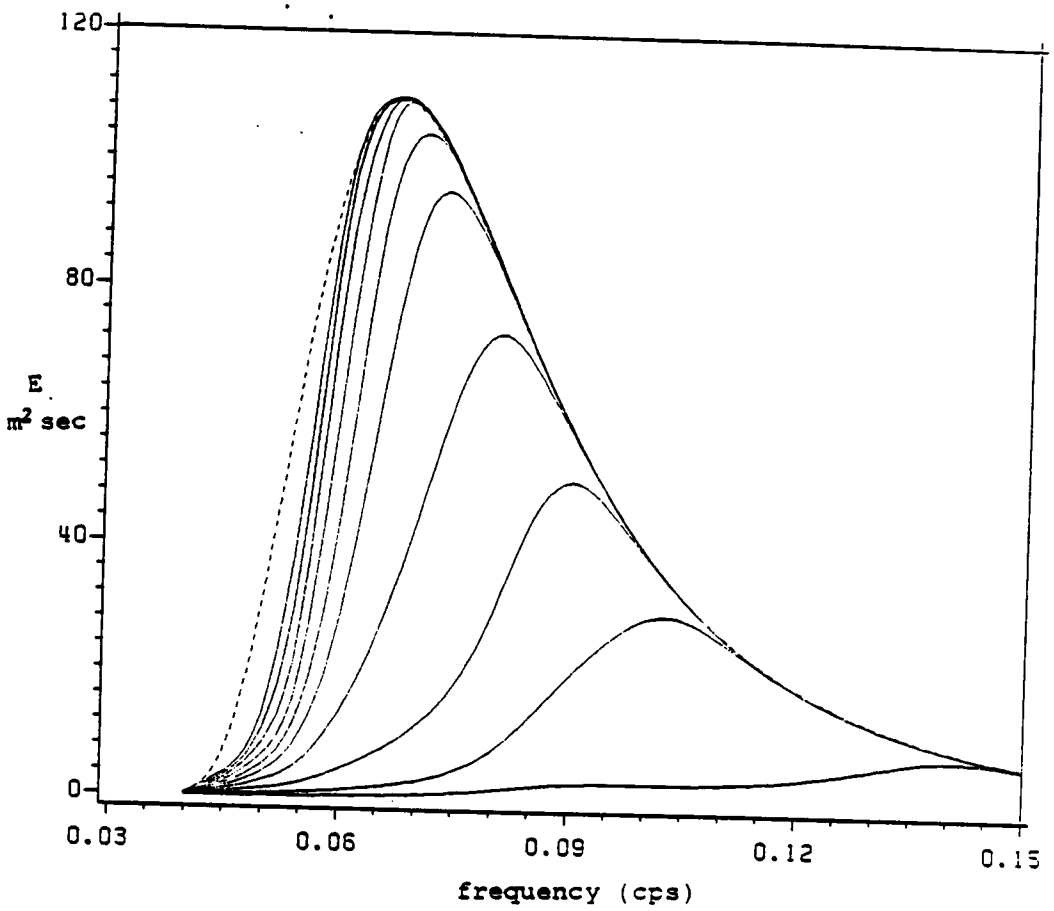

Fig. 18. Point spectrum evolution for a 40 knot wind oscillating in direction from VSOWM.

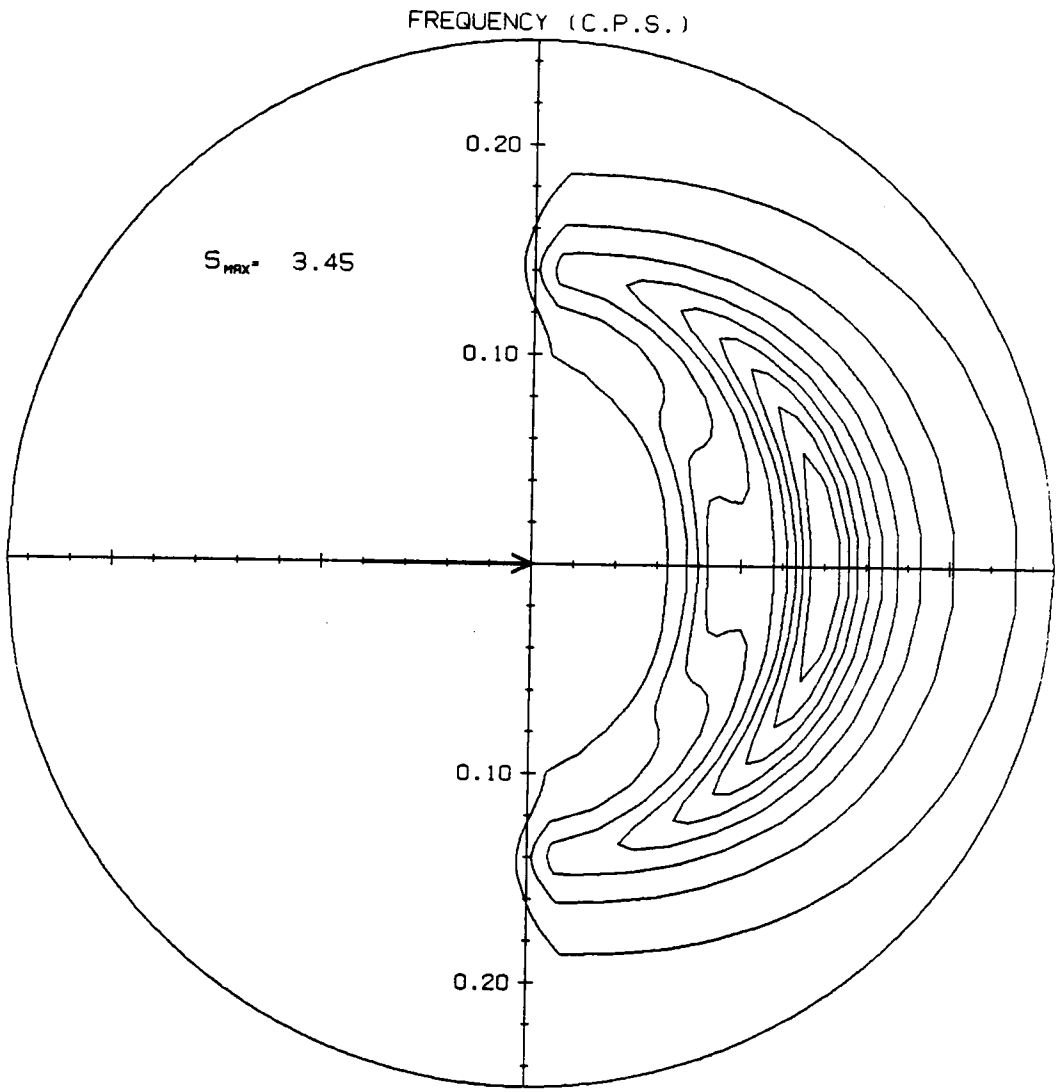

Fig. 19a. Contour plots of 2-D spectrum evolution for an oscillating 40 knot wind from VSOWM. T=3 hours

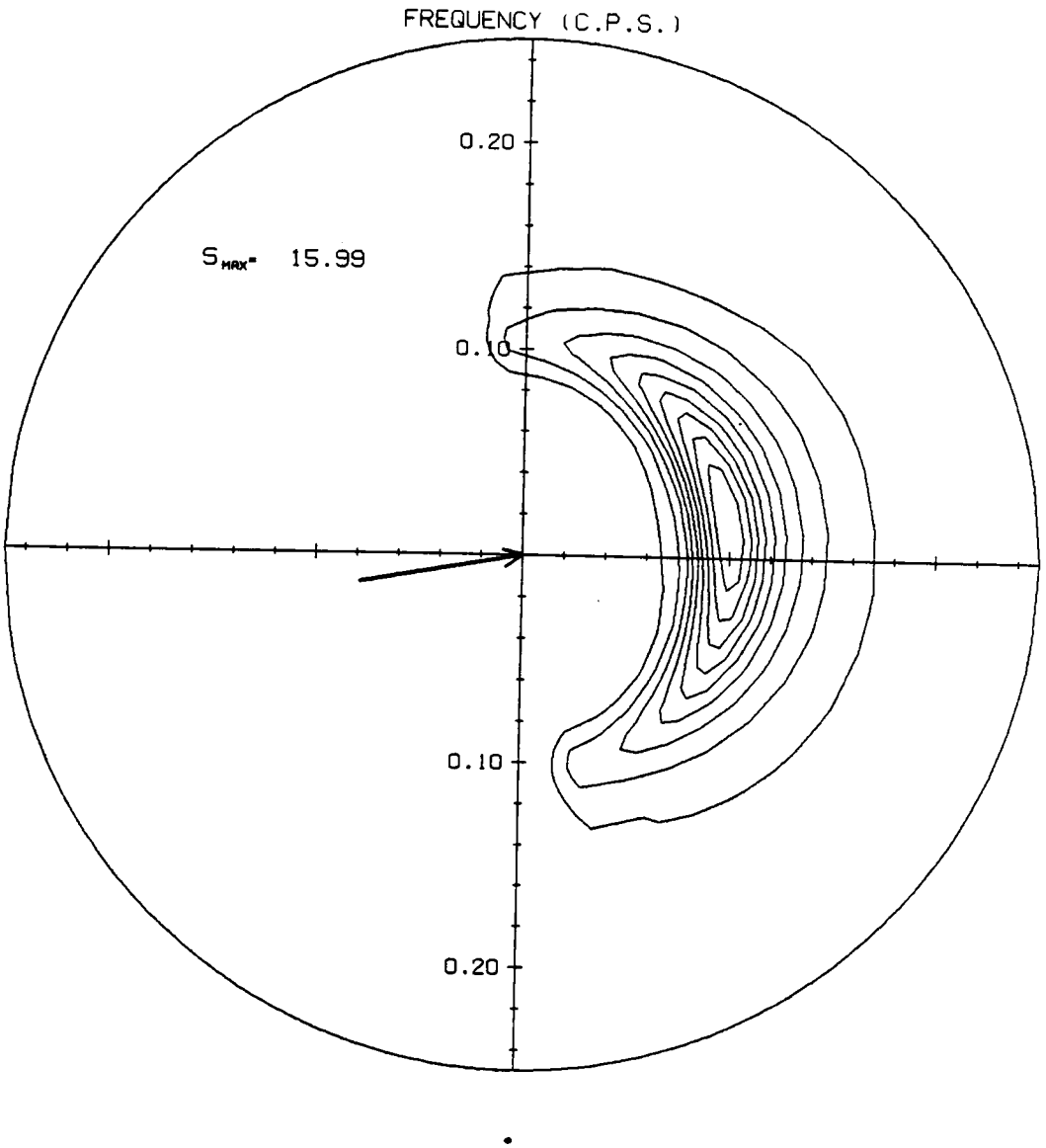

Fig. 19b. T=6 hours

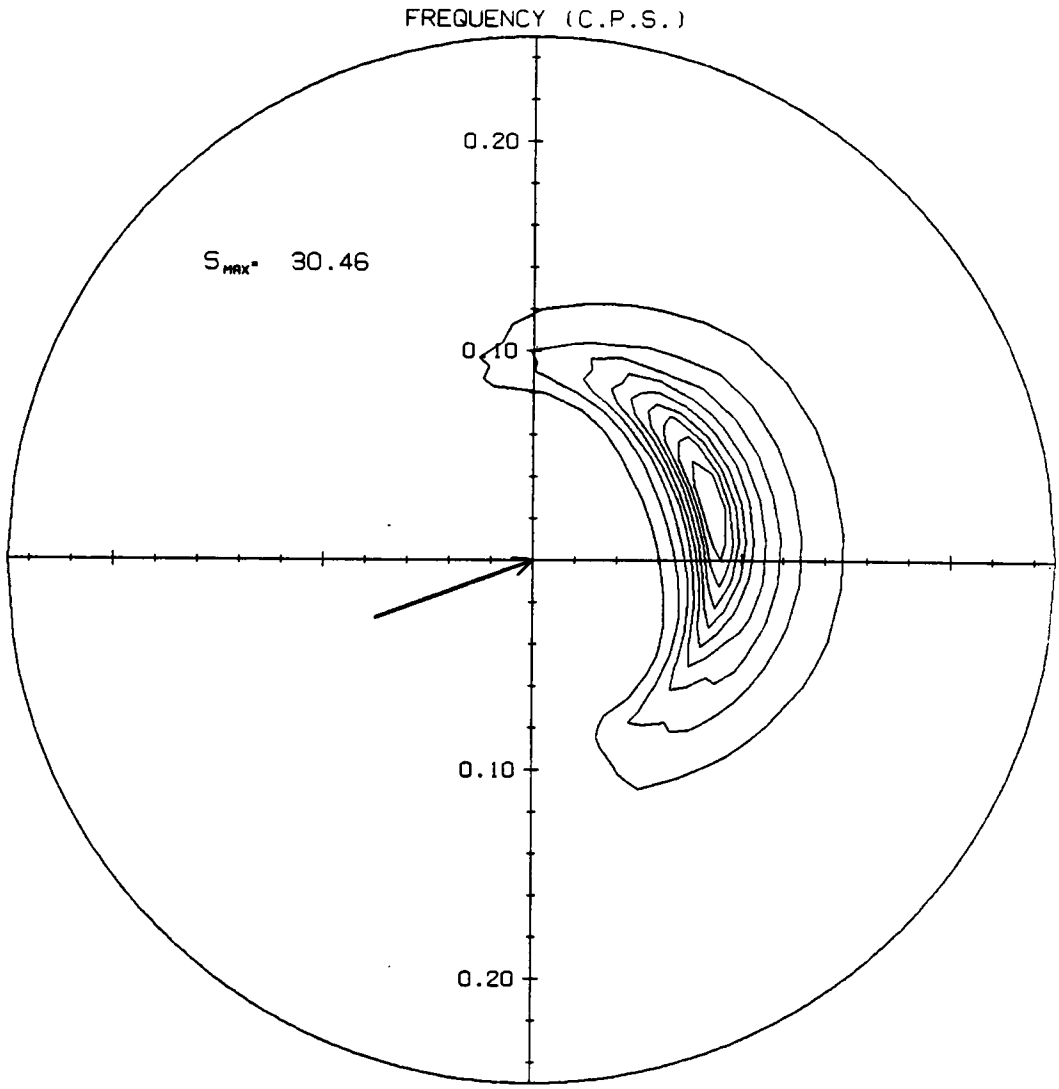

Fig. 19c. T=9 hours

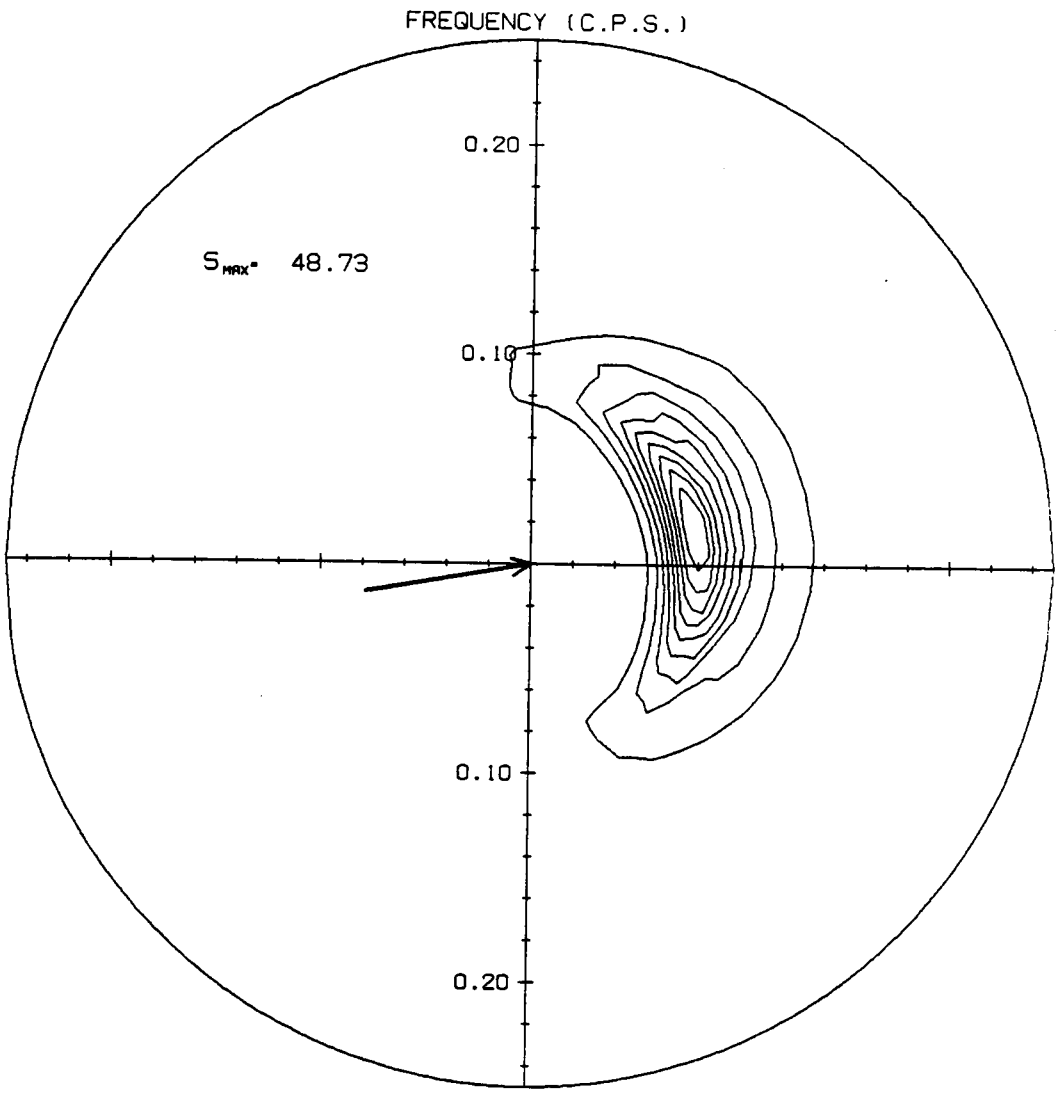

Fig. 19d. T=12 hours

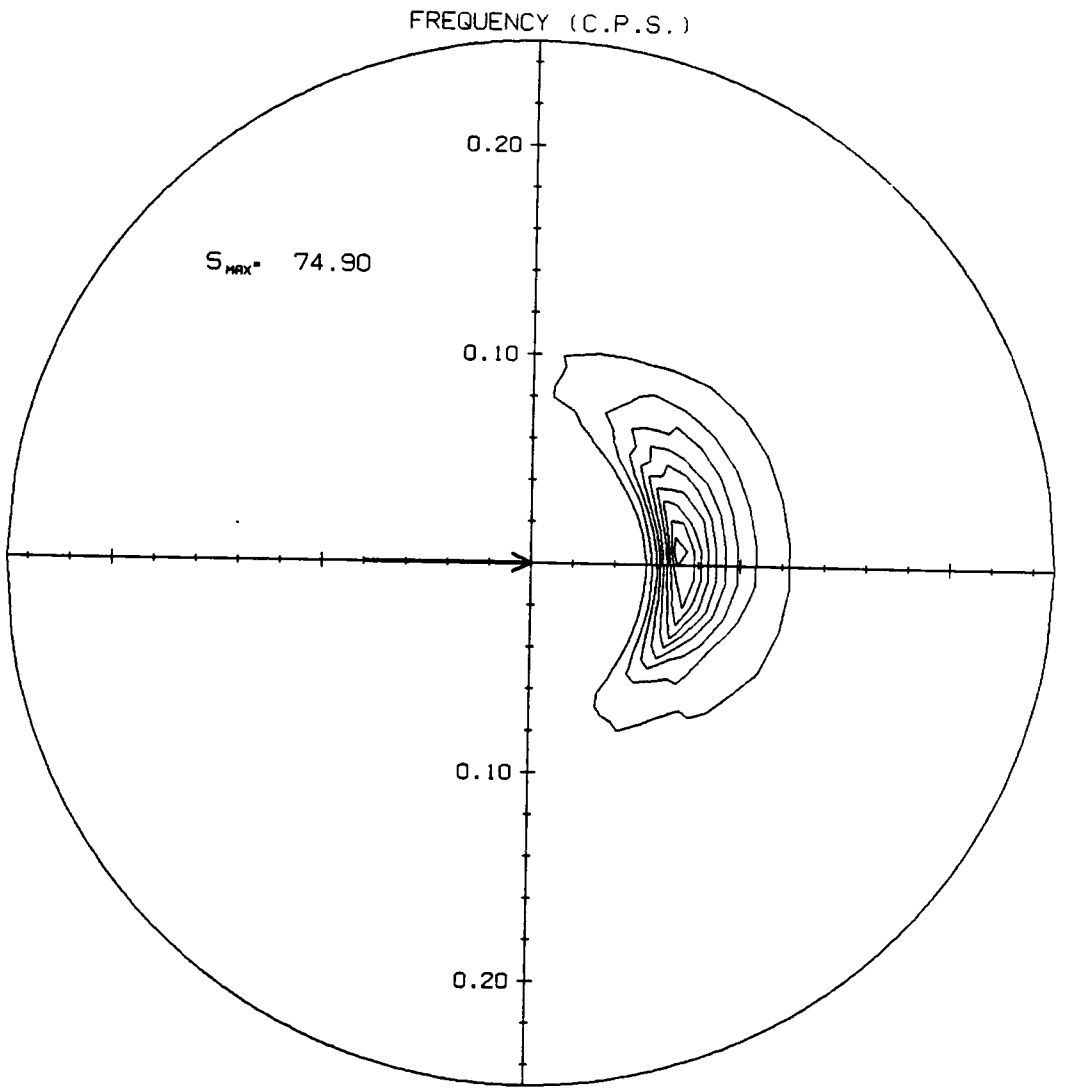

Fig. 19e. T=15 hours

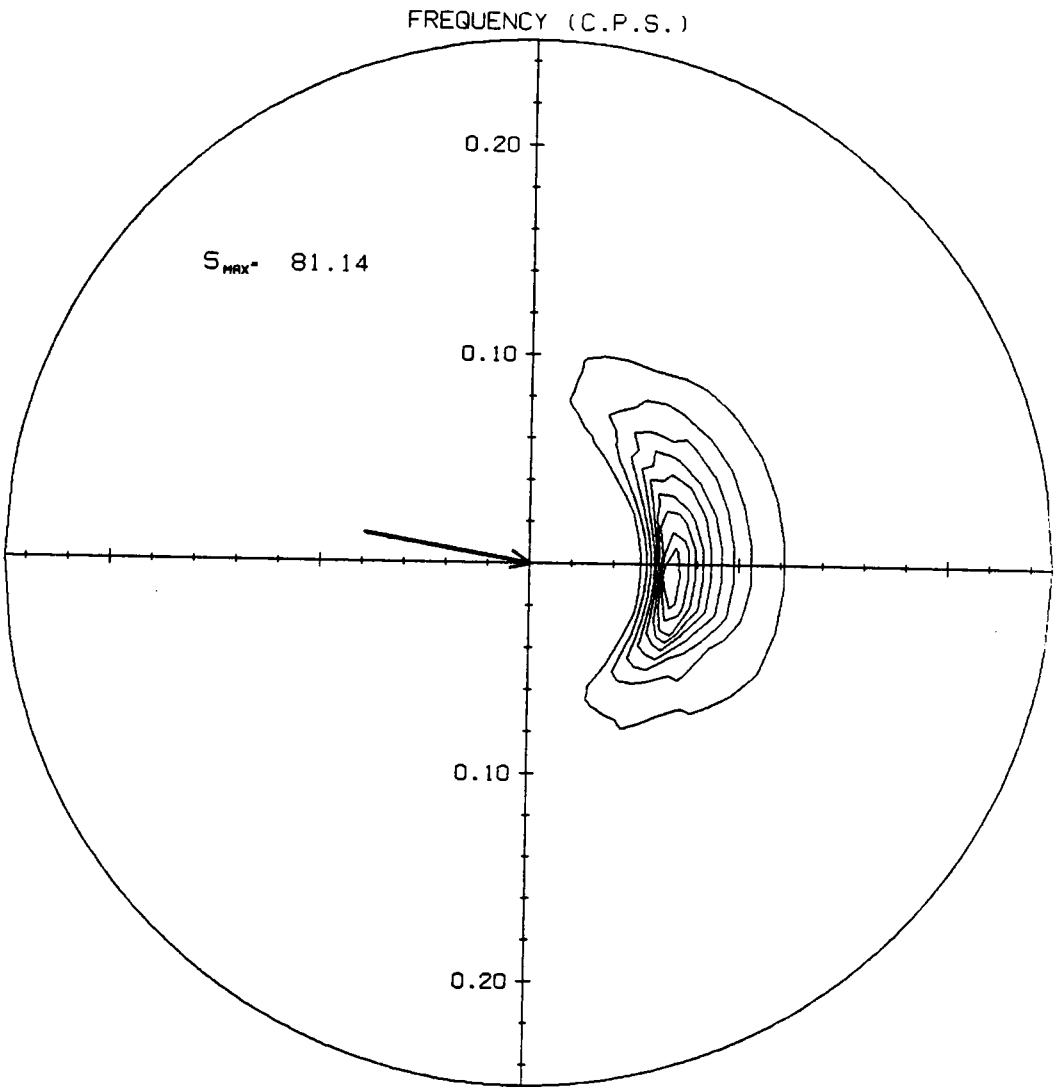

Fig. 19f. T=18 hours

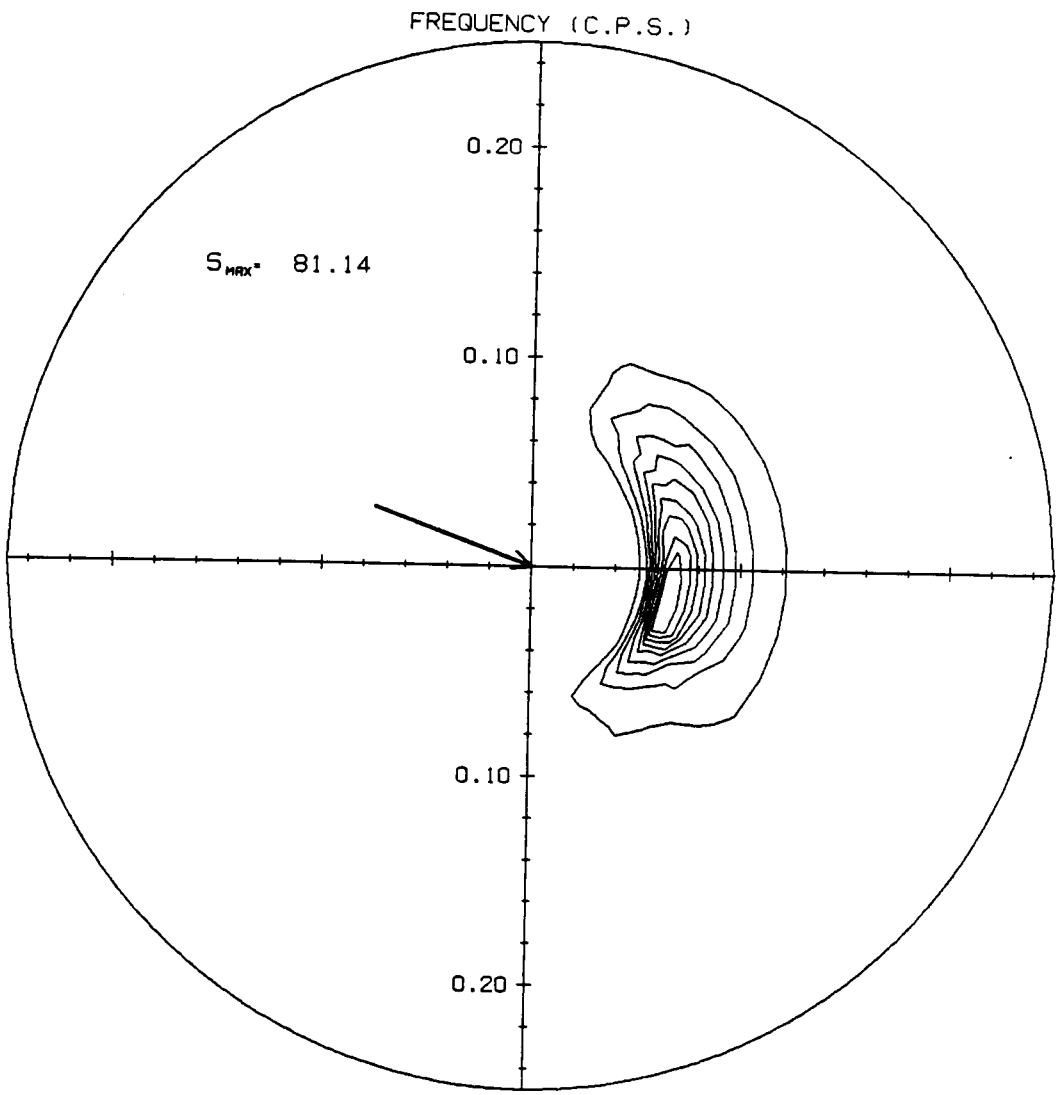

Fig. 19g. T=21 hours

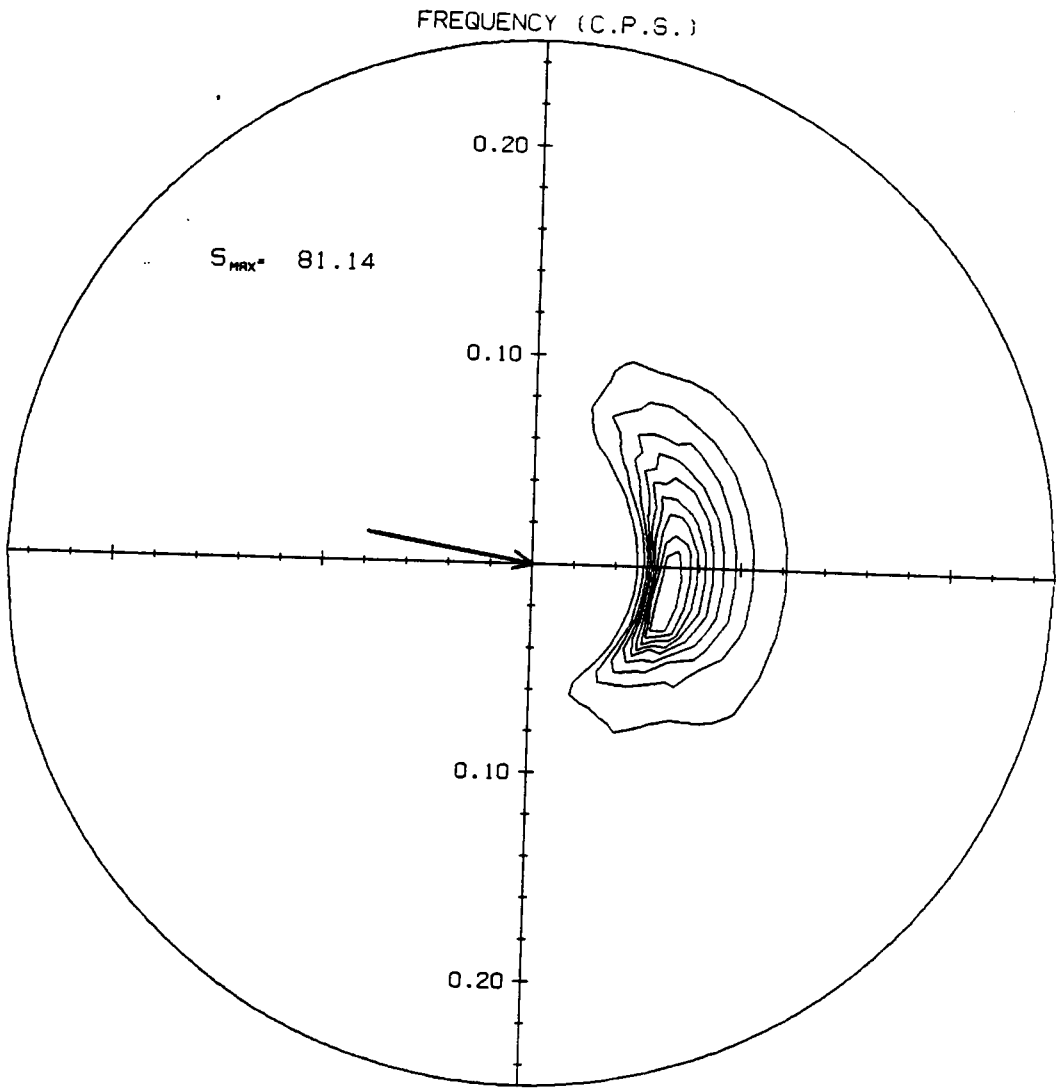

Fig. 19h. T=24 hours

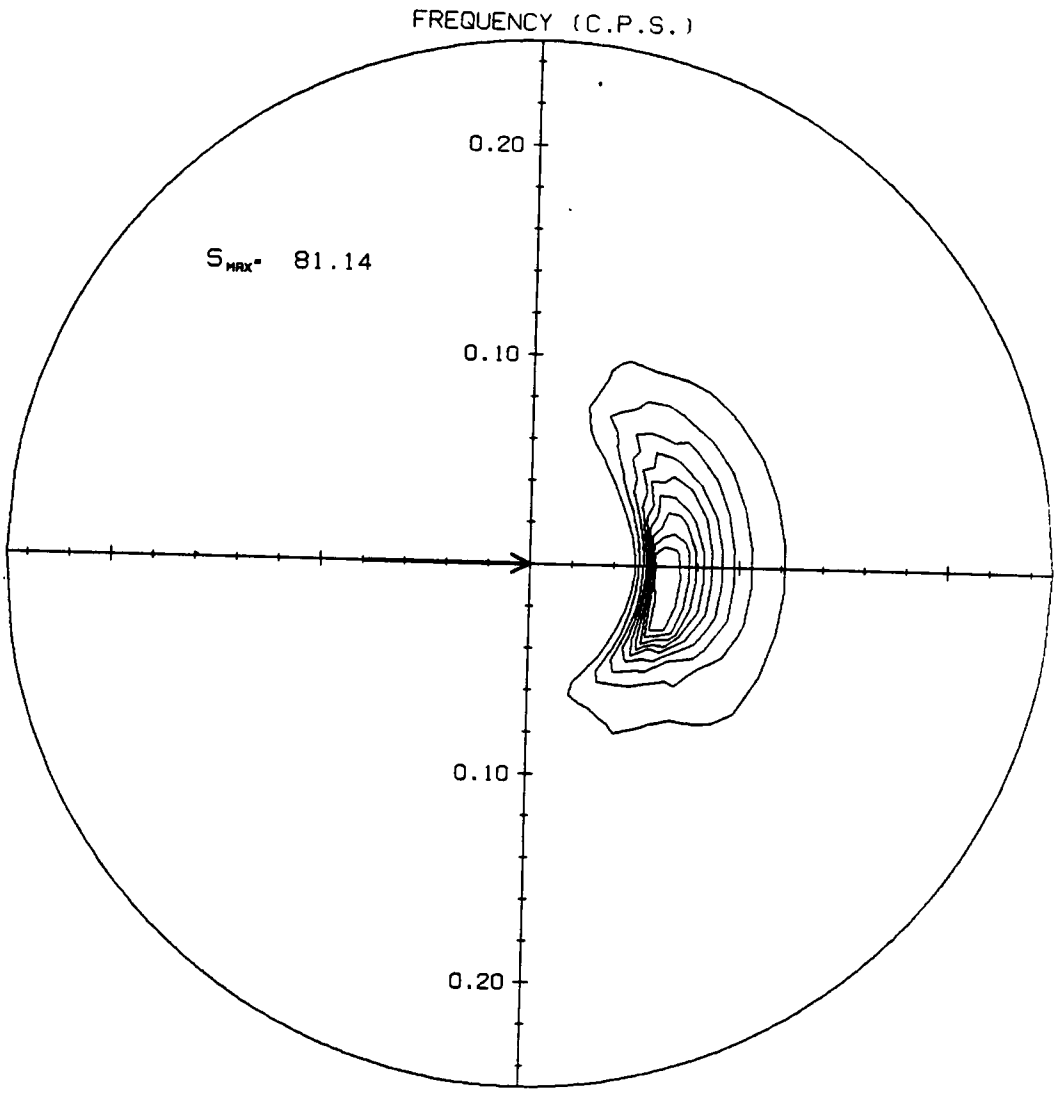

Fig. 19i. T=27 hours

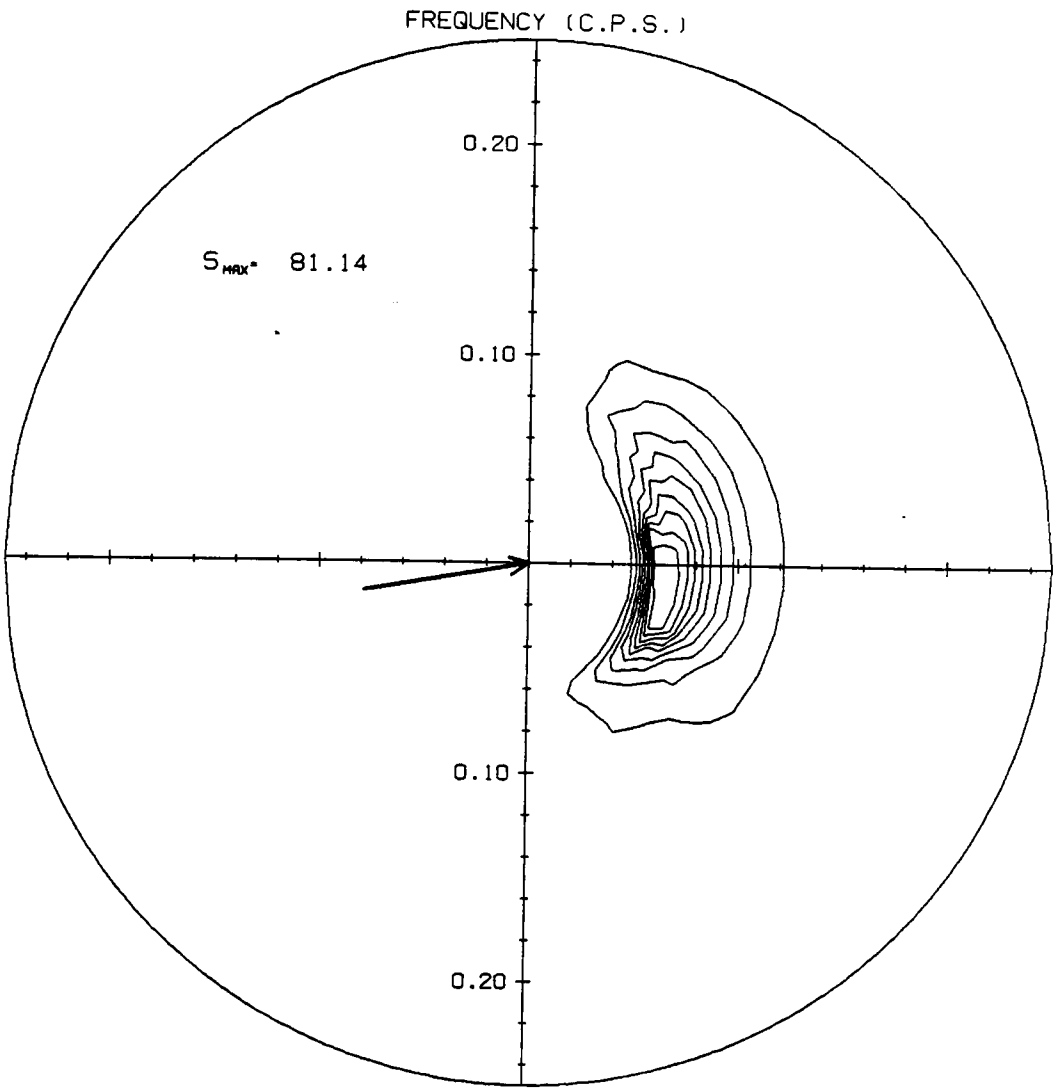

Fig. 19j. T=30 hours

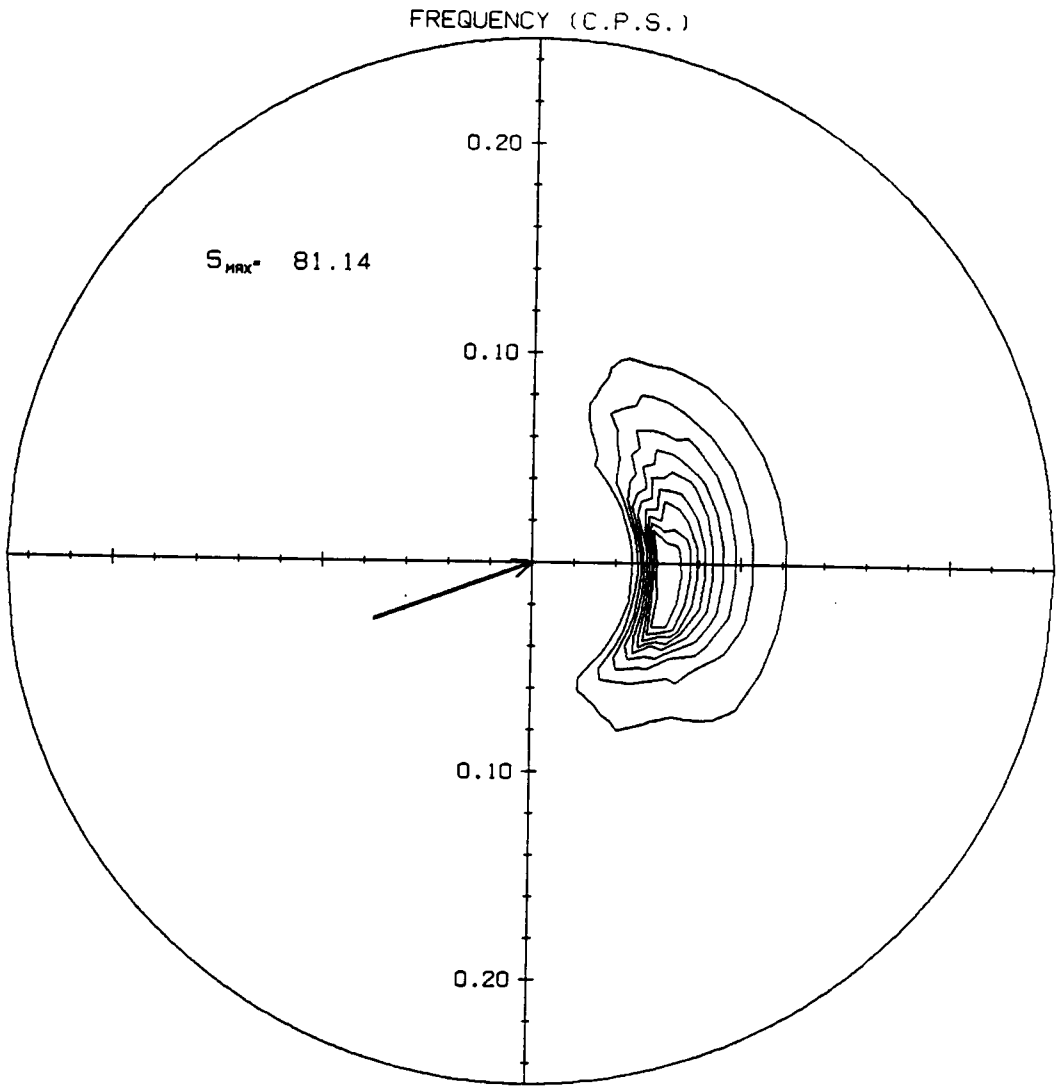

Fig. 19k. T=33 hours

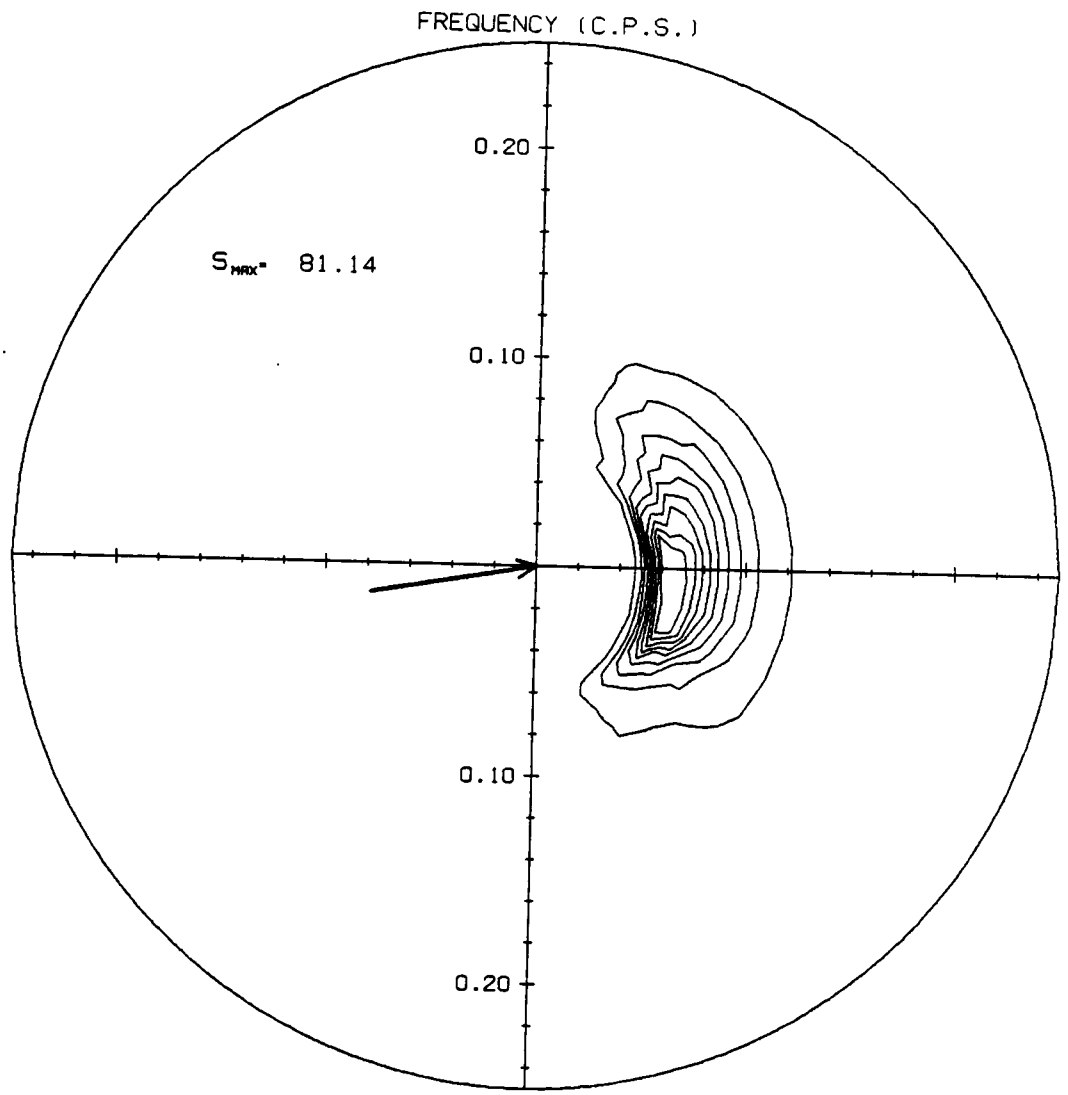

Fig. 191. T=36 hours

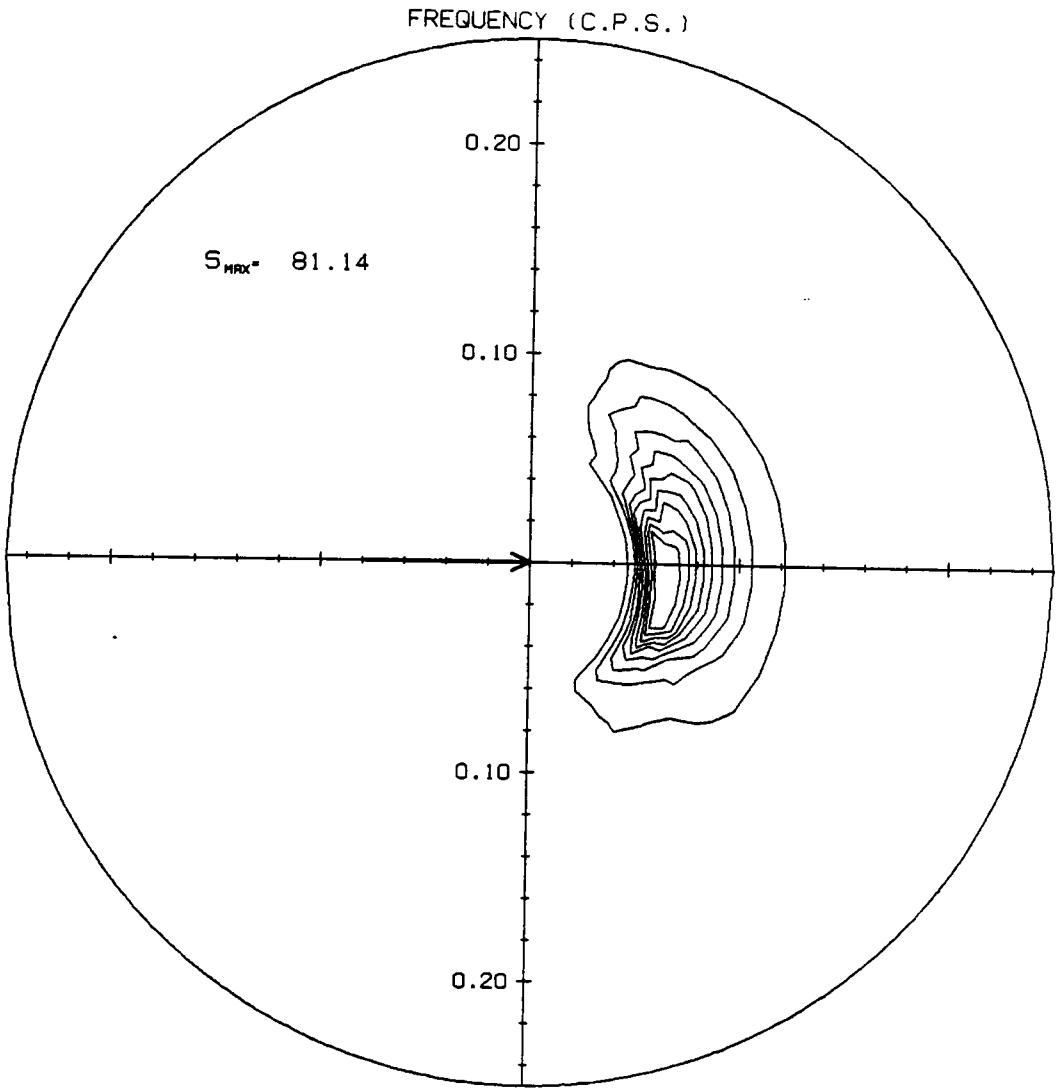

Fig. 19m. T=39 hours

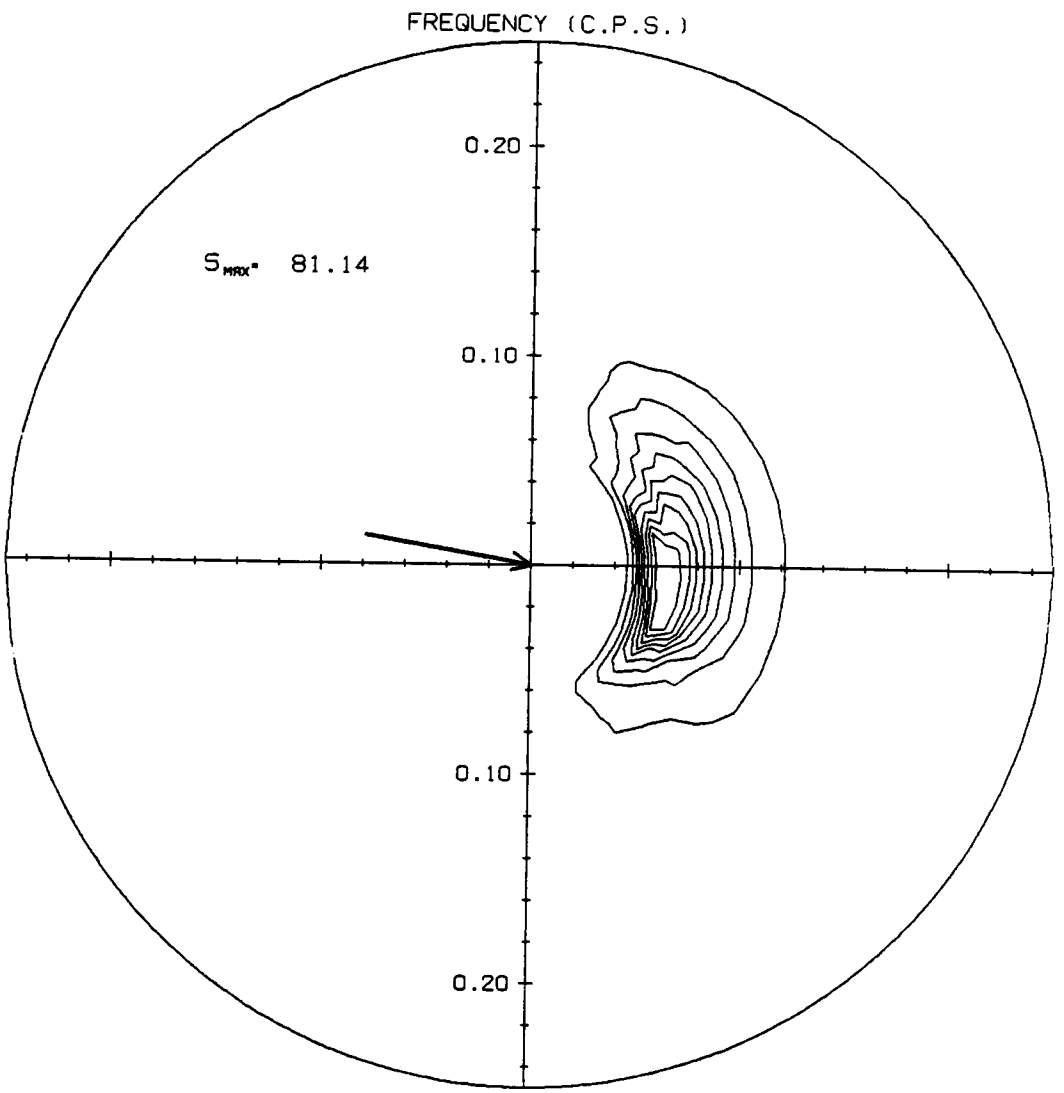

Fig. 19n. T=42 hours

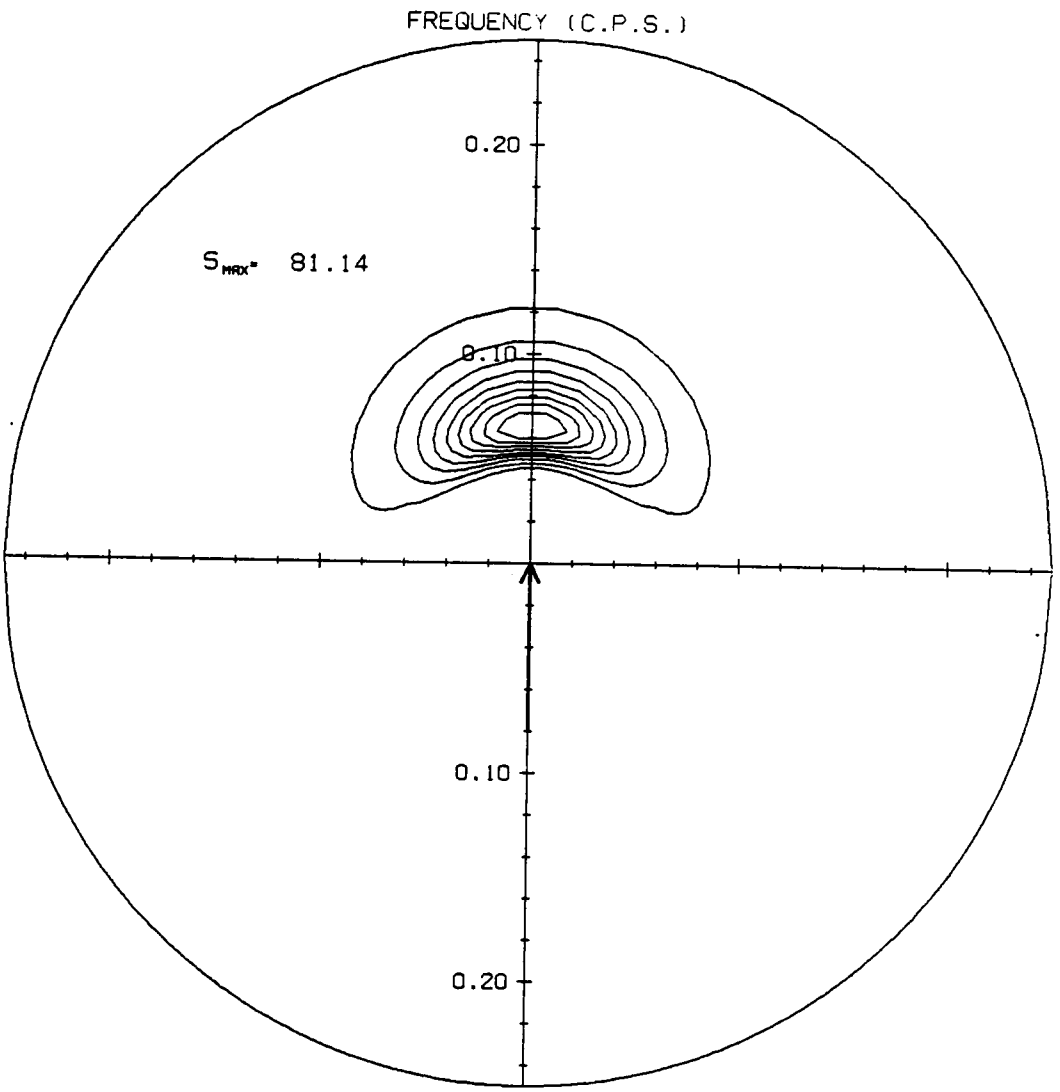

Fig. 20. Initial condition for 90 change of wind direction.

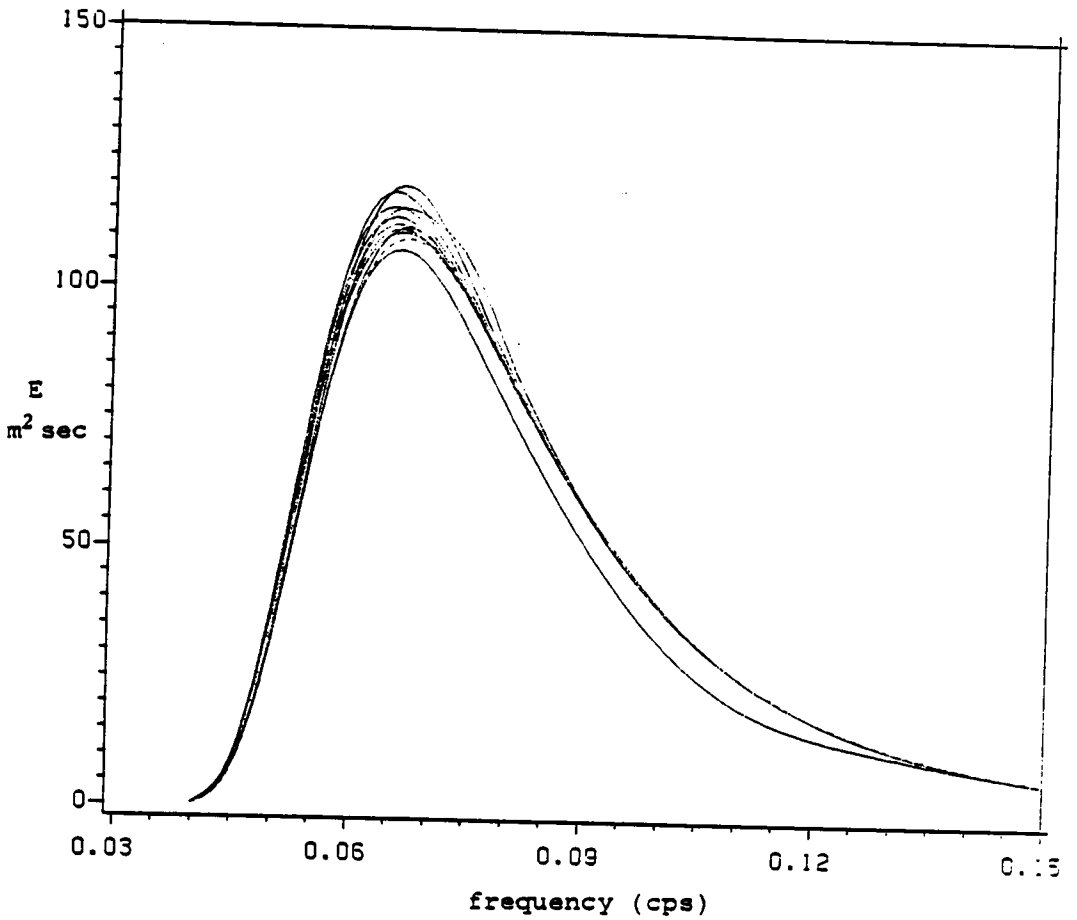

Fig. 21. Point spectrum evolution for 90° change of wind direction from VPINK.

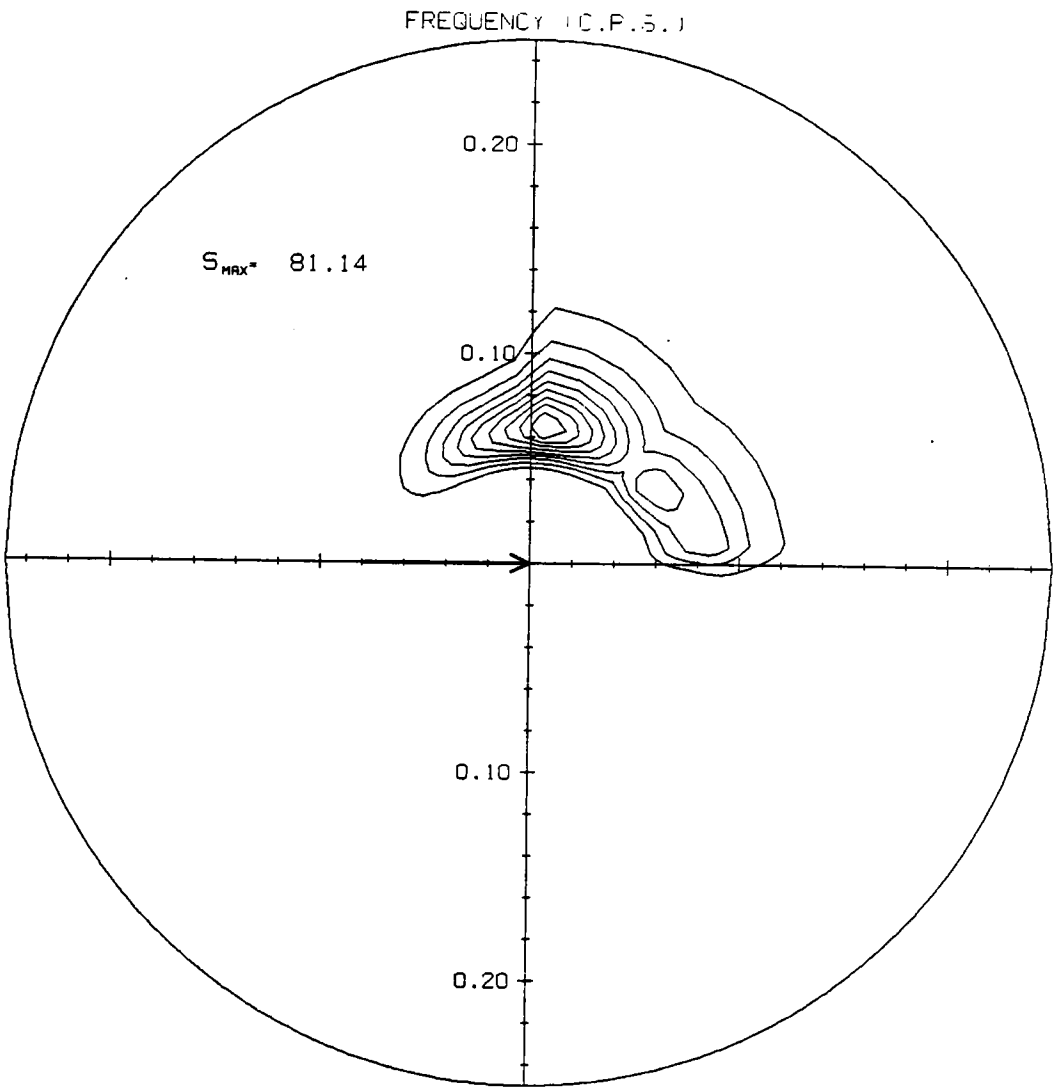

Fig. 22a. Contour plots of 2-D spectrum evolution for 90° change of wind direction from VPINK. T=3 hours

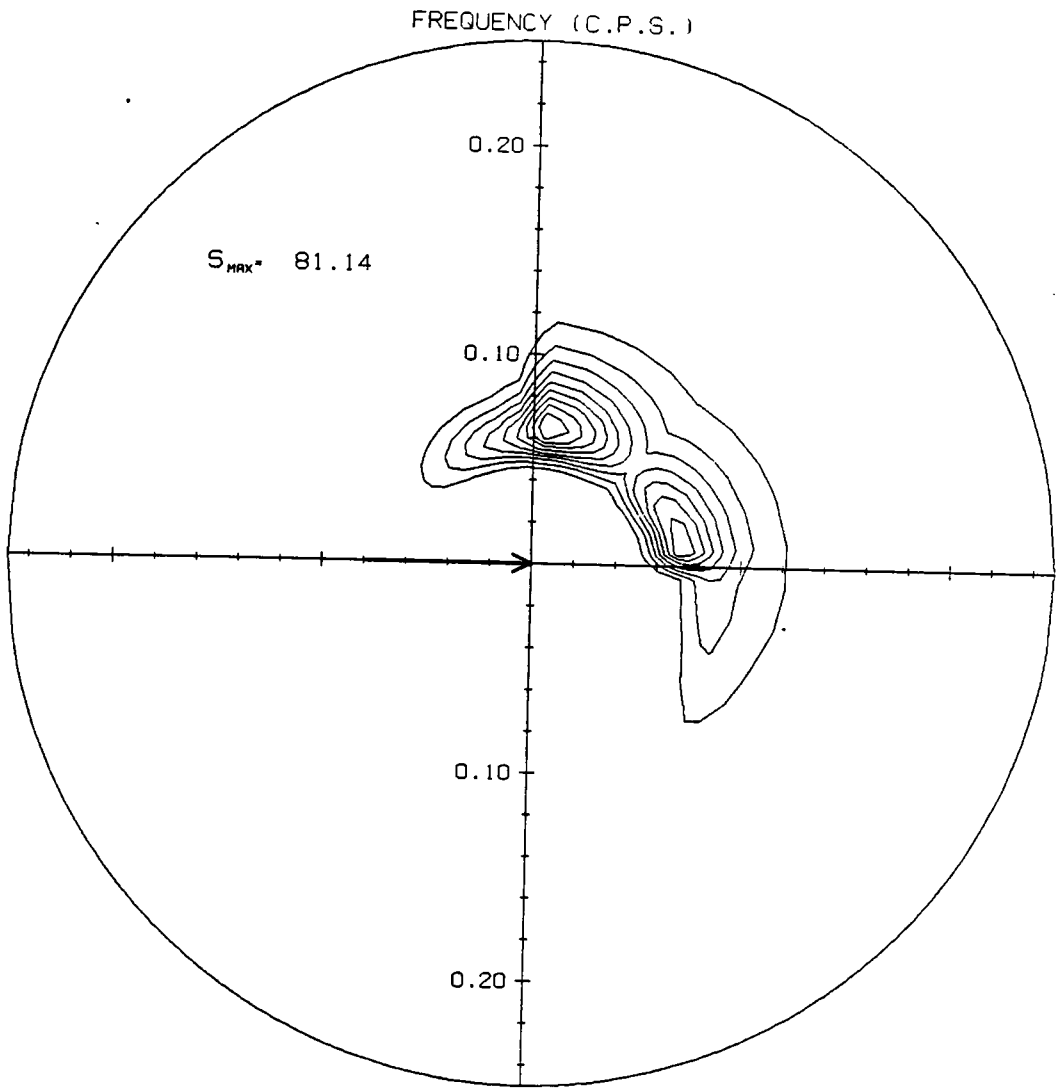

Fig. 22b. T=6 hours

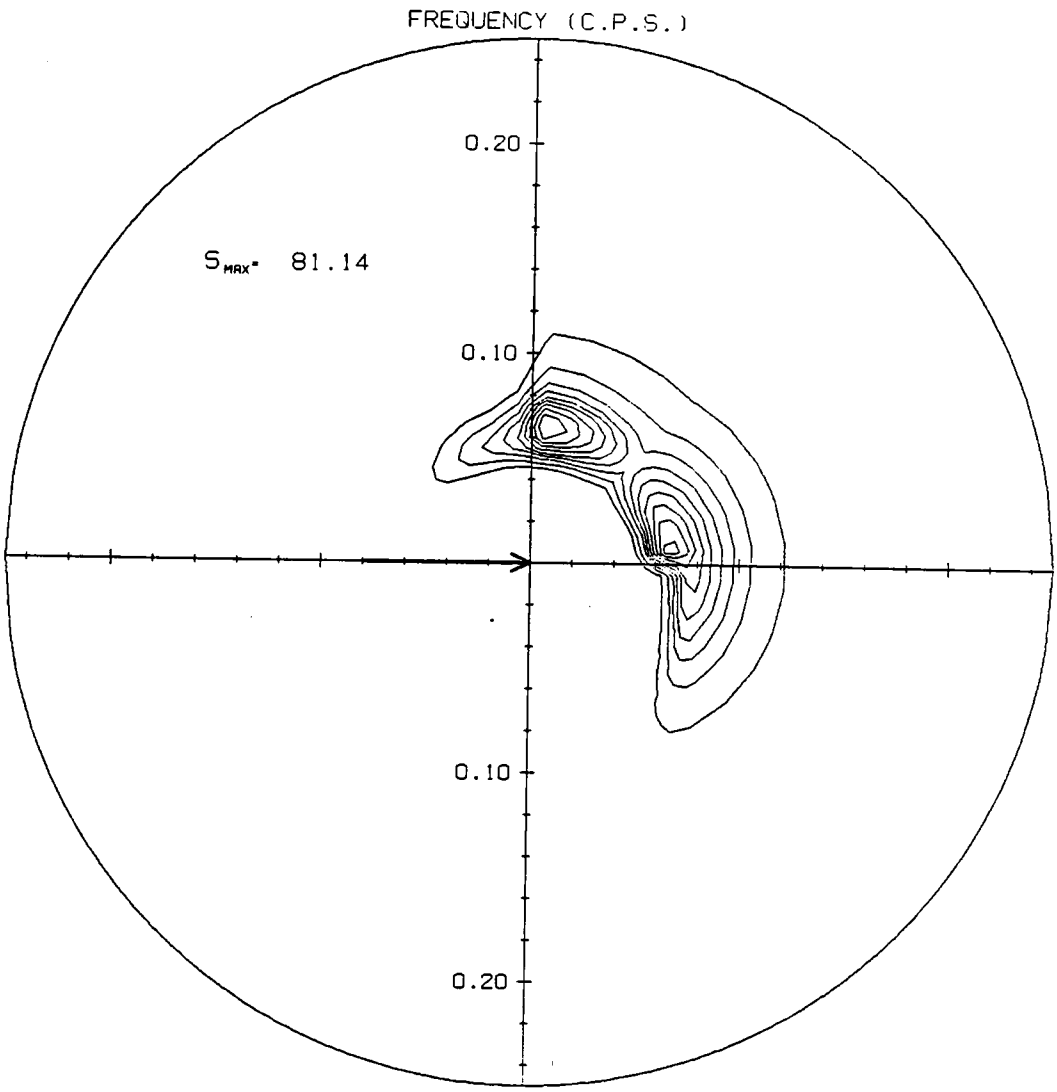

Fig. 22c. T=9 hours

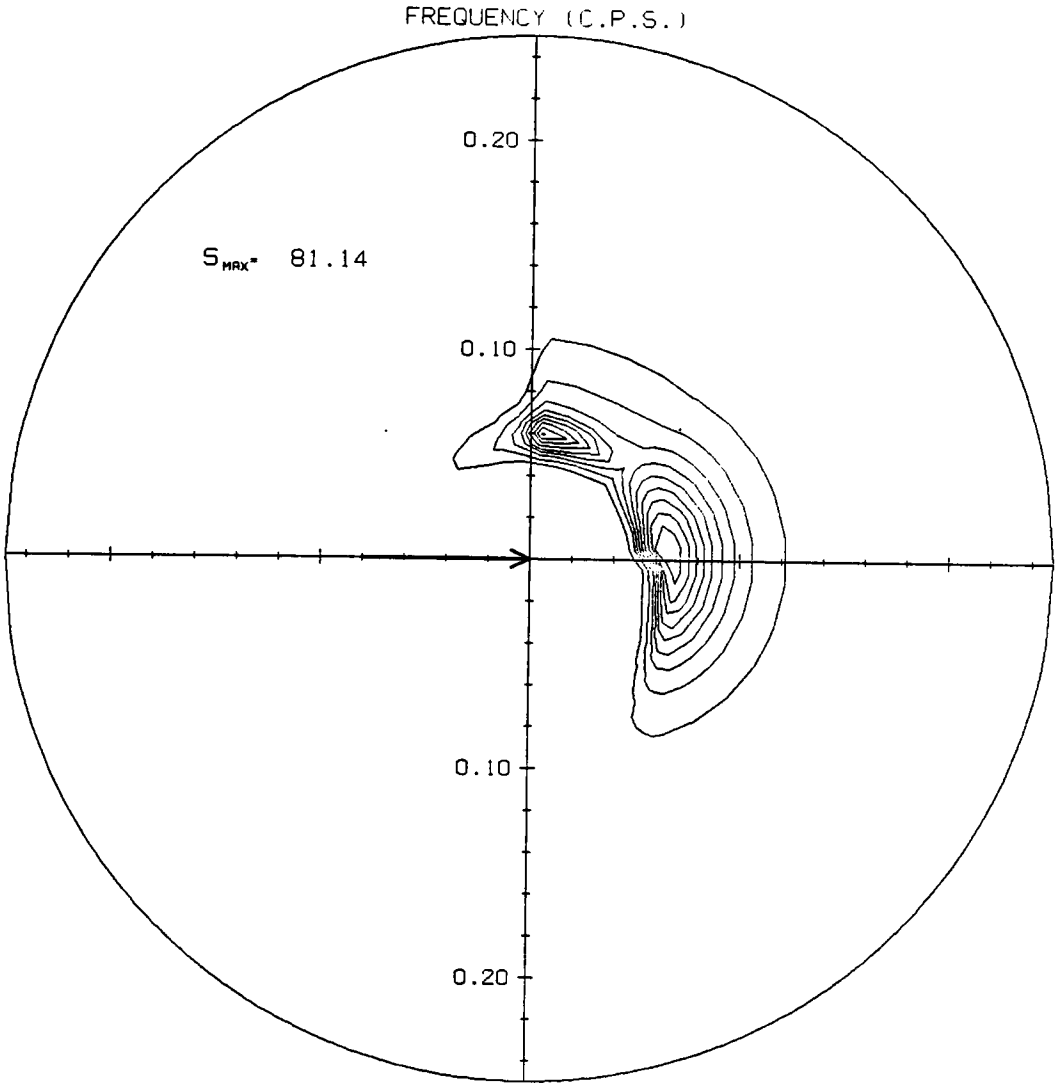

Fig. 22d. T=15 hours

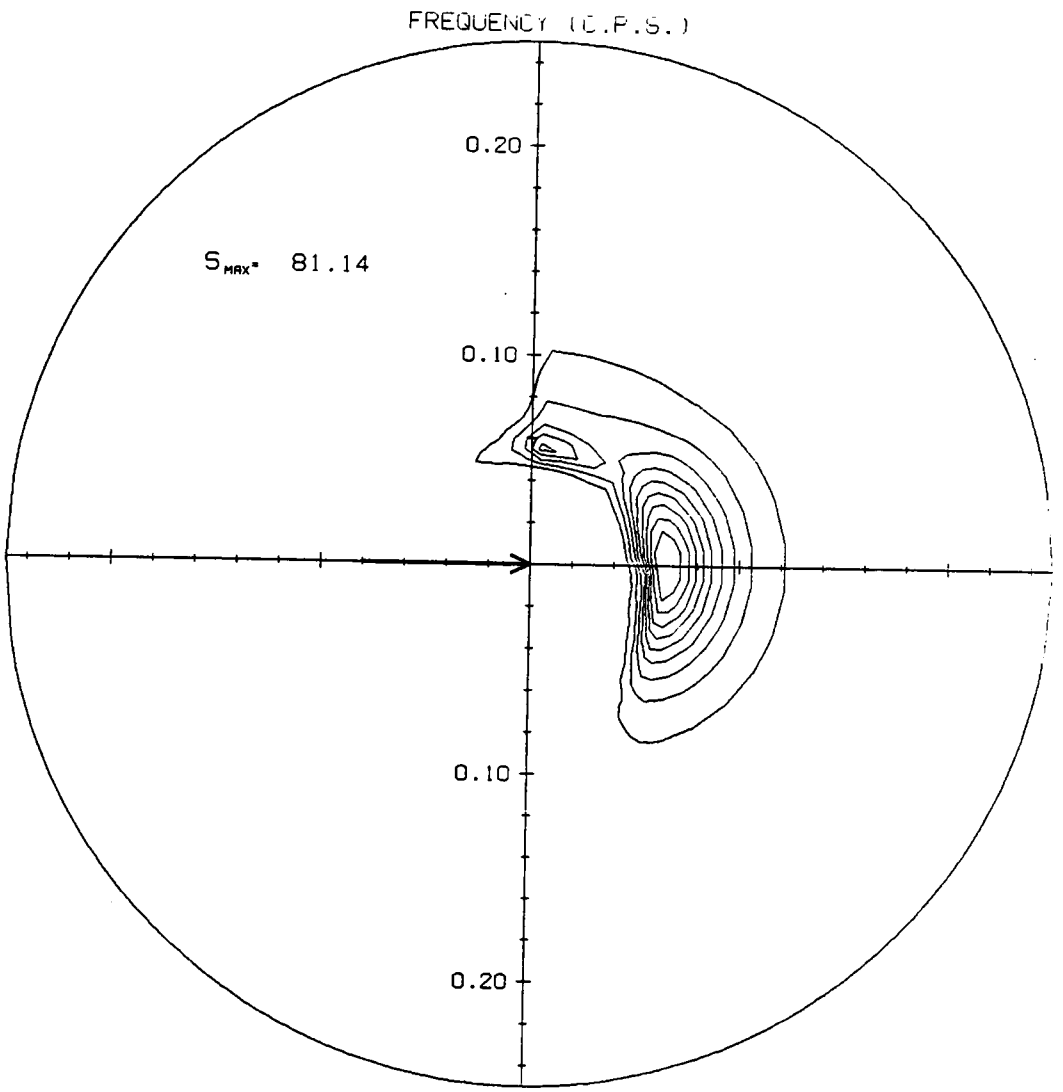

Fig. 22e. T=21 hours

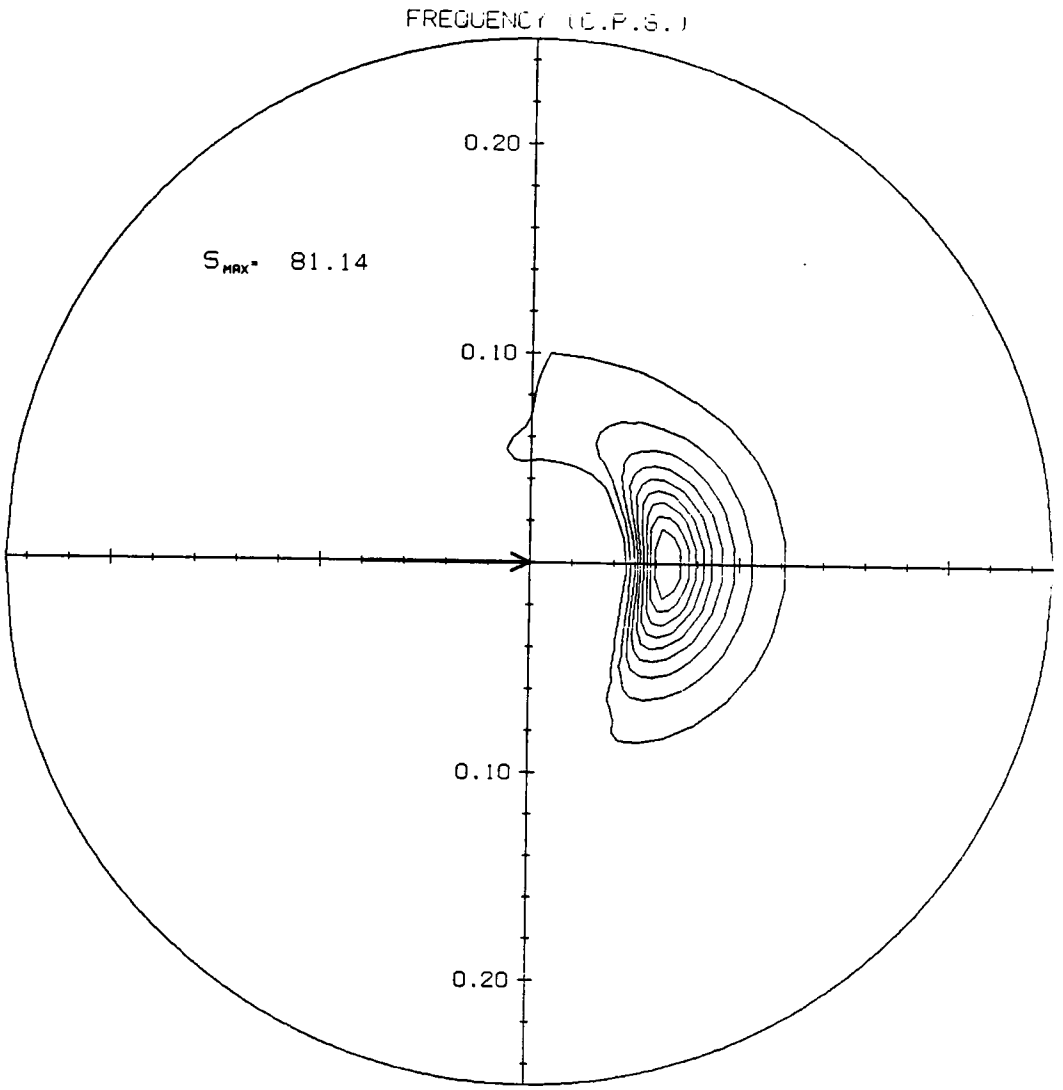

Fig. 22f. T=30 hours

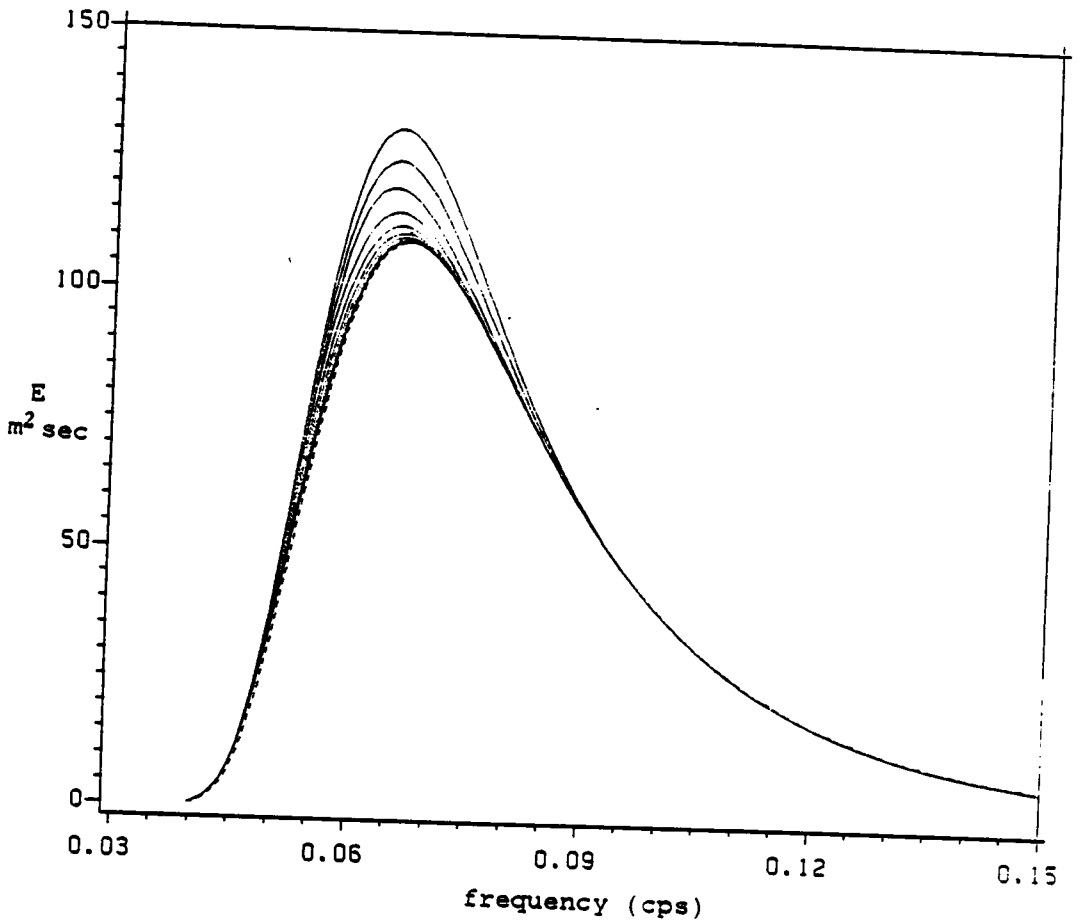

Fig. 23. Point spectrum evolution for 90 change of wind direction from VSCWM.

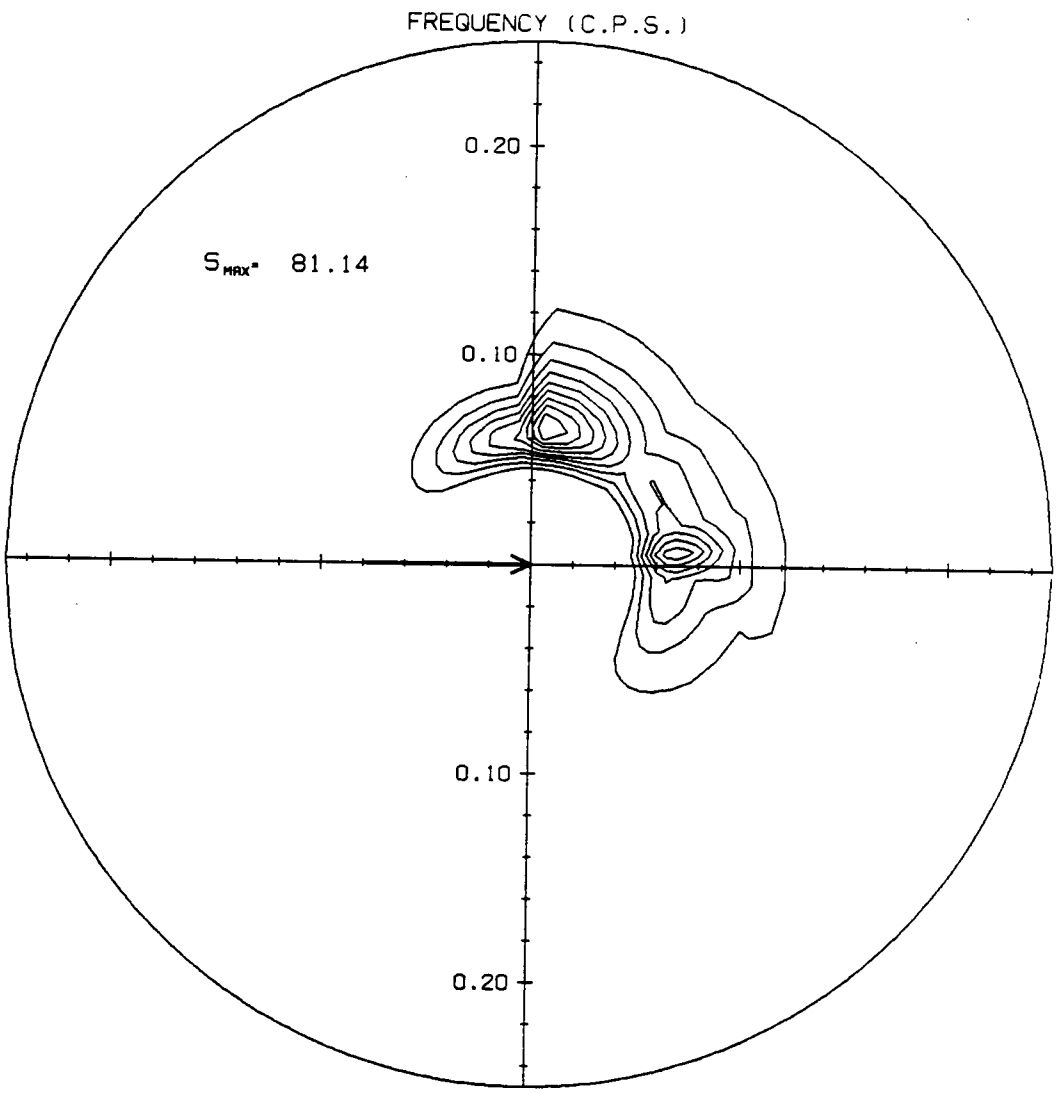

Fig. 24a. Contour plots of 2-D spectrum evolution for 90 change of wind direction from VSOWM. T=3 hours

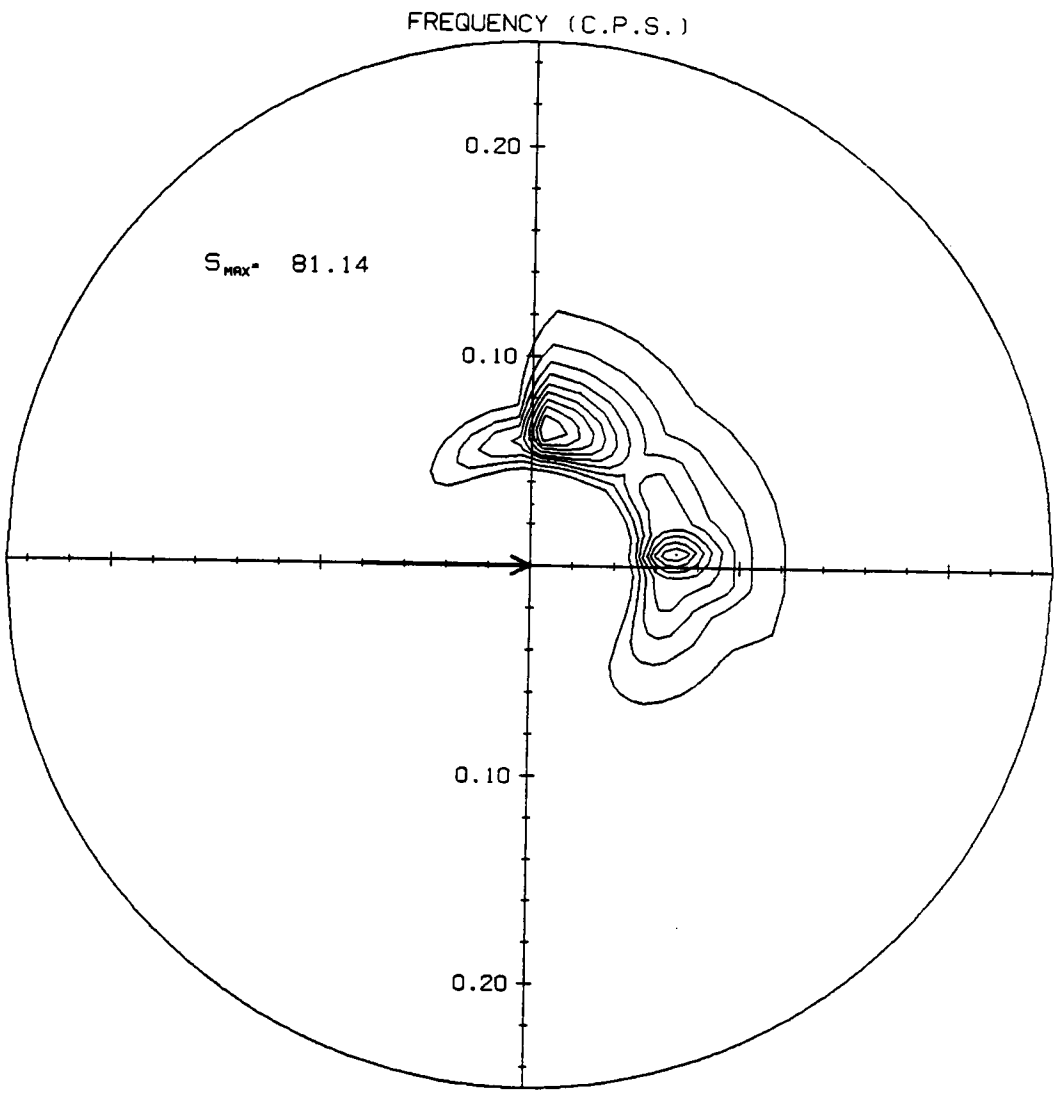

Fig. 24b. T=6 hours

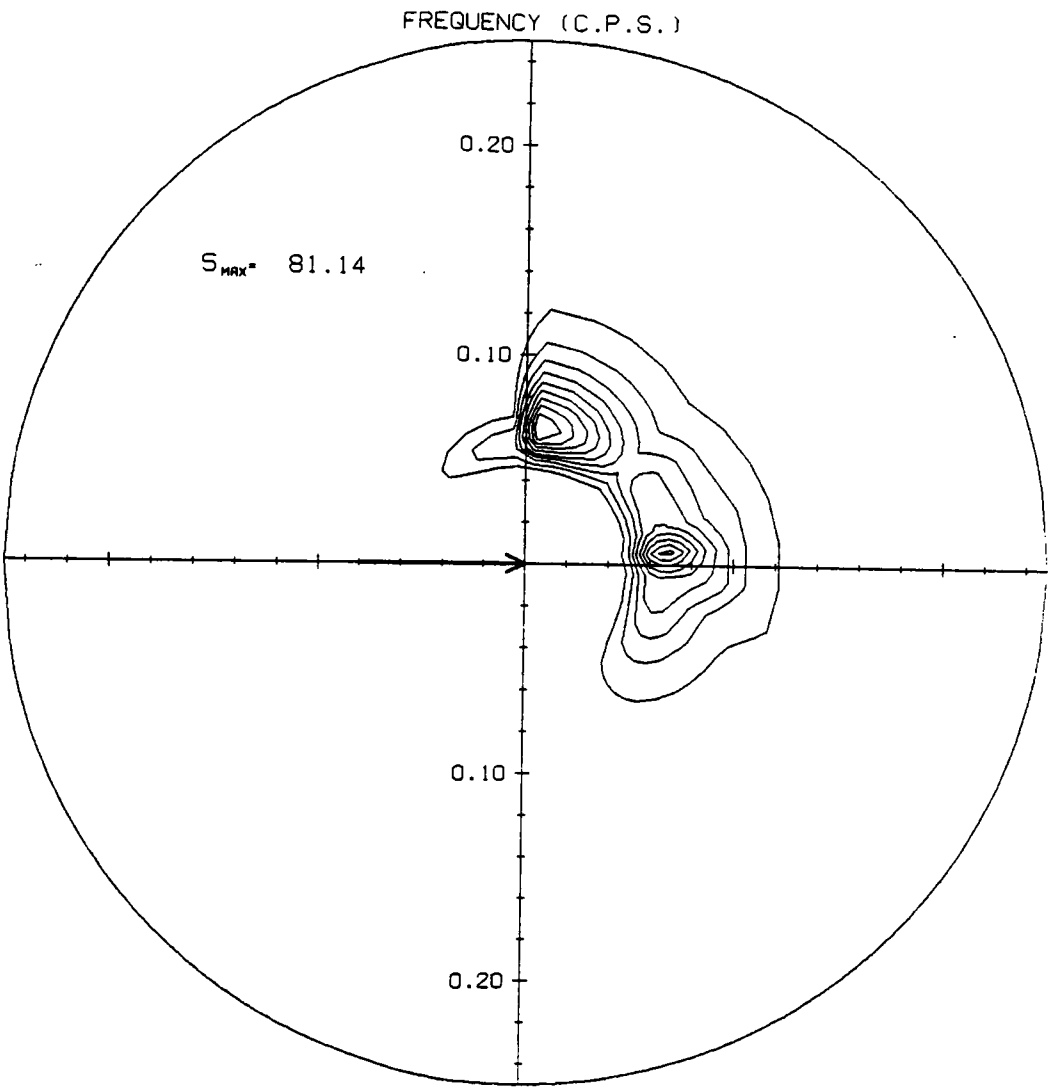

Fig. 24c. T=9 hours

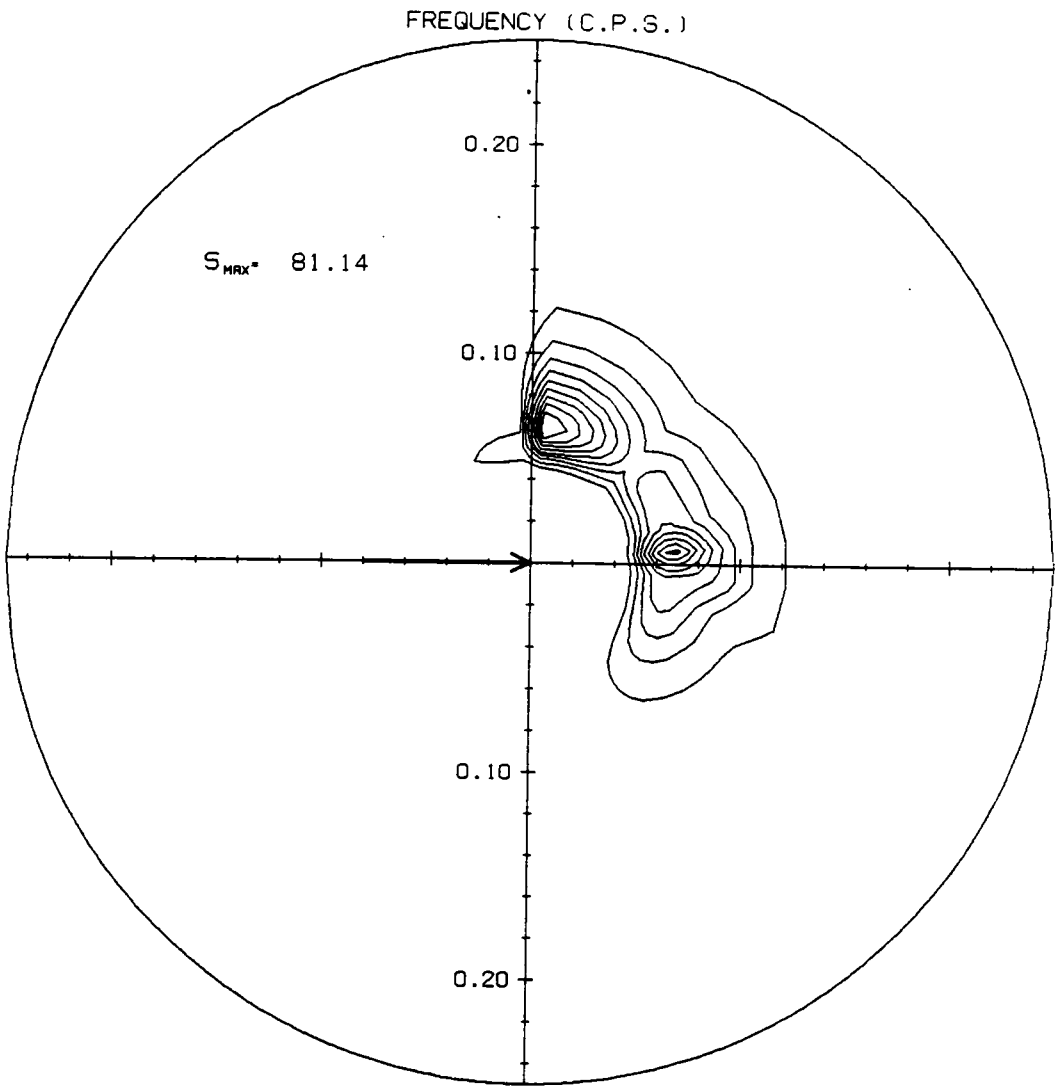

Fig. 24d. T=15 hours

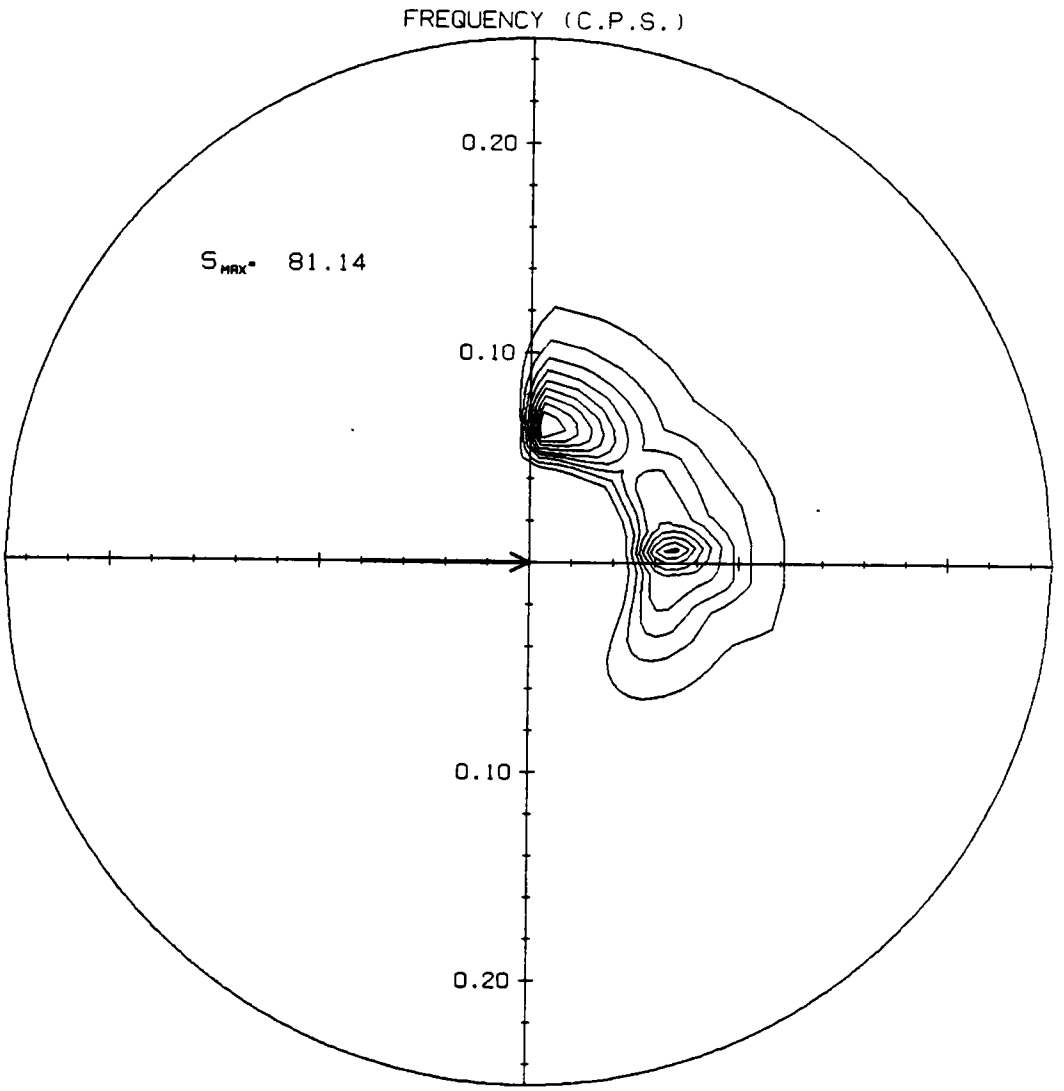

Fig. 24e. T=21 hours

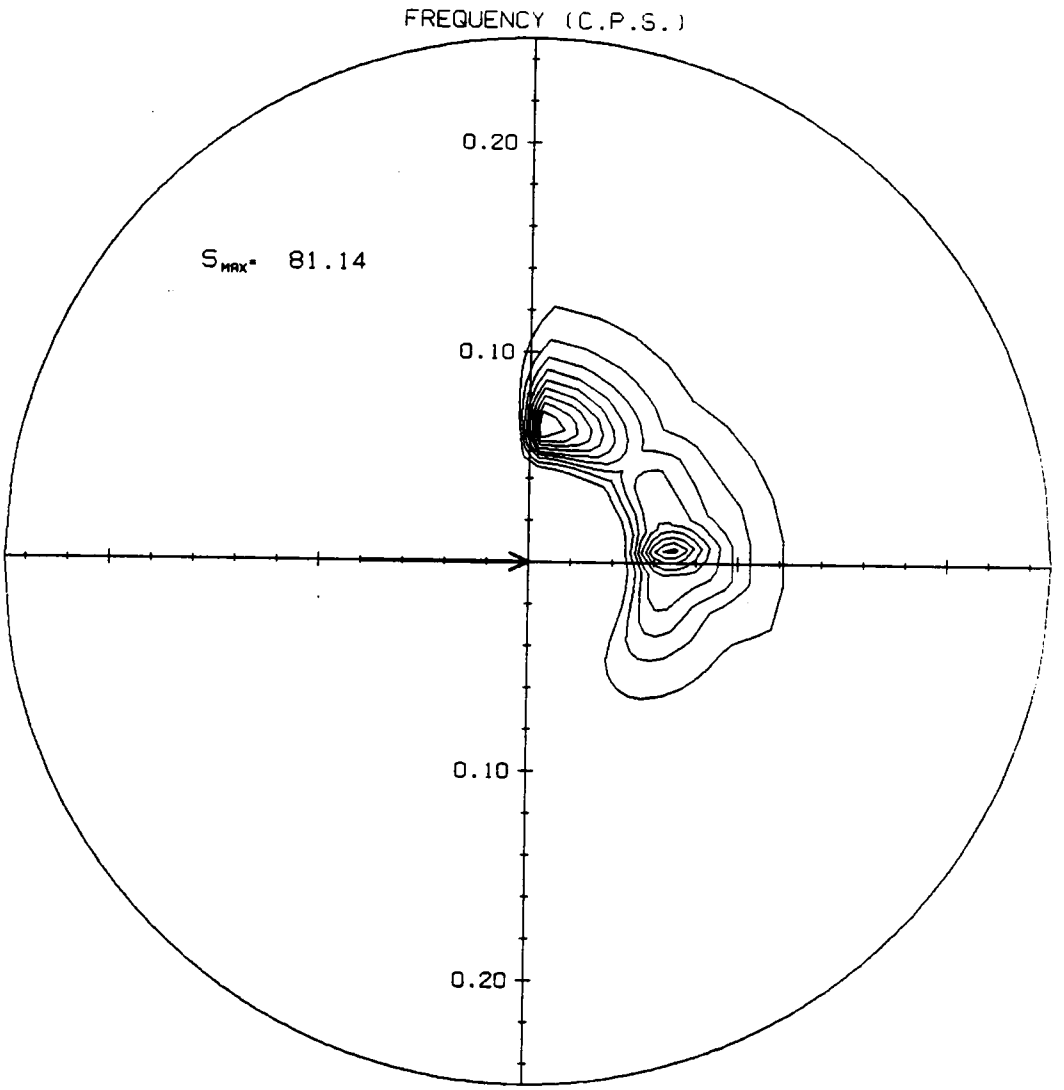

Fig. 24f. T=30 hours

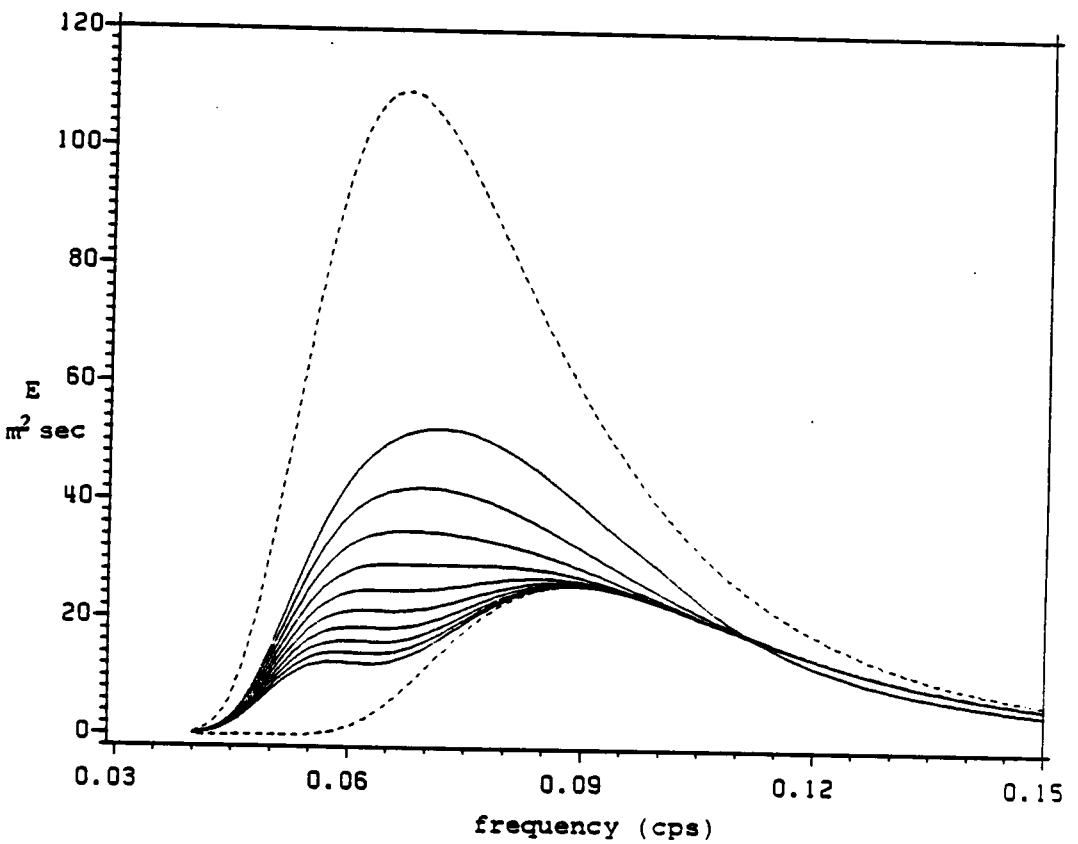

Fig. 25. Point spectrum evolution for 90° change of wind direction and drop in wind speed from VPINK in 3 hour time increments.

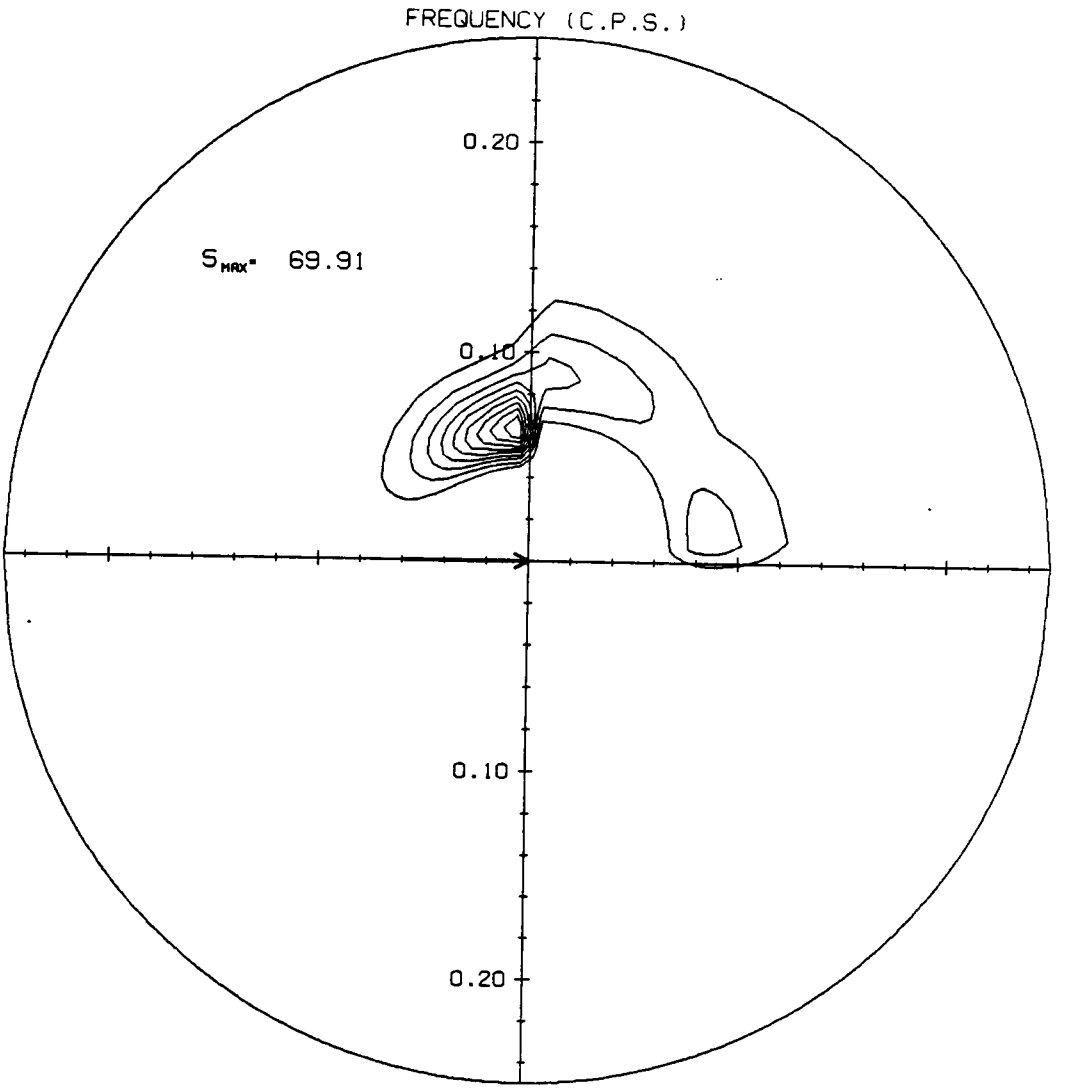

Fig. 26a. Contour plots of 2-D spectrum evolution for 90° change of wind direction and drop in wind speed from VPINK. T=3 hours

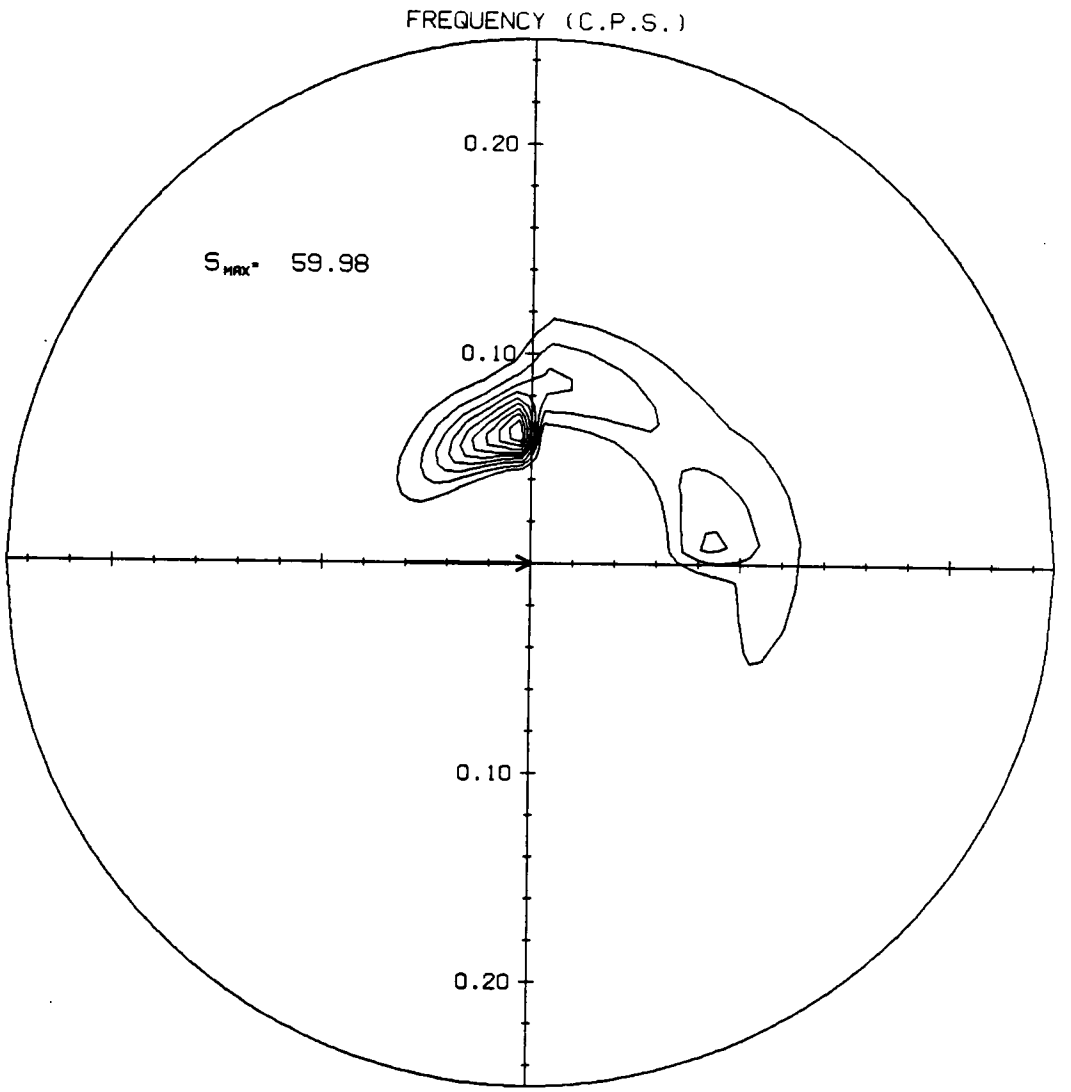

Fig. 26b. T=6 hours

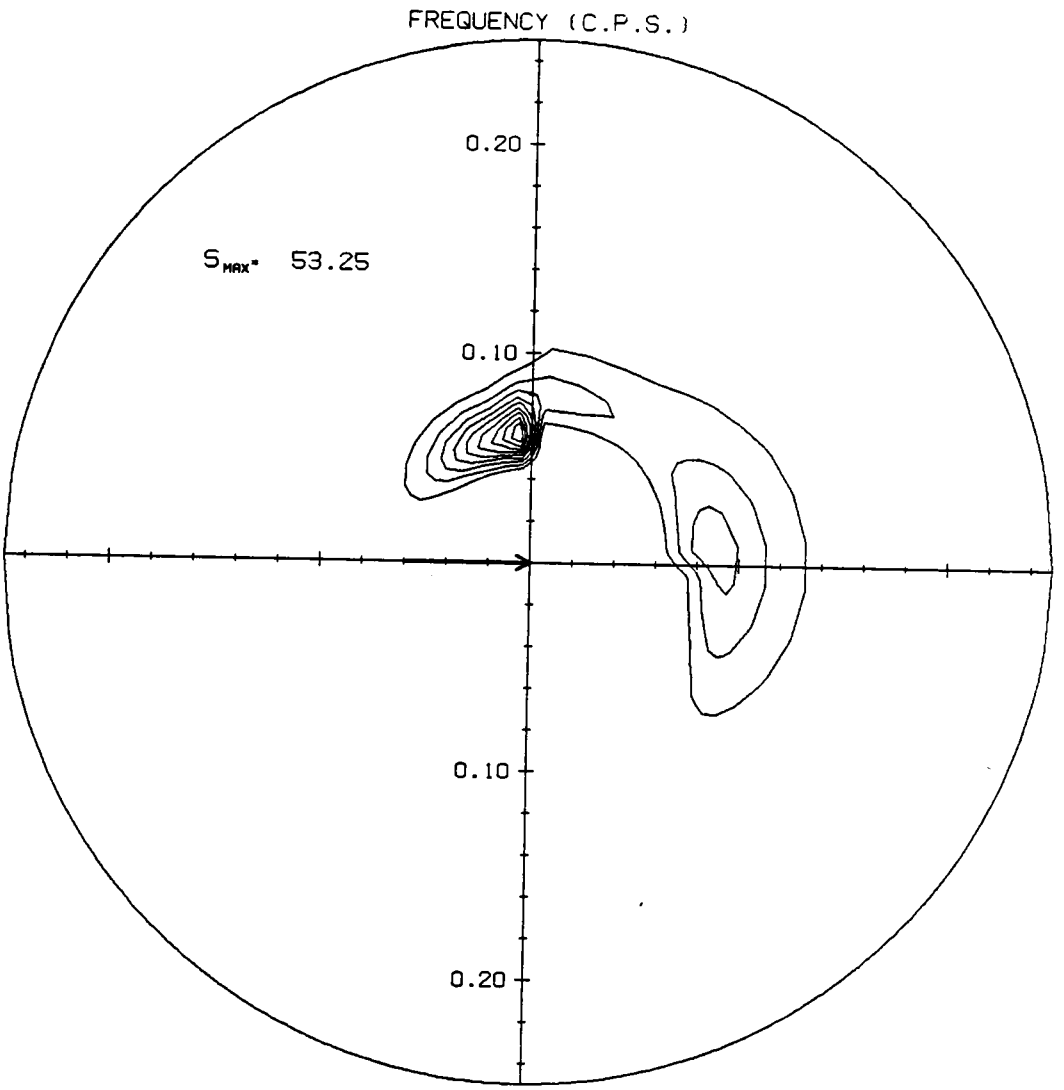

Fig. 26c. T=9 hours

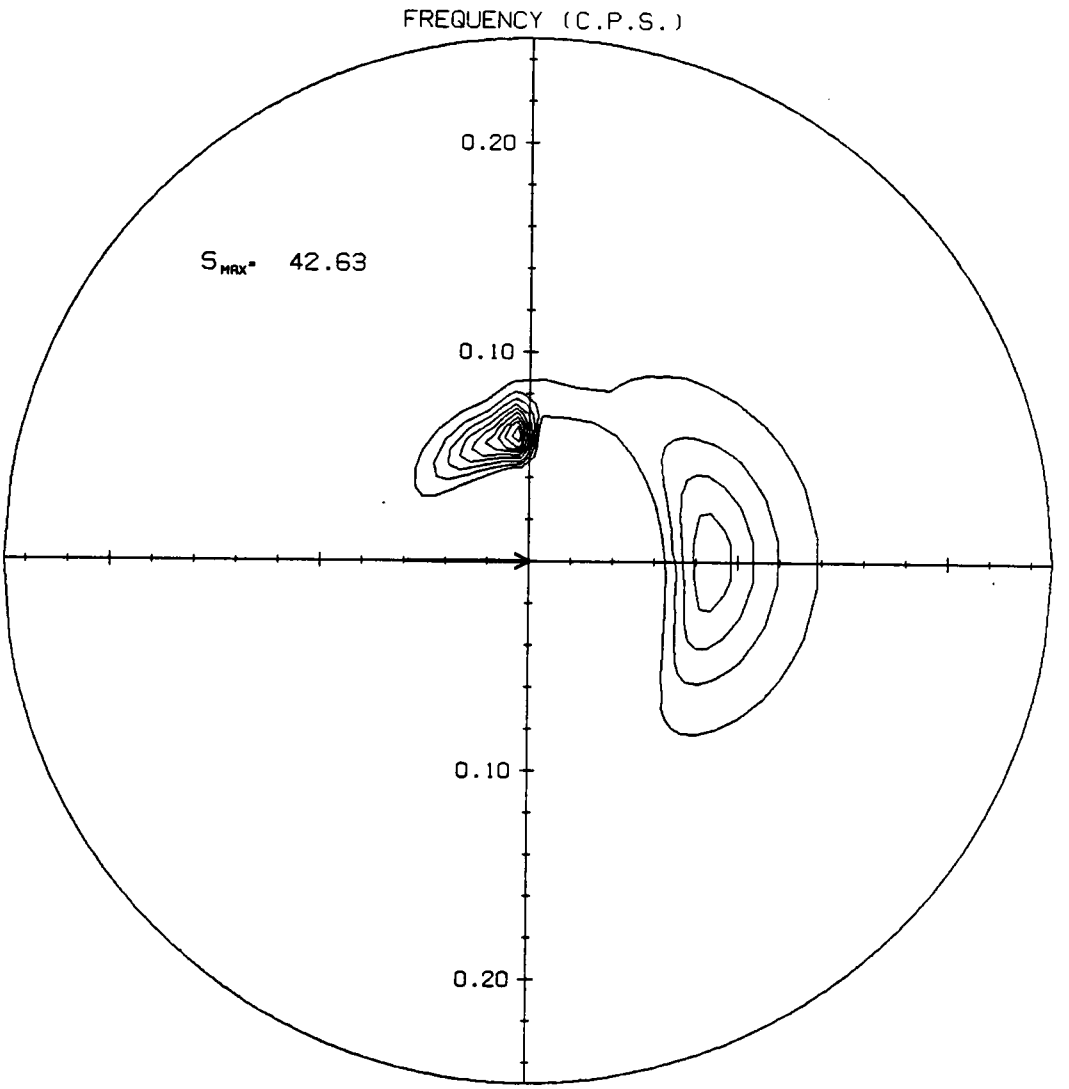

Fig. 26d. T=15 hours

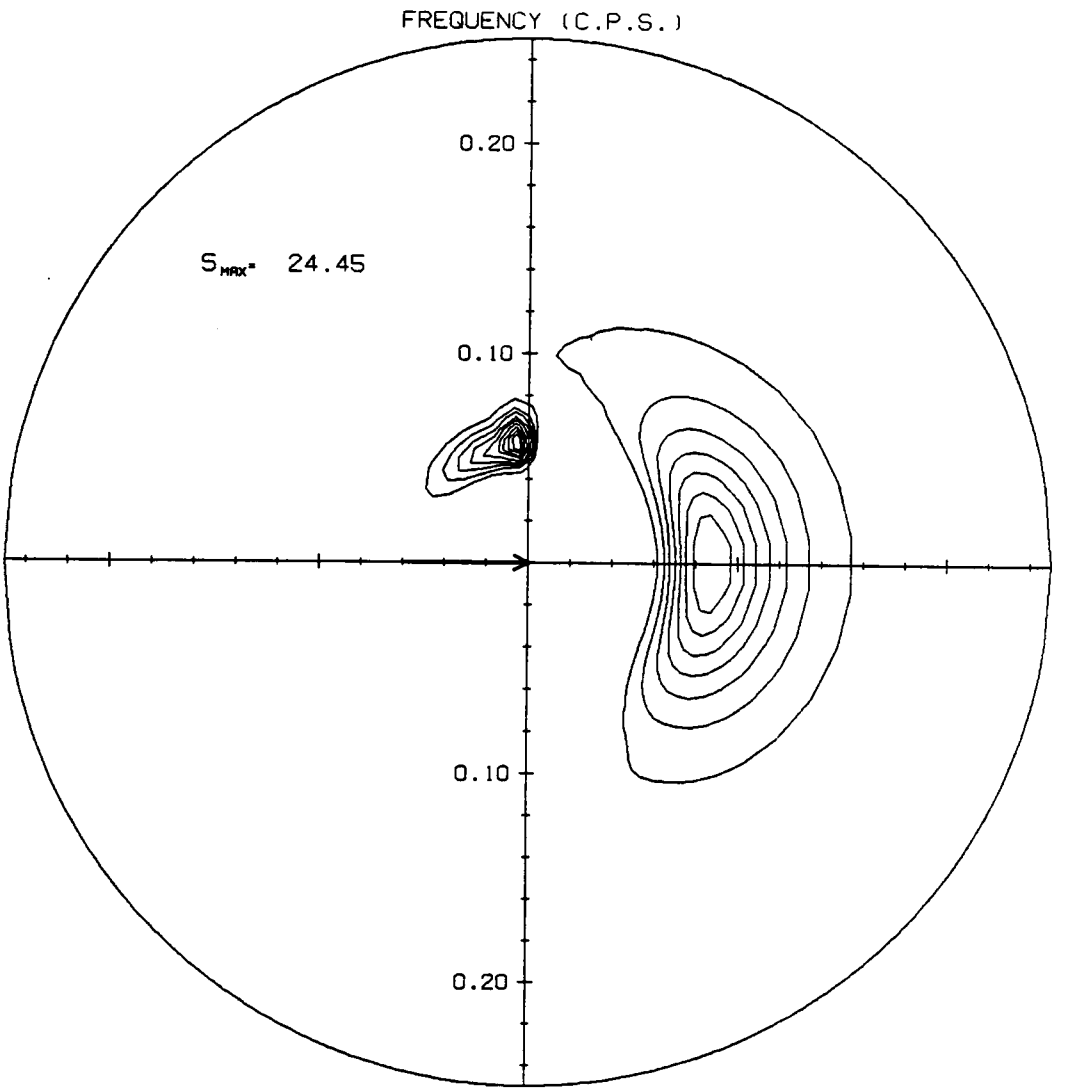

Fig. 26e. T=30 hours

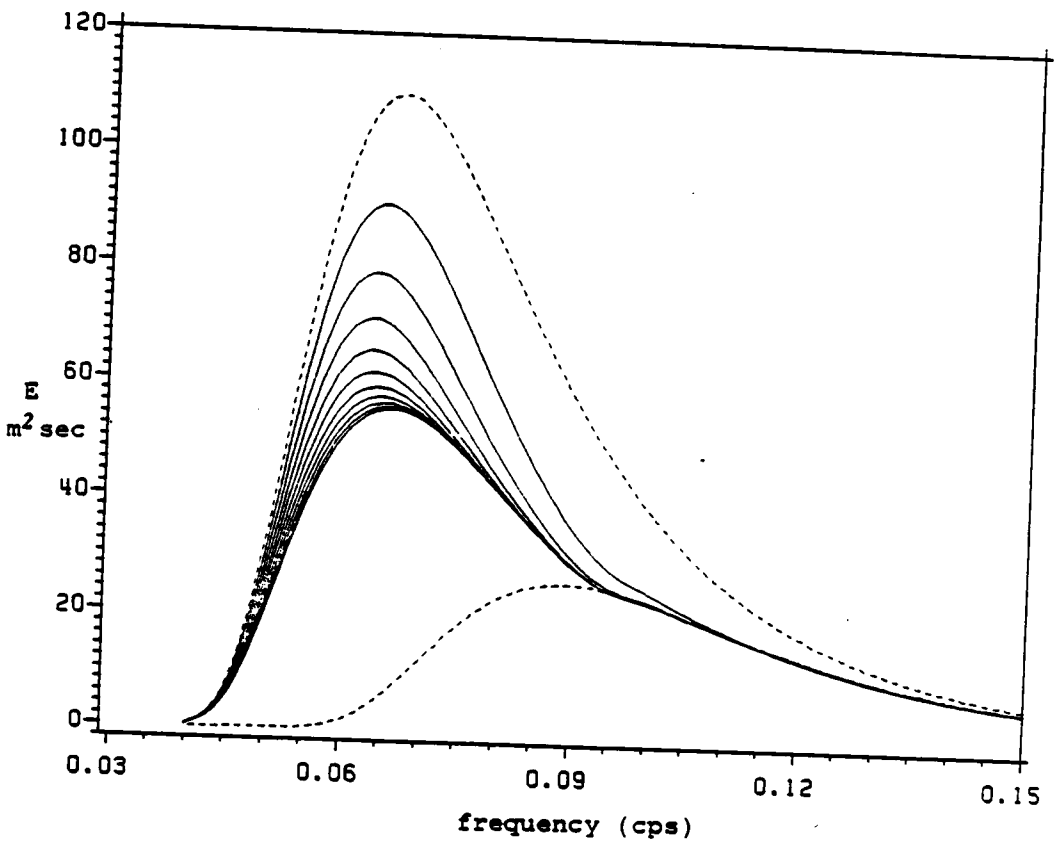

Fig. 27. Point spectrum evolution for 90° change of wind direction and drop in wind speed from VSOWM in 3 hour time increments.

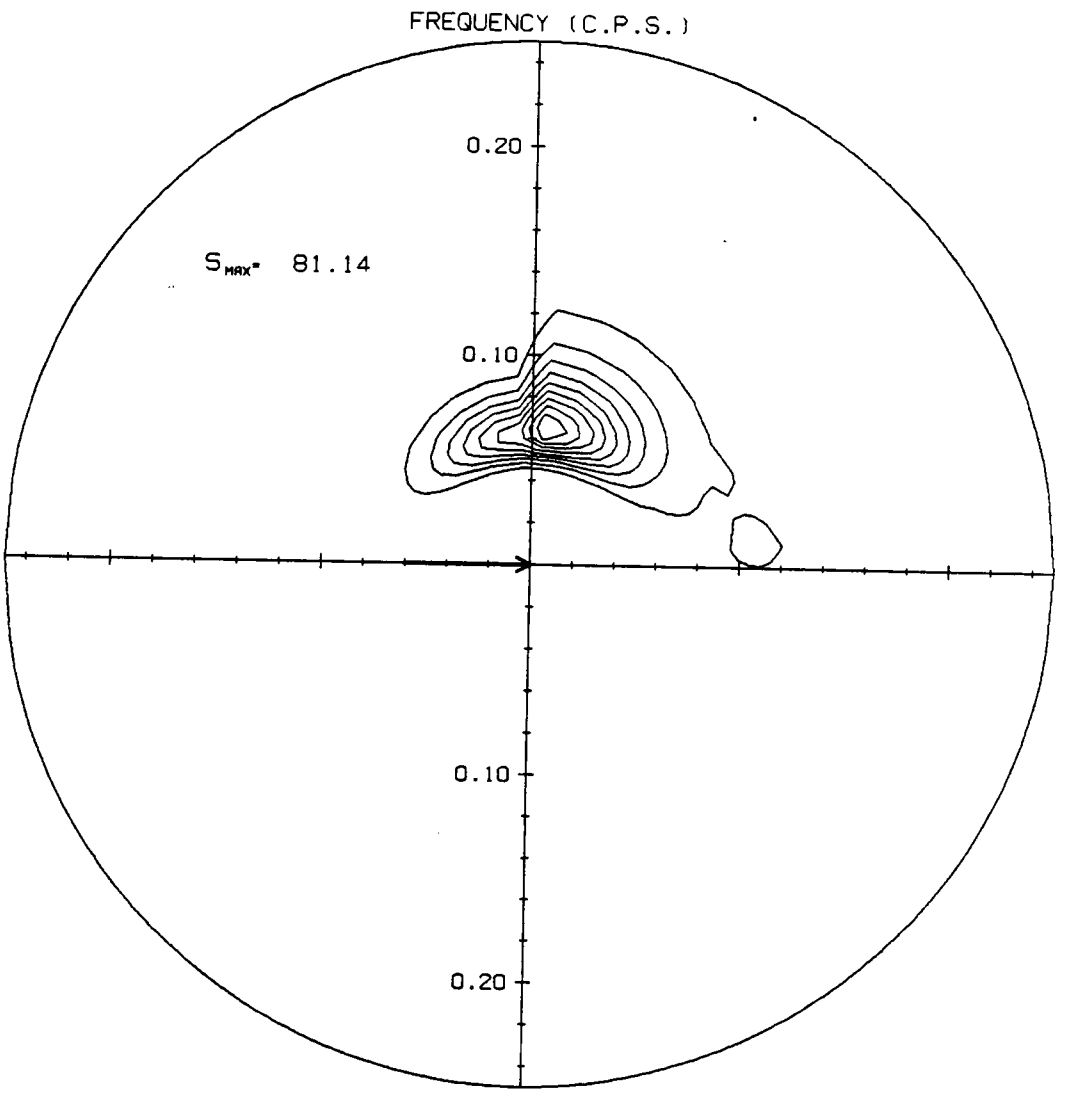

Fig. 28a. Contour plots of 2-D spectrum evolution for 90° change of wind direction and drop in wind speed from VSOWM. T=3 hours

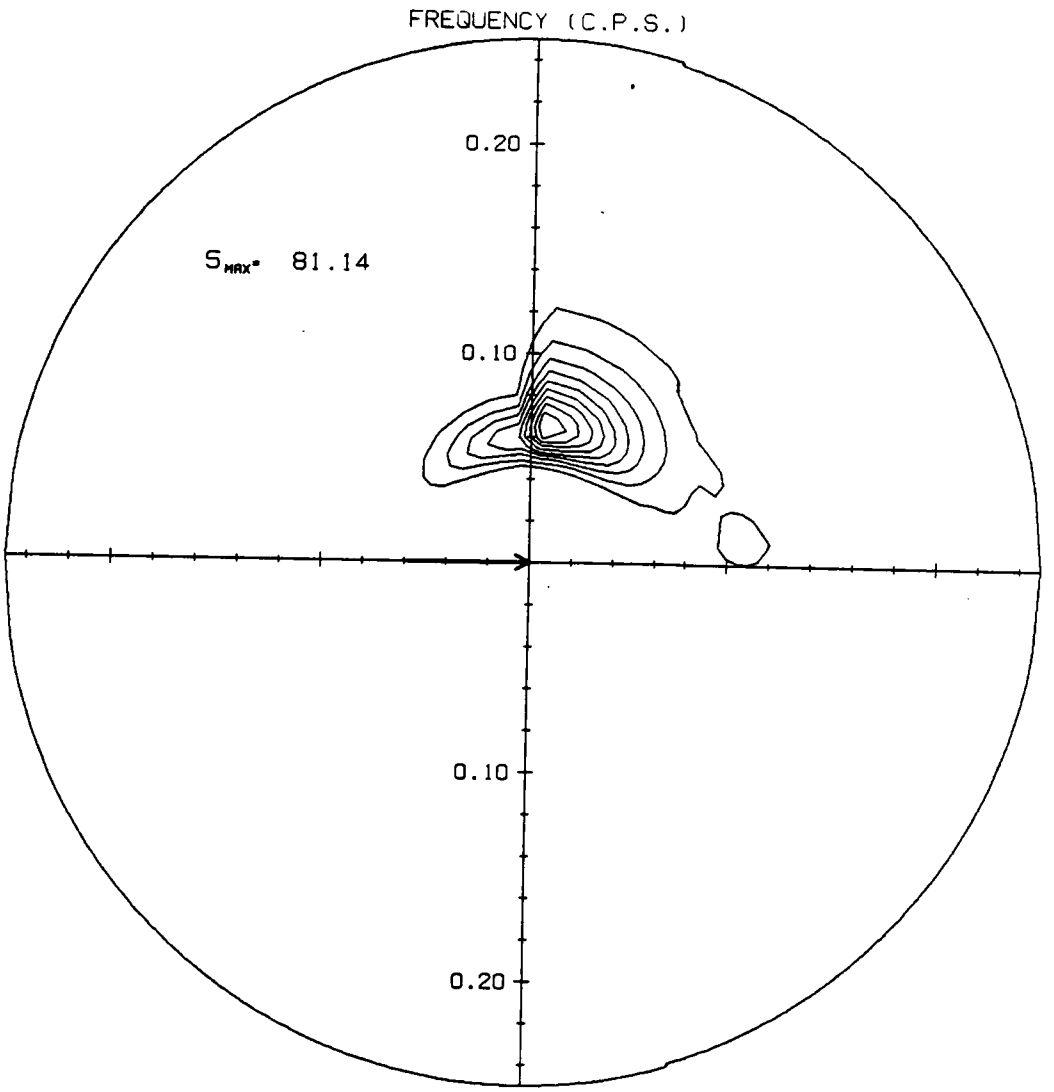

Fig. 28b. T=6 hours

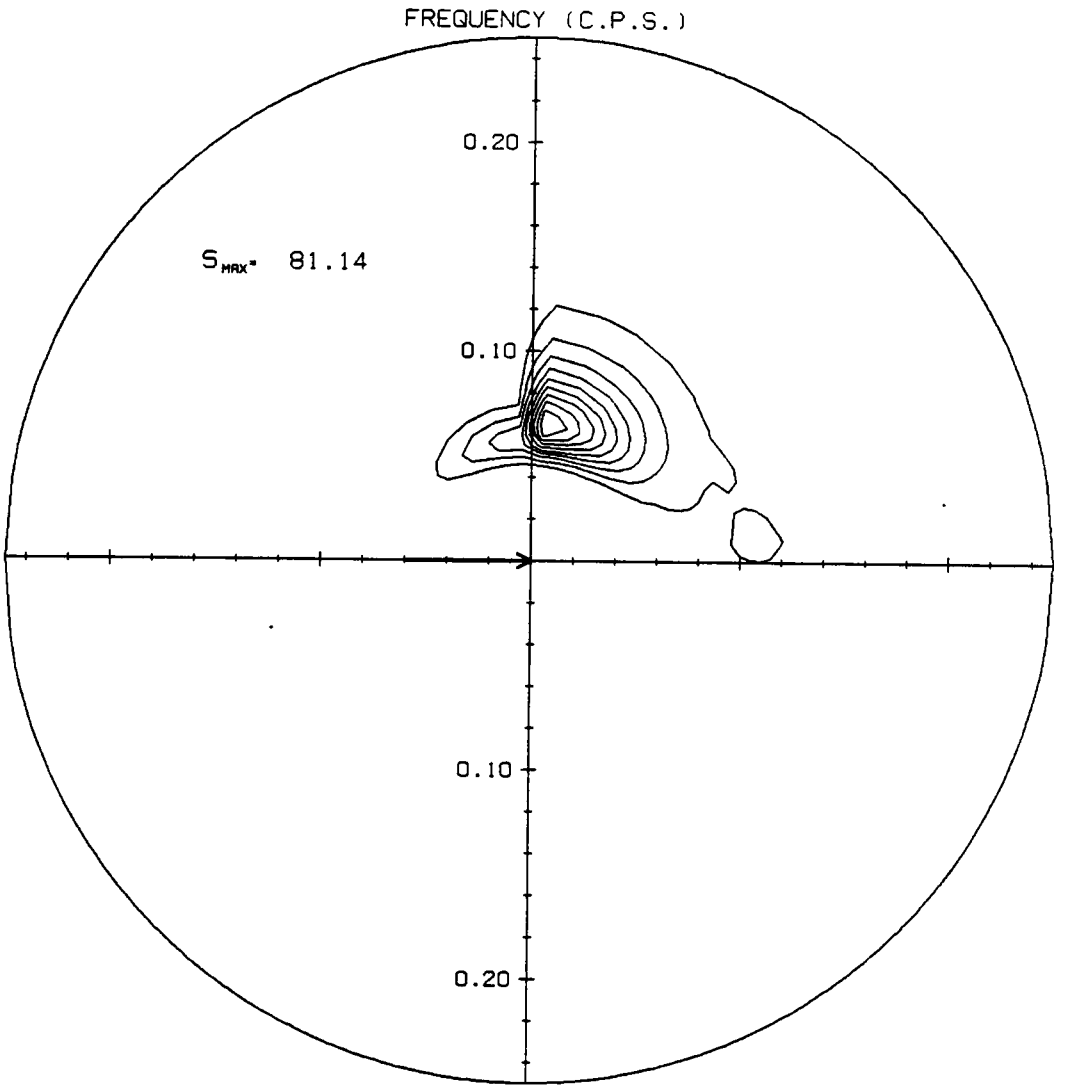

Fig. 28c. T=9 hours

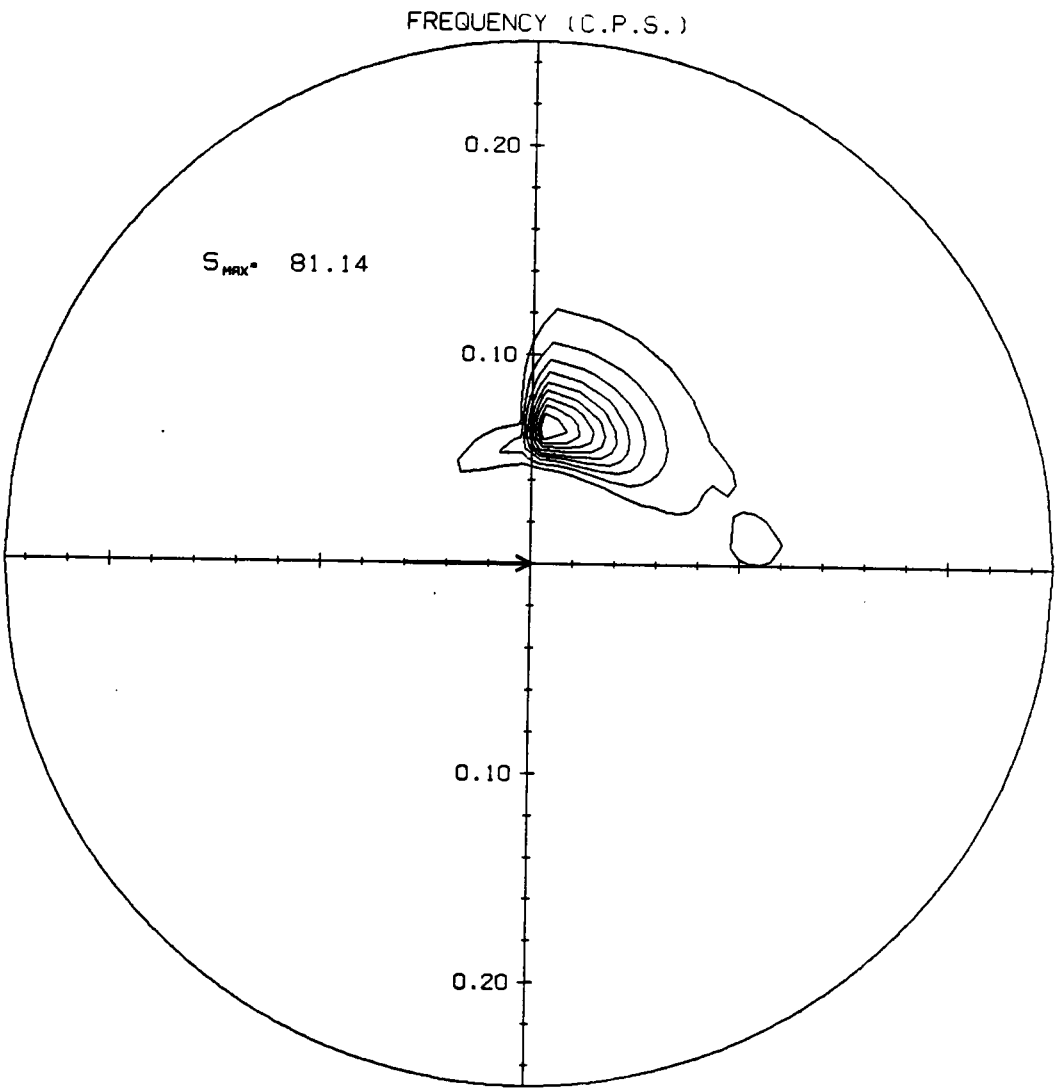

Fig. 28d. T=15 hours

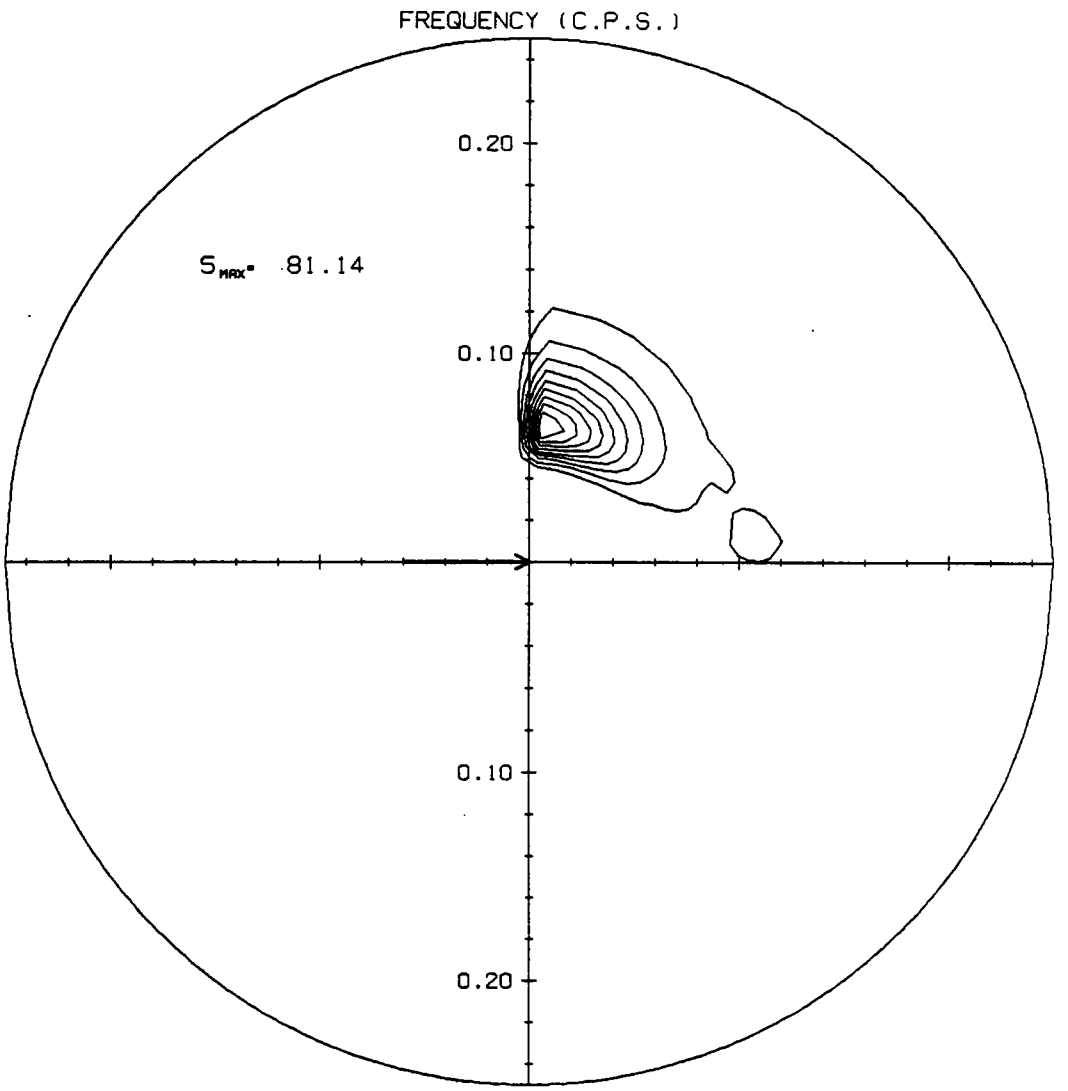

Fig. 28e. T=30 hours

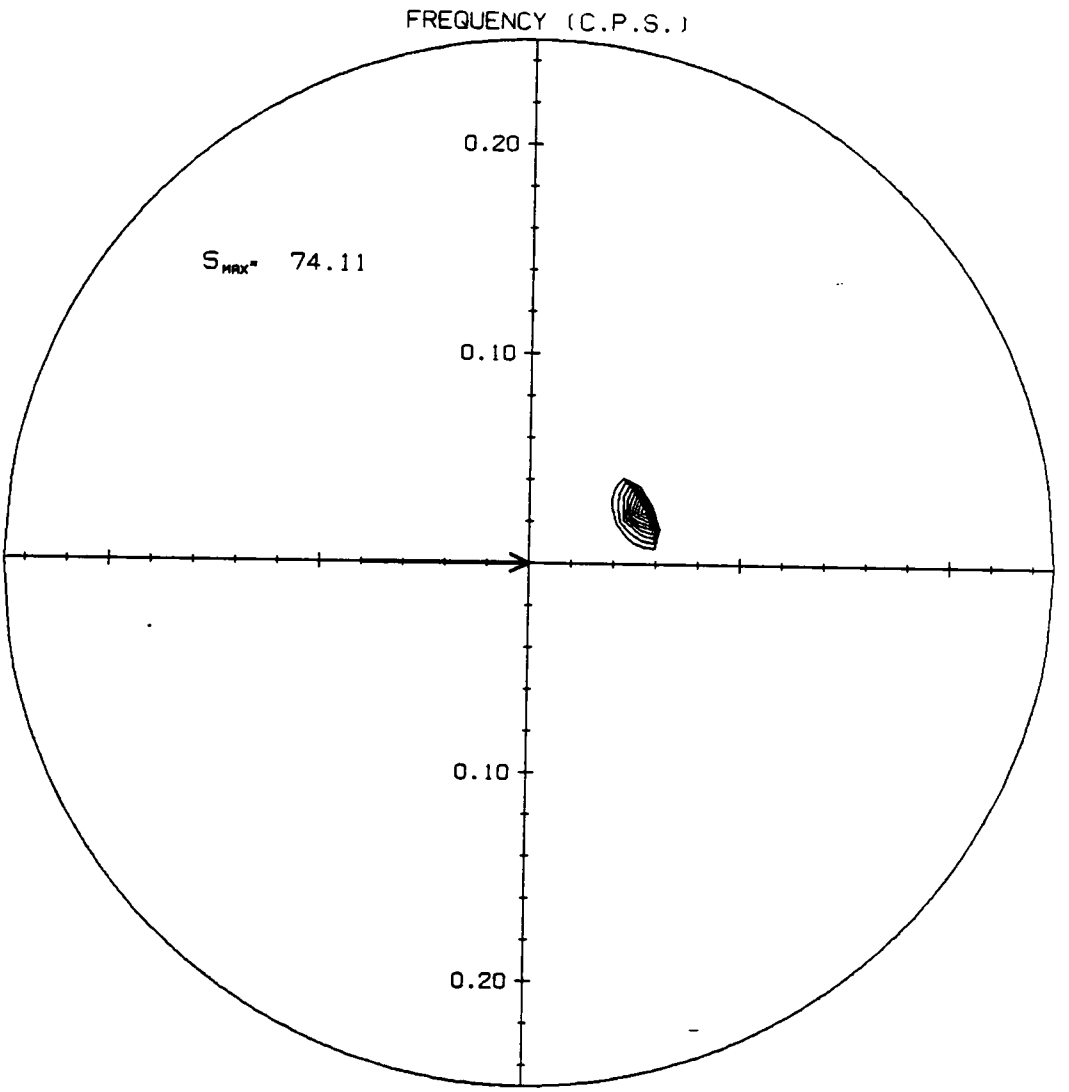

Fig. 29. Initial condition for wave growth in the presence of swell.

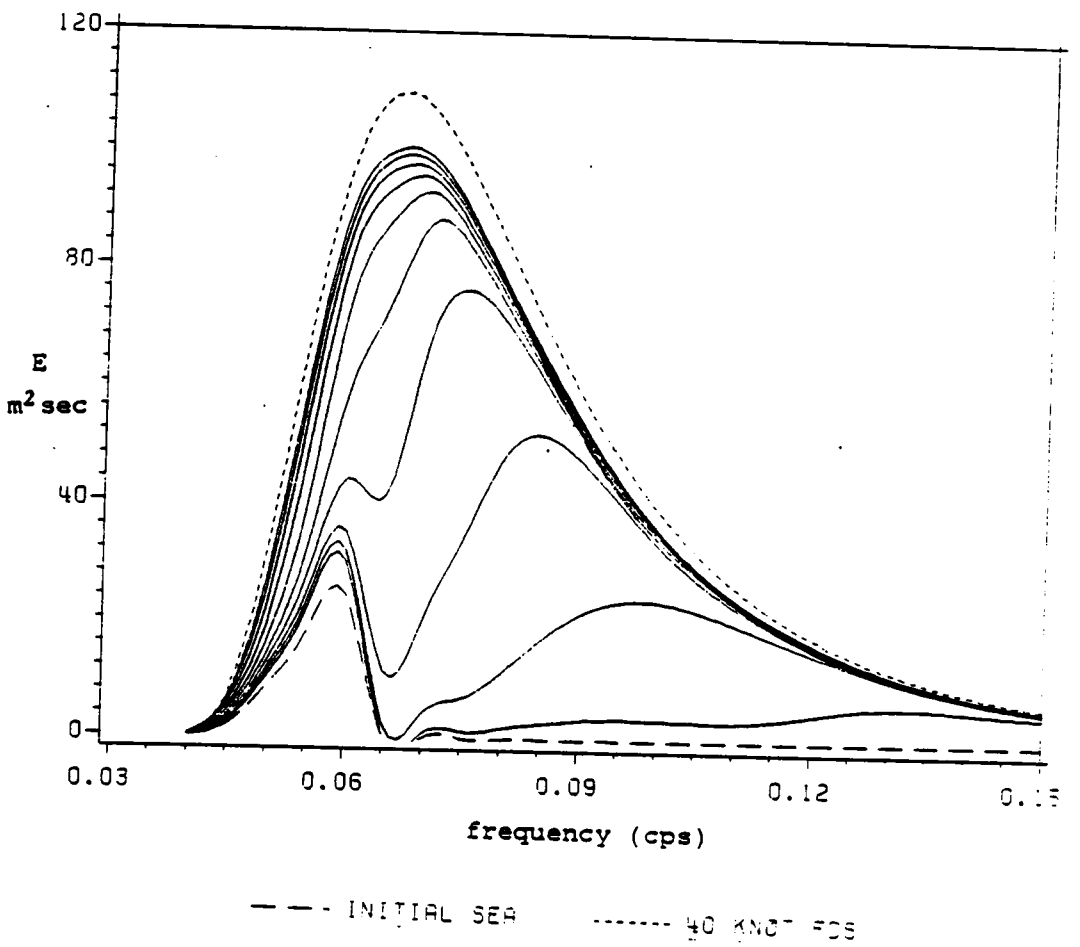

Fig. 30. Point spectrum evolution in the presence of swell from VPINK in 3 hour time increments.

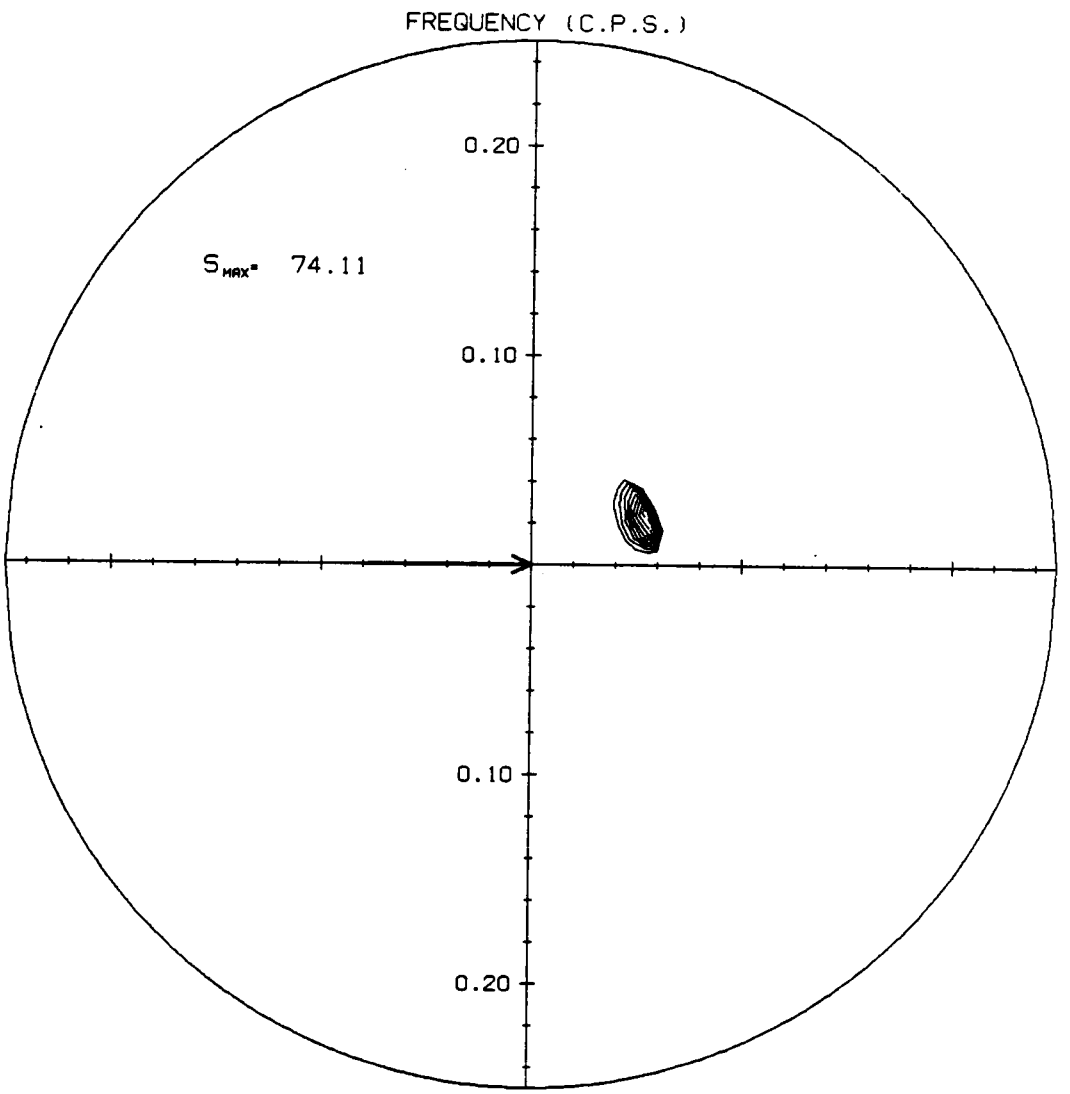

Fig. 31a. Contour plots of 2-D spectrum evolution in the presence of swell from VPINK. T=3 hours

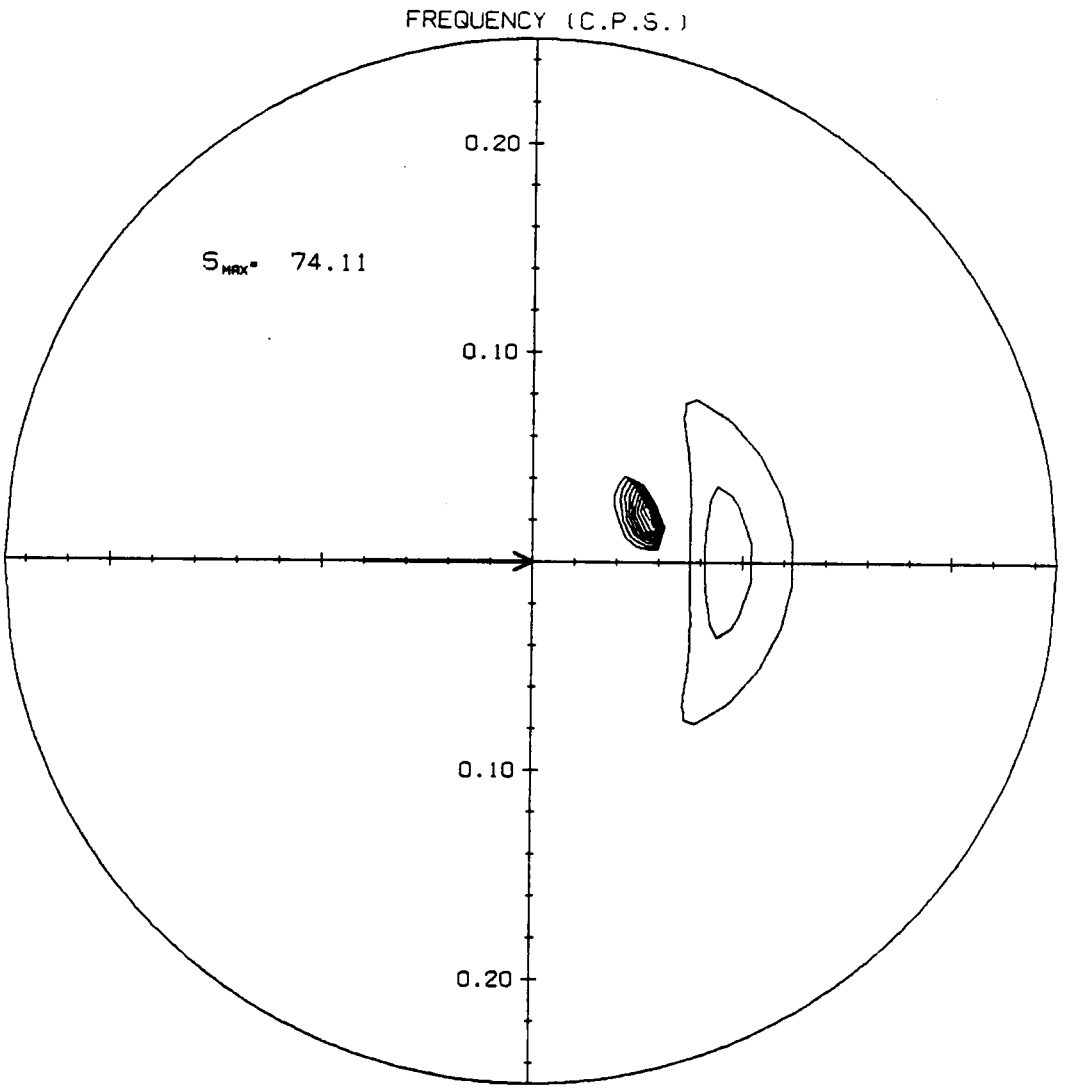

Fig. 31b. T=6 hours

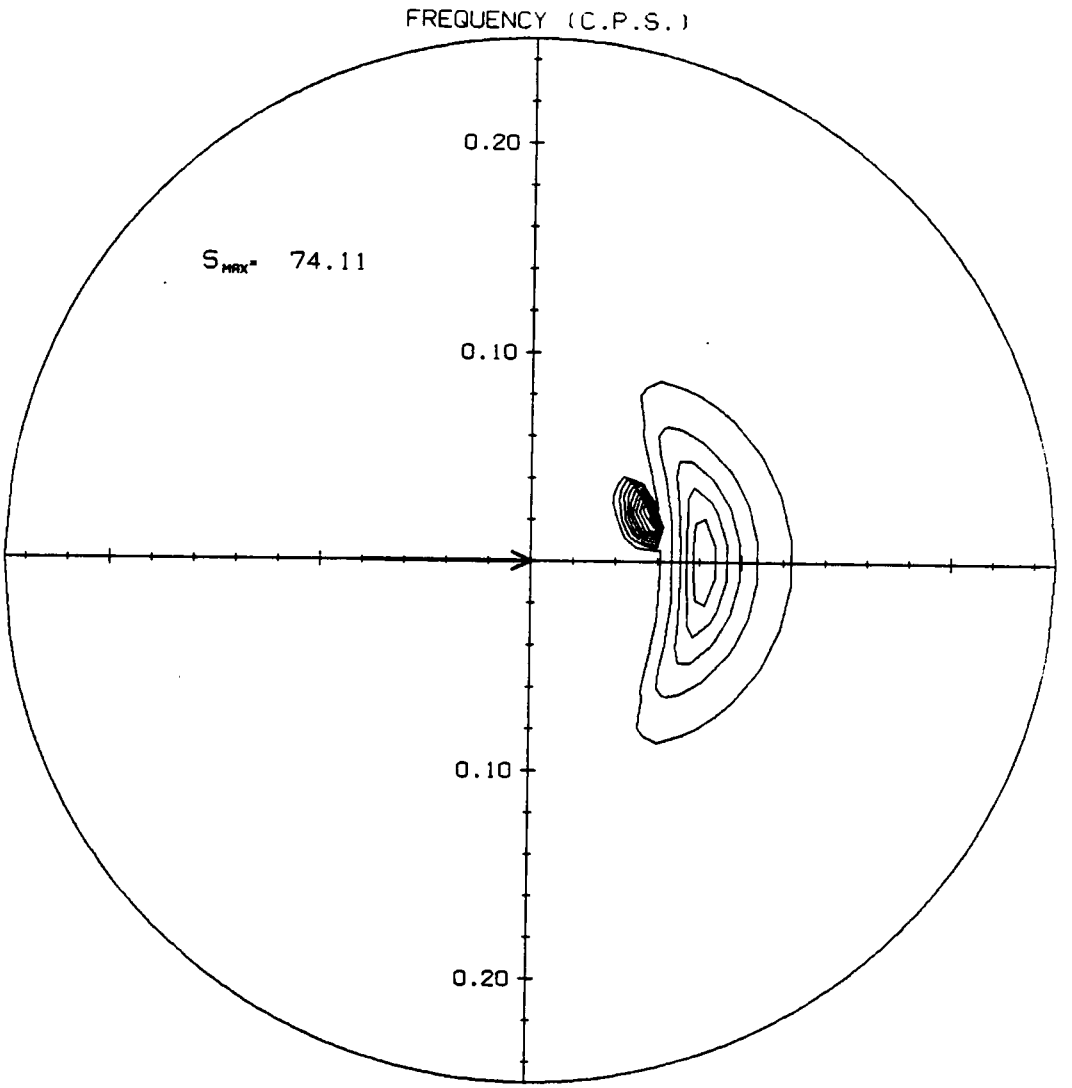

Fig. 31c. T=9 hours

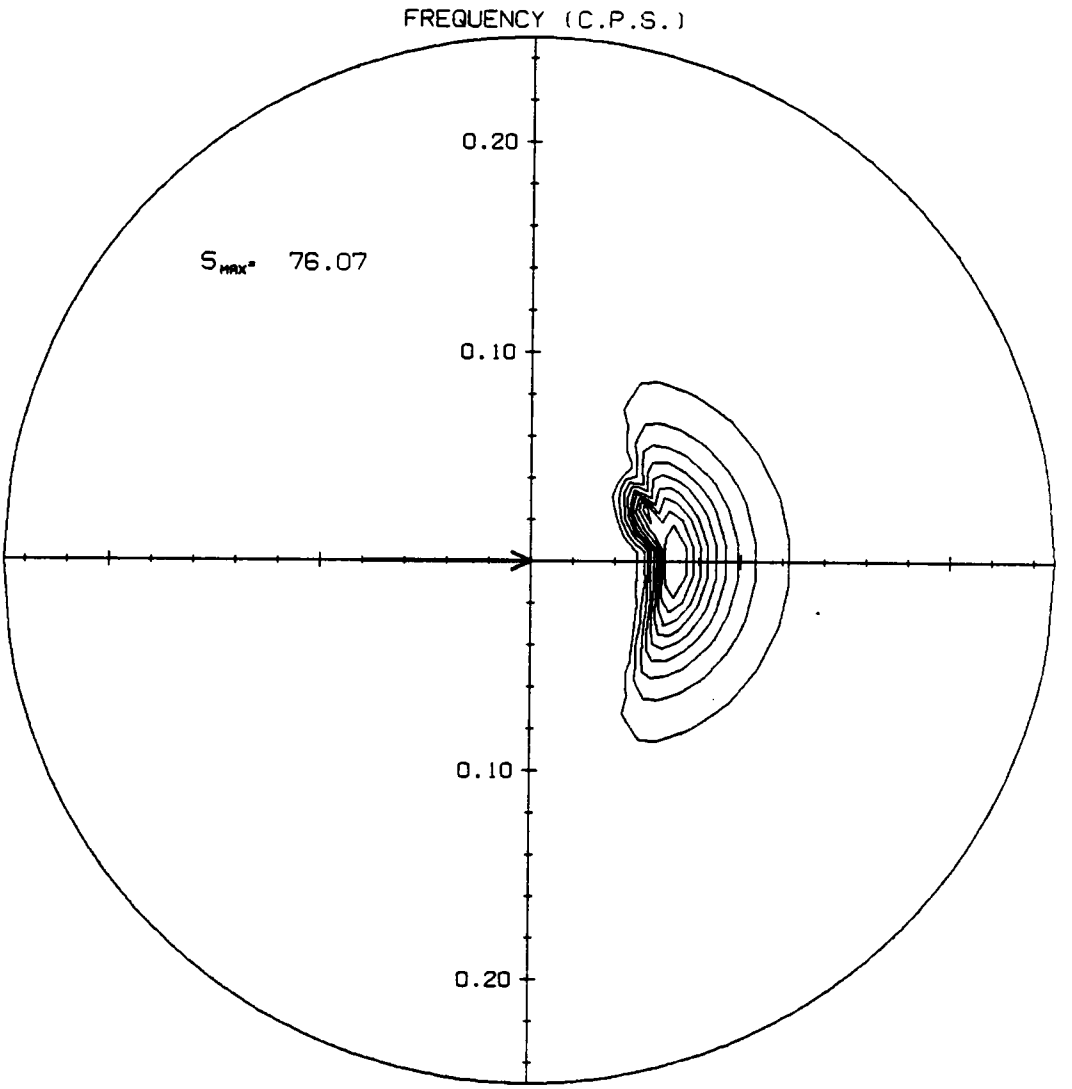

Fig. 31d. T=15 hours

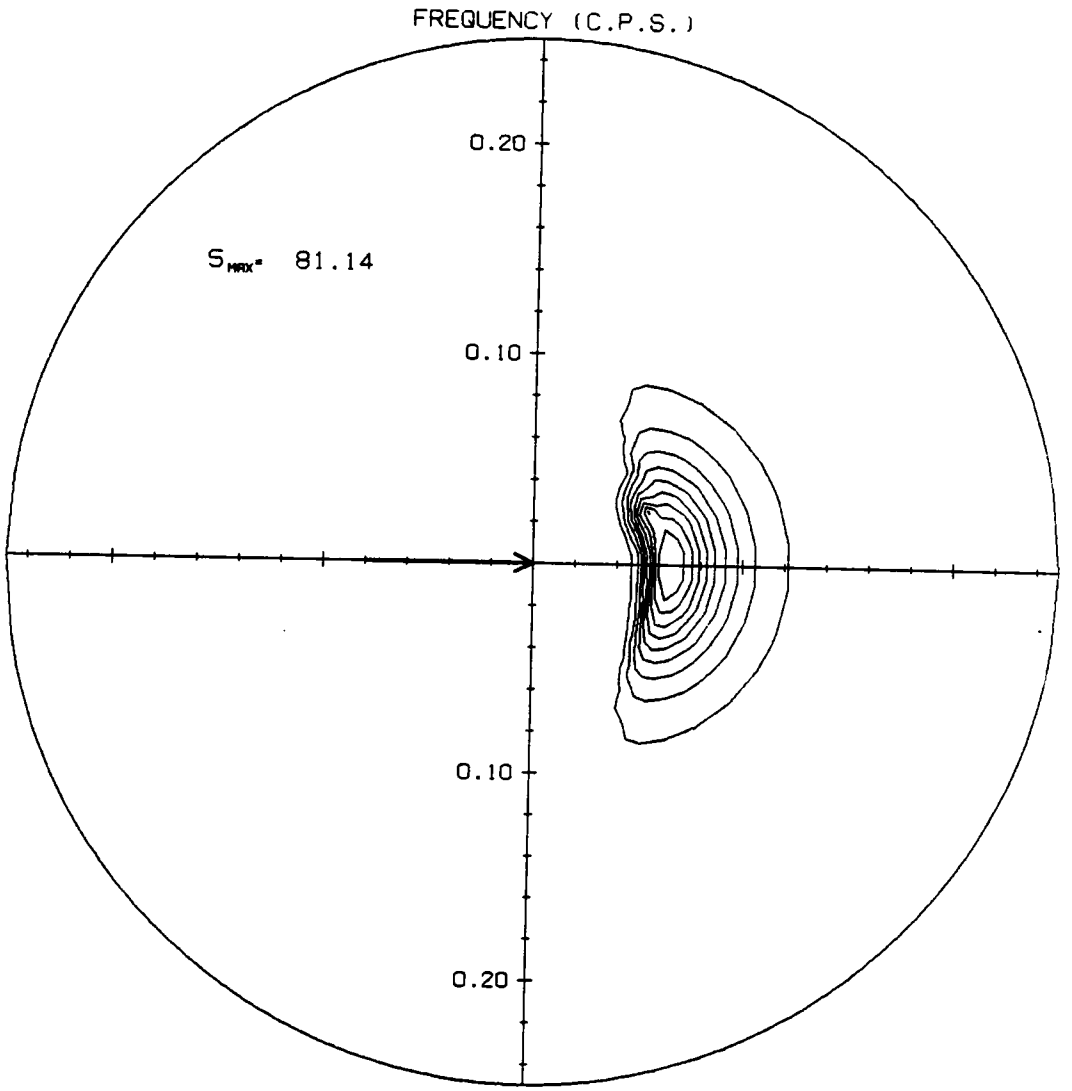

Fig. 31e. T=21 hours

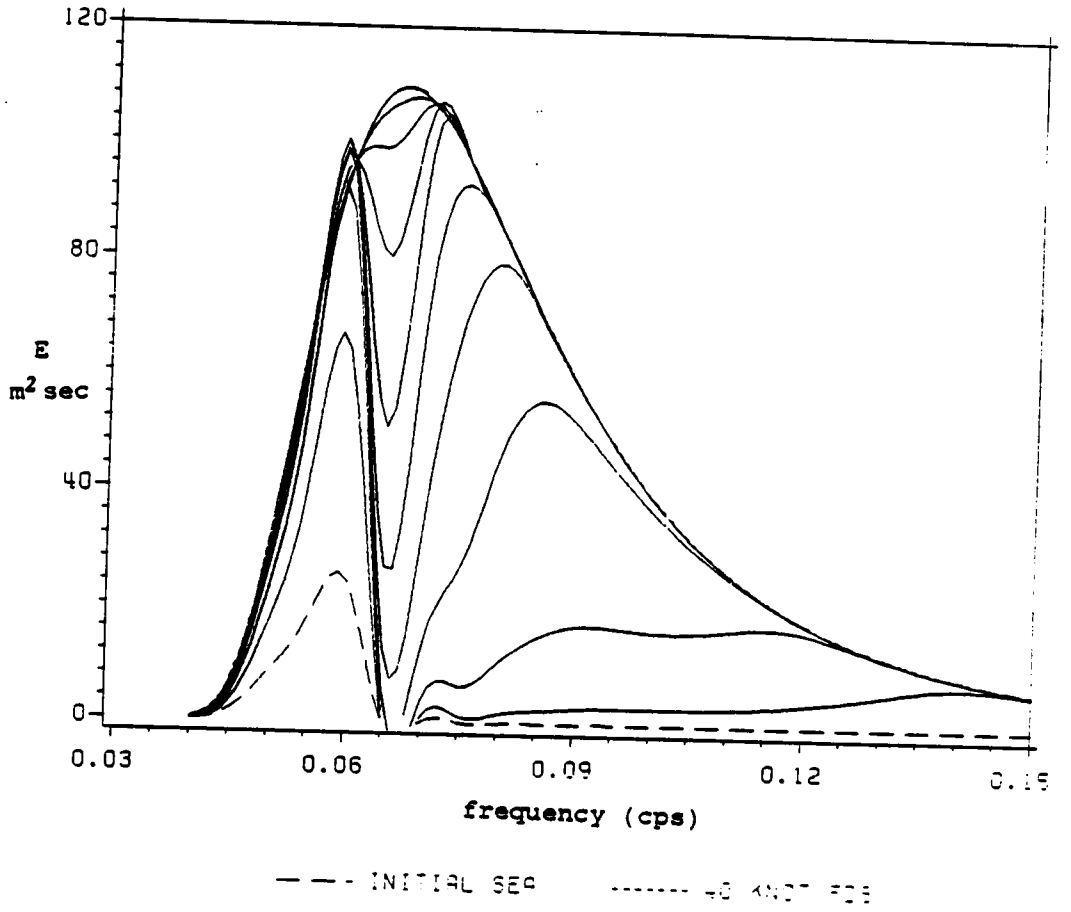

Fig. 32. Point spectrum evolution in the presence of swell from VSOWM in 3 hour time increments.

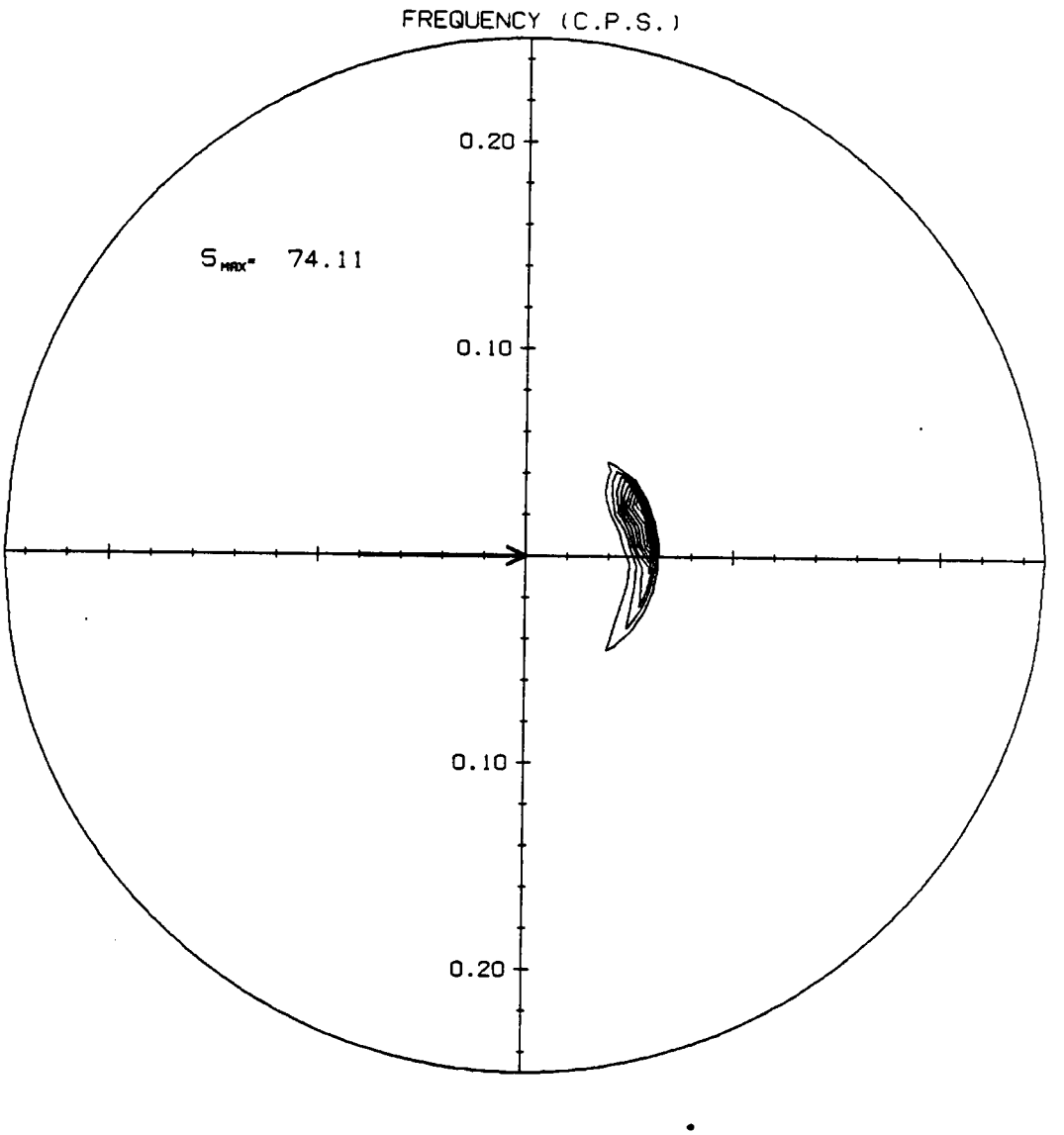

Fig. 33a. Contour plots of 2-D spectrum evolution in the presence of swell from VSOWM. T=3 hours

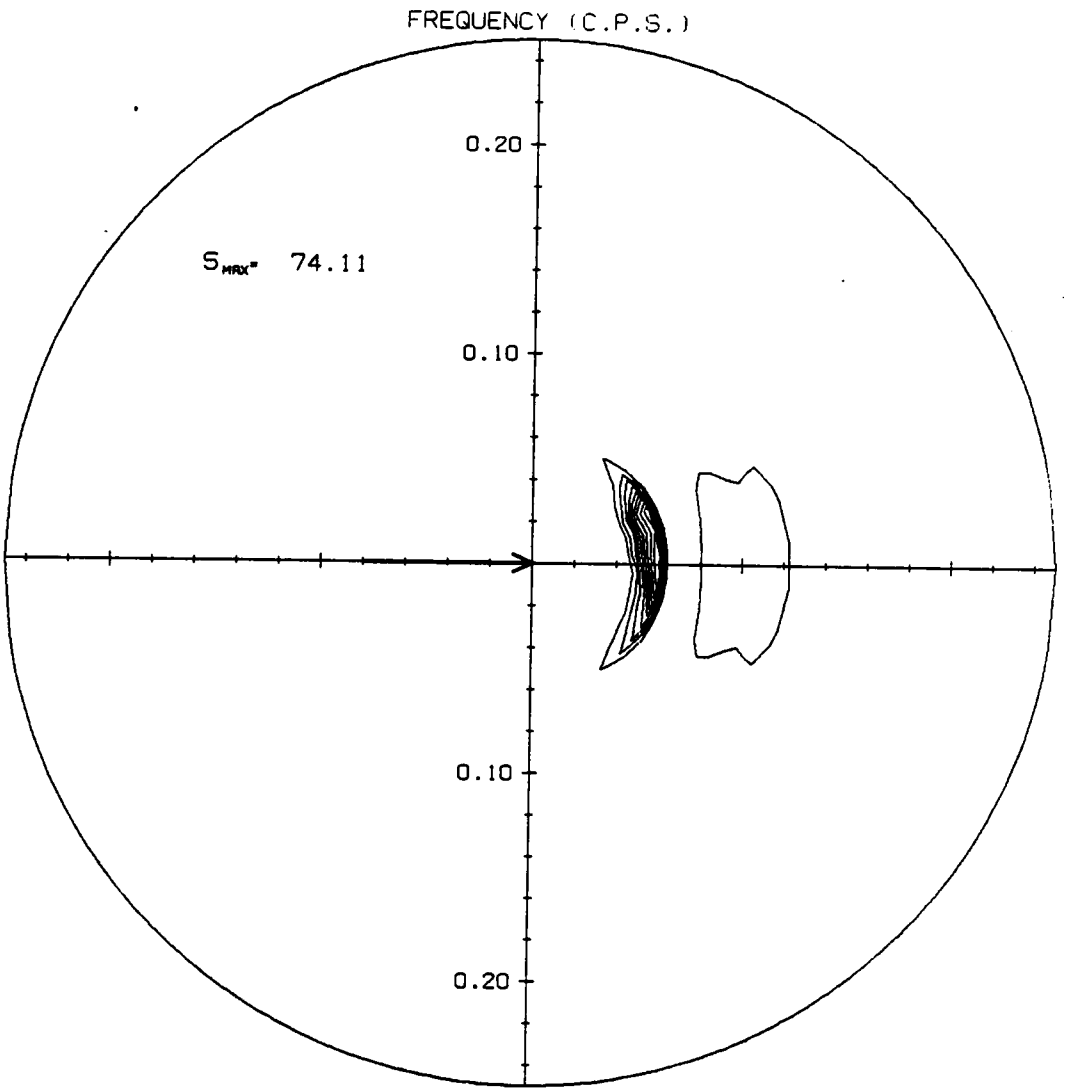

Fig. 33b. T=6 hours

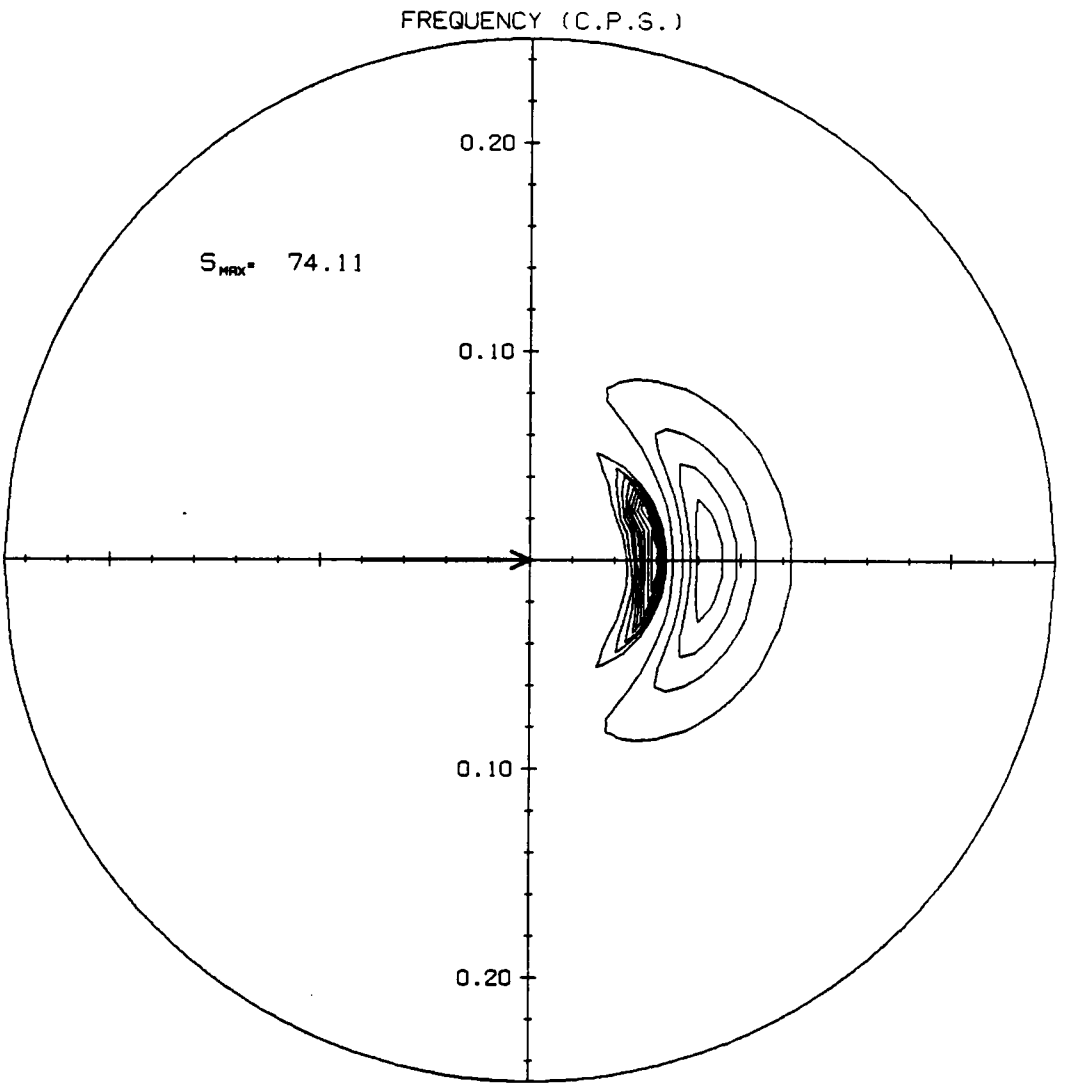

Fig. 33c. T=9 hours

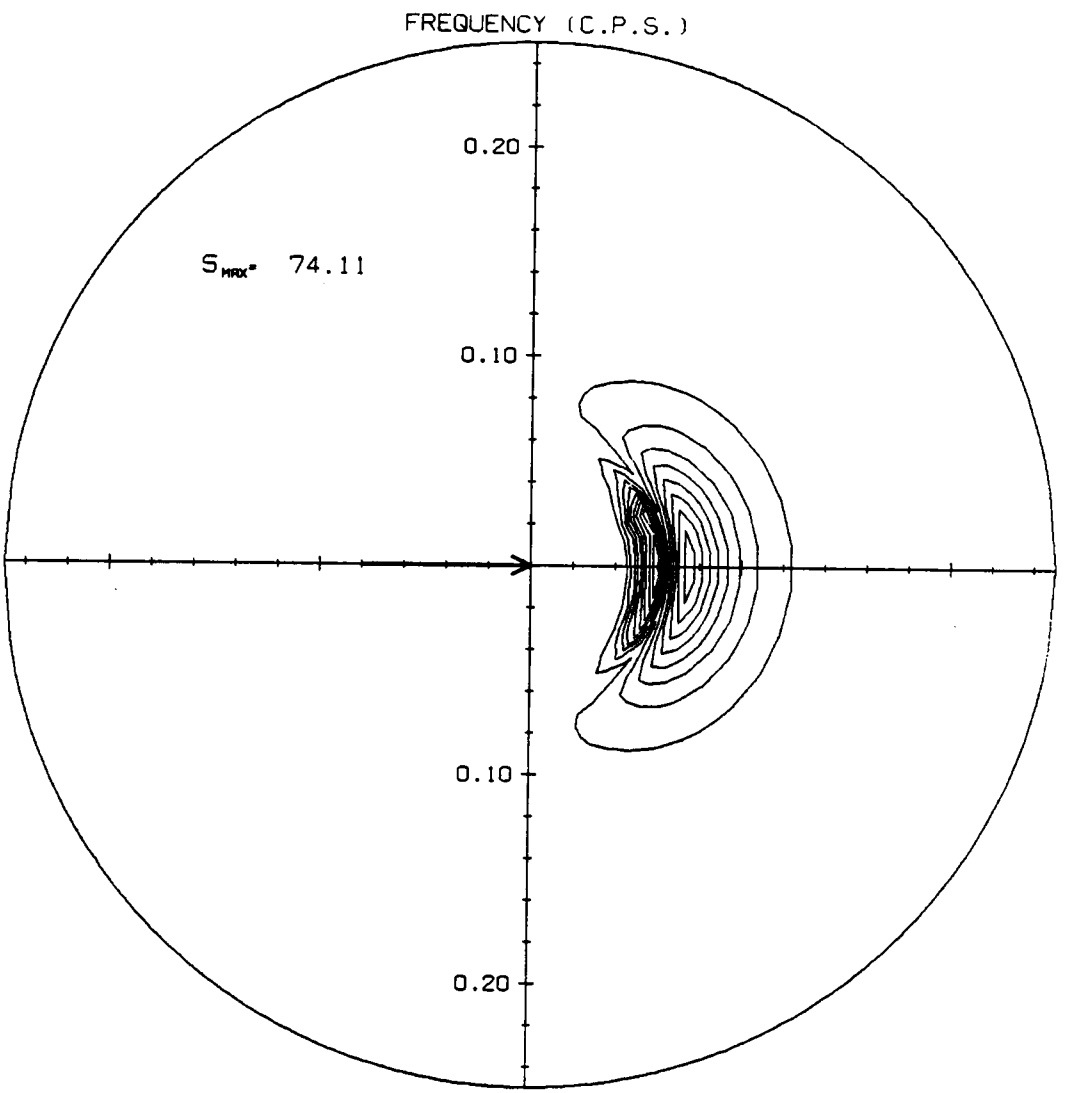

Fig. 33d. T=15 hours

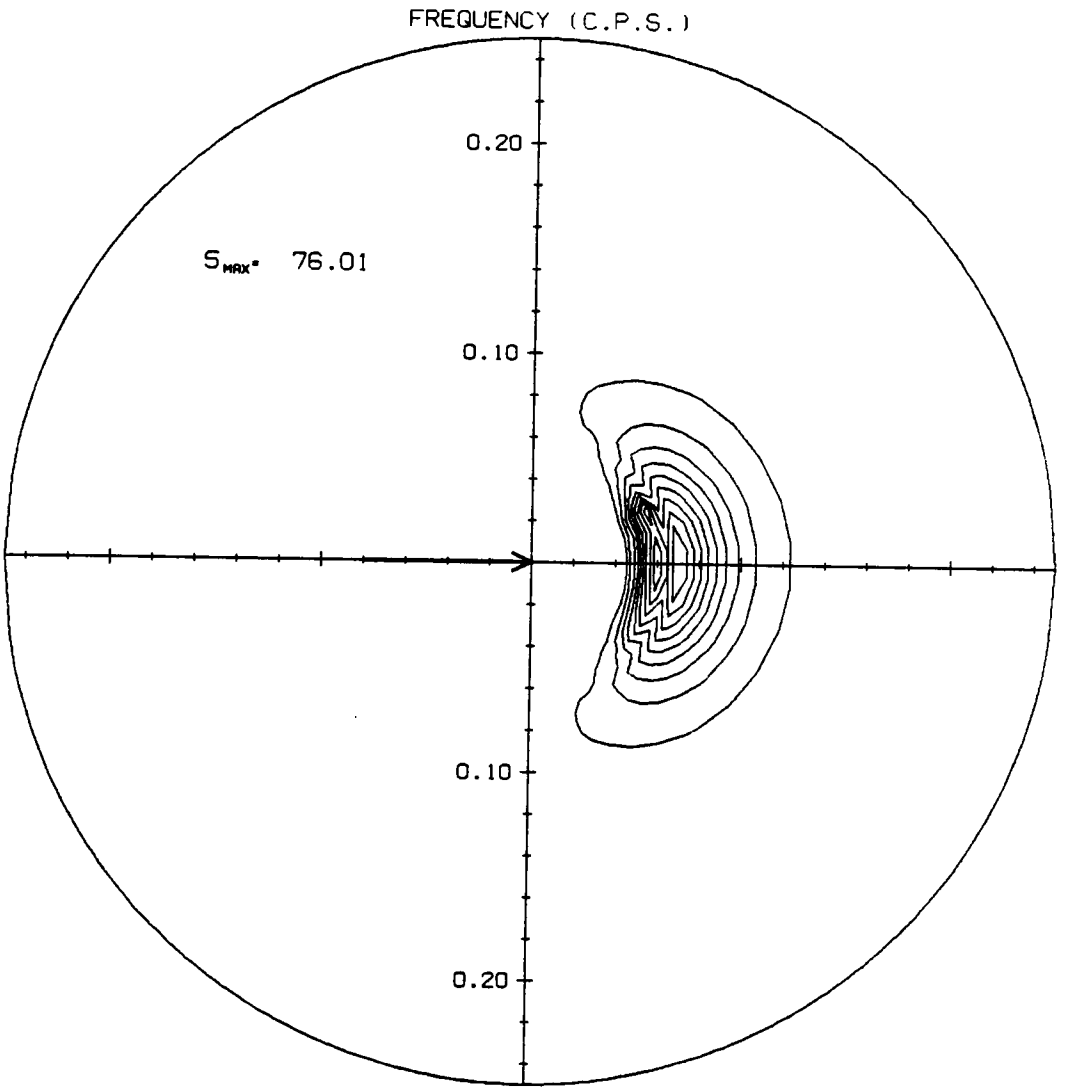

Fig. 33e. T=21 hours

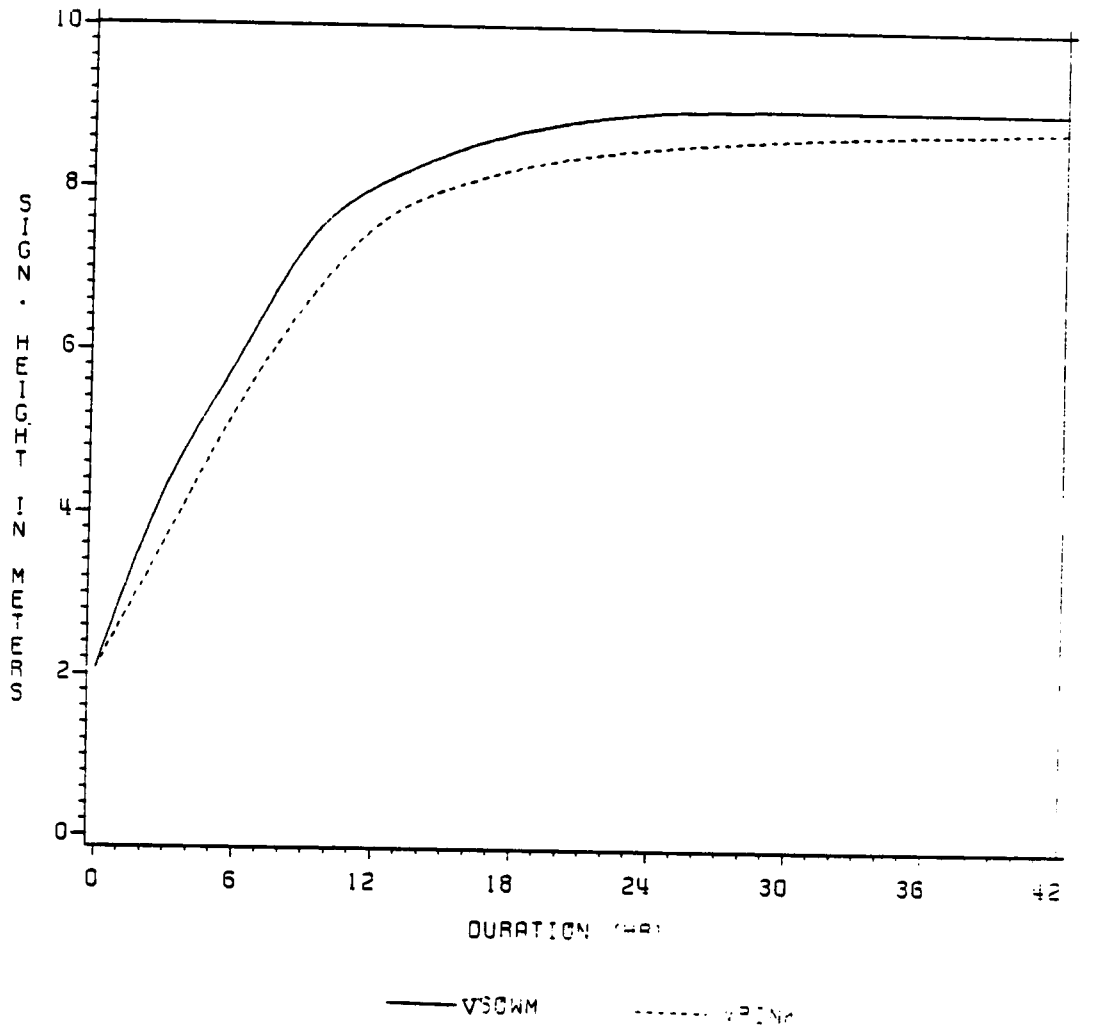

Fig. 34. Comparison of significant wave heights for growth in the presence of swell.

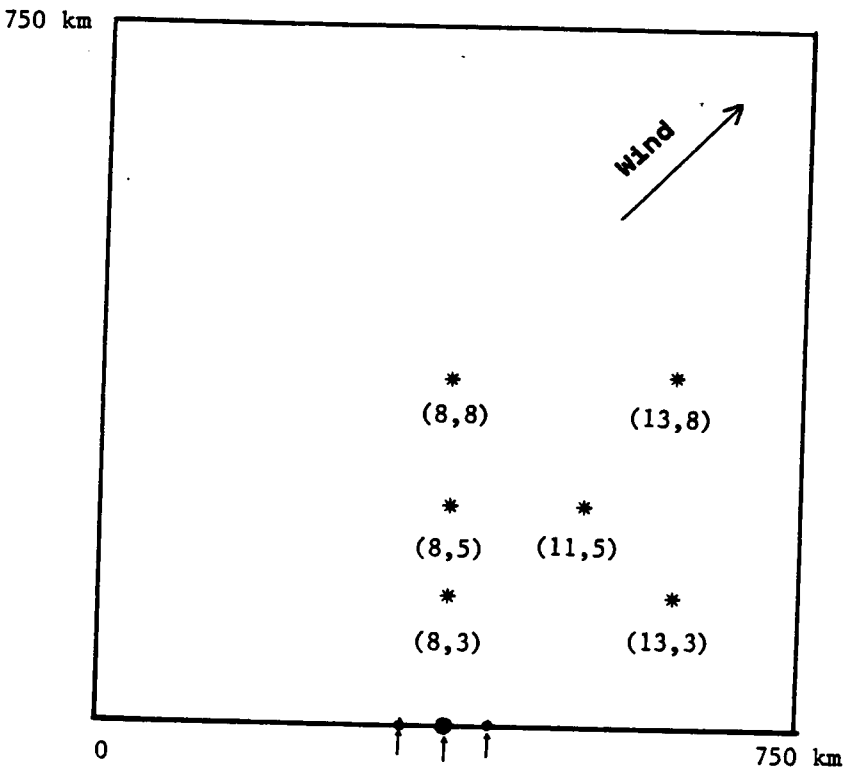

Fig. 35. Finite ocean geometry, output points and swell locations.

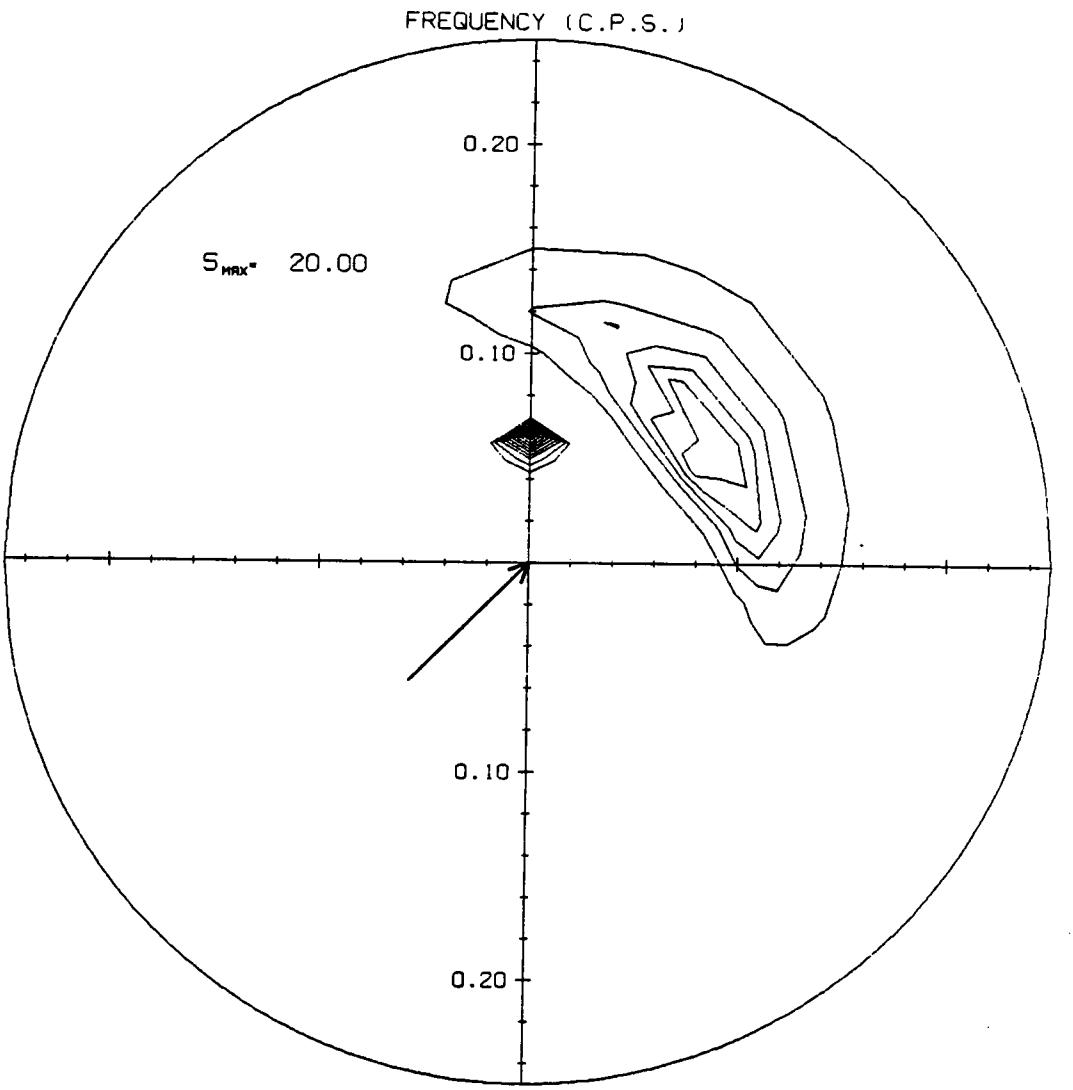

Fig. 36a Contour plots of 2-D spectrum evolution in the presence of swell from VPINK with propagation at location (8,3). T=5 hours

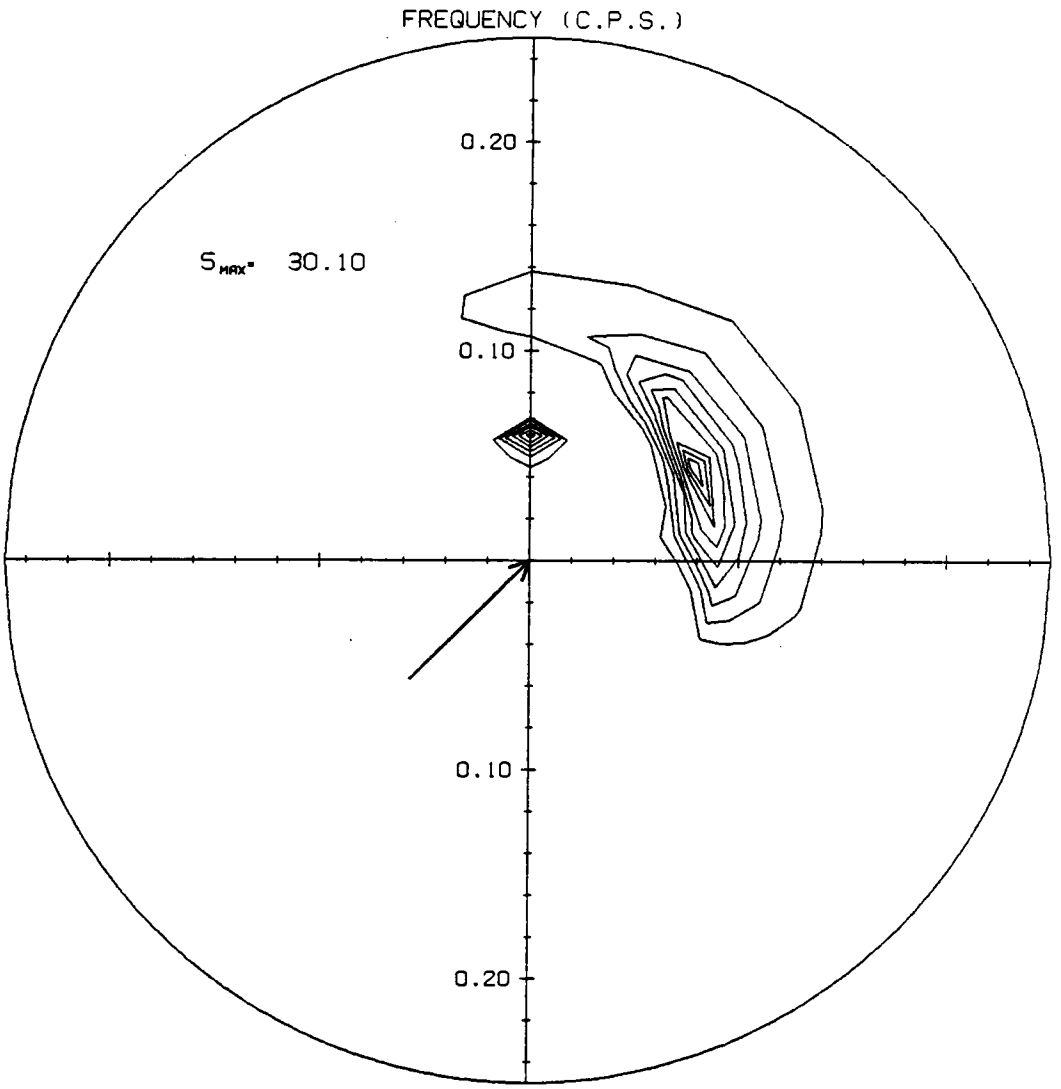

Fig. 36b T=10 hours

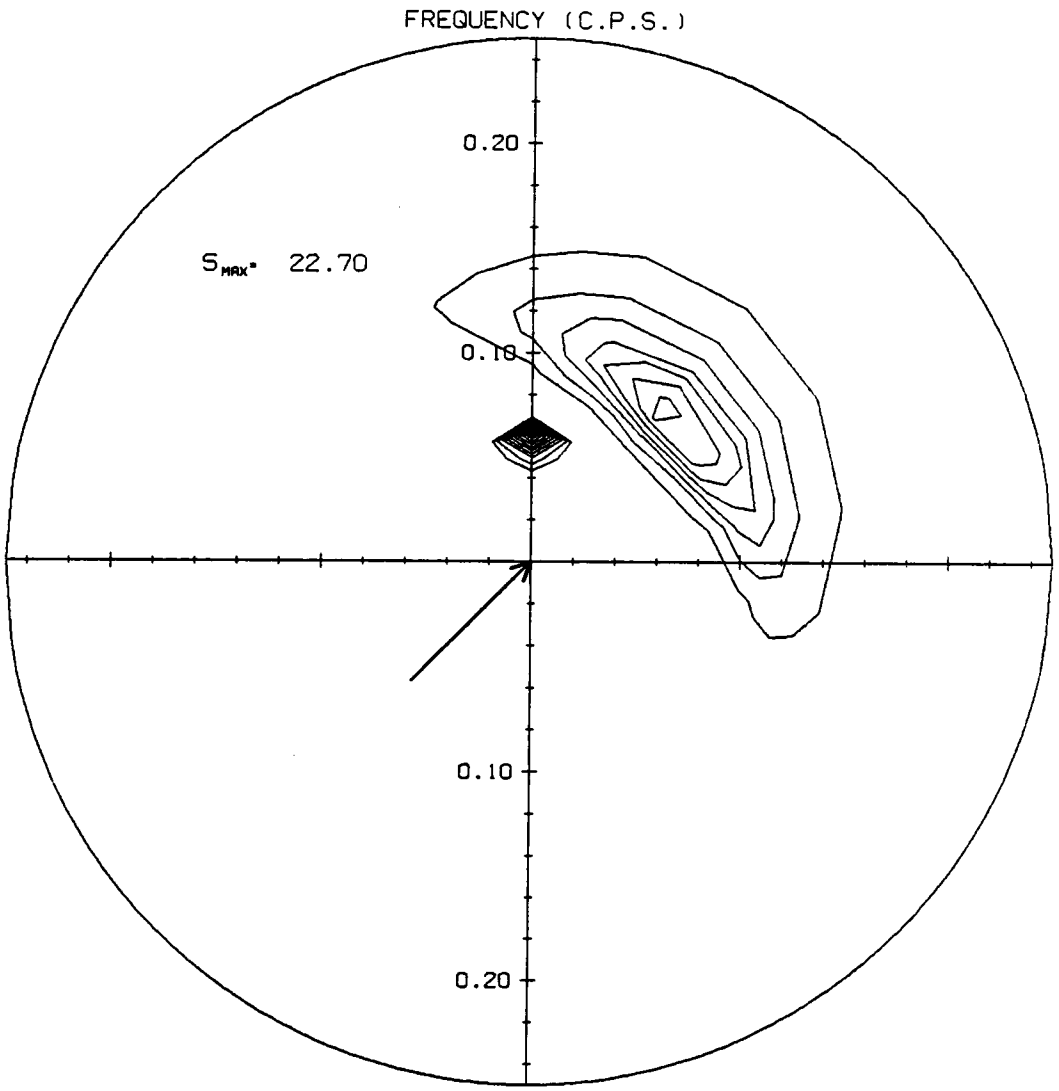

Fig. 37a Contour plots of 2-D spectrum evolution in the presence of swell from VPINK with propagation at location (8,5). T=5 hours

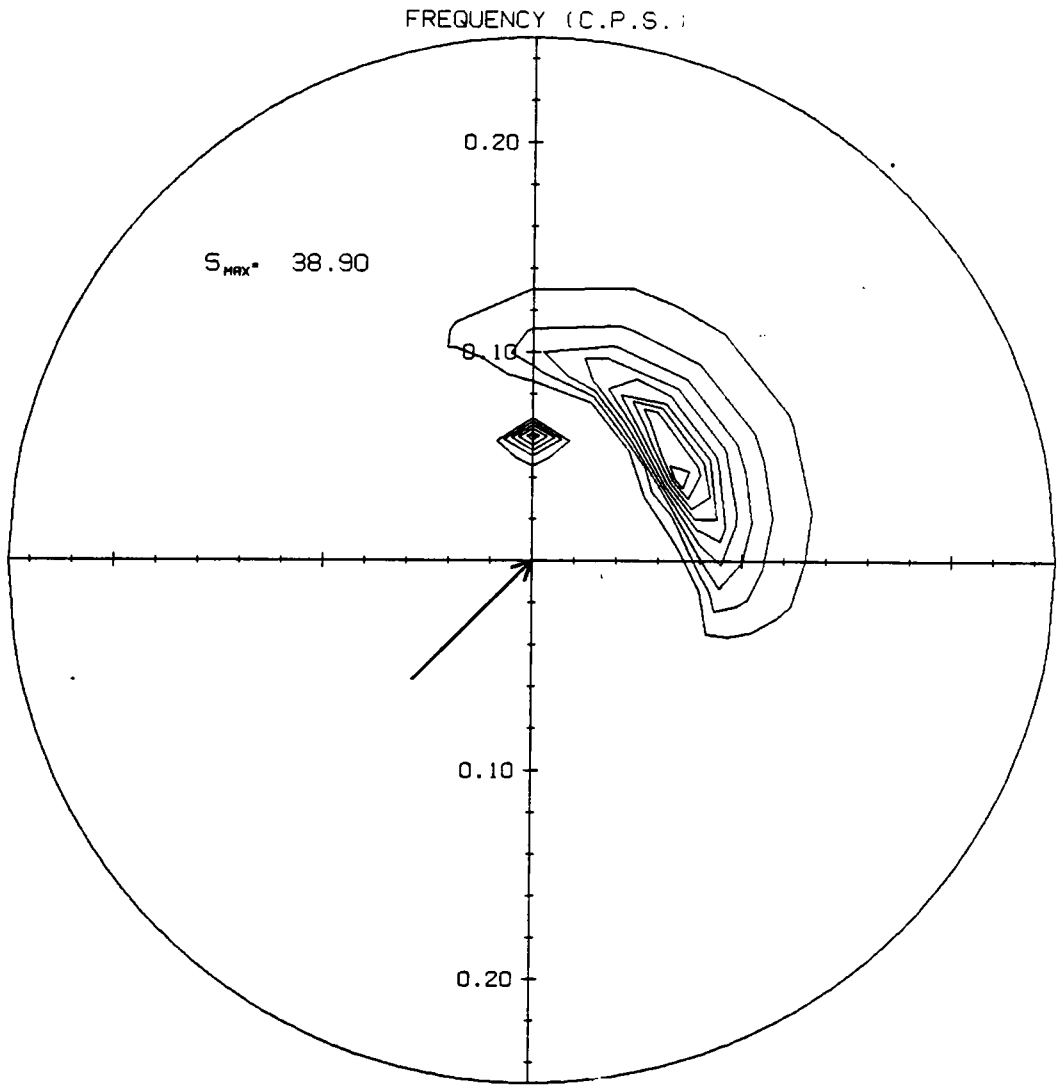

Fig. 37b T=10 hours

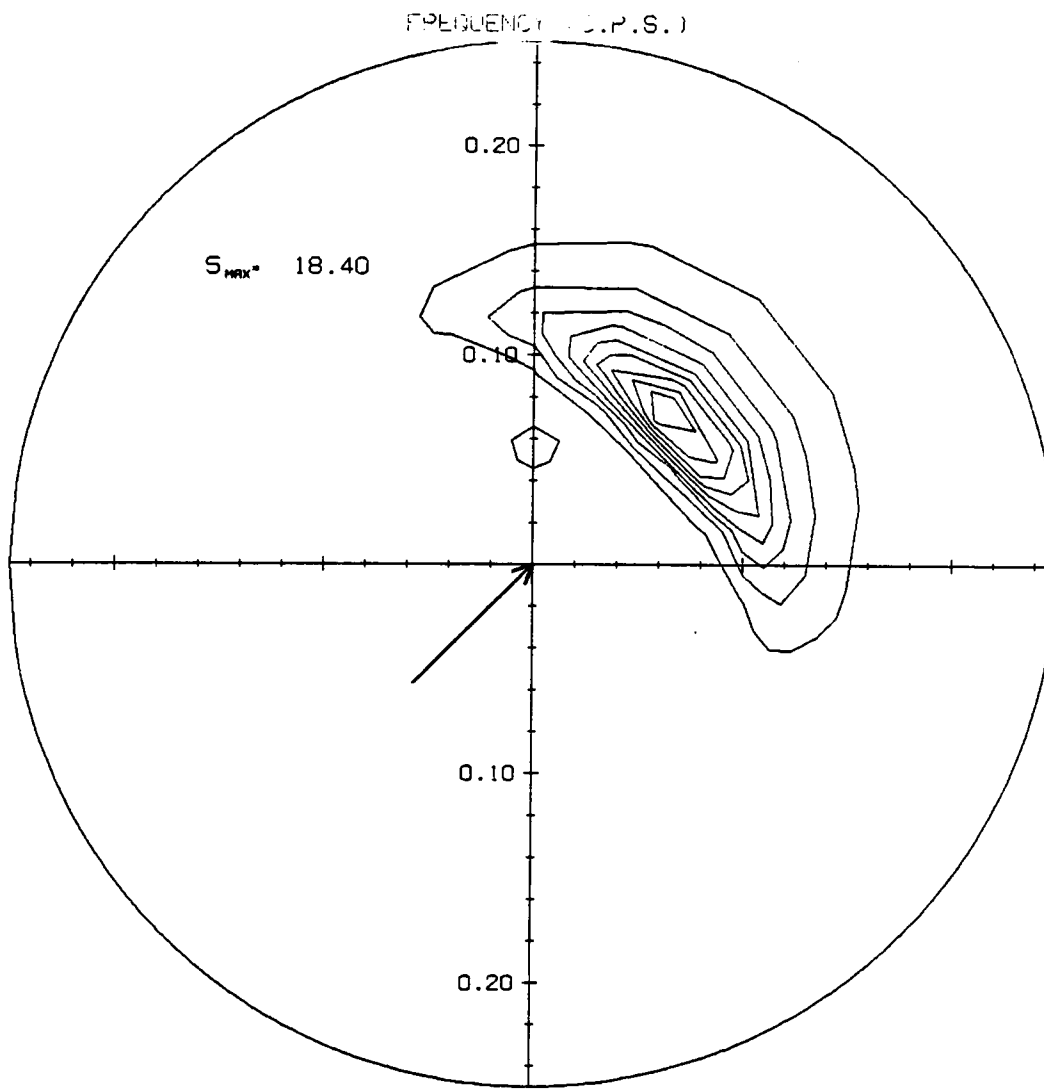

Fig. 38a Contour plots of 2-D spectrum evolution in the presence of swell from VPINK with propagation at location (8,8). T=5 hours

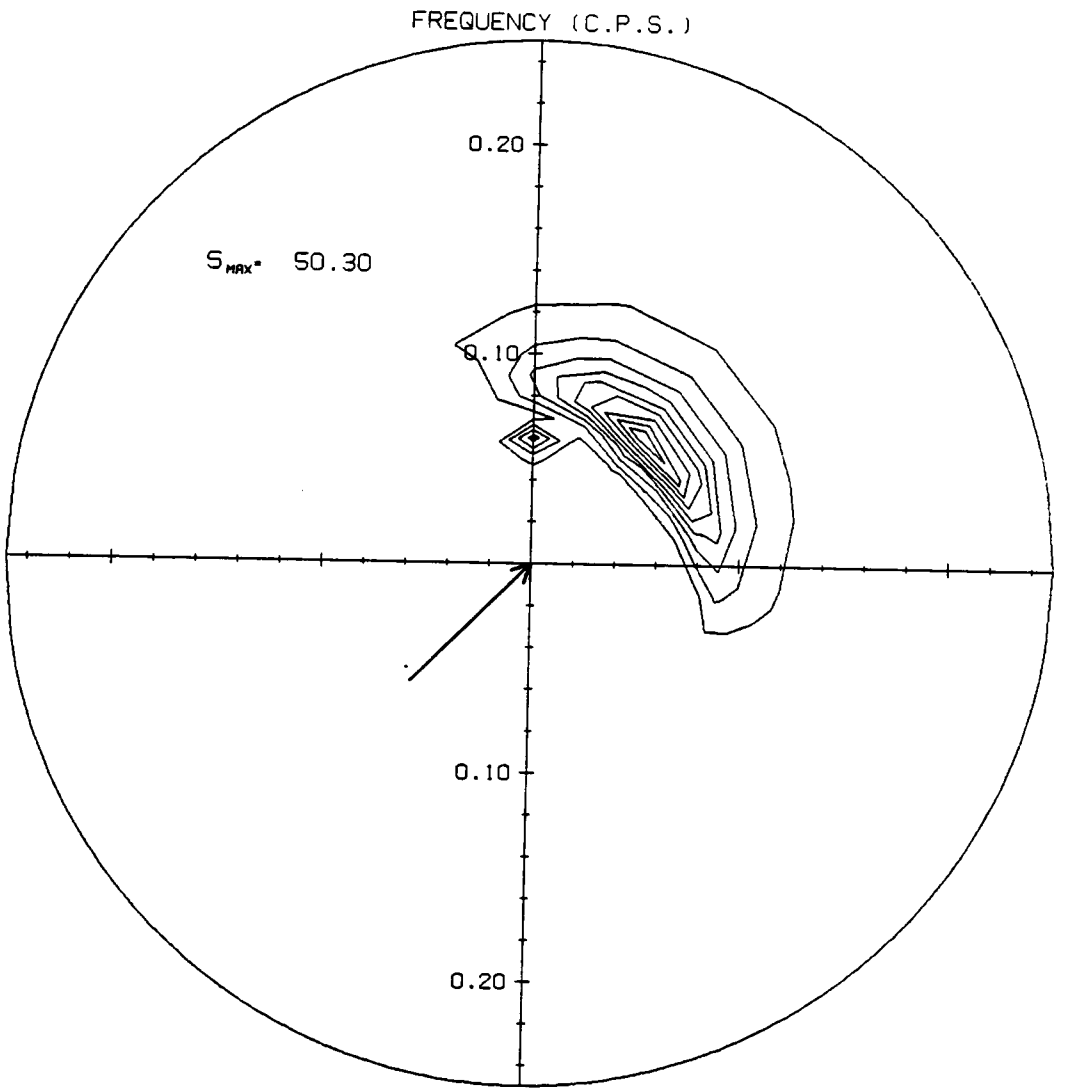

Fig. 38b T=10 hours

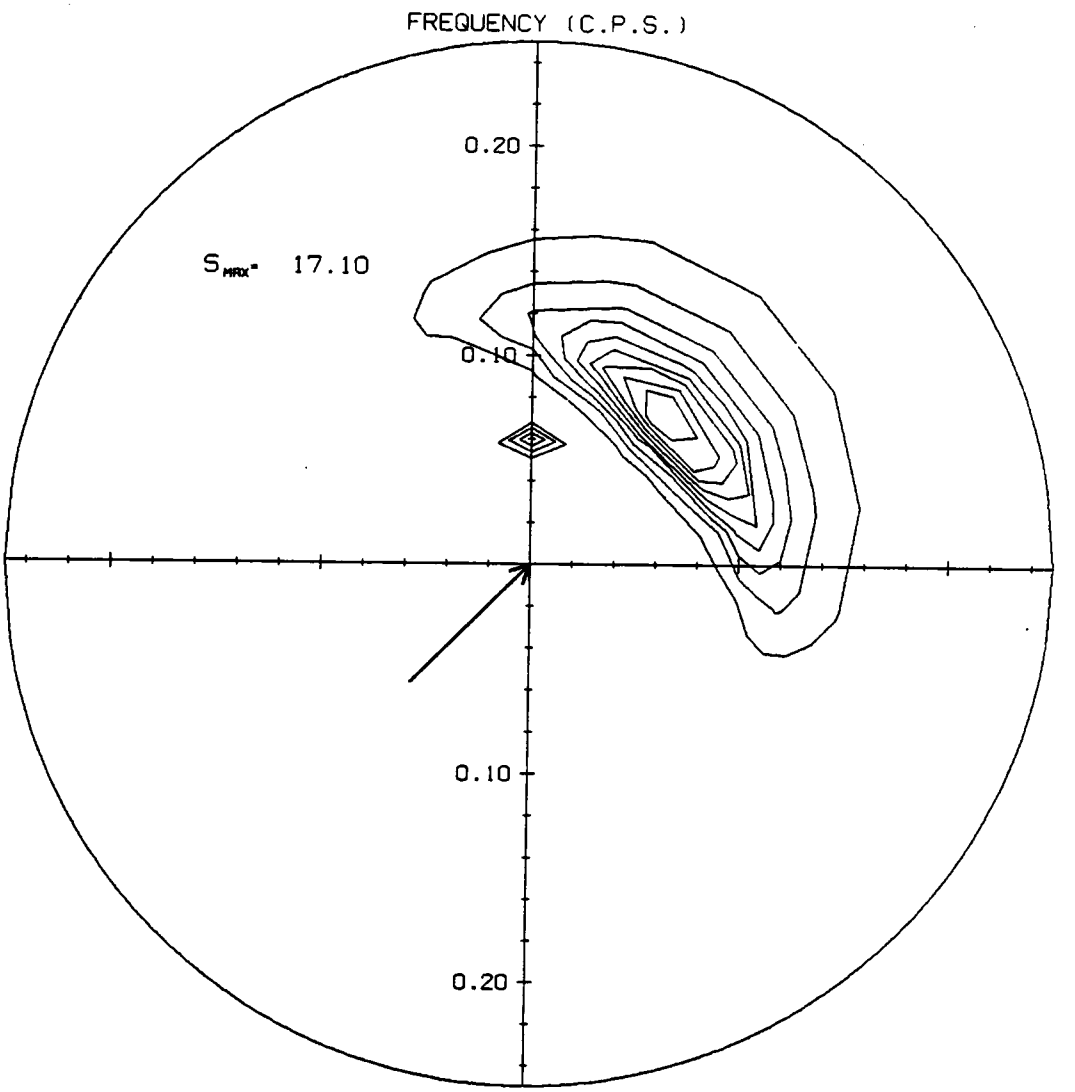

Fig. 39a Contour plots of 2-D spectrum evolution in the presence of swell from VPINK with propagation at location (11,5). T=5 hours

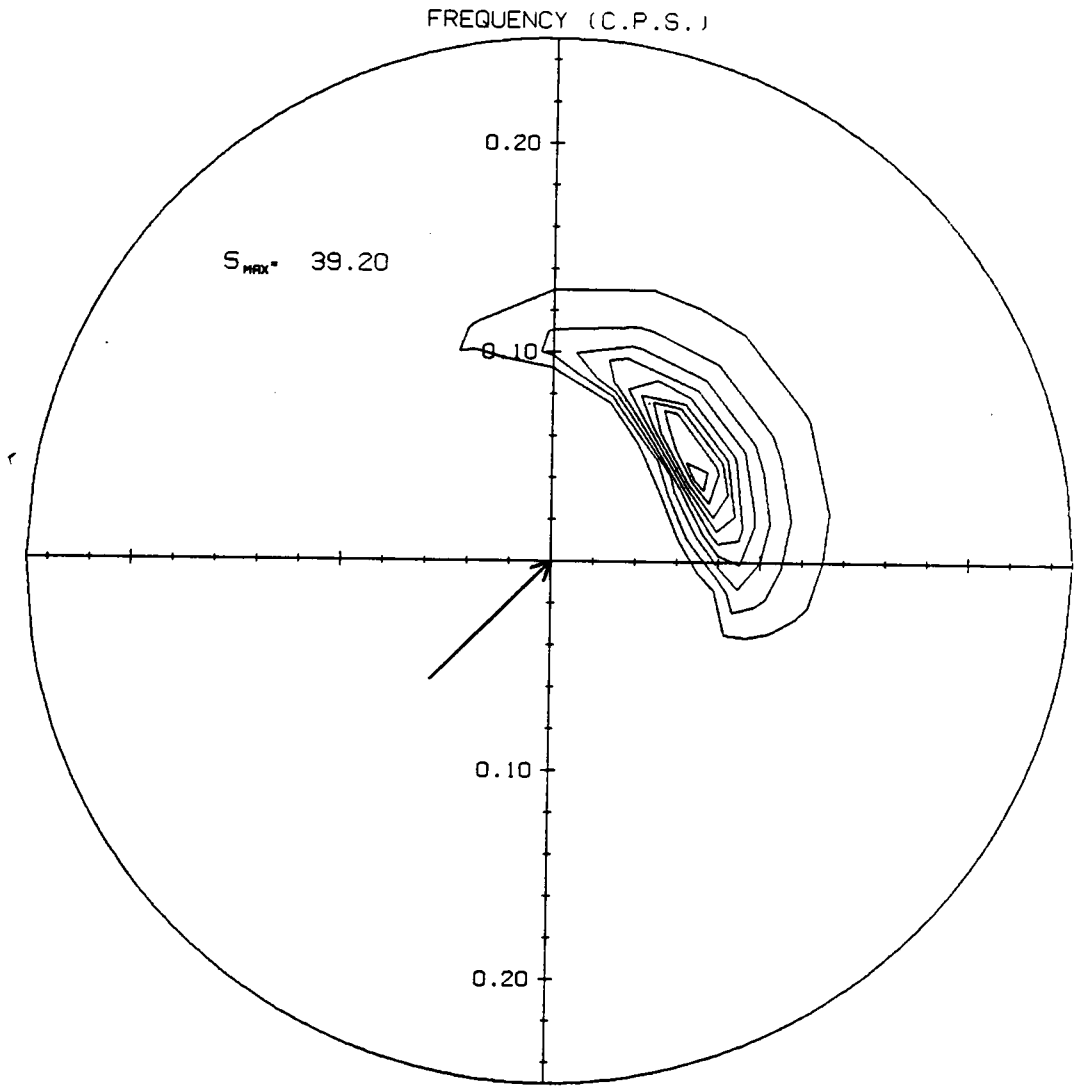

Fig. 39b T=10 hours

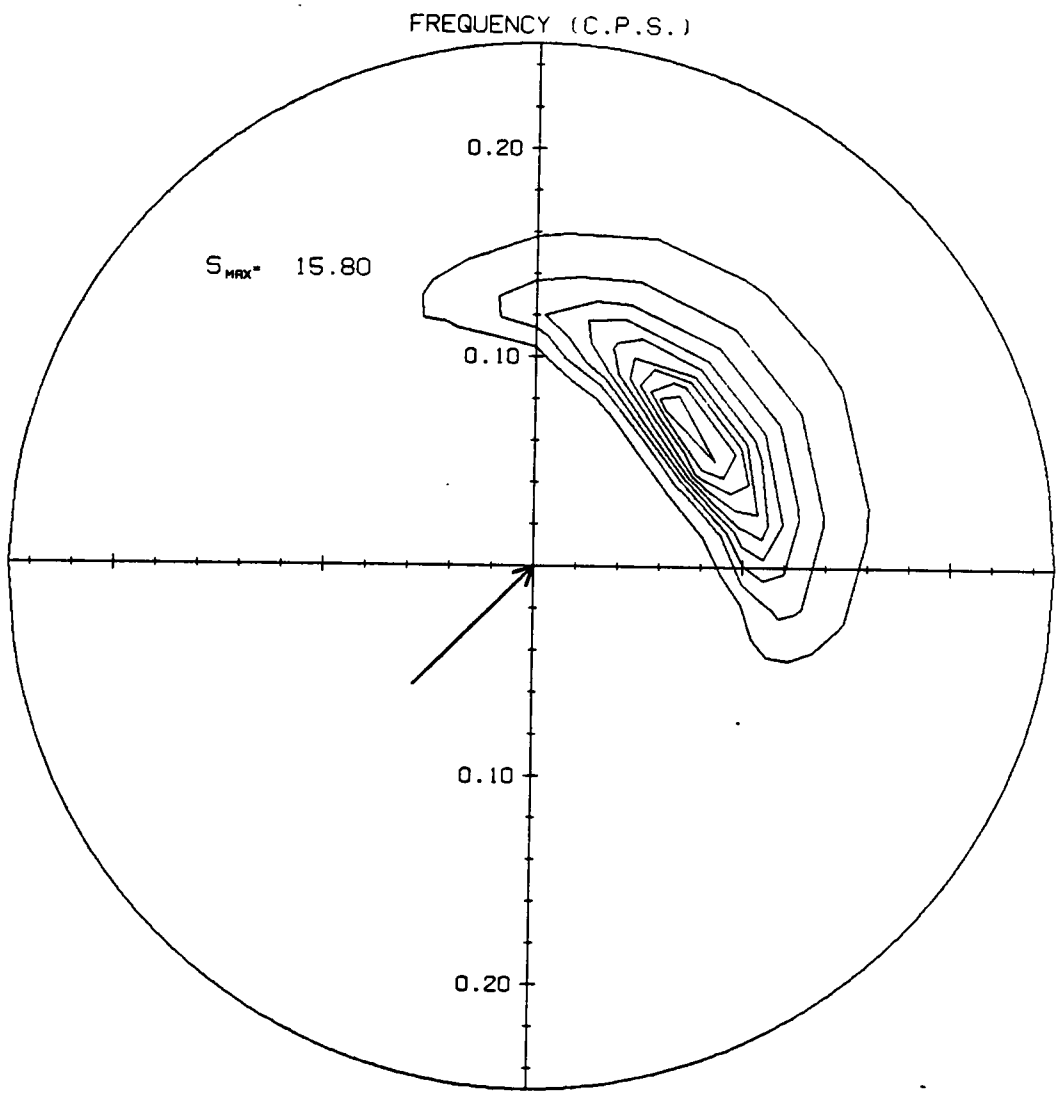

Fig. 40a Contour plots of 2-D spectrum evolution in the presence of swell from VPINK with propagation at location (13,3). T=5 hours

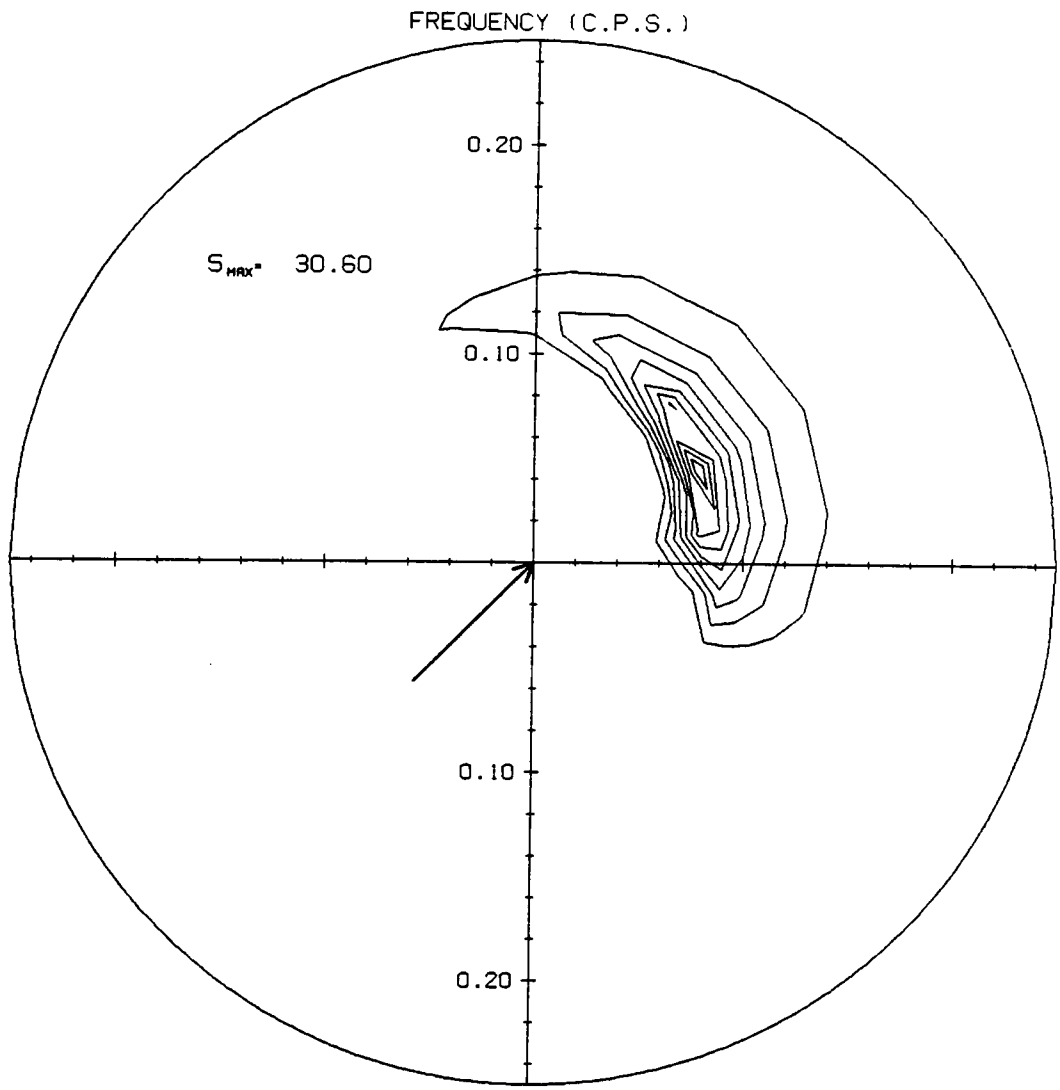

Fig. 40b T=10 hours

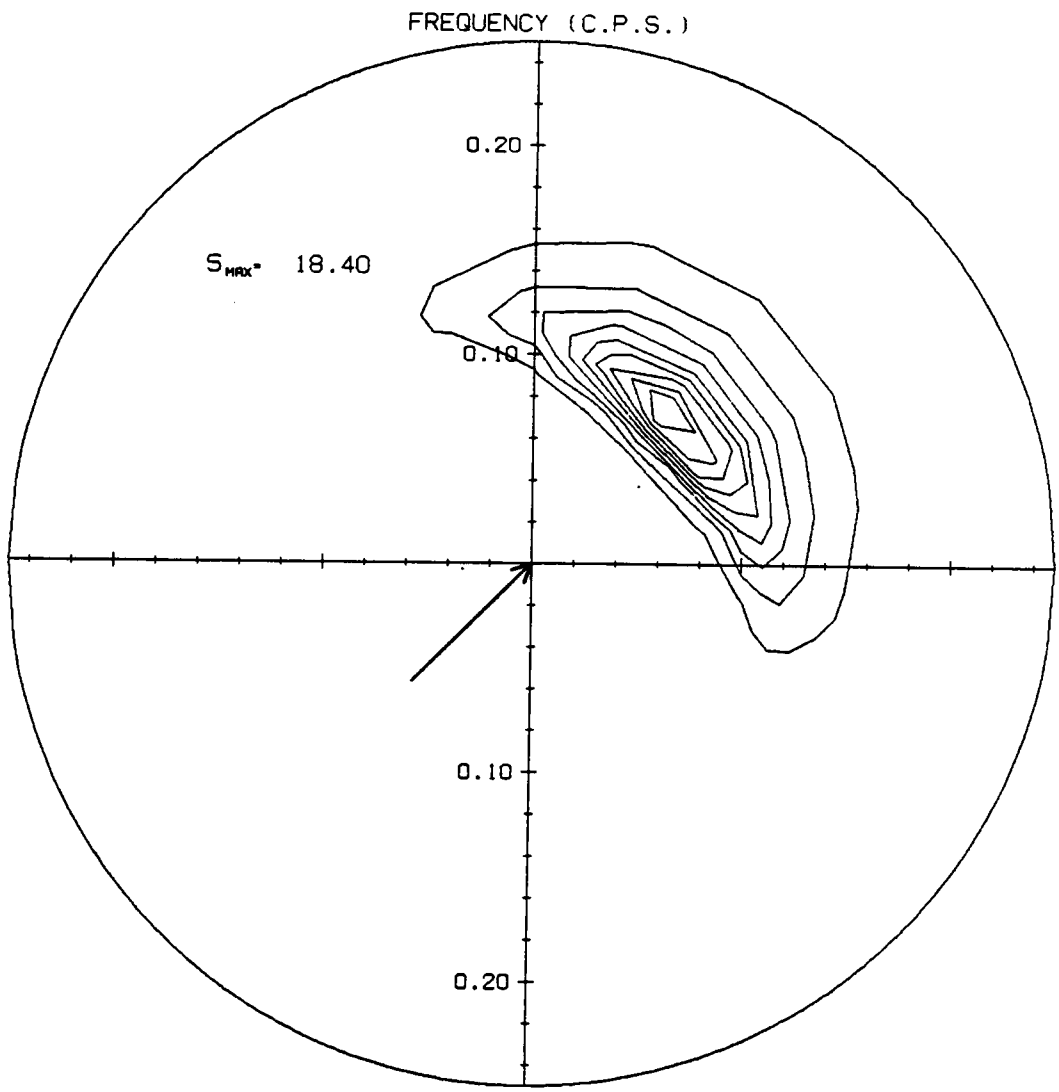

Fig. 41a Contour plots of 2-D spectrum evolution in the presence of swell from VPINK with propagation at location (13,8). T=5 hours

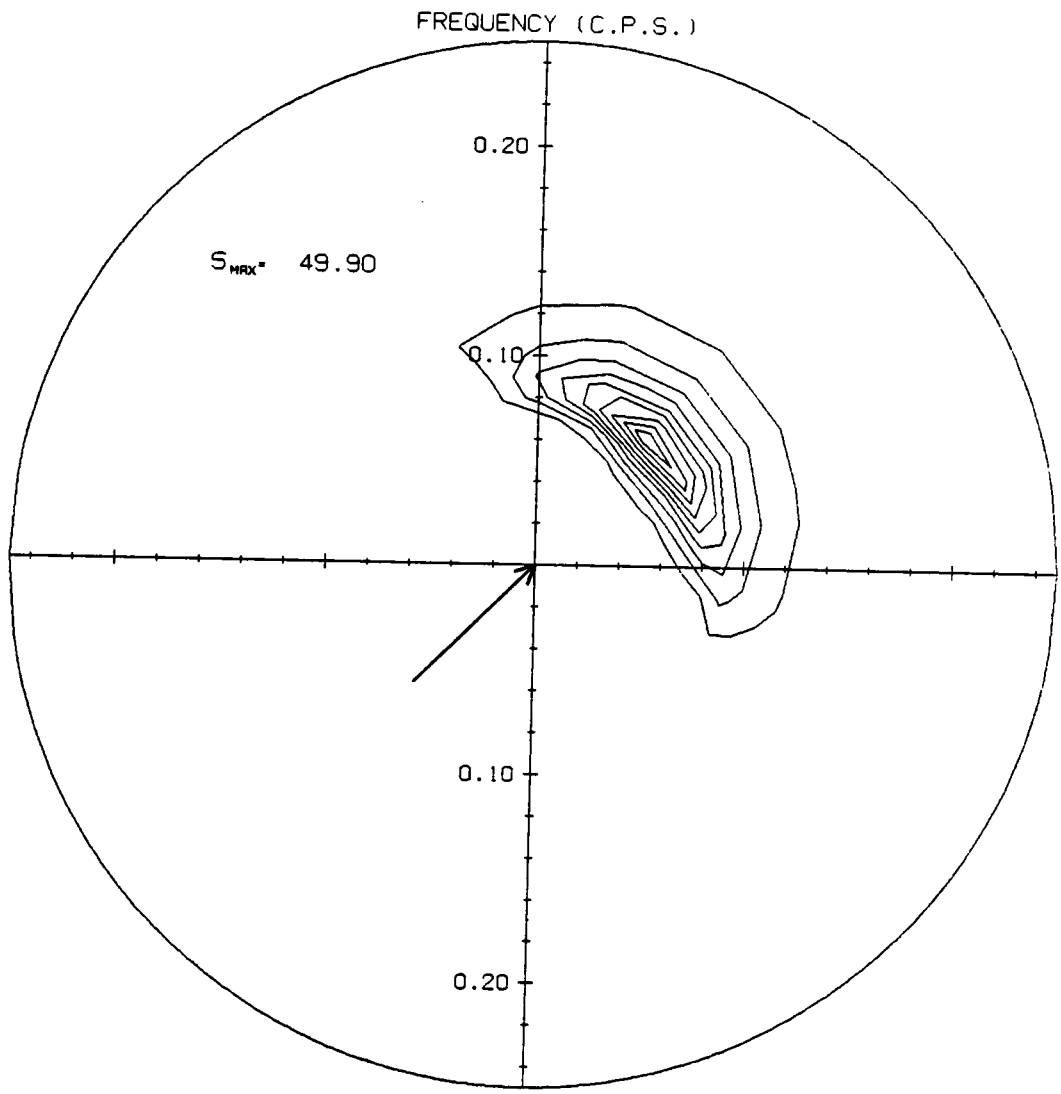

Fig. 41b T=10 hours

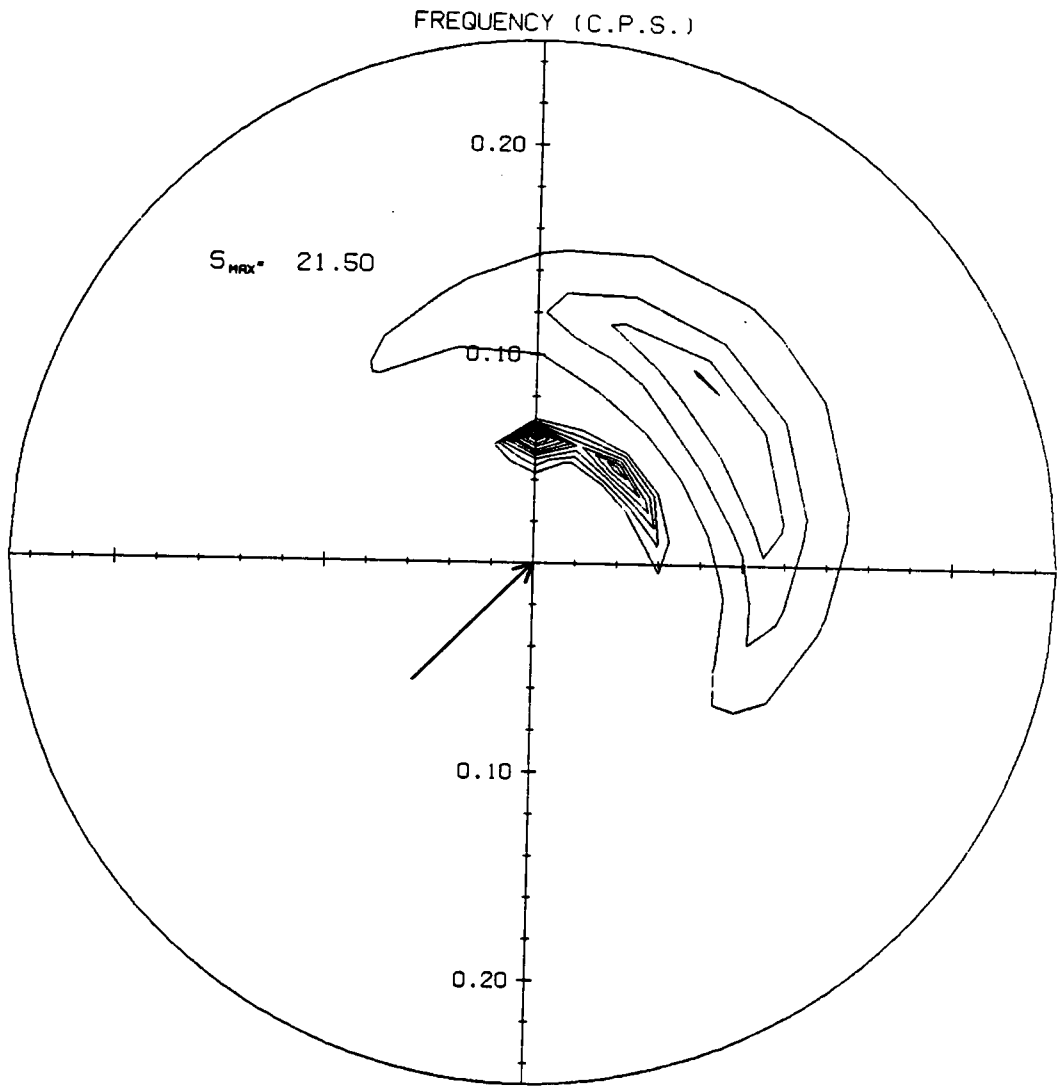

Fig. 42a Contour plots of 2-D spectrum evolution in the presence of swell from VSOWM with propagation at location (8,3). T=5 hours

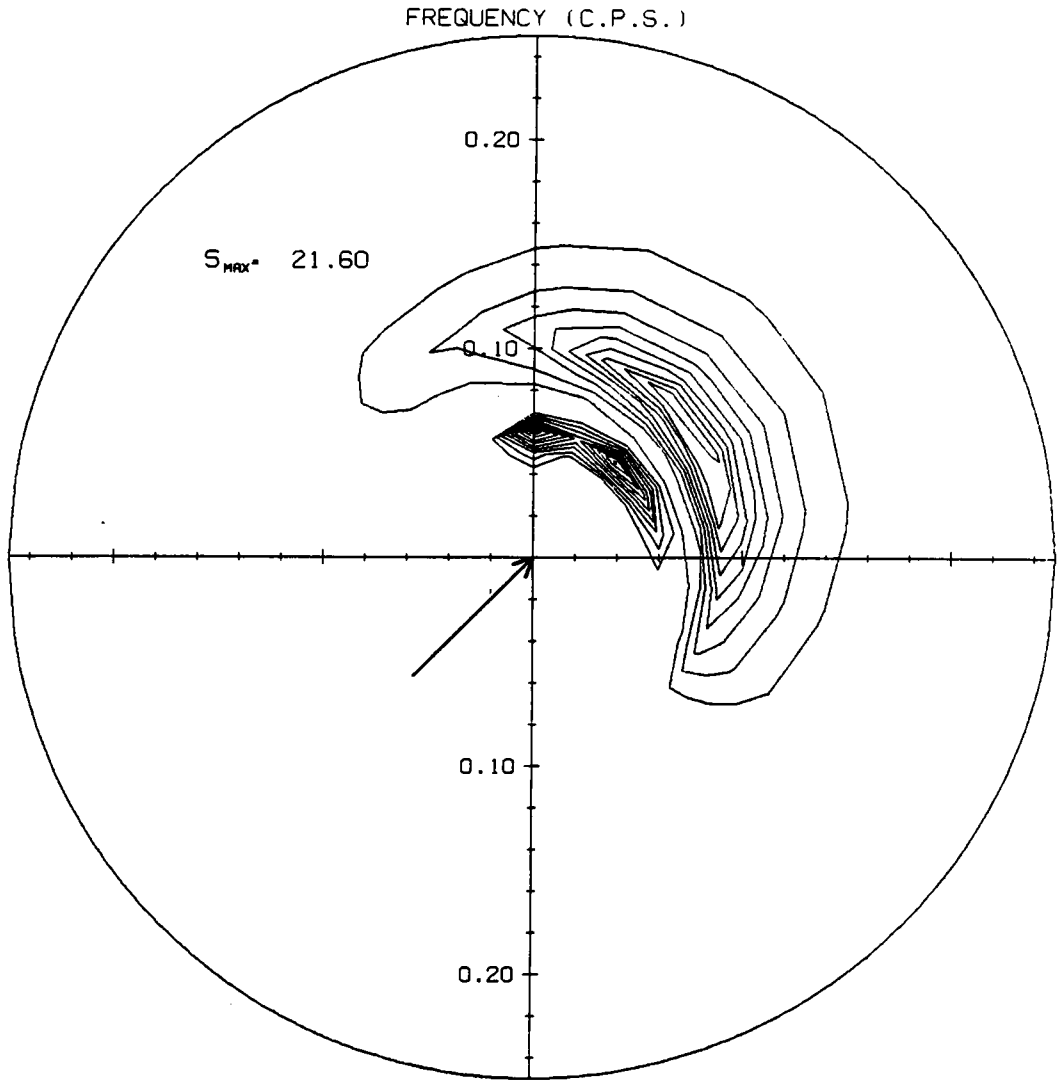

Fig. 42b T=10 hours

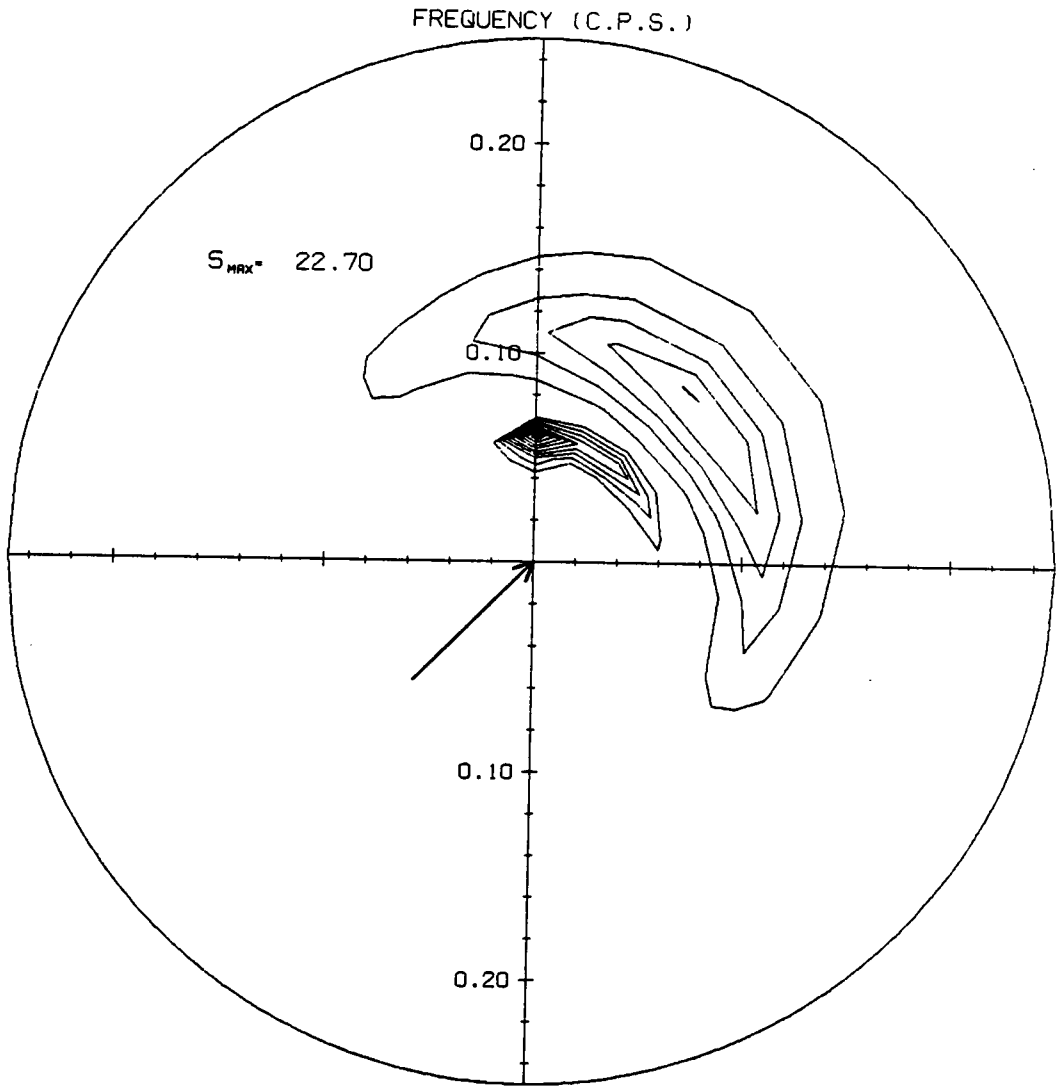

Fig. 43a Contour plots of 2-D spectrum evolution in the presence of swell from VSOWM with propagation at location (8,5). T=5 hours

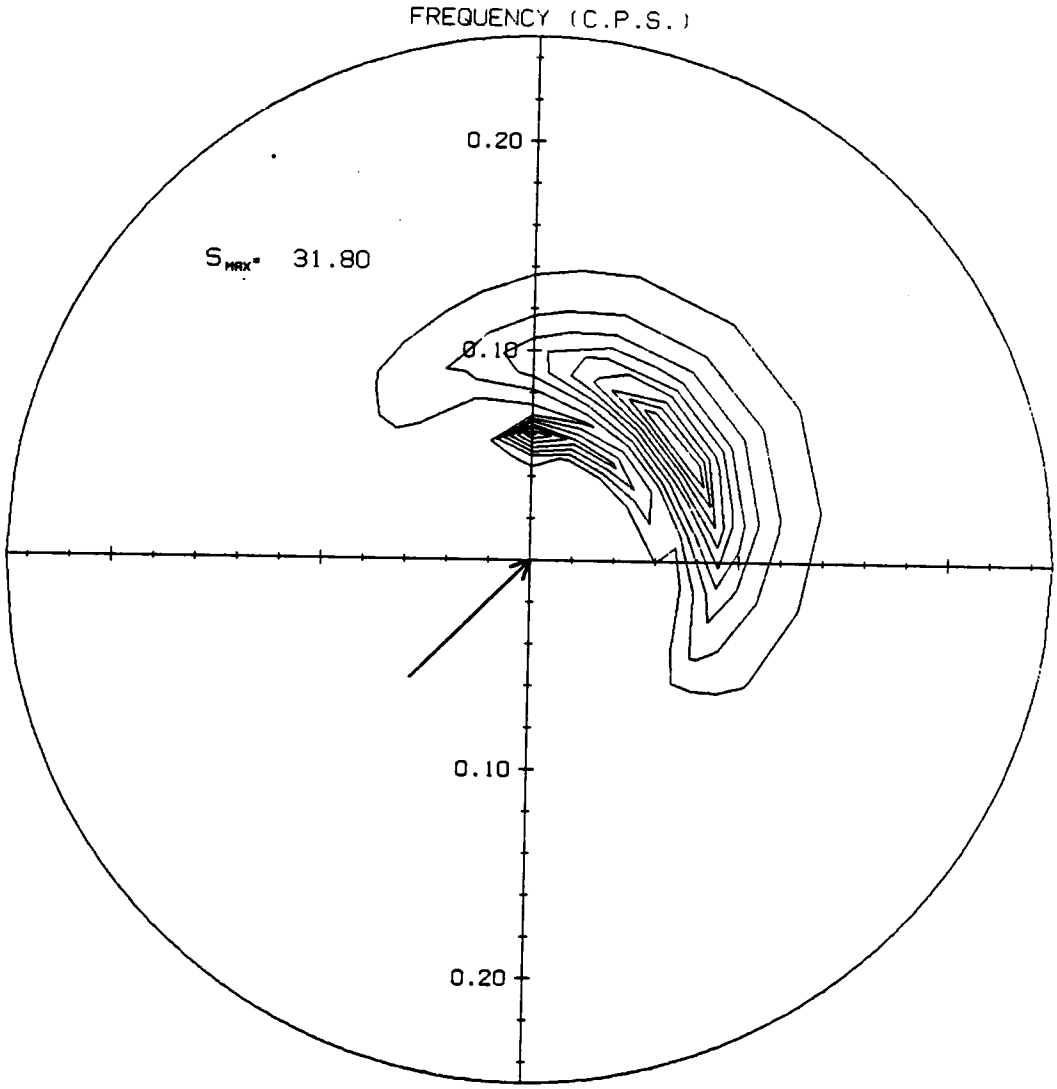

Fig. 43b T=10 hours

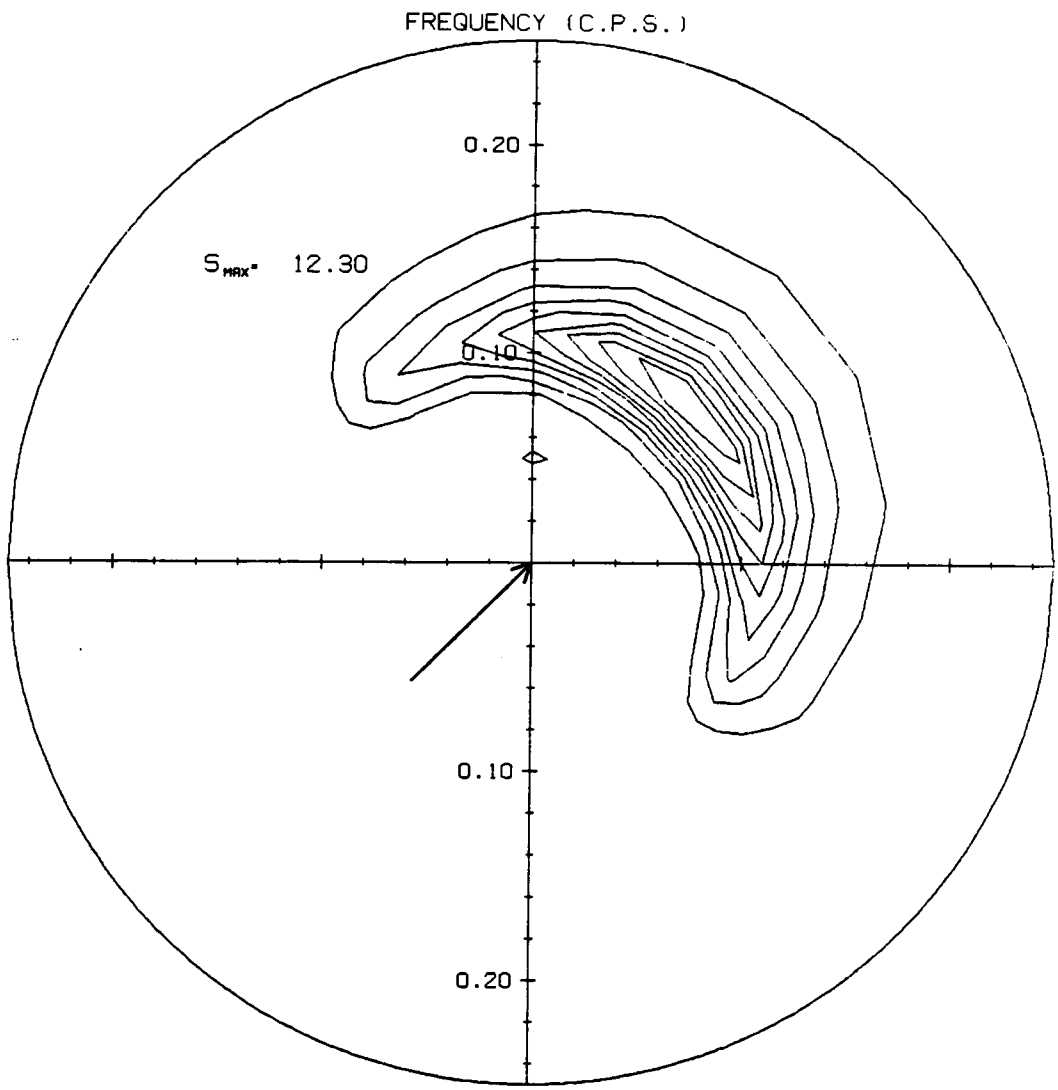

Fig. 44a Contour plots of 2-D spectrum evolution in the presence of swell from VSOWM with propagation at location (8,8). T=5 hours

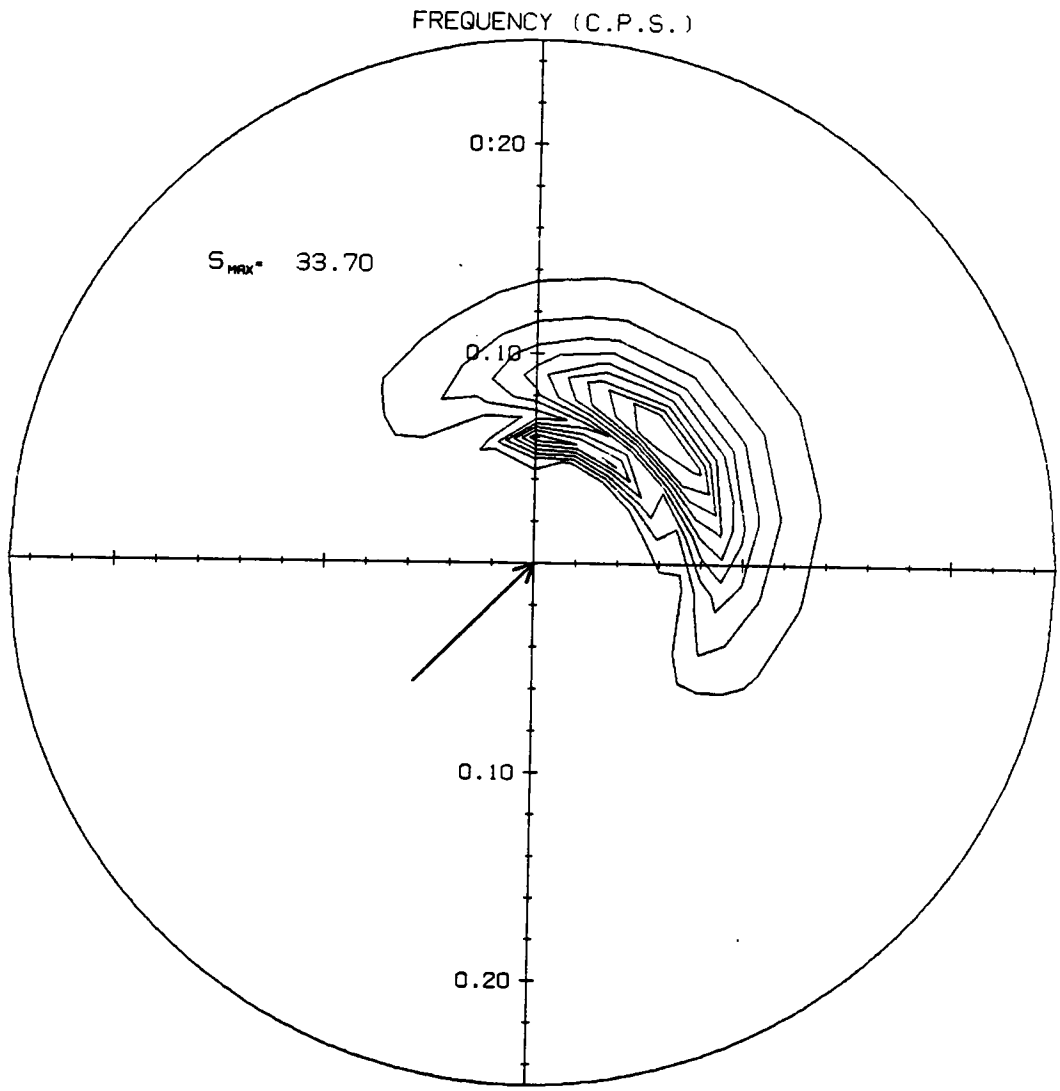

Fig. 44b T=10 hours

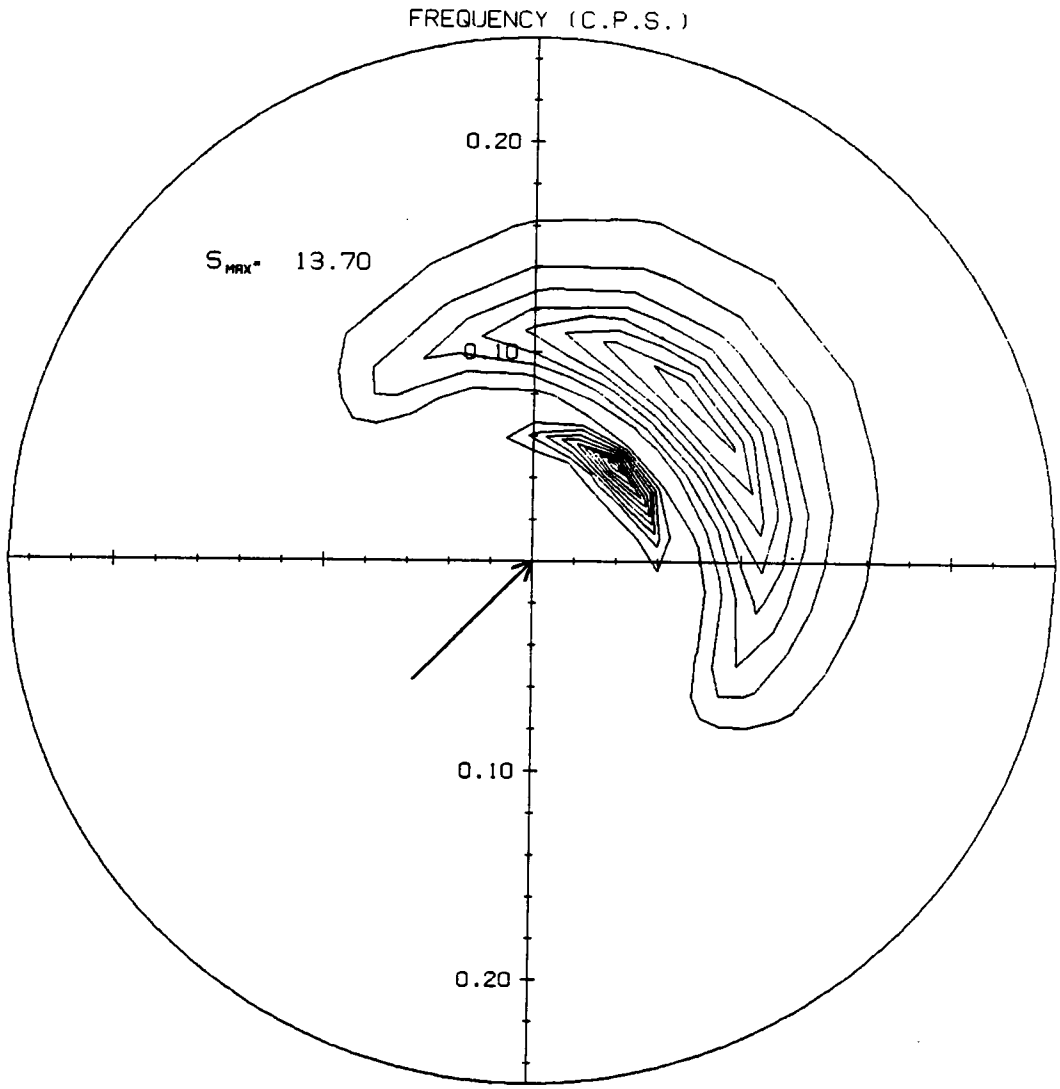

Fig. 45a Contour plots of 2-D spectrum evolution in the presence of swell from VSOWM with propagation at location (11,5). T=5 hours

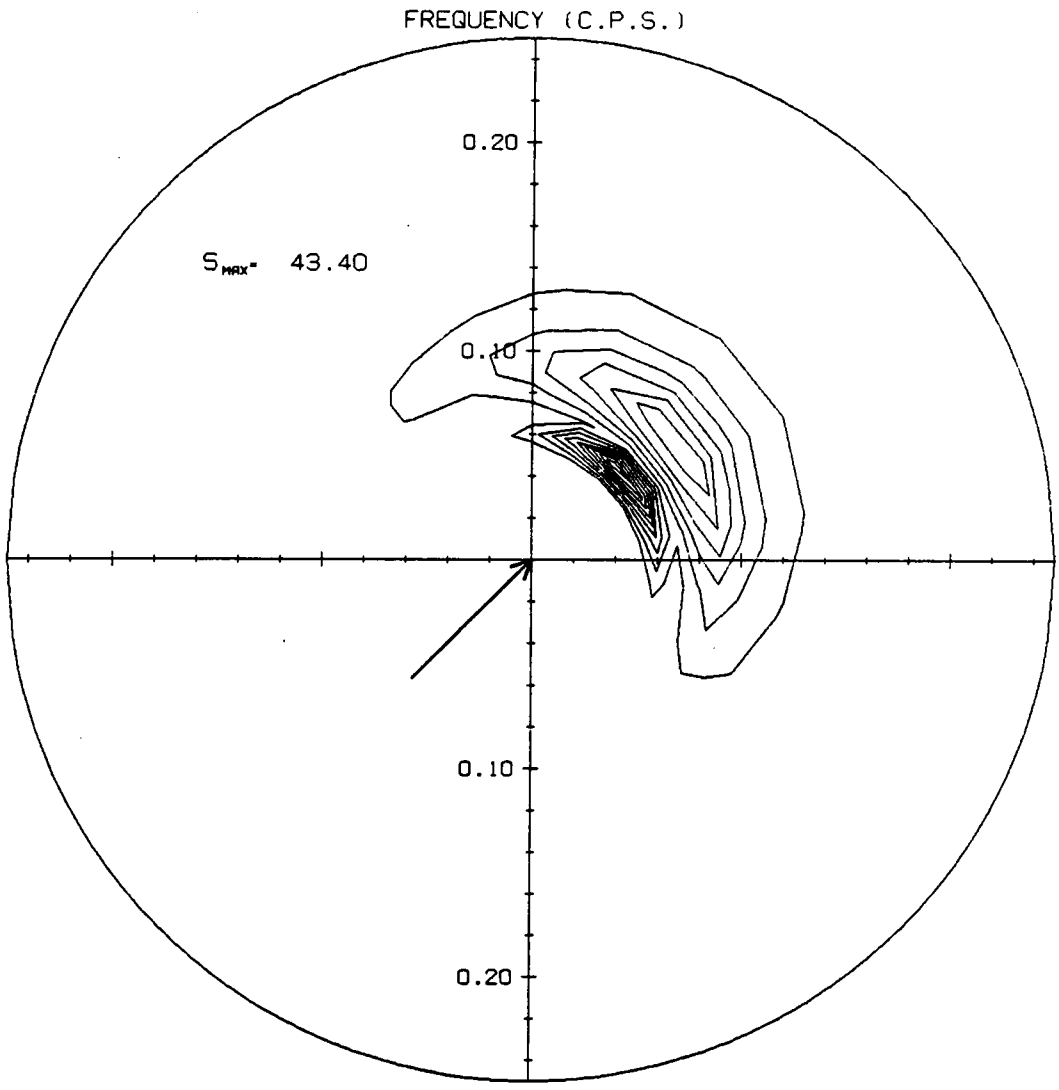

Fig. 45b T=10 hours

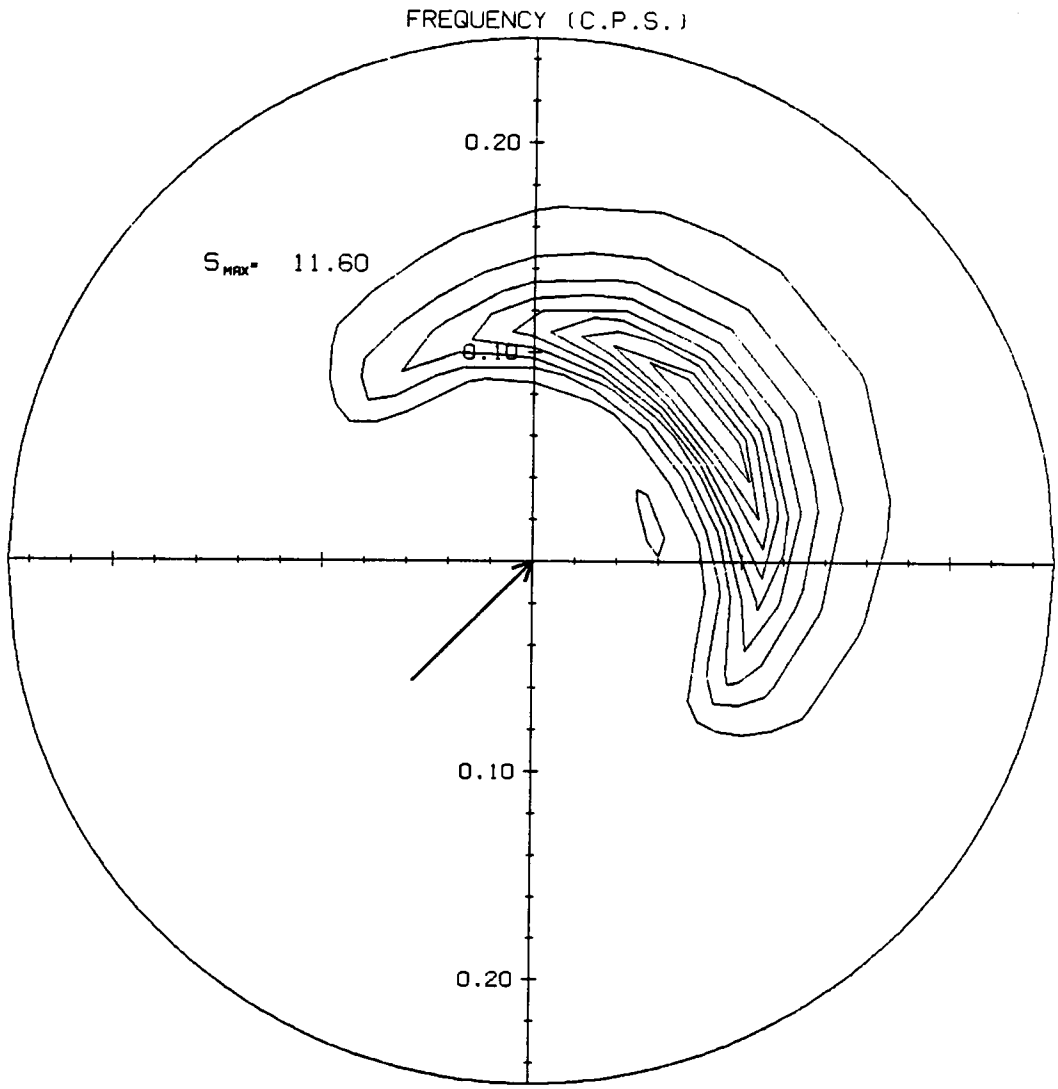

Fig. 46a Contour plots of 2-D spectrum evolution in the presence of swell from VSOWM with propagation at location (13,3). T=5 hours

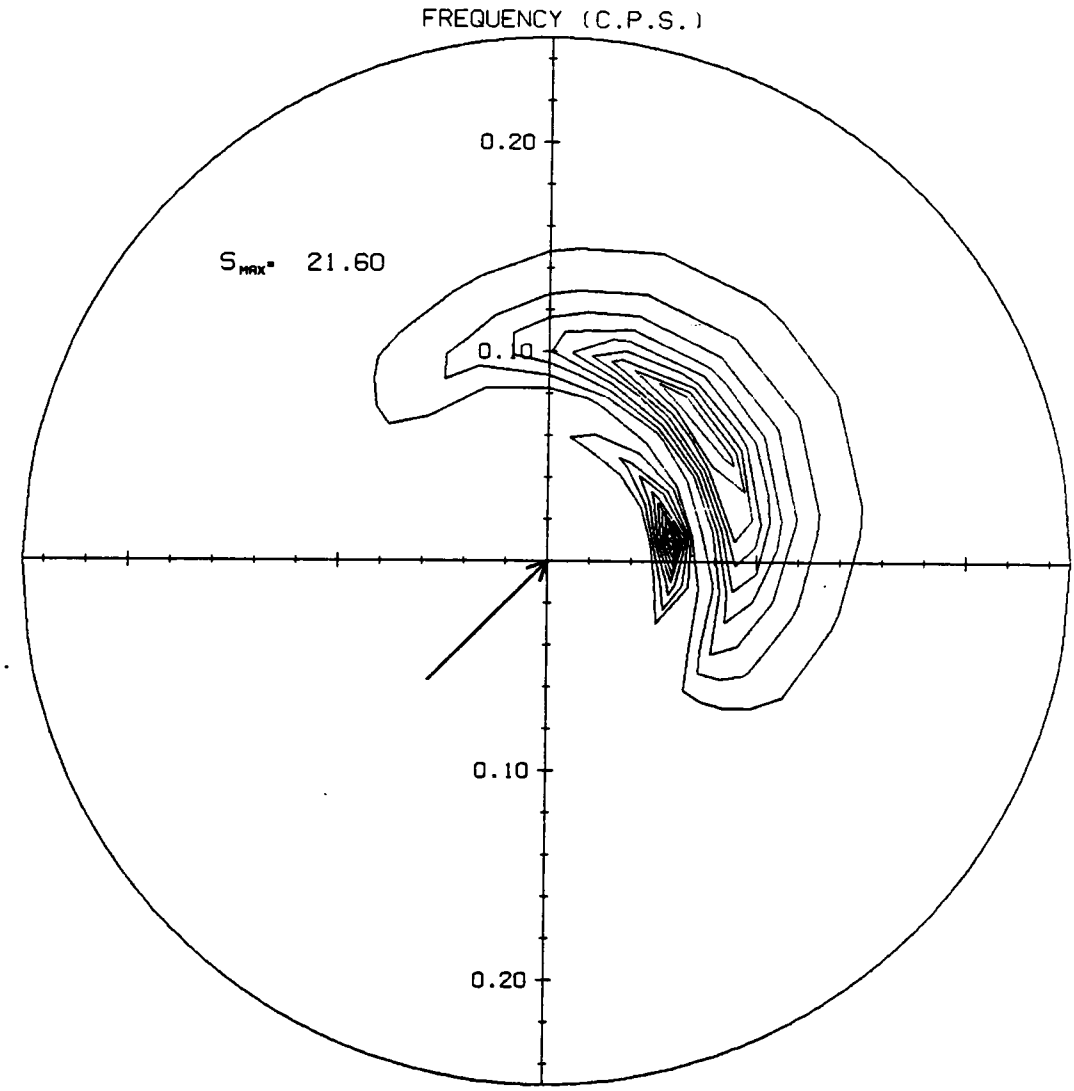

Fig. 46b T=10 hours

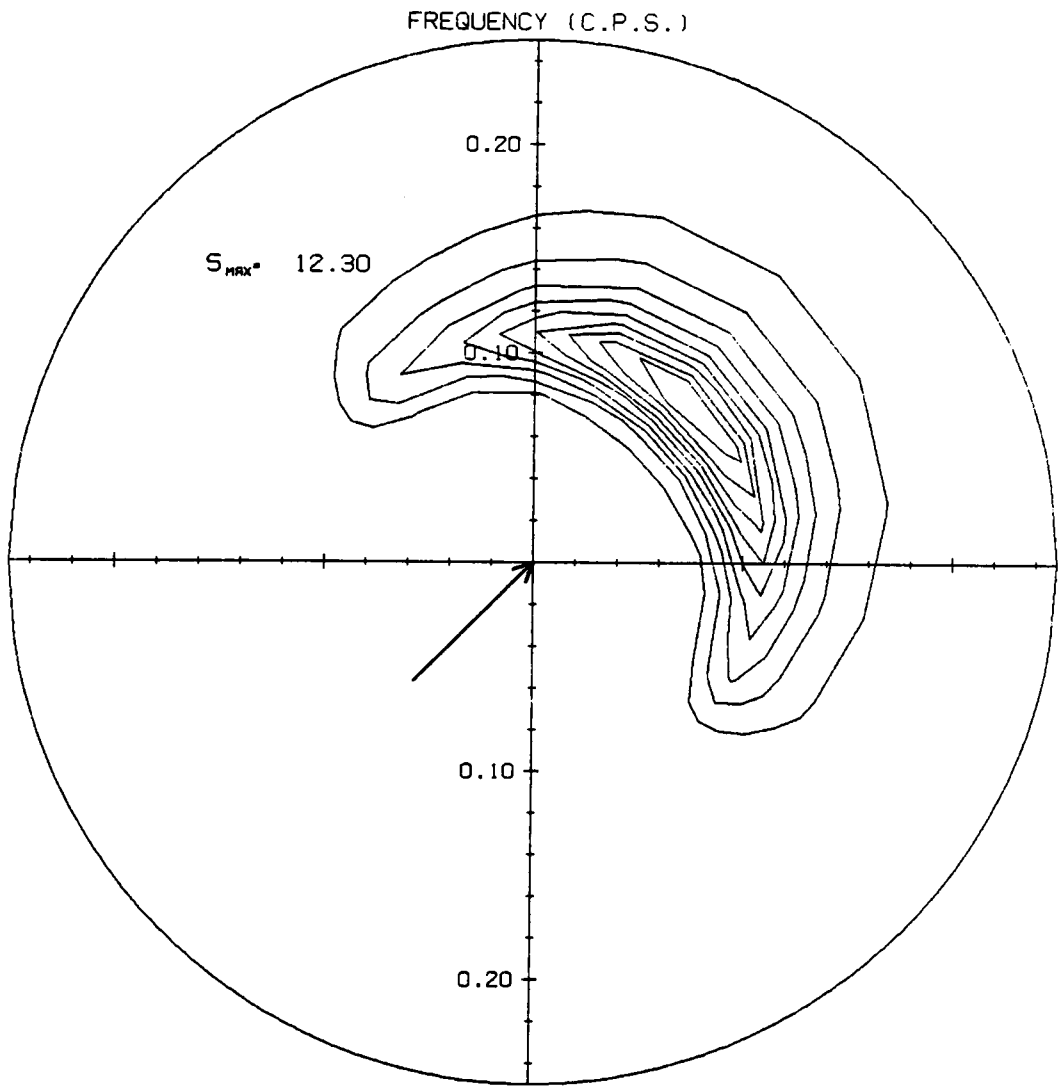

Fig. 47a Contour plots of 2-D spectrum evolution in the presence of swell from VSOWM with propagation at location (13,8). T=5 hours

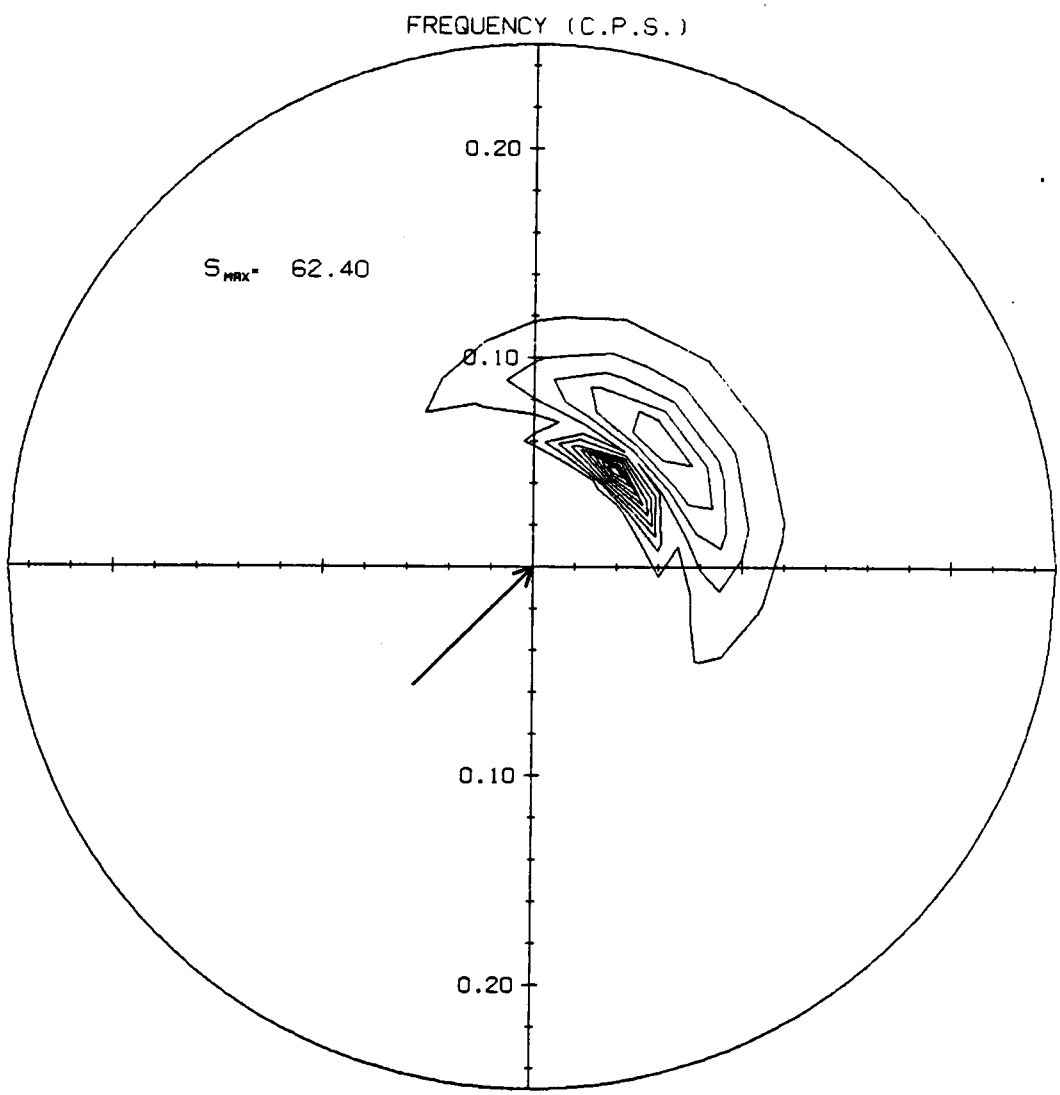

Fig. 47b T=10 hours

10. Table

Table 1. Integration limits for equation (4.21)

u^*/c	kz_m	kz_o	$k h_o$
0.01	0.7166E+12	0.1120E-05	0.7469E-04
0.02	0.3584E+04	0.4480E-05	0.2988E-03
0.03	0.8686E+01	0.1008E-04	0.6722E-03
0.04	0.5068E+00	0.1792E-04	0.1195E-02
0.05	0.1090E+00	0.2800E-04	0.1867E-02
0.06	0.3743E-01	0.4032E-04	0.2689E-02
0.07	0.1919E-01	0.5488E-04	0.3660E-02
0.08	0.1205E-01	0.7168E-04	0.4780E-02
0.09	0.8633E-02	0.9072E-04	0.6050E-02
0.10	0.6758E-02	0.1120E-03	0.7469E-02

The vita has been removed from the scanned document